





This is to certify that the

dissertation entitled

SYNTHESIS AND CHARACTERIZATION OF  
ETHYLENE OXIDE-SEGMENTED POLYMERS

presented by

Jun Qiao

has been accepted towards fulfillment  
of the requirements for

Ph.D. degree in Chemistry

  
Major professor

Date 9 August 1996

**LIBRARY  
Michigan State  
University**

**PLACE IN RETURN BOX to remove this checkout from your record.  
TO AVOID FINES return on or before date due.**

| <b>DATE DUE</b> | <b>DATE DUE</b> | <b>DATE DUE</b> |
|-----------------|-----------------|-----------------|
| _____           | _____           | _____           |
| _____           | _____           | _____           |
| _____           | _____           | _____           |
| _____           | _____           | _____           |
| _____           | _____           | _____           |
| _____           | _____           | _____           |
| _____           | _____           | _____           |

**SYNTHESIS AND CHARACTERIZATION OF ETHYLENE OXIDE-SEGMENTED  
POLYMERS**

**By**

**Jun Qiao**

**A DISSERTATION**

**Submitted to  
Michigan State University  
in partial fulfillment of the requirements  
for the degree of**

**DOCTOR OF PHILOSOPHY**

**Department of Chemistry**

**1996**

## ABSTRACT

### SYNTHESIS AND CHARACTERIZATION OF ETHYLENE OXIDE-SEGMENTED POLYMERS

By

Jun Qiao

Novel unsaturated ethylene oxide-segmented polymers were synthesized from oligo(ethylene glycol)  $\alpha,\omega$ -dialkenyl ethers *via* acyclic diene metathesis (ADMET) polymerization using Schrock's molybdenum alkylidene catalyst. The unsaturated polymers were prepared in high yields (above 92%) and the molecular weights were found to range from 15,100 to 93,900 Daltons according to gel permeation chromatography (GPC) measurements. The structures of the polymers were confirmed by  $^1\text{H}$  and  $^{13}\text{C}$  nuclear magnetic resonance (NMR) spectroscopy and infrared (IR) spectroscopy. Approximately 82 to 86% of the internal double bonds on the unsaturated polymer backbone were found to have a *trans* geometry by quantitative  $^{13}\text{C}$  NMR measurements. The polymers have good solubility in a variety of polar and nonpolar organic solvents.

The unsaturated polymers exhibited good thermal stability. Thermal gravimetric analysis (TGA) data indicated that the polymers were stable up to 300 °C, followed by rapid thermal breakdown above 300 °C. Differential scanning calorimetry (DSC) study revealed that the glass transition temperatures ( $T_g$ ) of the unsaturated polymers are segment length-dependent. Some of the

unsaturated polymers displayed interesting multiple crystallization and melting transitions in their DSC scans.

Perfectly alternating polyethylene/polyethylene oxide (AB)<sub>n</sub> copolymers were prepared by hydrogenating several unsaturated polymers. The thermal behavior of these hydrogenated polymers were studied by DSC.

Polymer electrolytes based on the unsaturated polymers were prepared using lithium perchlorate as salt. The Tg's of these polymer-salt complexes were dependent on the salt concentration, increasing with increasing salt content. The ionic conductivity of the electrolytes was obtained by impedance spectroscopy (IS) measurements. For each polymer electrolyte, as the salt content increased, the conductivity increased, reached a maximum and then dropped rapidly at higher salt concentrations. The conductivity was also found to increase with increasing temperature. The temperature-dependent conductivity fit the Vogel-Tammann-Fulcher (VTF) equation.

**To my wife Lei, my parents, and my brother Bin.**

hs

th

Co

re

en

Fi

De

re

## **ACKNOWLEDGMENTS**

I wish to express my deep appreciation to Professor Gregory L. Baker for his guidance, assistance and constant encouragement throughout the course of this research. I would also like to thank Professors James Jackson, Robert Cukier, Milton Smith and Peter Wagner for their guidance and assistance. My thanks go to all Baker group members as well, for making my stay in the lab an enjoyable one.

Financial support from Department of Chemistry and Center for Fundamental Materials Research at Michigan State University, and the U. S. Department of Energy is also acknowledged.

Finally, I want to thank my wife Lei for her constant love and support. I thank my parents and brother for their love and encouragement.

## TABLE OF CONTENTS

|   | <b>Page</b> |
|---|-------------|
| List of Schemes .....   | ix          |
| List of Tables .....  | xi          |
| List of Figures .....   | xiii        |
| <br>  |             |
| <b>INTRODUCTION</b> .....   | <b>1</b>    |
| I. <b>Polymer Electrolytes</b> .....  | <b>1</b>    |
| 1. <b>General</b> .....   | <b>1</b>    |
| 2. <b>PEO-based electrolytes</b> .....  | <b>2</b>    |
| 3. <b>Ionic conduction</b> .....  | <b>5</b>    |
| 4. <b>Synthesis of modified hosts</b> .....   | <b>7</b>    |
| II. <b>Target Polymers in This Work</b> .....   | <b>15</b>   |
| III. <b>ADMET Polymerization</b> .....  | <b>17</b>   |
| IV. <b>Ionic Conductivity Measurements</b> .....  | <b>28</b>   |
| <br>  |             |
| <b>RESULTS</b> .....  | <b>35</b>   |
| I. <b>Monomer Preparation</b> .....   | <b>35</b>   |
| II. <b>Unsaturated Ethylene Oxide-Segmented Polymers</b> .....  | <b>38</b>   |
| 1. <b>ADMET polymerization of oligo(ethylene glycol) <math>\alpha,\omega</math>-<br/>                dialkenyl ethers</b> ..... | <b>38</b>   |
| 2. <b>Properties of the unsaturated polymers</b> .....  | <b>40</b>   |
| 3. <b>Spectroscopic characterization of the unsaturated<br/>                polymers</b> .....                                  | <b>42</b>   |
| 4. <b>Thermal stability of the unsaturated polymers</b> .....   | <b>47</b>   |
| 5. <b>Thermal behavior of the unsaturated polymers</b> .....  | <b>52</b>   |
| III. <b>Alternating (AB)<sub>n</sub> Copolymers from the Unsaturated<br/>                Polymers</b> .....                     | <b>66</b>   |

|                    |  |     |
|--------------------|--|-----|
| 1.                 | Reduction of the unsaturated polymers.....                             | 66  |
| 2.                 | Physical properties of the hydrogenated polymers .....                 | 67  |
| 3.                 | Thermal behavior of the hydrogenated polymers.....                     | 71  |
| 4.                 | Morphology of the hydrogenated polymers.....                           | 77  |
| IV.                | Polymer Electrolytes Based on the Unsaturated Polymers .....           | 81  |
| 1.                 | Thermal behavior of the polymer electrolytes .....                     | 81  |
| 2.                 | Impedance spectroscopy of the polymer electrolytes .....               | 96  |
| 3.                 | Conductivity behavior of the polymer electrolytes.....                 | 99  |
| 4.                 | Temperature dependent conductivity.....                                | 107 |
| DISCUSSION.....    |  | 114 |
| I.                 | Scope of ADMET Polymerization in Synthesizing Target<br>Polymers. .... | 114 |
| 1.                 | ADMET polymerization catalysts.....                                    | 114 |
| 2.                 | Polymerizability of the monomers .....                                 | 116 |
| 3.                 | Controlling molecular weights .....                                    | 120 |
| II.                | Unsaturated Ethylene Oxide-Segmented Polymers .....                    | 122 |
| 1.                 | Segment length dependent glass transition<br>temperature.....          | 122 |
| 2.                 | Melting transitions.....   | 127 |
| III.               | Electrolytes from the Unsaturated Polymers .....                       | 129 |
| 1.                 | Conductivity and EO content.....                                       | 129 |
| 2.                 | Parameters in the VTF equation .....                                   | 130 |
| IV.                | Summary .....  | 132 |
| V.                 | Suggestions for Further Research .....                                 | 134 |
| EXPERIMENTAL ..... |  | 136 |
| I.                 | General .....  | 136 |
| 1.                 | Solvents .....   | 138 |
| 2.                 | Argon.....   | 139 |
| 3.                 | Sodium mirror.....   | 140 |
| II.                | Preparation of Monomers.....   | 141 |
| 1.                 | Diethylene glycol $\alpha,\omega$ -diallyl ether.....                  | 141 |
| 2.                 | Diethylene glycol $\alpha,\omega$ -di-3-butenyl ether .....            | 142 |
| 3.                 | Diethylene glycol $\alpha,\omega$ -di-4-pentenyl ether .....           | 142 |

|      |   |     |
|------|---|-----|
| 4.   | Triethylene glycol $\alpha,\omega$ -di-4-pentenyl ether .....                   | 144 |
| 5.   | Tetraethylene glycol $\alpha,\omega$ -di-4-pentenyl ether .....                 | 145 |
| 6.   | Diethylene glycol $\alpha,\omega$ -di-5-hexenyl ether .....                     | 145 |
| 7.   | Triethylene glycol $\alpha,\omega$ -di-5-hexenyl ether .....                    | 146 |
| 8.   | Tetraethylene glycol $\alpha,\omega$ -di-5-hexenyl ether .....                  | 146 |
| 9.   | Pentaethylene glycol $\alpha,\omega$ -di-5-hexenyl ether .....                  | 147 |
| 10.  | Diethylene glycol $\alpha,\omega$ -di-7-octenyl ether .....                     | 147 |
| 11.  | Tetraethylene glycol $\alpha,\omega$ -di-7-octenyl ether .....                  | 148 |
| <br> |   |     |
| III. | ADMET Polymerization Catalysts.....   | 150 |
| <br> |   |     |
| IV.  | Synthesis of Unsaturated Ethylene Oxide-Segmented<br>Polymers .....             | 151 |
| 1.   | Polymer from diethylene glycol $\alpha,\omega$ -di-3-butenyl ether.....         | 151 |
| 2.   | Polymer from diethylene glycol $\alpha,\omega$ -di-4-pentenyl ether....         | 151 |
| 3.   | Polymer from triethylene glycol $\alpha,\omega$ -di-4-pentenyl ether ...        | 152 |
| 4.   | Polymer from tetraethylene glycol $\alpha,\omega$ -di-4-pentenyl<br>ether ..... | 153 |
| 5.   | Polymer from diethylene glycol $\alpha,\omega$ -di-5-hexenyl ether.....         | 154 |
| 6.   | Polymer from triethylene glycol $\alpha,\omega$ -di-5-hexenyl ether....         | 154 |
| 7.   | Polymer from tetraethylene glycol $\alpha,\omega$ -di-5-hexenyl<br>ether .....  | 155 |
| 8.   | Polymer from pentaethylene glycol $\alpha,\omega$ -di-5-hexenyl<br>ether .....  | 155 |
| 9.   | Polymer from diethylene glycol $\alpha,\omega$ -di-7-octenyl ether.....         | 156 |
| 10.  | Polymer from tetraethylene glycol $\alpha,\omega$ -di-7-octenyl<br>ether .....  | 156 |
| <br> |   |     |
| V.   | Preparation of Saturated Ethylene Oxide-Segmented<br>Polymers .....             | 157 |
| 1.   | Hydrogenated polymer from PH2 .....   | 157 |
| 2.   | Hydrogenated polymer from PH3 .....   | 158 |
| 3.   | Hydrogenated polymer from PH4 .....   | 158 |
| 4.   | Hydrogenated polymer from PH5 .....   | 158 |
| <br> |   |     |
| VI.  | Preparation of Polymer Electrolytes .....                                       | 160 |
| <br> |   |     |
|      | APPENDIX.....   | 161 |
| <br> |   |     |
|      | BIBLIOGRAPHY .....  | 178 |

## LIST OF SCHEMES

| <b>Scheme</b> |  | <b>Page</b> |
|---------------|--|-------------|
| Scheme 1.     | Preparation of methylene-linked PEO copolymer.....                             | 7           |
| Scheme 2.     | Preparation of poly(dimethyl siloxane-co-ethylene oxide)s.....                 | 8           |
| Scheme 3.     | Copolymerization of ethylene oxide and propylene oxide.....                    | 9           |
| Scheme 4.     | Preparation of comb polymer with PEO branches.....                             | 10          |
| Scheme 5.     | Preparation of comb-branched poly(siloxanes) with PEO side chains.....         | 10          |
| Scheme 6.     | Preparation of MEEP from inorganic polyphosphazene.....                        | 11          |
| Scheme 7.     | Crosslinking PEO by hydrosilylation.....                                       | 14          |
| Scheme 8.     | Target polymer electrolyte hosts.....  | 15          |
| Scheme 9.     | General ADMET polymerization.....  | 17          |
| Scheme 10.    | ADMET polymerization mechanism.....  | 18          |
| Scheme 11.    | Synthesis of unsaturated polyalkanes <i>via</i> ADMET polymerization.....      | 21          |
| Scheme 12.    | Synthesis of unsaturated polyethers <i>via</i> ADMET polymerization .....      | 22          |
| Scheme 13.    | Synthesis of conjugated polyenes <i>via</i> ADMET polymerization..             | 24          |
| Scheme 14.    | Synthesis of liquid crystalline materials <i>via</i> ADMET polymerization..... | 25          |
| Scheme 15.    | Synthesis of cubane-containing polymer <i>via</i> ADMET polymerization.....    | 26          |
| Scheme 16.    | A generalized ADMET copolymerization.....                                      | 27          |

|   |            |
|---|------------|
| <b>Scheme 17. Monomer preparation by Williamson ether coupling .....</b>  | <b>36</b>  |
| <b>Scheme 18. Monomer preparation by reaction of ditosylates with sodium alkenoxides.....</b>                     | <b>37</b>  |
| <b>Scheme 19. ADMET polymerization of oligo(ethylene glycol) <math>\alpha,\omega</math>-dialkenyl ethers.....</b> | <b>38</b>  |
| <b>Scheme 20. Hydrogenation of the unsaturated polymers.....</b>  | <b>66</b>  |
| <b>Scheme 21. Failed ADMET polymerization to make an unsaturated polyether .....</b>                              | <b>117</b> |
| <b>Scheme 22. Competition between ring-closing metathesis reaction and ADMET polymerization.....</b>              | <b>118</b> |
| <b>Scheme 23. Mechanism for ring-closing metathesis reaction.....</b>   | <b>118</b> |
| <b>Scheme 24. An example of ring-closing metathesis reaction to prepare a cyclic ether.....</b>                   | <b>119</b> |

Table

## LIST OF TABLES

| <b>Table</b> |   | <b>Page</b> |
|--------------|---|-------------|
| Table 1.     | Some Representative ADMET Polymers Prepared by Wagener <i>et al.</i> .....                  | 23          |
| Table 2.     | Acronyms for Monomers.....  | 35          |
| Table 3.     | Polymerizability of Monomers by ADMET Polymerization Using Schrock's Mo Catalyst.....       | 40          |
| Table 4.     | Properties of the Unsaturated Polymers.....   | 41          |
| Table 5.     | Thermal Stability of the Unsaturated Polymers.....  | 51          |
| Table 6.     | Thermal Transition of the Unsaturated Polymers.....   | 64          |
| Table 7.     | GPC Data Comparison Between the Hydrogenated Polymers and Their Unsaturated Precursors..... | 70          |
| Table 8.     | Thermal Transition Temperatures for the Hydrogenated Polymers.....                          | 77          |
| Table 9.     | The Measured and Calculated $T_g$ of Some Unsaturated Polymers.....                         | 126         |
| Table 10.    | Peak Conductivity of the Unsaturated Polymers at 20 °C, 50 °C and 100 °C.....               | 130         |
| Table 11.    | The VTF Parameters for Polymer-Salt Complexes with an O:Li Ratio of 32.....                 | 131         |
| Table 12.    | Conductivity Data for PP2-LiClO <sub>4</sub> Complexes.....                                 | 172         |
| Table 13.    | Conductivity Data for PP3-LiClO <sub>4</sub> Complexes.....                                 | 173         |
| Table 14.    | Conductivity Data for PP4-LiClO <sub>4</sub> Complexes.....                                 | 174         |

Table 1:

Table 1:

Table 1:

|                  |  |            |
|------------------|--|------------|
| <b>Table 15.</b> | <b>Conductivity Data for PH<sub>3</sub>-LiClO<sub>4</sub> Complexes.....</b> | <b>175</b> |
| <b>Table 16.</b> | <b>Conductivity Data for PH<sub>4</sub>-LiClO<sub>4</sub> Complexes.....</b> | <b>176</b> |
| <b>Table 17.</b> | <b>Conductivity Data for PH<sub>5</sub>-LiClO<sub>4</sub> Complexes.....</b> | <b>177</b> |

## LIST OF FIGURES

| <b>Figure</b> |  | <b>Page</b> |
|---------------|--|-------------|
| Figure 1.     | Arrhenius plot of temperature-dependent conductivity in PEO-LiClO <sub>4</sub> complex (O:Li = 6) reported by Chabagno.....                            | 3           |
| Figure 2.     | Conductivity of the amorphous PEO-LiClO <sub>4</sub> electrolytes of different salt concentrations at 50 °C reported by Prud'homme <i>et al.</i> ..... | 4           |
| Figure 3.     | Li <sup>+</sup> ion transport in PEO-salt complex as the combined result of polymer segmental motion and Li <sup>+</sup> ion movement.....             | 5           |
| Figure 4.     | Conductivity scale for different materials.....  | 29          |
| Figure 5.     | Polymer electrolyte contained between two inert electrodes: before (left) and after (right) a <i>d.c.</i> voltage of fixed potential is applied.....   | 30          |
| Figure 6.     | Current decay as a function of time when a <i>d.c.</i> voltage is applied to a polymer electrolyte sample.....   | 31          |
| Figure 7.     | The sinusoidal voltage applied to a polymer electrolyte cell and the resulting current.....  | 32          |
| Figure 8.     | Complex impedance vector <b>Z</b> and the real and imaginary components in the rectangular complex plane. The phase angle is $\theta$ .....            | 33          |
| Figure 9.     | Complex impedance diagram of a polymer electrolyte cell sandwiched between two inert electrodes.....   | 34          |
| Figure 10.    | A schematic cross section polymer electrolyte cell of known dimensions.....  | 34          |
| Figure 11.    | <sup>1</sup> H NMR spectra of monomer <b>P3</b> (top) and polymer <b>PP3a</b> (bottom).....  | 43          |

|            |   |    |
|------------|---|----|
| Figure 12. | $^{13}\text{C}$ NMR spectra of monomer <b>P3</b> (top) and polymer <b>PP3a</b> (bottom).....  | 45 |
| Figure 13. | IR spectra of monomer <b>P3</b> (top) and polymer <b>PP3a</b> (bottom)...                     | 46 |
| Figure 14. | TGA profiles of <b>PP2</b> (heating rate 10 °C/min).....                                      | 48 |
| Figure 15. | TGA profiles of <b>PP4</b> and PEG10K in nitrogen (heating rate 10 °C/min).....               | 49 |
| Figure 16. | TGA profiles of <b>PH2</b> (heating rate 10 °C/min).....                                      | 50 |
| Figure 17. | Second DSC heating and cooling scans for <b>PB2</b> (heating and cooling rate 10 °C/min)..... | 53 |
| Figure 18. | Second DSC heating and cooling scans for <b>PP2</b> (heating and cooling rate 10 °C/min)..... | 54 |
| Figure 19. | Second DSC heating and cooling scans for <b>PP3</b> (heating and cooling rate 10 °C/min)..... | 55 |
| Figure 20. | Second DSC heating and cooling scans for <b>PP4</b> (heating and cooling rate 10 °C/min)..... | 57 |
| Figure 21. | Second DSC heating and cooling scans for <b>PH2</b> (heating and cooling rate 10 °C/min)..... | 58 |
| Figure 22. | Second DSC heating and cooling scans for <b>PH3</b> (heating and cooling rate 10 °C/min)..... | 59 |
| Figure 23. | Second DSC heating and cooling scans for <b>PH4</b> (heating and cooling rate 10 °C/min)..... | 60 |
| Figure 24. | Second DSC heating and cooling scans for <b>PH5</b> (heating and cooling rate 10 °C/min)..... | 61 |
| Figure 25. | Second DSC heating and cooling scans for <b>PO2</b> (heating and cooling rate 10 °C/min)..... | 62 |
| Figure 26. | Second DSC heating and cooling scans for <b>PO4</b> (heating and cooling rate 10 °C/min)..... | 63 |
| Figure 27. | $^1\text{H}$ NMR spectrum of hydrogenated polymer <b>PH5H</b> .....                           | 68 |

|            |   |    |
|------------|---|----|
| Figure 12. | <sup>13</sup> C NMR spectra of monomer <b>P3</b> (top) and polymer <b>PP3a</b> (bottom).....  | 45 |
| Figure 13. | IR spectra of monomer <b>P3</b> (top) and polymer <b>PP3a</b> (bottom)...                     | 46 |
| Figure 14. | TGA profiles of <b>PP2</b> (heating rate 10 °C/min).....                                      | 48 |
| Figure 15. | TGA profiles of <b>PP4</b> and PEG10K in nitrogen (heating rate 10 °C/min).....               | 49 |
| Figure 16. | TGA profiles of <b>PH2</b> (heating rate 10 °C/min).....                                      | 50 |
| Figure 17. | Second DSC heating and cooling scans for <b>PB2</b> (heating and cooling rate 10 °C/min)..... | 53 |
| Figure 18. | Second DSC heating and cooling scans for <b>PP2</b> (heating and cooling rate 10 °C/min)..... | 54 |
| Figure 19. | Second DSC heating and cooling scans for <b>PP3</b> (heating and cooling rate 10 °C/min)..... | 55 |
| Figure 20. | Second DSC heating and cooling scans for <b>PP4</b> (heating and cooling rate 10 °C/min)..... | 57 |
| Figure 21. | Second DSC heating and cooling scans for <b>PH2</b> (heating and cooling rate 10 °C/min)..... | 58 |
| Figure 22. | Second DSC heating and cooling scans for <b>PH3</b> (heating and cooling rate 10 °C/min)..... | 59 |
| Figure 23. | Second DSC heating and cooling scans for <b>PH4</b> (heating and cooling rate 10 °C/min)..... | 60 |
| Figure 24. | Second DSC heating and cooling scans for <b>PH5</b> (heating and cooling rate 10 °C/min)..... | 61 |
| Figure 25. | Second DSC heating and cooling scans for <b>PO2</b> (heating and cooling rate 10 °C/min)..... | 62 |
| Figure 26. | Second DSC heating and cooling scans for <b>PO4</b> (heating and cooling rate 10 °C/min)..... | 63 |
| Figure 27. | <sup>1</sup> H NMR spectrum of hydrogenated polymer <b>PH5H</b> .....                         | 68 |

|            |   |    |
|------------|---|----|
| Figure 28. | $^{13}\text{C}$ NMR spectrum of hydrogenated polymer <b>PH5H</b> .....  | 69 |
| Figure 29. | Second DSC heating and cooling scans for <b>PH2H</b> (heating and cooling rate $10\text{ }^\circ\text{C}/\text{min}$ ).....   | 72 |
| Figure 30. | Second DSC heating and cooling scans for <b>PH3H</b> (heating and cooling rate $10\text{ }^\circ\text{C}/\text{min}$ ).....   | 73 |
| Figure 31. | Second DSC heating and cooling scans for <b>PH4H</b> (heating and cooling rate $10\text{ }^\circ\text{C}/\text{min}$ ).....   | 75 |
| Figure 32. | Second DSC heating and cooling scans for <b>PH5H</b> (heating and cooling rate $10\text{ }^\circ\text{C}/\text{min}$ ).....   | 76 |
| Figure 33. | Polarized light optical micrograph of <b>PH2H</b> .....   | 78 |
| Figure 34. | Polarized light optical micrograph of <b>PH3H</b> .....   | 79 |
| Figure 35. | 2nd heating DSC scans of <b>PP2</b> and its $\text{LiClO}_4$ salt complexes at different salt concentrations. Numbers refer to molar O:Li ratios for each sample. Heating rate is $10\text{ }^\circ\text{C}/\text{min}$ ..... | 82 |
| Figure 36. | $T_g$ as a function of the salt molar fraction for <b>PP2</b> -salt complexes.....  | 83 |
| Figure 37. | 2nd heating DSC scans of <b>PP3</b> and its $\text{LiClO}_4$ salt complexes at different salt concentrations. Numbers refer to molar O:Li ratios for each sample. Heating rate is $10\text{ }^\circ\text{C}/\text{min}$ ..... | 84 |
| Figure 38. | $T_g$ as a function of the salt molar fraction for <b>PP3</b> -salt complexes.....  | 85 |
| Figure 39. | 2nd heating DSC scans of <b>PP4</b> and its $\text{LiClO}_4$ salt complexes at different salt concentrations. Numbers refer to molar O:Li ratios for each sample. Heating rate is $10\text{ }^\circ\text{C}/\text{min}$ ..... | 87 |
| Figure 40. | $T_g$ as a function of the salt molar fraction for <b>PP4</b> -salt complexes.....  | 88 |
| Figure 41. | 2nd heating DSC scans of <b>PH3</b> and its $\text{LiClO}_4$ salt complexes at different salt concentrations. Numbers refer to molar O:Li ratios for each sample. Heating rate is $10\text{ }^\circ\text{C}/\text{min}$ ..... | 89 |
| Figure 42. | $T_g$ as a function of the salt molar fraction for <b>PH3</b> -salt complexes.....  | 90 |

Fig

|            |   |     |
|------------|---|-----|
| Figure 43. | 2nd heating DSC scans of <b>PH4</b> and its $\text{LiClO}_4$ salt complexes at different salt concentrations. Numbers refer to molar O:Li ratios for each sample. Heating rate is $10\text{ }^\circ\text{C}/\text{min}$ ..... | 92  |
| Figure 44. | $T_g$ as a function of the salt molar fraction for <b>PH4</b> -salt complexes.....  | 93  |
| Figure 45. | 2nd heating DSC scans of <b>PH5</b> and its $\text{LiClO}_4$ salt complexes at different salt concentrations. Numbers refer to molar O:Li ratios for each sample. Heating rate is $10\text{ }^\circ\text{C}/\text{min}$ ..... | 94  |
| Figure 46. | $T_g$ as a function of the salt molar fraction for <b>PH5</b> -salt complexes.....  | 95  |
| Figure 47. | Complex impedance diagram for <b>PP4</b> -salt complex (O:Li = 4) at $50\text{ }^\circ\text{C}$ .....   | 97  |
| Figure 48. | Complex impedance diagram for <b>PH4</b> -salt complex (O:Li = 32) at $30\text{ }^\circ\text{C}$ .....  | 98  |
| Figure 49. | Conductivity of <b>PP2</b> - $\text{LiClO}_4$ complexes as a function of salt content at $20\text{ }^\circ\text{C}$ , $50\text{ }^\circ\text{C}$ and $100\text{ }^\circ\text{C}$ .....  | 100 |
| Figure 50. | Conductivity of <b>PP3</b> - $\text{LiClO}_4$ complexes as a function of salt content at $20\text{ }^\circ\text{C}$ , $50\text{ }^\circ\text{C}$ and $100\text{ }^\circ\text{C}$ .....  | 101 |
| Figure 51. | Conductivity of <b>PP4</b> - $\text{LiClO}_4$ complexes as a function of salt content at $20\text{ }^\circ\text{C}$ and $50\text{ }^\circ\text{C}$ .....  | 102 |
| Figure 52. | Conductivity of <b>PH3</b> - $\text{LiClO}_4$ complexes as a function of salt content at $20\text{ }^\circ\text{C}$ , $50\text{ }^\circ\text{C}$ and $100\text{ }^\circ\text{C}$ .....  | 103 |
| Figure 53. | Conductivity of <b>PH4</b> - $\text{LiClO}_4$ complexes as a function of salt content at $20\text{ }^\circ\text{C}$ , $50\text{ }^\circ\text{C}$ and $100\text{ }^\circ\text{C}$ .....  | 104 |
| Figure 54. | Conductivity of <b>PH5</b> - $\text{LiClO}_4$ complexes as a function of salt content at $20\text{ }^\circ\text{C}$ , $50\text{ }^\circ\text{C}$ and $100\text{ }^\circ\text{C}$ .....  | 105 |
| Figure 55. | VTF plots for <b>PP2</b> - $\text{LiClO}_4$ complexes with O:Li ratio of 32, 16, 12, and 4.....   | 108 |
| Figure 56. | VTF plots for <b>PP3</b> - $\text{LiClO}_4$ complexes with O:Li ratio of 64, 32, 16, and 12.....  | 109 |

|   |     |
|---|-----|
| Figure 57. VTF plots for <b>PP4-LiClO<sub>4</sub></b> complexes with O:Li ratio of 64, 32, 16, and 8..... | 110 |
| Figure 58. VTF plots for <b>PH3-LiClO<sub>4</sub></b> complexes with O:Li ratio of 64, 32, 8, and 4.....  | 111 |
| Figure 59. VTF plots for <b>PH4-LiClO<sub>4</sub></b> complexes with O:Li ratio of 64, 32, and 4.....     | 112 |
| Figure 60. VTF plots for <b>PH5-LiClO<sub>4</sub></b> complexes with O:Li ratio of 64, 32, 8, and 4.....  | 113 |
| Figure 61. Ethylene oxide segment length dependent <b>T<sub>g</sub></b> in unsaturated polymers.....      | 123 |
| Figure 62. Methylene unit dependent <b>T<sub>g</sub></b> in several unsaturated polymers.....             | 124 |
| Figure 63. Melting temperature as a function number of ethylene oxide units in unsaturated polymers.....  | 127 |
| Figure 64. TGA profiles of <b>PB2</b> (heating rate 10 °C/min).....                                       | 162 |
| Figure 65. TGA profiles of <b>PP2a</b> (heating rate 10 °C/min).....                                      | 163 |
| Figure 66. TGA profiles of <b>PP3a</b> (heating rate 10 °C/min).....                                      | 164 |
| Figure 67. TGA profiles of <b>PP3</b> (heating rate 10 °C/min).....                                       | 165 |
| Figure 68. TGA profiles of <b>PP4a</b> (heating rate 10 °C/min).....                                      | 166 |
| Figure 69. TGA profiles of <b>PH3</b> (heating rate 10 °C/min).....                                       | 167 |
| Figure 70. TGA profiles of <b>PH4</b> (heating rate 10 °C/min).....                                       | 168 |
| Figure 71. TGA profiles of <b>PH5</b> (heating rate 10 °C/min).....                                       | 169 |
| Figure 72. TGA profiles of <b>PO2</b> (heating rate 10 °C/min).....                                       | 170 |
| Figure 73. TGA profiles of <b>PO4</b> (heating rate 10 °C/min).....                                       | 171 |

ISS

ION

OW

WI

(of

copy

see

See

copy

can

Ma

avo

Th

sto

Suc

and

# INTRODUCTION

## I. Polymer Electrolytes

### 1. General

Polymer electrolytes<sup>1-4</sup> refer to polymer-salt complexes formed by dissolving salts (mainly alkali metal salts) in appropriate polymers. After the pioneering work done by Wright and coworkers<sup>5</sup> in 1973, and Armand and coworkers<sup>6</sup> in 1979, polymer electrolytes have attracted considerable interest owing to their potential applications as new solid ionic conductors.

The ionic conductivities of polymer electrolytes usually range from  $10^{-8}$  to  $10^{-6}$  S/cm at room temperature, and reach  $10^{-4}$  to  $10^{-3}$  S/cm at 100 °C for many polymer-salt complexes. Although their conductivity at ambient temperature needs to improve in order to be useful for many applications, solid polymer electrolytes can be processed into very thin films with large surface area, so that power densities comparable to liquid electrolytes or molten salts ( $>100$  W/dm<sup>3</sup>) can be maintained. However, in contrast to conventional ionic conducting materials, they have the advantage of operating in solvent-free conditions and avoid the use of flammable organic solvents or corrosive aqueous solutions. Thus, polymer electrolytes can find applications in energy generation and storage as rechargeable solid state lithium batteries, in electrochromic devices such as sunglasses and smart windows, as well as in solid state ionic sensors and photoelectrochemical cells.

at

se

oo

oo

wh

en

co

ab

po

mo

the

am

ele

com

cry

How

and

copy

As an ideal electrolyte host, a polymer should have electron donating atoms or groups that can form coordinate bonds with cations, good chain segmental mobility to enable transport of ions,<sup>7</sup> and a suitable distance between coordinating sites. While a number of polymers, including polyethers,<sup>8-9</sup> polyimines,<sup>10-11</sup> polythioethers<sup>12</sup> and polyesters<sup>13-15</sup> fit these criteria, the most widely studied polymer host to date has been poly(ethylene oxide) (PEO).

## 2. PEO-based electrolytes

PEO is usually prepared by the catalyzed ring-opening polymerization of ethylene oxide. Since the linear PEO chains adopt a regular helical conformation,<sup>16</sup> PEO is a highly crystalline material with a degree of crystallinity above 70% at room temperature. Depending on molecular weight, the melting point of PEO ranges from 60 °C for a molecular weight of 4,000 to 66 °C as the molecular weight reaches 200,000. Due to the presence of traces of catalyst, the ionic conductivity of commercial PEO is between  $10^{-11}$  to  $10^{-9}$  S/cm.

When a salt is dissolved in PEO, the resulting PEO-salt complex can be amorphous, semi-crystalline or crystalline, depending on composition of the electrolyte and temperature, as illustrated in a phase diagram for PEO-LiClO<sub>4</sub> complex reported by Robitaille *et al.*<sup>17</sup> According to the phase diagram, a crystalline phase exists with an O:Li ratio of 10 and it melts around 65 °C. However, conductivity is adversely affected by the crystallinity in the electrolyte, and as studies by Berthier and coworkers<sup>18</sup> confirmed, the amorphous phase in polymer electrolytes is responsible for the high ionic conductivity. The crystalline

cha  
ove  
the  
but  
stat  
elec

Fig  
com

phase in a polymer electrolyte reinforces the mechanical strength, but lowers the overall conductivity. At elevated temperatures, the crystalline phase melts and the conductivities of PEO-salt complexes are promising ( $> 10^{-4}$  S/cm at 100 °C), but the disappearance of crystalline phase leads to decreased dimensional stability. The temperature-dependent conductivity of a PEO-based polymer electrolyte is exemplified in **Figure 1**.

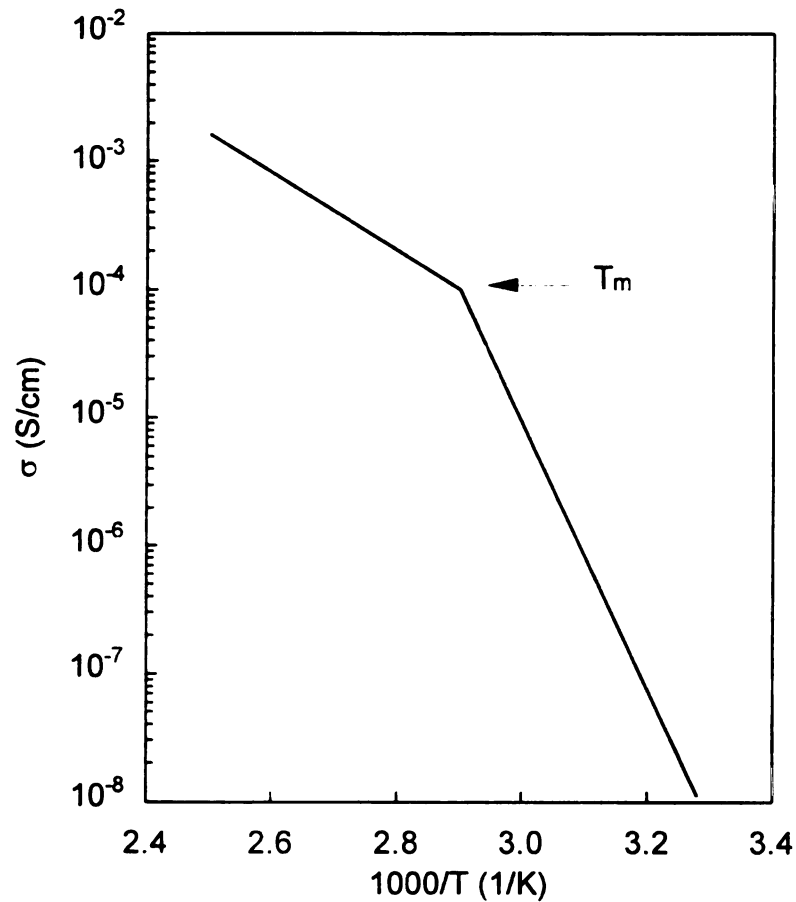


**Figure 1.** Arrhenius plot of temperature-dependent conductivity in PEO-LiClO<sub>4</sub> complex (O:Li = 6) reported by Chabagno.<sup>19</sup>

The conductivity of a PEO-salt complex is also closely related to its salt content. **Figure 2** shows that at low salt concentration, the conductivity increases with increasing salt content and reaches a peak value. However, with

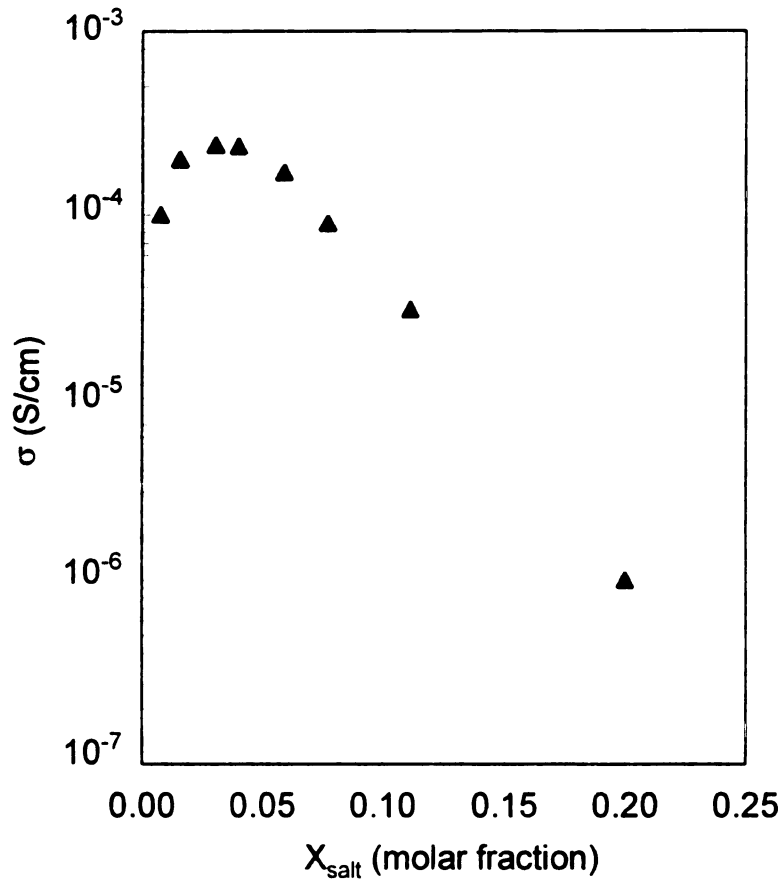


**Figure 2.** Conductivity of the amorphous PEO-LiClO<sub>4</sub> electrolytes of different salt concentrations at 50 °C reported by Prud'homme *et al.*<sup>9</sup>

continued increases in salt concentration, the ions tend to form aggregates that are much larger in mass and thus have a greatly reduced mobility. Also, the oxygen-ion coordination complexes act as transient crosslinking points that

decrease the chain mobility and conductivity. At the highest salt concentrations, the number of oxygen atoms available to form new coordinating sites decreases. As a result of these factors, the conductivity drops significantly when more salt is added.

### 3. Ionic conduction

Mechanistically, ion transport in PEO-based electrolytes can be illustrated by the model in **Figure 3**. In a PEO matrix, a  $\text{Li}^+$  cation forms a complex with surrounding oxygen atoms from a single PEO chain or from different chains.

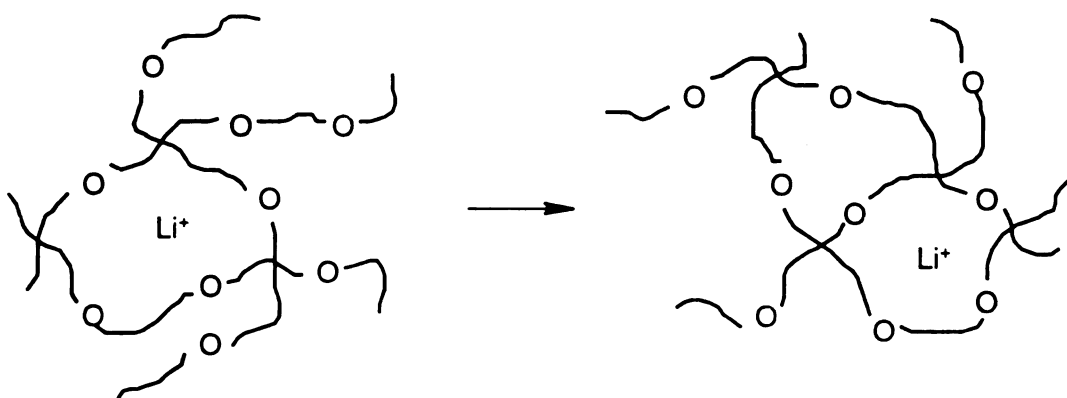


**Figure 3.**  $\text{Li}^+$  ion transport in PEO-salt complex as the combined result of polymer segmental motion and  $\text{Li}^+$  ion movement.

The Li-O complexes are in dynamic equilibrium. Local polymer segmental motion and  $\text{Li}^+$  ion movement result in diffusion of  $\text{Li}^+$  ions from one site to a neighboring site. Without an electric field, cation diffusion is random, but in an

electric field, the ions diffuse preferentially in the field direction and transport charge.

The electrical conductivity in such a polymer electrolyte can be expressed by the general equation

$$\sigma = \sum_i n_i \mu_i Q_i$$

where  $\sigma$  is conductivity,  $n_i$ ,  $\mu_i$ , and  $Q_i$  are the total number, mobility and charge of the species  $i$  respectively. This equation includes contributions from all charge carriers, both cations and anions, and relates the conductivity to the mobility of each carrier. The mobility of a charge carrier,  $\mu_i$ , is temperature dependent. In order to describe the relationship of temperature and conductivity of a homogeneous electrolyte, an Arrhenius type equation, the Vogel-Tammann-Fulcher (VTF) equation was derived<sup>4</sup>

$$\sigma(T) = A \exp[-B/(T - T_0)]$$

In the VTF equation,  $A$  and  $B$  are empirical terms related to the number of charge carriers and the activation energy for ion transport, and  $T_0$  is the temperature at which the conductivity is zero and is usually taken as the glass transition temperature of the electrolyte determined from thermal analysis. This equation indicates that the lower the glass transition temperature of a polymer electrolyte, the higher the conductivity at a certain temperature  $T$ . Therefore it is desirable to make polymer electrolytes with low  $T_g$ 's. Furthermore, the conductivity increases exponentially with increasing values of  $(T - T_0)$ .

#### 4. Synthesis of modified hosts

Practical solid state electrolytes require both a high ionic conductivity and stable mechanical properties, but the preparation of polymer electrolytes that combine both of these characteristics has been problematic. Not surprisingly, numerous synthetic efforts have aimed at altering the basic PEO structure to obtain both high conductivity and mechanical stability. In general, three approaches have been attempted to achieve this goal: introducing defects into regular PEO backbone to reduce crystallinity, making comb-branched polymers that have low  $T_g$  backbones and flexible oligo(ethylene oxide) side chains, and crosslinking the polymer to stabilize dimensional stability.

##### 1) introducing defects into regular PEO backbone

Defects have been introduced into PEO backbones to eliminate crystallinity. Booth and colleagues<sup>20-22</sup> inserted methylene units into regular PEO chains by stepwise condensation polymerization of oligo(ethylene glycol)s and methylene chloride as shown in **Scheme 1**.

##### **Scheme 1. Preparation of methylene-linked PEO copolymer**

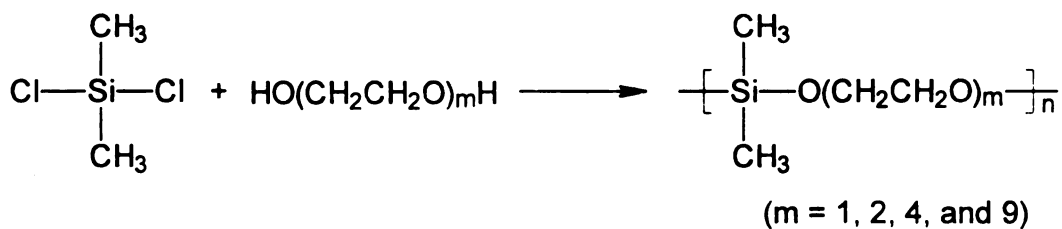


Depending on the length of the ethylene glycol segment used, the resulting oxymethylene-linked PEO has a lower melting point (below 26 °C) and a reduced

degree of crystallinity (below 31 %). The ionic conductivity of polymer-LiCF<sub>3</sub>SO<sub>3</sub> complexes reached 5x10<sup>-5</sup> S/cm at room temperature.

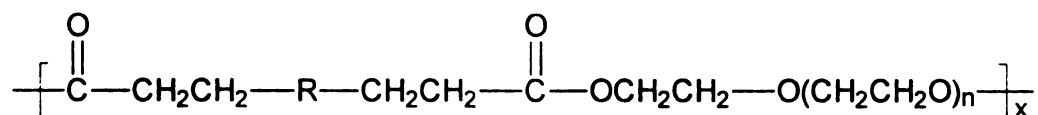
Similarly, a series of linear poly(dimethyl siloxane-co-ethylene oxide)s, were prepared by Nagaoka, Naruse, Shinohara and Watanabe<sup>23</sup> by condensation polymerization of dimethyldichlorosilane and oligo(ethylene glycol)s (**Scheme 2**).

**Scheme 2. Preparation of poly(dimethyl siloxane-co-ethylene oxide)s**



The peak ionic conductivity of the amorphous copolymer-LiClO<sub>4</sub> complexes was determined to be 1.5x10<sup>-4</sup> S/cm for m = 4 at room temperature. However, these polymers were neither chemically nor mechanical stable when used as real electrolyte hosts.

Likewise, highly viscous liquid polyesters of the general structure



where R is a sulfur atom or CH<sub>2</sub> group and n ranged from 0 to 4, were prepared and studied as electrolyte hosts.<sup>24</sup> The low molecular weights (M<sub>n</sub> in the range of 970 to 4,340) and low T<sub>g</sub>'s (in the range of -40 to -54 °C) of these materials led to

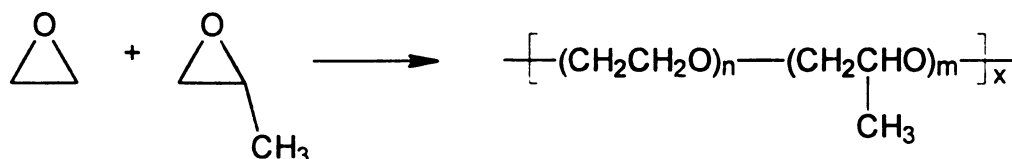
r  
P  
C  
C  
C  
h  
M  
AS

Ex.  
Poly.  
al  
Side-

room temperature conductivities of the order of  $10^{-5}$  S/cm for the resulting polymer-LiClO<sub>4</sub> complexes.

The copolymerization of ethylene oxide and propylene oxide was carried out by Passiniemi et al.<sup>25</sup> to give random copolymers, whose  $T_g$  and  $T_m$  were dependent on the composition of the two monomers. The increase in propylene oxide content resulted in a decrease of both  $T_g$  and  $T_m$ , as the methyl group on the oxypropylene repeating unit disrupts the PEO crystalline structure. However, the total conductivity of the copolymer-LiClO<sub>4</sub> complexes was found to decrease as PO content in the copolymer increased.

**Scheme 3. Copolymerization of ethylene oxide and propylene oxide**



2) comb-branched polymers

Coordinating oligo(ethylene oxide) side chains have been attached to flexible backbones with low  $T_g$ 's to form comb-branched polymers. For example, polysiloxanes usually have low  $T_g$ 's ( $-127$  °C), therefore Hall *et al.*<sup>26</sup> and Smid *et al.*<sup>27-29</sup> used the following catalyzed reaction to obtain liquid oligo(ethylene oxide) side-chain poly(methyl siloxane) comb polymers (**Scheme 4**).

The

room

at the

Sc

The p

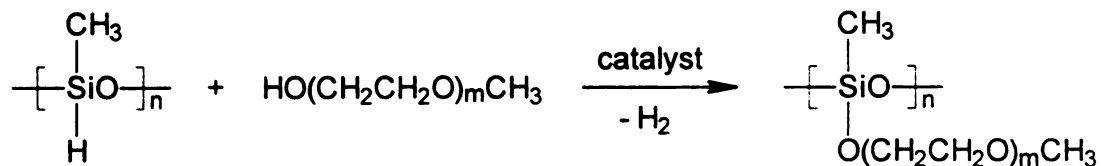
oligo

branch

polym

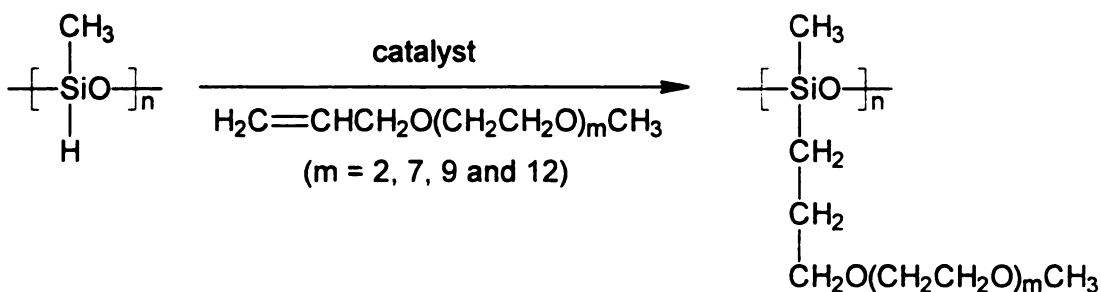
sodium

**Scheme 4. Preparation of comb polymer with PEO branches**



The highest conductivity for such polymer-LiClO<sub>4</sub> complexes was 1x10<sup>-4</sup> S/cm at room temperature. Hydrosilation reactions of poly(methyl siloxane) with allyl ethers were carried out to produce similar polymers (Scheme 5).<sup>28</sup>

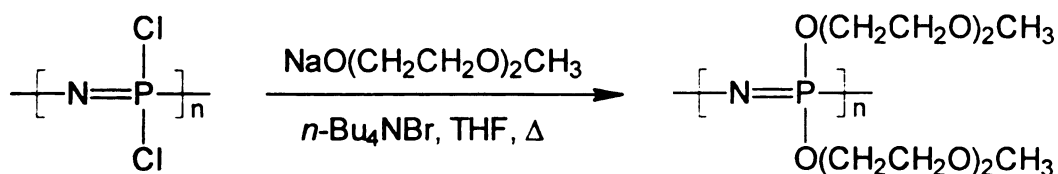
**Scheme 5. Preparation of comb-branched poly(siloxanes) with PEO side chains**



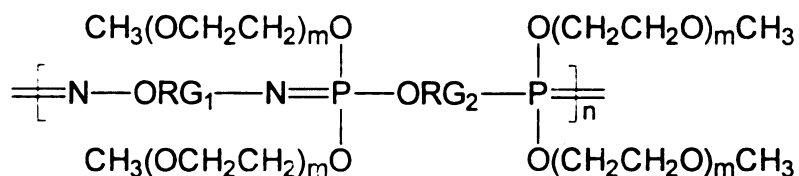
The polymers had similar conductivities to those obtained using Scheme 4.

Polyphosphazene has a T<sub>g</sub> of -70 °C. Polyphosphazenes with oligo(ethylene oxide) side chains<sup>7, 30-34</sup> represent another class of comb-branched polymers synthesized and studied as electrolyte hosts. The first such polymer, MEEP, was prepared by reaction of poly(dichlorophosphazene) with sodium 2-(2-methoxyethoxy) ethoxide as illustrated in Scheme 6.

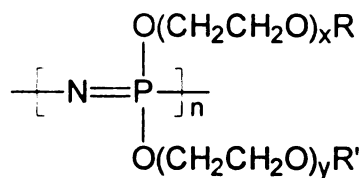
**Scheme 6. Preparation of MEEP from inorganic polyphosphazene**



Compared to traditional electrolytes from PEO, MEEP-LiCF<sub>3</sub>SO<sub>3</sub> complexes showed improved ionic conductivity (2x10<sup>-5</sup> S/cm) at room temperature, however, these materials lack the mechanical stability needed for most applications. Aside from cross-linking,<sup>34-36</sup> Pomerantz *et al.*<sup>37</sup> reported polyphosphazene-based electrolytes with enhanced mechanical properties by modifying the polymer backbone with organo-λ<sup>5</sup>-phosphazenes of the kind



where ORG<sub>1</sub> and ORG<sub>2</sub> were organic spacer groups. The conductivity of one of these polymer-LiCF<sub>3</sub>SO<sub>3</sub> complexes reached 3.2x10<sup>-6</sup> S/cm at 22 °C. The mixed side chains were adjusted on phosphazene backbones of



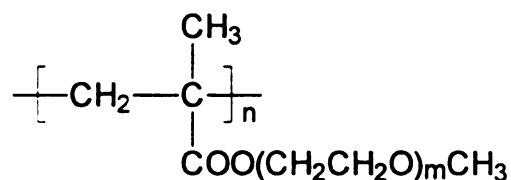
b  
a  
L  
re  
a  
D  
W  
T  
D  
S

W  
W  
of 3  
The  
S

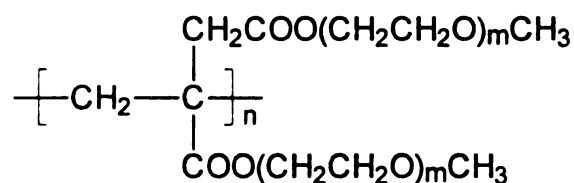
where

by Allcock and his colleagues,<sup>33</sup> where R and R' could be CH<sub>3</sub> and/or C<sub>12</sub>H<sub>25</sub>, and x and y were variables. The peak conductivities of some of these polymer-LiCF<sub>3</sub>SO<sub>3</sub> complexes were found to be between 1.6x10<sup>-6</sup> and 3.9x10<sup>-5</sup> S/cm.

Comb-branched polymers with low T<sub>g</sub> backbones usually have the required chain flexibility for a highly conductive electrolyte. Unfortunately most are not mechanically stable enough to allow their use as electrolyte hosts at room temperature. In order to overcome this drawback, main chain flexibility was sometimes intentionally sacrificed to gain good dimensional stability. For this reason, flexible oligo(ethylene oxide) side chains were incorporated into polymers with relatively rigid backbones. Polymethacrylates with pendant PEO side chains, poly(MEEMA), of the formula



where m was of varying values, were designed and prepared as host materials with improved mechanical strength.<sup>37-39</sup> A recent study<sup>39</sup> reported a conductivity of 3x10<sup>-5</sup> S/cm at 25 °C for poly(MEEMA) with a short (m = 2) side PEO chain. The need for more PEO content in the polymer and more flexible side chains gave rise to related materials, poly(itaconate ester)-based polymers<sup>40</sup>



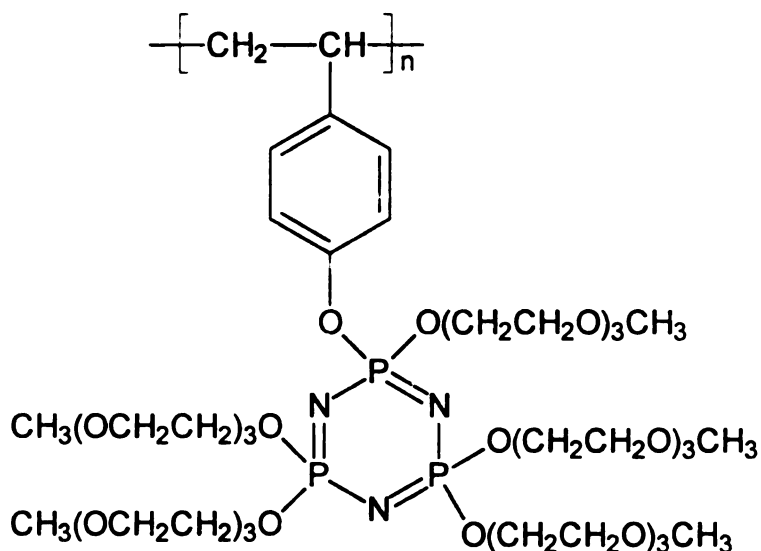
where two PEO-containing side chains were attached to each repeating unit.

1  
C  
E  
r

form  
inclu  
sche

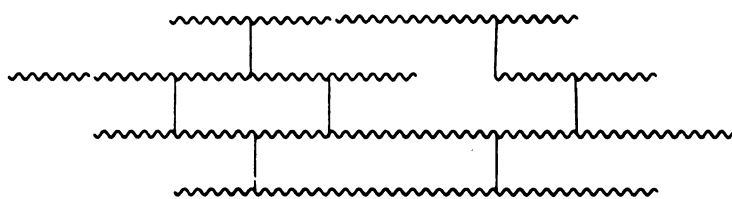
Usual  
result

Recently, Inoue and coworkers<sup>41-42</sup> reported their work on a polycascade polymer, poly(STEP) (shown below). Though the conducting side chains were connected to a relatively rigid polystyrene backbone, the conductivity of poly(STEP)-LiClO<sub>4</sub> complexes was found to be  $1.5 \times 10^{-5}$  S/cm at 30 °C and reached as high as  $10^{-4}$  S/cm at 60 °C.



### 3) crosslinking polymers to stabilize mechanical properties

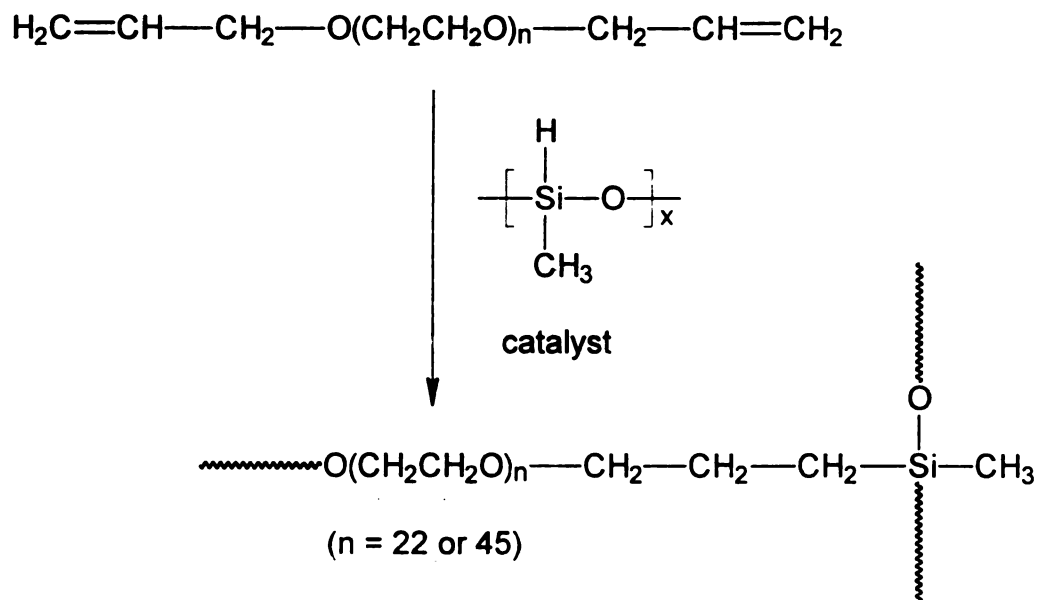
The polymer electrolytes are often crosslinked as final processing step to form a three-dimensional network of reasonable stability. Crosslinking methods include photo-irradiation to give polymer electrolytes that have the following schematic structure.



Usually crosslinked electrolytes have lower conductivities after crosslinking as a result of reduced chain mobility.

An example of crosslinking PEO by hydrosilylation is shown in **Scheme 7**.  
 7.<sup>43</sup> Conductivity for the crosslinked polymer-salt complexes reached  $10^{-5}$  to  $10^{-6}$  S/cm at room temperature.

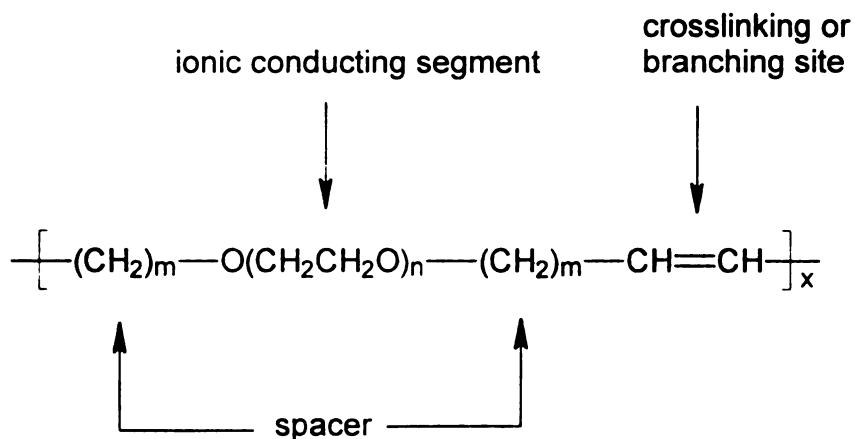
**Scheme 7. Crosslinking PEO by hydrosilylation**



## II. Target Polymers in This Work

In this project, a new series of polymer electrolyte hosts was designed to have the general structure depicted in **Scheme 8**. It is desirable for a polymer electrolyte to have a low glass transition temperature, high ionic conductivity and stable mechanical properties. The target polymers satisfy these important requirements for a good electrolyte host in the following ways: (1) with mainly polyethylene and PEO segments in the polymers, the glass transition temperature was expected to be low; (2) oligo(ethylene oxide) blocks were incorporated into the polymer backbone as ionic conducting segments; (3) adjustable spacers were expected to stabilize the mechanical strength of the material some extent; (4) carbon-carbon double bonds were introduced as crosslinking or branching sites to modify the structure of the material.

**Scheme 8. Target polymer electrolyte hosts**

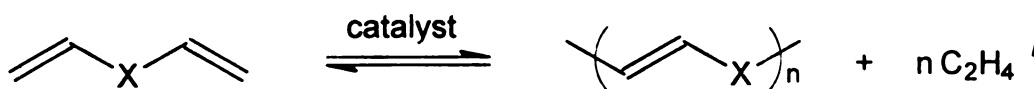


From the synthetic point of view, it should be possible to prepare the target polymers by an easy, clean and straightforward polymerization in large quantity. Recent developments in acyclic diene metathesis (ADMET) polymerization<sup>44-57</sup> offer a convenient synthetic route to the target polymers.

### III. ADMET Polymerization

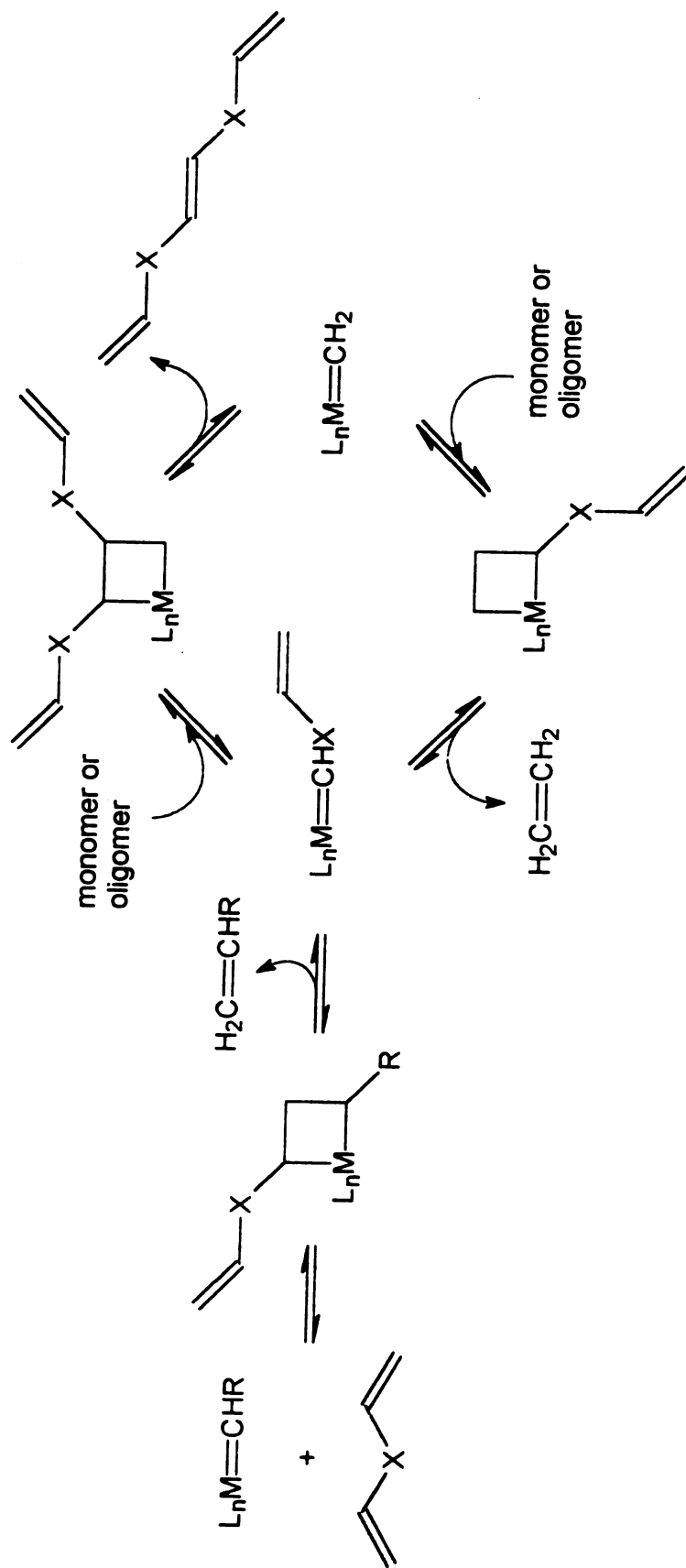
ADMET polymerization is a stepwise condensation polymerization as generalized in **Scheme 9**. In the presence of a metathesis catalyst, an acyclic  $\alpha,\omega$ -diene can be polymerized to give an unsaturated linear polymer by equilibrium polymerization. Like common condensation polymerizations,<sup>58</sup> a volatile small molecule by-product (ethylene) is eliminated from the reaction, and the removal of ethylene drives the equilibrium towards high molecular weights.

**Scheme 9. General ADMET polymerization**



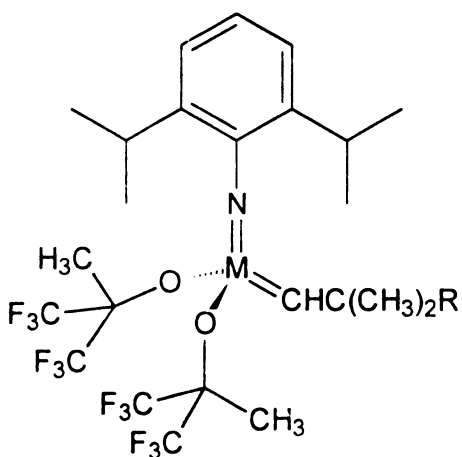
The mechanism of ADMET chemistry (**Scheme 10**) as proposed by Wagener *et al.*<sup>45</sup> consists of an initiation step followed by a polymerization cycle. In the initiation step, the initiator (for example, a metal alkylidene) reacts with monomer to generate a metallocyclobutane, which decomposes to form a metallocarbene species derived from the monomer. This step is an example of the olefin metathesis reaction. The polymerization cycle involves the formation of metallocyclobutane intermediates that leads to dimer, trimer, etc., and eventually leads to high polymers. As noted in the scheme, each step is reversible, and removal of ethylene is crucial for obtaining high molecular weights.

Scheme 10. ADMET polymerization mechanism.



There are two types of ADMET polymerization catalysts that have been reported in the literature. The first type includes classical olefin metathesis catalysts. In 1987 Wagener and his colleagues<sup>44</sup> employed the  $WCl_6/EtAlCl_2$  catalyst system to polymerize 1,9-decadiene and 1,5-hexadiene. Later Nubel *et al.*<sup>54</sup> described  $WCl_6/EtAlCl_2/PrOAc$  as a modified catalyst to synthesize polypentenamer from 1,5-hexadiene. However, both catalysts polymerized hydrocarbon diene monomers with limited success. Since classical metathesis catalysts are generally strong Lewis acids, they do not tolerate a wide variety of organic functional groups in monomers.

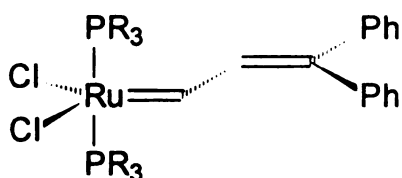
The second type of catalyst, Lewis acid-free transition metal alkylidene complexes have been very successful in carrying out ADMET polymerization of diene monomers having different organic functionalities. The most widely used ADMET catalysts were developed by Schrock and coworkers<sup>59-62</sup> and have the following general structure:



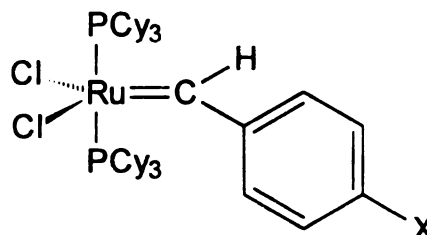
where the metal is either tungsten or molybdenum ( $M = W$ ,  $R = CH_3$ ;  $M = Mo$ ,  $R = Ph$ ). The homogeneous W catalyst has a much higher reactivity than the Mo

analog, but due to its reactivity, the tungsten catalyst has a shorter lifetime, less tolerance towards functional groups and less control over metathesis reactions. This makes Schrock's Mo catalyst the favored choice for most ADMET polymerizations.

Grubbs reported that ruthenium carbene metathesis catalysts<sup>63-65</sup> (shown below) are effective for ring-opening metathesis polymerization.<sup>63 66-69</sup> Recent work by Walba *et al.*<sup>56</sup> showed the ruthenium catalyst was also a good catalyst for ADMET polymerization. These well-defined ruthenium complexes are much less sensitive to oxygen and are more tolerant of organic functional groups.



(R = Ph or Cy)



(X = H or Cl)

The reaction conditions for ADMET are relatively mild. Polymerization initiated by Schrock's alkylidene catalysts requires that the temperature not exceed 60 °C. Above this limit the catalysts tend to decompose and lose reactivity. The work by Walba *et al.*<sup>56</sup> indicated that the Grubbs' ruthenium catalyst can be used at 80 °C for 24 hours.

A number of unsaturated linear polymers containing different organic functional groups have been synthesized *via* ADMET polymerization. The first high molecular weight polymers from ADMET were reported in 1991.<sup>45</sup> By using Schrock's W alkylidene catalyst, Wagener *et al.* prepared two unsaturated

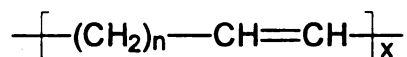
polyalkanes (**Scheme 11**). The polymerization generated clean polymers and ethylene without any other products.

**Scheme 11. Synthesis of unsaturated polyalkanes *via* ADMET**

**polymerization**

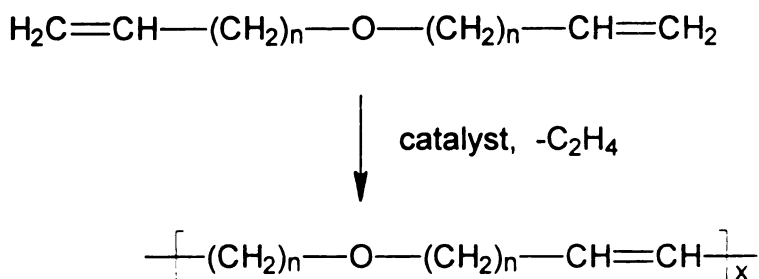


Schrock's W alkylidene catalyst



$n = 6, M_n = 108,000; n = 2, M_n = 28,000$

Unsaturated polyethers, which are structurally relevant to the target polymers in this project, were the next polymers prepared *via* ADMET polymerization.<sup>46</sup> As **Scheme 12** shows, polymers were obtained when  $n = 3$  and 4. It was found, however, that high polymers were not produced when there were less than three methylene units separating the oxygen atom and the terminal vinyl group in the monomers ( $n = 0, 1$  or 2). This was attributed to catalyst poisoning caused by the interaction of the vinyl group and the oxygen atom with the metal center that blocked further metathesis steps.

**Scheme 12. Synthesis of unsaturated polyethers via ADMET****polymerization**

ADMET polymerization also found application in the synthesis of unsaturated polycarbosilanes,<sup>47</sup> unsaturated polycarbosiloxanes,<sup>50</sup> and unsaturated polythioethers<sup>52</sup> (Table 1). Two other types of polymers prepared *via* ADMET polymerization are unsaturated polyesters<sup>48</sup> and unsaturated polycarbonates.<sup>49</sup> Metathesis reactions involving compounds with carbonyl groups led to catalyst poisoning before Schrock's Lewis acid-free catalysts were invented, and the successful preparation of polymers containing carbonyl groups demonstrates the versatility of ADMET polymerization with these improved catalyst systems.

One interesting aspect of the ADMET chemistry is the relationship between the monomer structure and its polymerizability. More specifically, it has been found that when a functional group is separated by three or more methylene units from terminal vinyl group, unsaturated linear polymers can be prepared. However, monomers with two or less methylene units may not be polymerized by ADMET. This phenomenon was termed the "negative

**Table 1. Some Representative ADMET Polymers Prepared by Wagener***et al.*<sup>47-50,52</sup>

| Unsaturated polymer | Structure   |
|---------------------|---|
| polycarbosilane     | $\left[ \text{CH}_2 - \underset{\text{CH}_3}{\overset{\text{CH}_3}{\text{Si}}} - \text{C}_6\text{H}_4 - \underset{\text{CH}_3}{\overset{\text{CH}_3}{\text{Si}}} - \text{CH}_2 - \text{CH}=\text{CH} \right]_x$   |
| polycarbosiloxane   | $\left[ \text{CH}_2 - \underset{\text{CH}_3}{\overset{\text{CH}_3}{\text{Si}}} - \text{O} - \underset{\text{CH}_3}{\overset{\text{CH}_3}{\text{Si}}} - \text{O} - \underset{\text{CH}_3}{\overset{\text{CH}_3}{\text{Si}}} - \text{CH}_2 - \text{CH}=\text{CH} \right]_x$ |
| polythioether       | $\left[ (\text{CH}_2)_4 - \text{S} - (\text{CH}_2)_4 - \text{CH}=\text{CH} \right]_x$   |
| polyesters          | $\left[ (\text{CH}_2)_n - \text{O} - \overset{\text{O}}{\parallel}{\text{C}} - \text{C}_6\text{H}_4 - \overset{\text{O}}{\parallel}{\text{C}} - \text{O} - (\text{CH}_2)_n \right]_x$ <p style="text-align: center;">(n = 2, 3, and 4)</p>                                |
| polycarbonates      | $\left[ (\text{CH}_2)_n - \text{O} - \overset{\text{O}}{\parallel}{\text{C}} - \text{O} - (\text{CH}_2)_n \right]_x$ <p style="text-align: center;">(n = 2, 3, and 4)</p>   |

ne

SP

ca

we

pr

S

H

The

mor

the

afe

ach.

dig

cha

holic

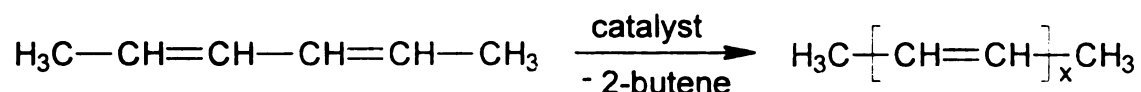
cryst

othe

neighboring group effect". Since we intended to vary the number of methylene spacers to adjust the mechanical properties of the target polymers, attention was paid to how this would affect the polymerizability of the monomers.

ADMET polymerization of conjugated monomers has been explored as well.<sup>53</sup> Methyl terminated polyenes with up to 20 conjugated double bonds were prepared from 2,4-hexadiene (**Scheme 13**).

**Scheme 13. Synthesis of conjugated polyenes via ADMET polymerization**



The effect of double bond substitution on the ADMET polymerizability of a monomer is of general interest,<sup>70</sup> yet in this reaction, neither monosubstitution on the terminal carbon atoms of the double bonds nor conjugation in the monomer affected the ADMET reactivity of the monomer. The determining factor in achieving high molecular weight seemed to be the solubility of the resulting oligomers or polymers, as their precipitation prevented further growth of the chains.

ADMET polymerization proved to be a convenient method to prepare liquid crystalline materials as well. A series of main-chain ferroelectric liquid crystalline oligomers were synthesized by ADMET polymerization using Grubbs' ruthenium carbene metathesis catalyst, illustrated in **Scheme 14**.<sup>56</sup>

H<sub>2</sub>

S

The

poly

spec

inter

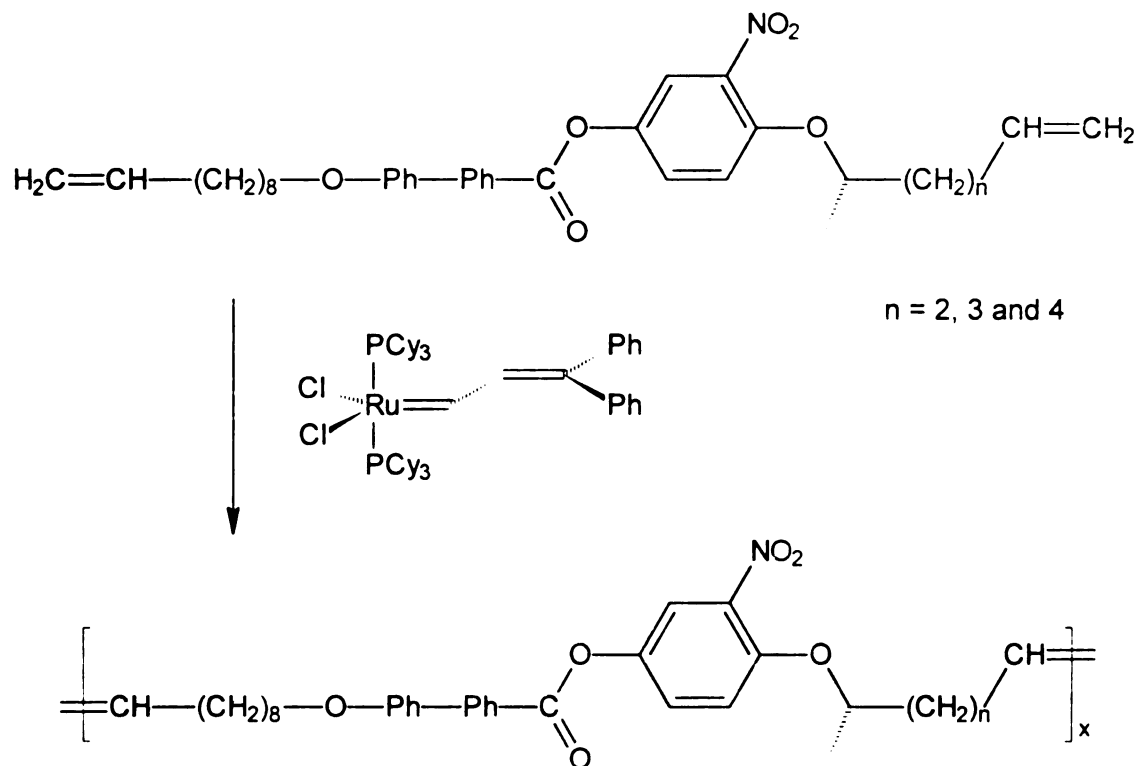
Saus

whic

1100

**Scheme 14. Synthesis of liquid crystalline materials via ADMET**

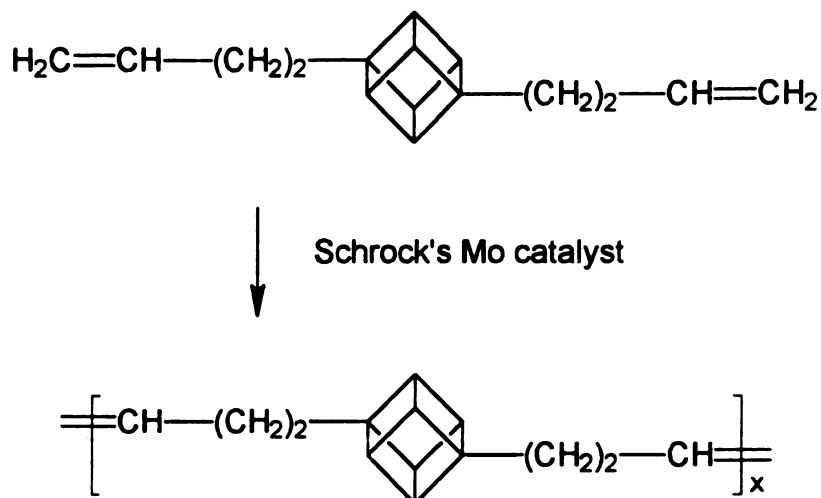
**polymerization**



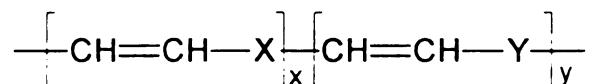
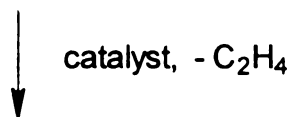
The polymerization was carried out in bulk at 80 °C for 24 hours. The degree of polymerization was about 10, determined by end group analysis from  $^1\text{H}$  NMR spectra.

An unsaturated polymer with a cubane-containing backbone, which is of interest as high-energy material, was synthesized recently by Chauvin and Saussine<sup>57</sup> through ADMET chemistry (**Scheme 15**). The molecular weight, which was limited by the poor solubility of the polymer, was determined to be 1,100 to 1,300 by  $^1\text{H}$  NMR end group analysis.

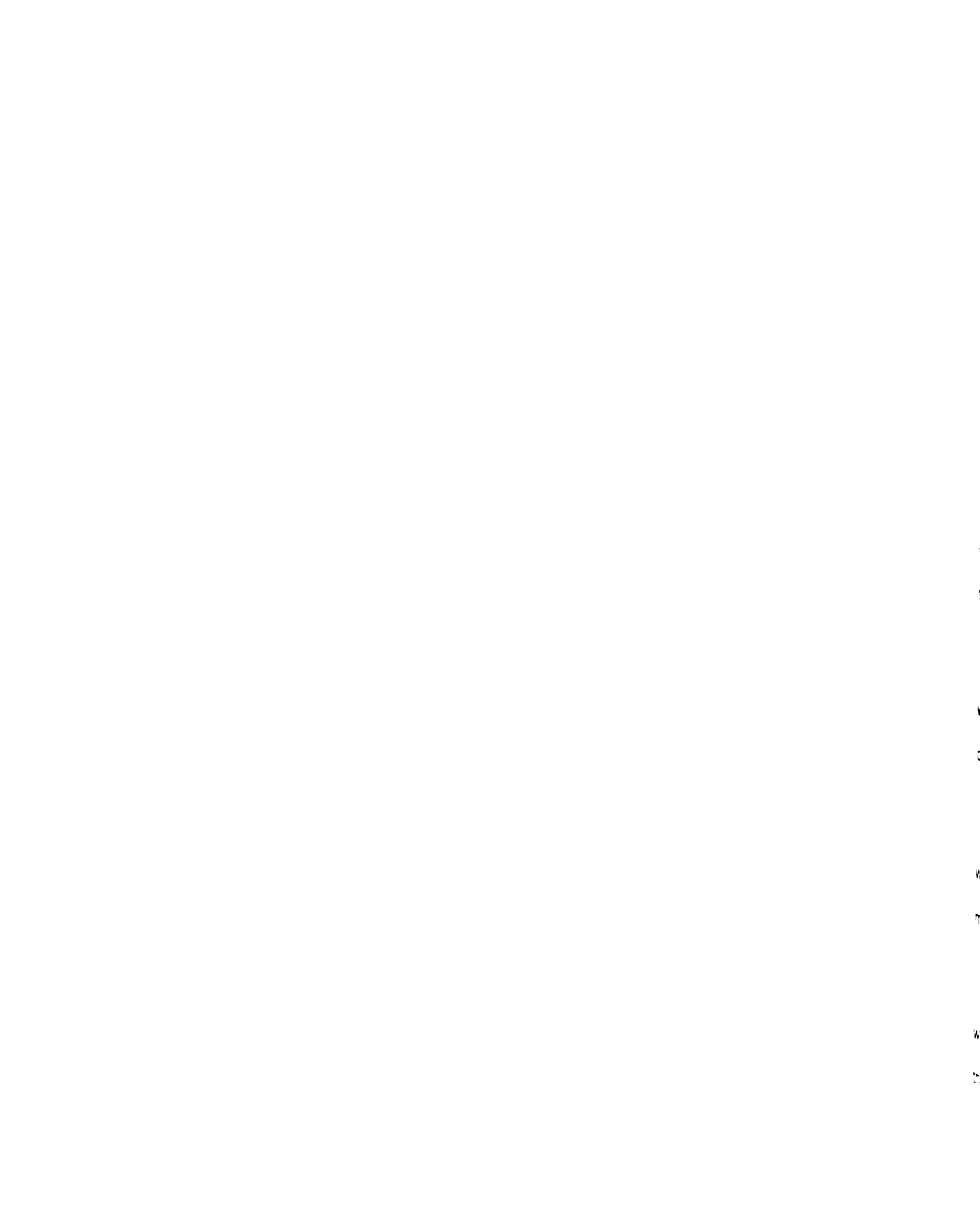
**Scheme 15. Synthesis of cubane-containing polymer via ADMET  
polymerization**



ADMET polymerization can also be used to generate copolymers from two  $\alpha,\omega$ -diene monomers. When two dienes can be polymerized through ADMET individually, they are able to form random ADMET copolymers as well (**Scheme 16**). ADMET copolymerization was performed in several systems,<sup>46,48,52,57</sup> and the process can be easily explained by **Scheme 10**, where either monomer can add to the reactive species in the polymerization cycle, thus producing a random copolymer.

**Scheme 16. A generalized ADMET copolymerization**

Finally, it is worthwhile to mention the geometry of the internal double bonds in the ADMET polymers. The ratio of the *cis* and *trans* double bonds are usually determined by quantitative  $^{13}\text{C}$  NMR measurements. The content of *trans* double bonds in ADMET polymers has been reported to range from 40 to 93%, but most polymerizations yield around 80% *trans* content.



#### IV. Ionic Conductivity Measurements

There are two distinct types of conducting materials in terms of charge carriers. Electronic conducting materials conduct electric currents by the flow of electrons. Metals, semiconductors such as Si, and conjugated polymers all are examples of electronic conductors. Ionic conducting materials, as the name implies, conduct electricity by the migration of ions. Molten salts, some inorganic conductors, aqueous electrolyte solutions, and polymer electrolytes fall into this category. **Figure 4** lists various conducting materials and their conductivity.

Like all other conducting materials, the most important electric property of a polymer electrolyte is its conductivity. Conductivity,  $\sigma$ , is defined as the reciprocal of resistivity  $\rho$

$$\sigma = \frac{1}{\rho}$$

while resistivity, an intrinsic physical property of a material which is independent of its geometry, is given by

$$\rho = R \frac{A}{l}$$

where  $A$  is the area and  $l$  is the length of the sample. The resistance  $R$  can be measured or calculated using Ohm's law

$$R = \frac{V}{I}$$

where  $V$  is the applied voltage and  $I$  is the resulting current. Ohm's law reveals that for a metal conductor of fixed dimension, there exists a linear relationship



betw

mea

hold

samp

Figur

by the

positi

polym

the re

res:sta

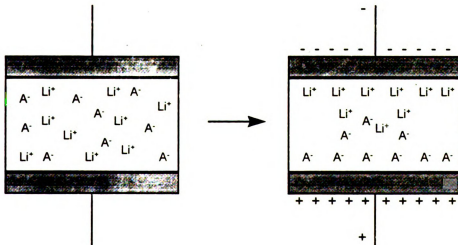
electro

Figure 5

(left) and

between the voltage applied and the current. Thus the resistance can be measured and the conductivity of the sample can be derived.

However, the linear relationship between voltage and current does not hold when a *d.c.* voltage of fixed potential is applied to a polymer electrolyte sample contained between two inert electrodes (Figure 5). As shown in Figure 6, the current decays as a function of time. This phenomenon is caused by the accumulation of cations at the negative electrode and anions at the positive electrode, and the reduction in number of charge carriers in the bulk polymer electrolyte (Figure 5). The current decay makes it difficult to measure the resistance and thus conductivity by direct current methods. Moreover, resistance at the interface between the bulk polymer electrolyte and the electrodes makes *d.c.* measurements complicated.



**Figure 5.** Polymer electrolyte contained between two inert electrodes: before (left) and after (right) a *d.c.* voltage of fixed potential is applied.

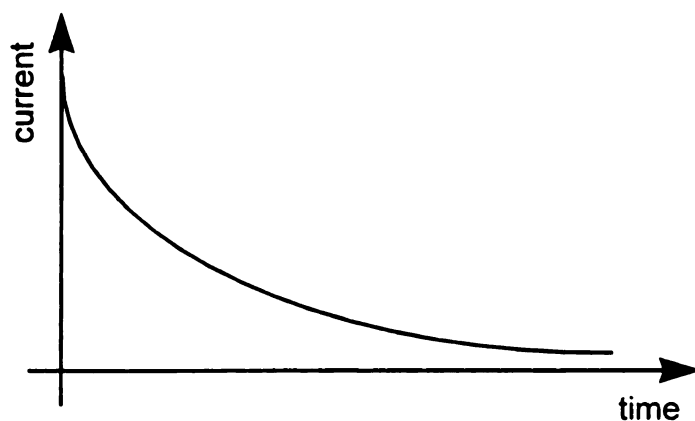


**Figure 6.** Current decay as a function of time when a *d.c.* voltage is applied to a polymer electrolyte sample.

While the measurement of ionic conductivity of polymer electrolytes by direct current methods has some difficulties, impedance spectroscopy<sup>71-75</sup> (IS), an alternating current method, proves more successful. When an alternating voltage signal of a certain frequency is applied to a polymer electrolyte cell, a resulting *a.c.* current, usually not in phase with the voltage, can be measured (**Figure 7**). The voltage *V* and current *I* can be expressed in their sinusoidal forms as

$$V = |V| \sin (\omega t)$$

and

$$I = |I| \sin (\omega t - \phi)$$

where  $|V|$  is the potential magnitude and  $|I|$  is the current magnitude,  $\omega$  is the angular frequency of the *a.c.* voltage, which is related to the applied frequency

as  $\omega = 2\pi f$ ,  $t$  is the time, and  $\phi$  is the phase shift of the current from the voltage and is dependent on the angular frequency.

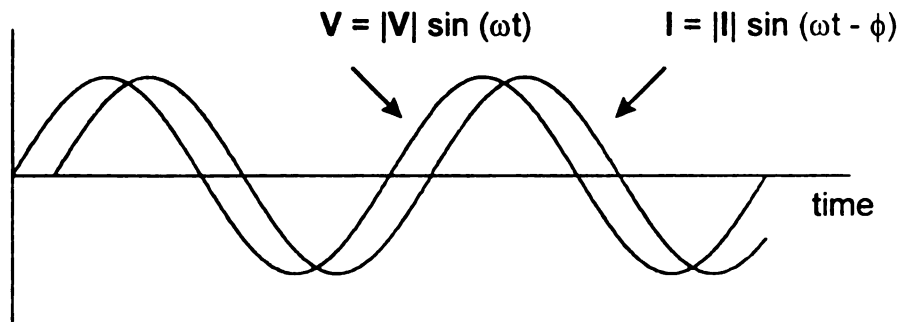


**Figure 7.** The sinusoidal voltage applied to a polymer electrolyte cell and the resulting current.

The concept of impedance is introduced when Ohm's law is applied in the *a.c.* measurement. Impedance  $Z$  is given by  $Z = V / I$ , the same form as its *d.c.* counterpart, resistance  $R$ , but  $Z$  is a function of frequency of the voltage. Impedance is a vector quantity and can be treated in complex form as

$$Z = Z' - jZ''$$

where  $Z'$  is the real component,  $Z''$  is the imaginary component, and  $j$  is the imaginary symbol. **Figure 8** shows how the complex impedance vector  $Z$  relates to its real and imaginary components in the rectangular complex plane at a phase angle of  $\theta$ .

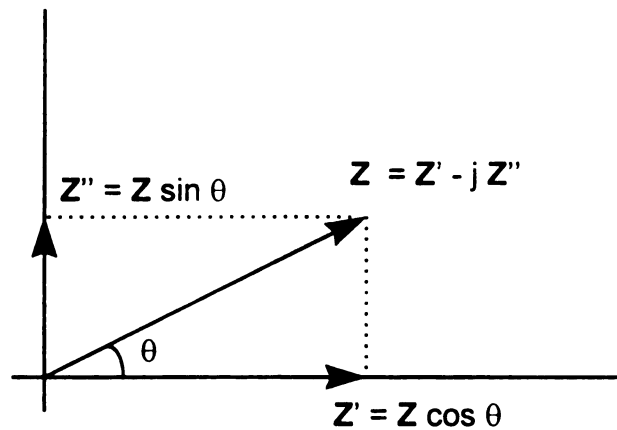


**Figure 8.** Complex impedance vector  $Z$  and the real and imaginary components in the rectangular complex plane. The phase angle is  $\theta$ .

In a typical IS measurement, the magnitude of the applied voltage is fixed at an appropriate value, but the frequency is changed over a wide range, usually from several hertz to several megahertz. At each frequency, the complex impedance is obtained and is plotted as a point in the complex plane. **Figure 9** displays the complex impedance diagram of a polymer electrolyte cell. The plotted data is composed of a semicircle for impedance data in the high frequency range followed by a linear spike for low frequency data. The real bulk impedance of the electrolyte,  $R_b$ , is taken as the intercept of the linear spike on the real axis.

Since the dimensions of the polymer electrolyte cell are known (**Figure 10**), the conductivity of the bulk polymer electrolyte can be calculated according to

$$\sigma = \frac{1}{R_b} \times \frac{l}{A}$$

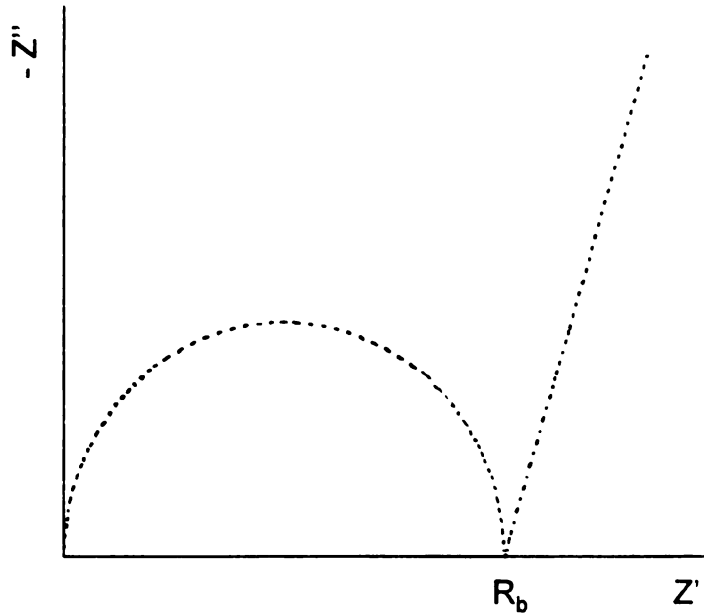


**Figure 9.** Complex impedance diagram of a polymer electrolyte cell sandwiched between two inert electrodes.

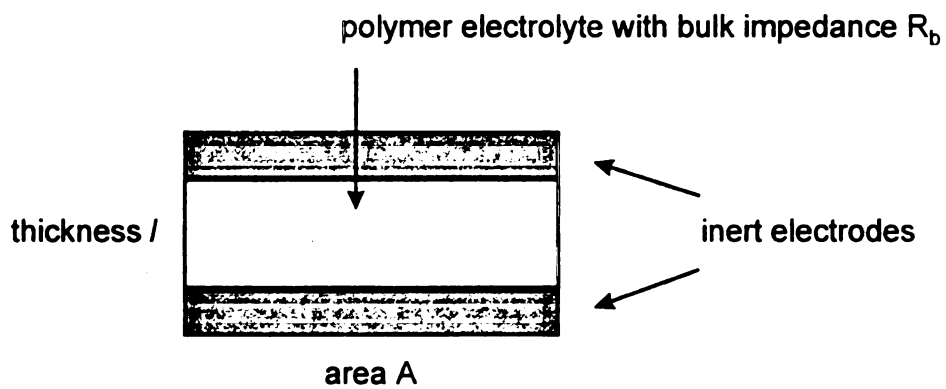


**Figure 10.** A schematic cross section polymer electrolyte cell of known dimensions.

# RESULTS

## I. Monomer Preparation

In order to synthesize the target polymers *via* ADMET polymerization, oligo(ethylene glycol)  $\alpha,\omega$ -dialkenyl ethers were prepared that have the general structure shown in **Table 2**. For simplicity, the nomenclature shown in **Table 2** is used in place of the full names of the monomers. The corresponding abbreviations for the polymers are "P" followed by the monomer abbreviation.

**Table 2. Acronyms for Monomers<sup>a</sup>**

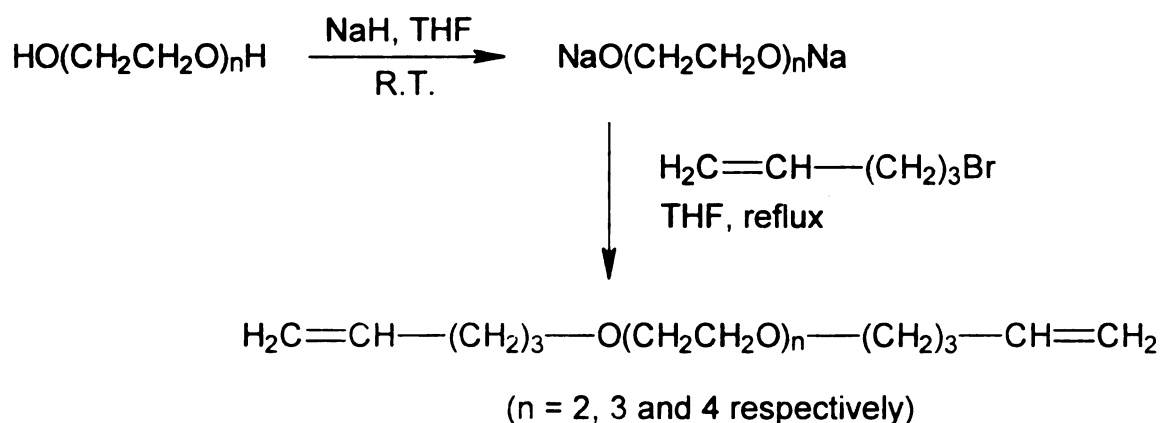


| n | 2         | 3         | 4         | 5         |
|---|-----------|-----------|-----------|-----------|
| m |           |           |           |           |
| 1 | <b>A2</b> |           |           |           |
| 2 | <b>B2</b> |           |           |           |
| 3 | <b>P2</b> | <b>P3</b> | <b>P4</b> |           |
| 4 | <b>H2</b> | <b>H3</b> | <b>H4</b> | <b>H5</b> |
| 6 | <b>O2</b> |           | <b>O4</b> |           |

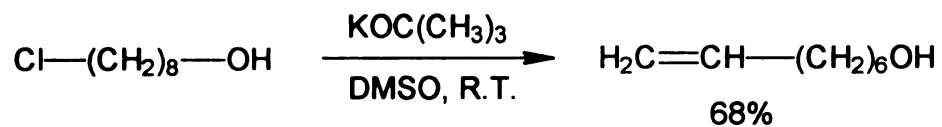
<sup>a</sup> A, B, P, H, O refer to allyl, 3-butenyl, 4-pentenyl, 5-hexenyl, and 7-octenyl respectively.

Two synthetic routes were chosen to prepare the monomers with different numbers of methylene units between the terminal vinyl groups and the oligo(ethylene oxide) segment. The first route (**Scheme 17**) involved the Williamson coupling of 4-bromo-1-pentene with the di-sodium salt of di-, tri-, and tetra-ethylene glycol to make **P2**, **P3** and **P4** respectively. The yields (not optimized) ranged from 62% to 81%.

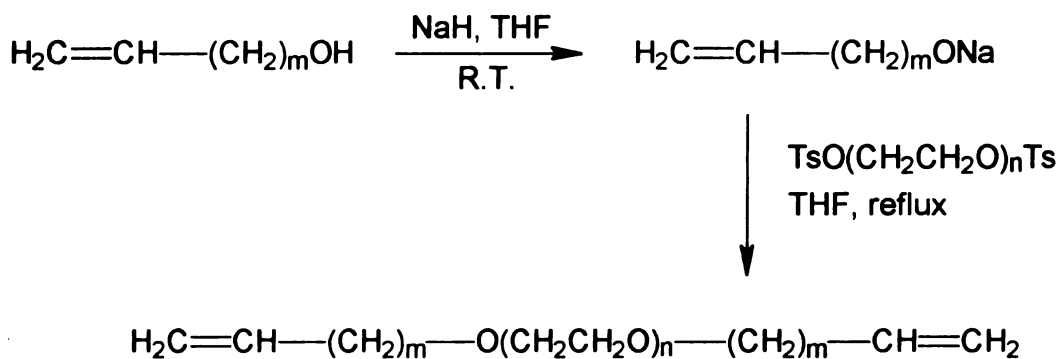
**Scheme 17. Monomer preparation by Williamson ether coupling**



All other monomers were prepared in 64 to 88% yield by coupling the sodium salts of alkenols and oligo(ethylene glycol) ditosylates (**Scheme 18**). The key reagents, allyl alcohol, 3-buten-1-ol, and 5-hexen-1-ol were purchased from commercial sources. 7-Octen-1-ol was prepared by the following one-step elimination reaction:



**Scheme 18. Monomer preparation by reaction of ditosylates with sodium alkenoxides**



$m = 1: n = 2;$        $m = 2: n = 2;$   
 $m = 4: n = 2, 3, 4, \text{ and } 5;$   
 $m = 6: n = 2 \text{ and } 4.$

The purification of the monomers was performed by repeated vacuum distillation over calcium hydride. Most monomers were further dried by stirring over a fresh sodium mirror under argon, followed by distillation in *vacuo*. All purified monomers were stored in a drybox for future polymerization.

I

A

P

w

ir

u

P

g

S

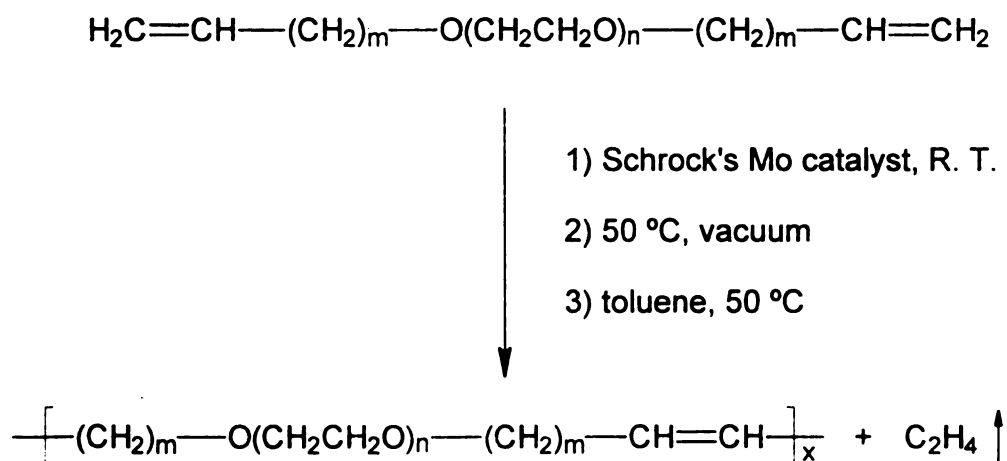
## II. Unsaturated Ethylene Oxide-Segmented Polymers

### 1. ADMET polymerization of oligo(ethylene glycol) $\alpha,\omega$ -dialkenyl ethers

Both  $WCl_6/Sn(CH_3)_4/PrOAc$  and Schrock's Mo catalyst were tested as ADMET polymerization catalysts in this research. Attempted ADMET polymerization of **P3** and **H4** using  $WCl_6/Sn(CH_3)_4/PrOAc$  as the catalyst system was carried out in the same manner as described in literature. No sign of initiation and polymerization was observed.

ADMET polymerizations of oligo(ethylene glycol)  $\alpha,\omega$ -dialkenyl ethers using Schrock's molybdenum alkylidene catalyst were successful. Polymerization of monomers were carried out in scale running from 0.5 g to 15.0 g as generalized in **Scheme 19**.

#### **Scheme 19. ADMET polymerization of oligo(ethylene glycol) $\alpha,\omega$ -dialkenyl ethers**

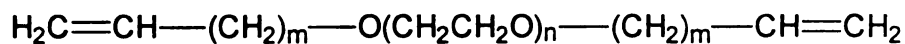


In most cases, the addition of catalyst to monomers resulted in an immediate, vigorous release of ethylene gas and the mixtures became homogeneous. Since the monomers and oligomers have high boiling points and their volatility at room temperature is minimal, high vacuum was applied throughout the bulk polymerization stage. After 6 h, the polymerization temperature was raised to 50 °C. When the polymerization systems became too viscous to stir, dry toluene was added to lower the viscosity and vacuum was only occasionally applied. With time the color of the polymerization changed from yellow to orange to dark brown, presumably due to partial decomposition of the catalyst. After a certain period of time the polymerization was terminated by exposing it to air.

When **A2** and Schrock's Mo catalyst were mixed, the immediate evolution of ethylene was also observed. However, the polymerization stopped at early stage and no high molecular weight polymer was obtained.

Except for **A2**, whose polymerizability needs further investigation, all monomers in **Table 3** were polymerized to give high molecular weight polymers via ADMET polymerization. The polymer work-up procedure included precipitating the polymers from toluene solutions into *n*-heptane and drying under high vacuum until constant weight was obtained. The polymers were all prepared in good yield (92% and above).

**Table 3. Polymerizability of Monomers by ADMET Polymerization Using Schrock's Mo Catalyst<sup>a</sup>**



| n | 2 | 3 | 4 | 5 |
|---|---|---|---|---|
| m |   |   |   |   |
| 1 | ± |   |   |   |
| 2 | + |   |   |   |
| 3 | + | + | + |   |
| 4 | + | + | + | + |
| 6 | + |   | + |   |

<sup>a</sup> (+) monomer has been polymerized into polymer. (±)

needs further investigation; no polymer was obtained

## 2. Properties of the unsaturated polymers

The properties of the unsaturated polymers are collected in **Table 4**. The molecular weights are comparable to the published results for other ADMET polymerizations.<sup>45-52</sup> The polydispersity index (PDI) values are all near 2, typical for step-growth polymerizations. Despite attempts to remove all catalyst residues, the purified polymers had a slight greenish-brown tinge that is believed to correspond to catalyst residues. All the polymers, except for **PO2** and **PO4**, were extremely tacky regardless of molecular weight. Polymers **PO2** and **PO4**

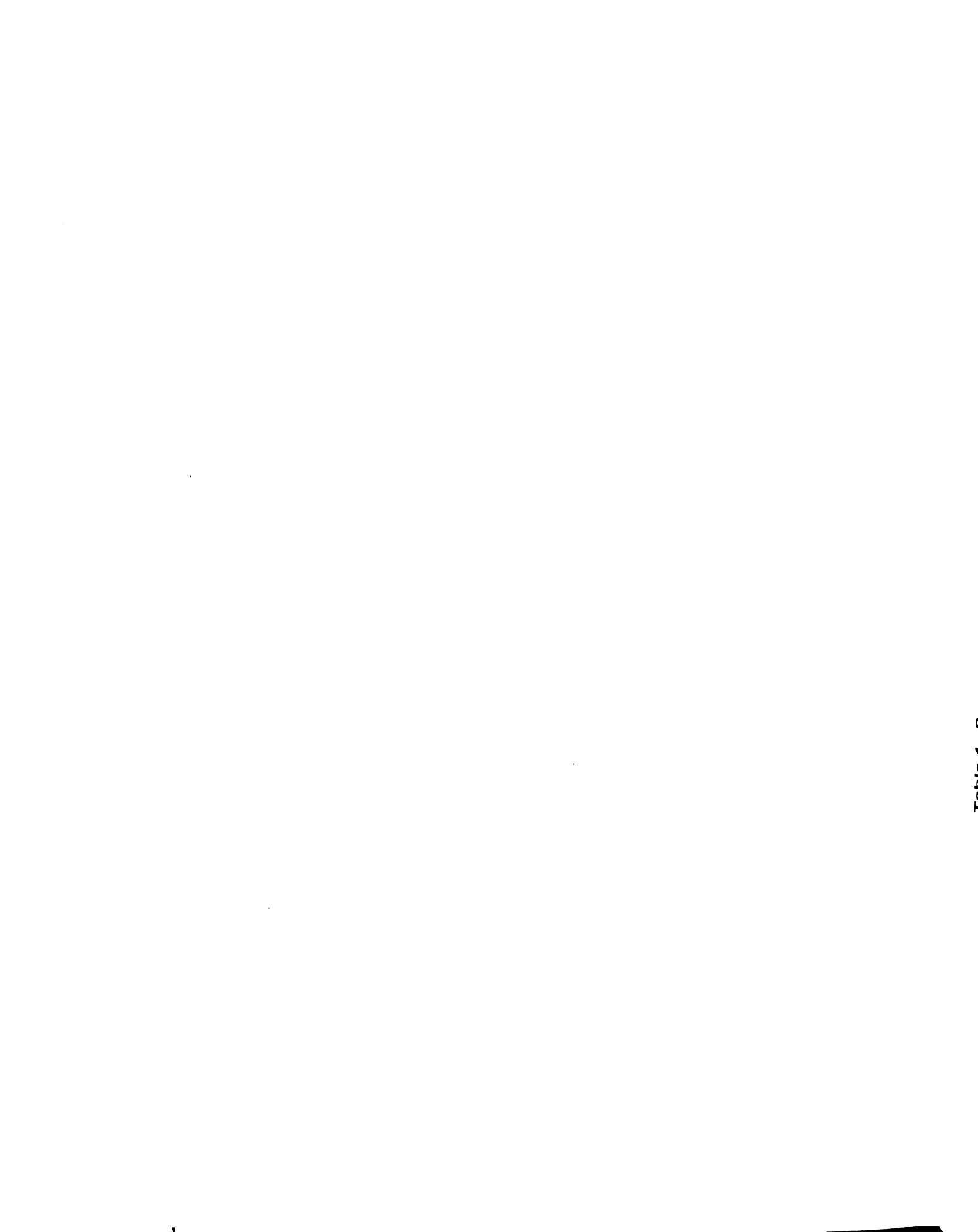


**Table 4. Properties of Unsaturated Polymers**



| Polymer     | m | n | polymerization<br>time (h) | Yield (%) | M <sub>n</sub> | PDI  | % trans C=C<br>bonds |
|-------------|---|---|----------------------------|-----------|----------------|------|----------------------|
| <b>PB2</b>  | 2 | 2 | 168                        | 92.8      | 15,100         | 1.86 | 86                   |
| <b>PP2a</b> | 3 | 2 | 48                         | 95.0      | 17,700         | 2.15 | 84                   |
| <b>PP2</b>  | 3 | 2 | 168                        | 97.8      | 93,900         | 2.29 | 83                   |
| <b>PP3a</b> | 3 | 3 | 48                         | 95.3      | 18,300         | 3.10 | 83                   |
| <b>PP3</b>  | 3 | 3 | 168                        | 95.9      | 55,000         | 2.57 | 84                   |
| <b>PP4a</b> | 3 | 4 | 48                         | 96.7      | 37,300         | 2.21 | 85                   |
| <b>PP4</b>  | 3 | 4 | 168                        | 97.8      | 66,400         | 2.24 | 85                   |
| <b>PH2</b>  | 4 | 2 | 168                        | 94.4      | 44,700         | 2.74 | 82                   |
| <b>PH3</b>  | 4 | 3 | 168                        | 97.2      | 32,200         | 2.12 | 84                   |
| <b>PH4</b>  | 4 | 4 | 168                        | 96.9      | 28,100         | 2.16 | 83                   |
| <b>PH5</b>  | 4 | 5 | 168                        | 97.6      | 31,500         | 2.01 | 86                   |
| <b>PO2</b>  | 6 | 2 | 96                         | 96.1      | 57,100         | 2.45 | 84                   |
| <b>PO4</b>  | 6 | 4 | 96                         | 95.0      | 35,400         | 2.35 | 82                   |

o  
n  
eth  
mon  
simi  
mono  
figure  
ethyle  
polyme  
resonar  
while a  
correspo

both have six methylene units on each side of oligo(ethylene oxide) segment in the repeating unit, and appear to be crystalline and stiff.

The polymers are soluble in an unusually broad range of organic solvents, including toluene, tetrahydrofuran, chloroform, carbon tetrachloride, methanol, acetonitrile, acetone, and ethyl acetate. This high solubility likely results from the combination of hydrophobic (alkenyl) and hydrophilic (ethylene oxide) segments in the polymer backbone.

### 3. Spectroscopic characterization of the unsaturated polymers

The chemical structures of the unsaturated polymers were characterized by  $^1\text{H}$  NMR,  $^{13}\text{C}$  NMR and FTIR spectroscopy. The spectroscopic data appears in the Experimental section.

Monomers having same terminal alkenyl groups and different number of ethylene oxide units in the middle are homologous, and the spectra of these monomers look very similar. Polymers from these monomers also have very similar NMR spectra. As a representative example, the  $^1\text{H}$  NMR spectra of monomer **P3** and polymer **PP3a** are shown in **Figure 11** for comparison. In this figure, peaks between 3.64 and 3.54 ppm, corresponding to protons on the ethylene oxide segment, are common to all monomers and unsaturated polymers and show no shift in going from monomer to polymer. However, resonances at 5.80 and 4.97 ppm from vinyl protons on monomer **P3** disappear, while a new peak appears at 5.38 ppm in the spectrum of polymer **PP3a** that corresponds to the protons on the internal double bonds.

a  
b  
c  
d  
e  
O(CH<sub>2</sub>CH<sub>2</sub>O)<sub>3</sub>

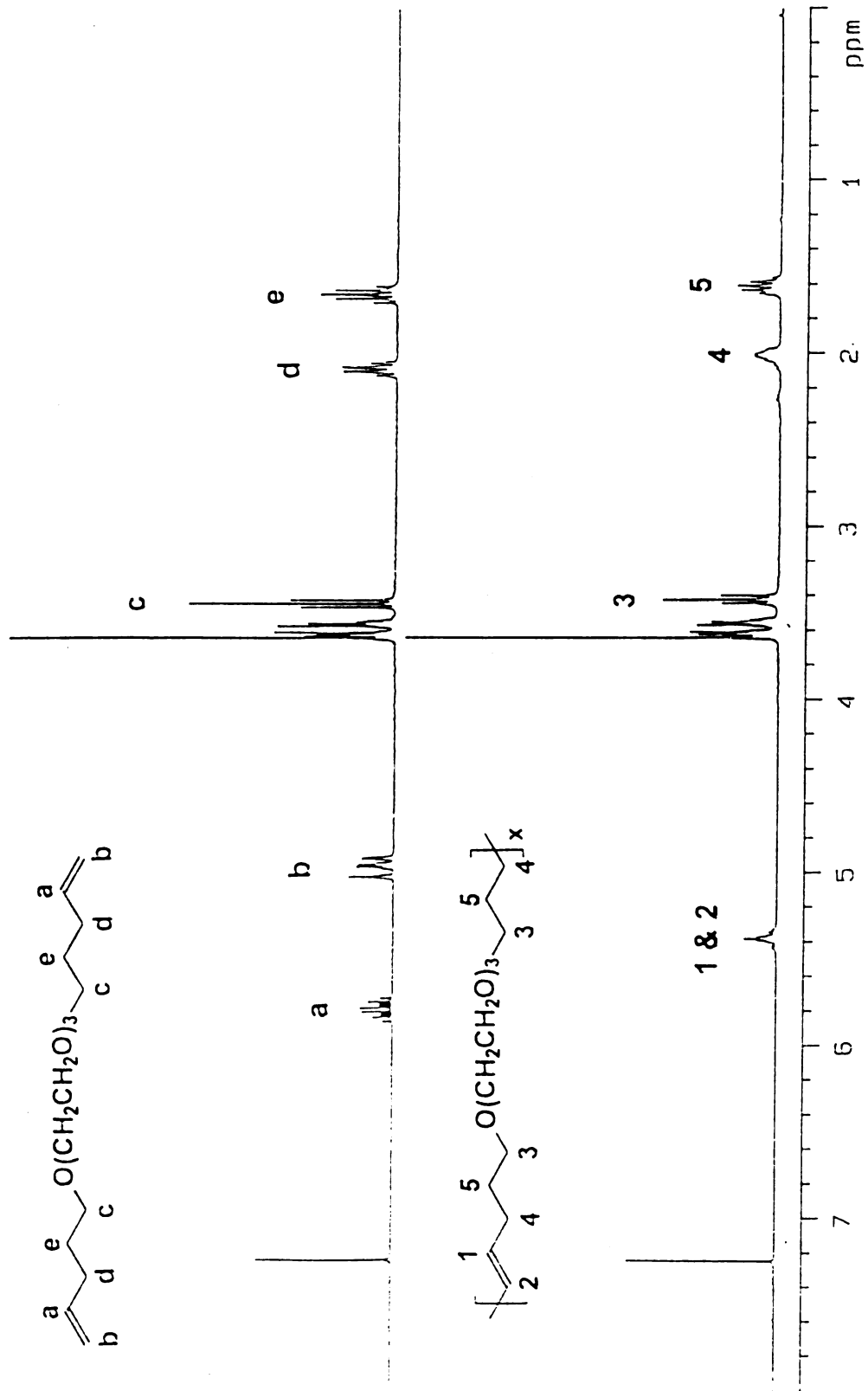


**Figure 11.** <sup>1</sup>H NMR spectra of monomer P3 (top) and polymer PP3a (bottom).

c

an

tra

agre

poly

with

also ne

absorp

O-C asy

994 and

while a n

cm<sup>1</sup>. The

In the  $^{13}\text{C}$  NMR spectra (**Figure 12**), signals from carbon atoms of the ethylene oxide unit appear at 70.8 and 70.5 ppm. Peaks from the terminal vinyl groups of the monomer at 138.3 and 114.7 ppm disappear, while two new resonances appear at 130.0 and 129.5 ppm that correspond to the *trans* and *cis* double bond carbons respectively. The peak at 30.2 ppm in the monomer spectrum splits into two resonances (29.5 and 23.6 ppm) in the polymer spectrum, corresponding to the *trans* and *cis* geometries of carbon 4 in the polymer.

The relative proportion of *cis* and *trans* carbon-carbon double bonds in the polymers was determined by comparing the integration of the peaks at 130.0 and 129.5 ppm from quantitative  $^{13}\text{C}$  NMR measurements. The percentage of *trans* double bonds in the polymers was consistently between 82-86%, which agrees well with results by other research groups who reported that ADMET polymerizations result in *trans* double bond contents ranging from 40% to 90%, with most around 80%.<sup>45-52</sup>

Spectroscopic changes in going from monomer **P3** to polymer **PP3a** are also noticeable in the IR spectra (**Figure 13**). Not surprisingly, the strong absorption at  $1121\text{ cm}^{-1}$  is the common feature in the spectra, attributable to C-O-C asymmetrical stretching in ethers. As expected, the bands at 3080, 1642, 994 and  $914\text{ cm}^{-1}$  characteristic of the vinyl group disappear after polymerization, while a new sharp band corresponding to the *trans* double bond appears at  $968\text{ cm}^{-1}$ . The absorption band for the *cis* internal double bond,

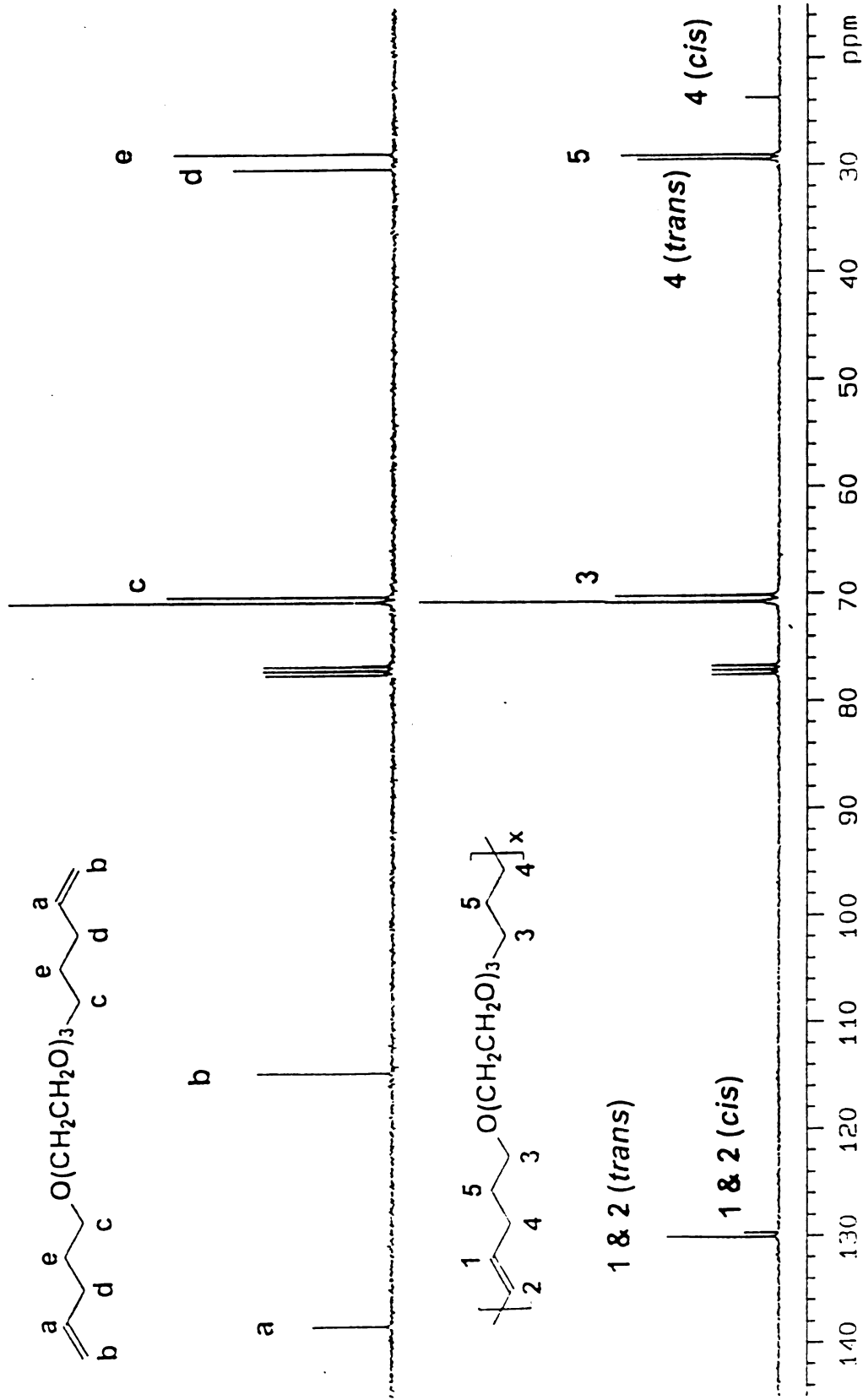


**Figure 12.**  $^{13}\text{C}$  NMR spectra of monomer P3 (top) and polymer PP3a (bottom).



which was expected to appear between 730-665  $\text{cm}^{-1}$  was not seen, due to the low *cis* double bond content in the polymer and overlap from other bands.

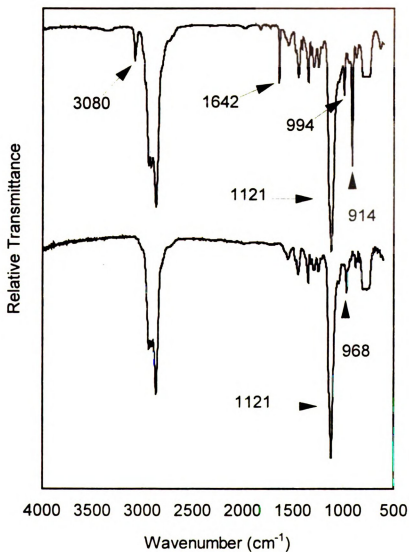


**Figure 13.** IR spectra of monomer P3 (top) and polymer PP3a (bottom).

the

bot

14

bot

On

the

be

mo

The

bre

ind

sta

of

Co

ter

the

Ap

#### 4. Thermal stability of the unsaturated polymers

The thermal stability of the unsaturated polymers was investigated by thermogravimetric analysis (TGA). For each polymer, measurements were taken both in inert (nitrogen) and in oxidative (air) atmospheres.

Typical TGA curves of an unsaturated polymer are represented in **Figure 14**. It shows that the onset of decomposition for polymer **PP2** is above 320 °C in both nitrogen and air, and the polymer decomposes rather rapidly afterwards. Only trace residues remained above 500 °C. There is no significant difference in thermal stability for **PP2** in nitrogen and in air, although the samples appeared to be slightly more stable in inert atmosphere.

The nitrogen TGA profiles of polymer **PP4** and polyethylene glycol with a molecular weight of 10,000 (**PEG10K**) are plotted in **Figure 15** for comparison. The TGA curves of **PP4** look similar to those of **PP2**, with the onset of thermal breakdown at comparable temperatures. The similarity in the TGA profiles indicates that the unsaturated polymer and **PEG10K** have similar thermal stabilities, and implies that ether breakdown is responsible for the decomposition of the polymers.

Thermal decomposition of **PH2**, shown in **Figure 16**, gave similar results. Compared with **PP2** and **PP4**, the degradation onset for **PH2** occurred at a lower temperature, and following a slow initial decomposition it rapidly degraded like the previous polymers.

The TGA profiles of the other unsaturated polymers appear in the Appendix. **Table 5** compiles the temperatures for 5%, 50% and 90% weight

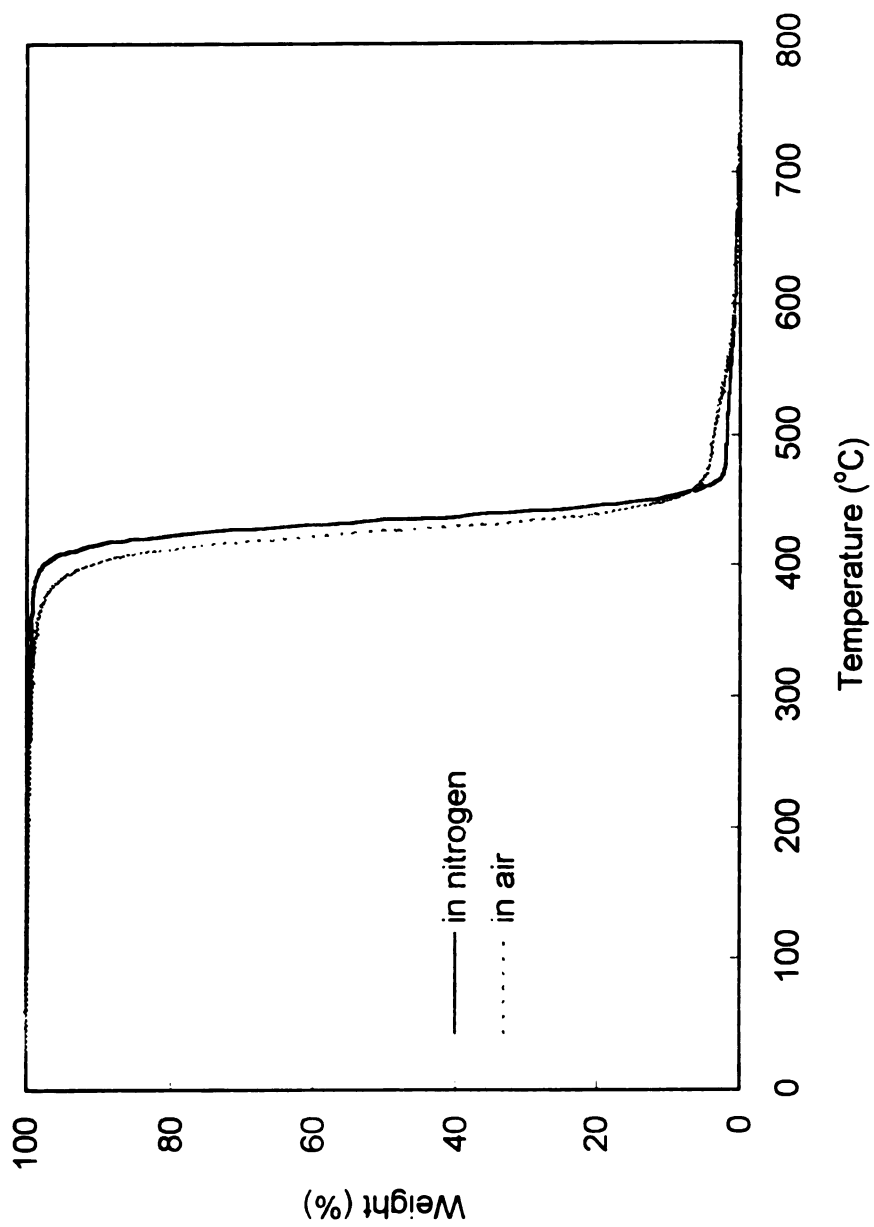


**Figure 14.** TGA profiles of PP2 (heating rate 10 °C/min).

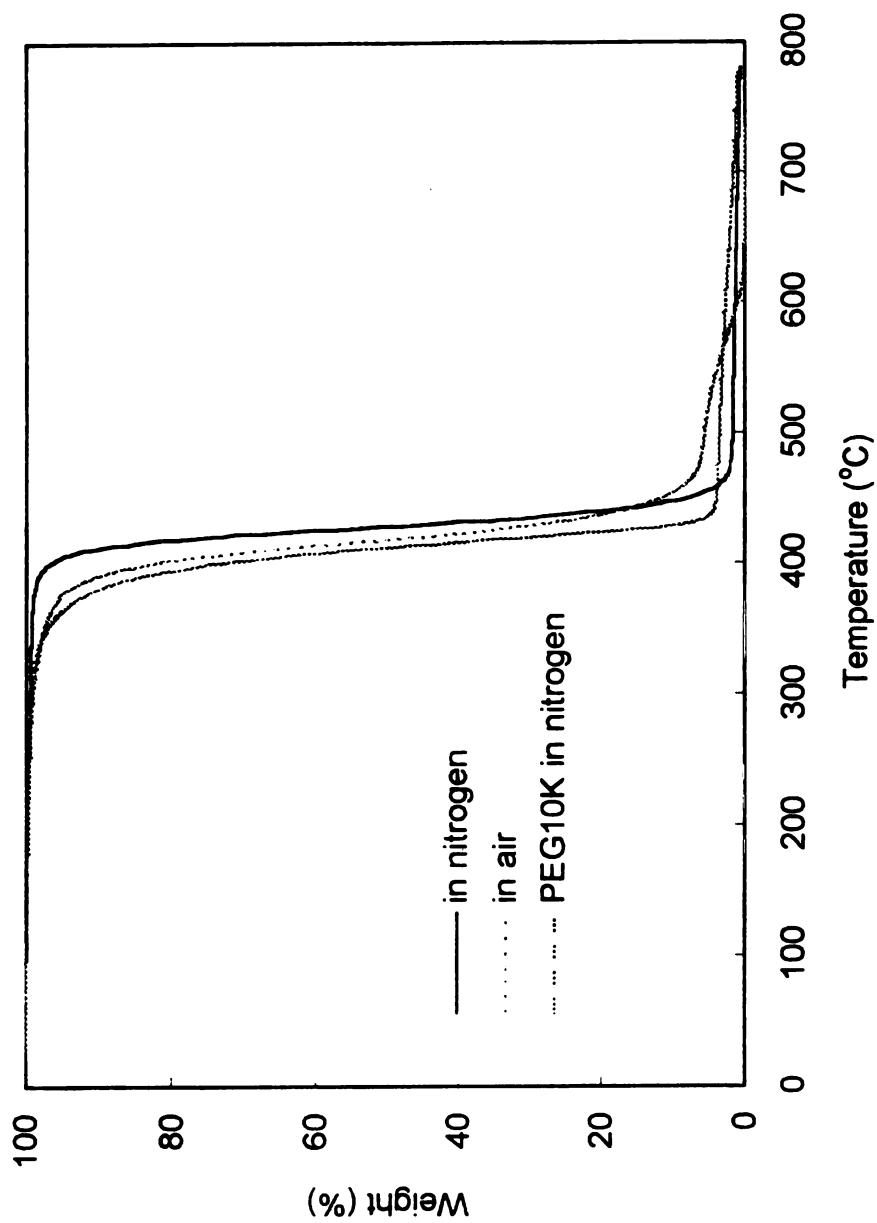


**Figure 15.** TGA profiles of PP4 and PEG10K in nitrogen (heating rate 10 °C/min).

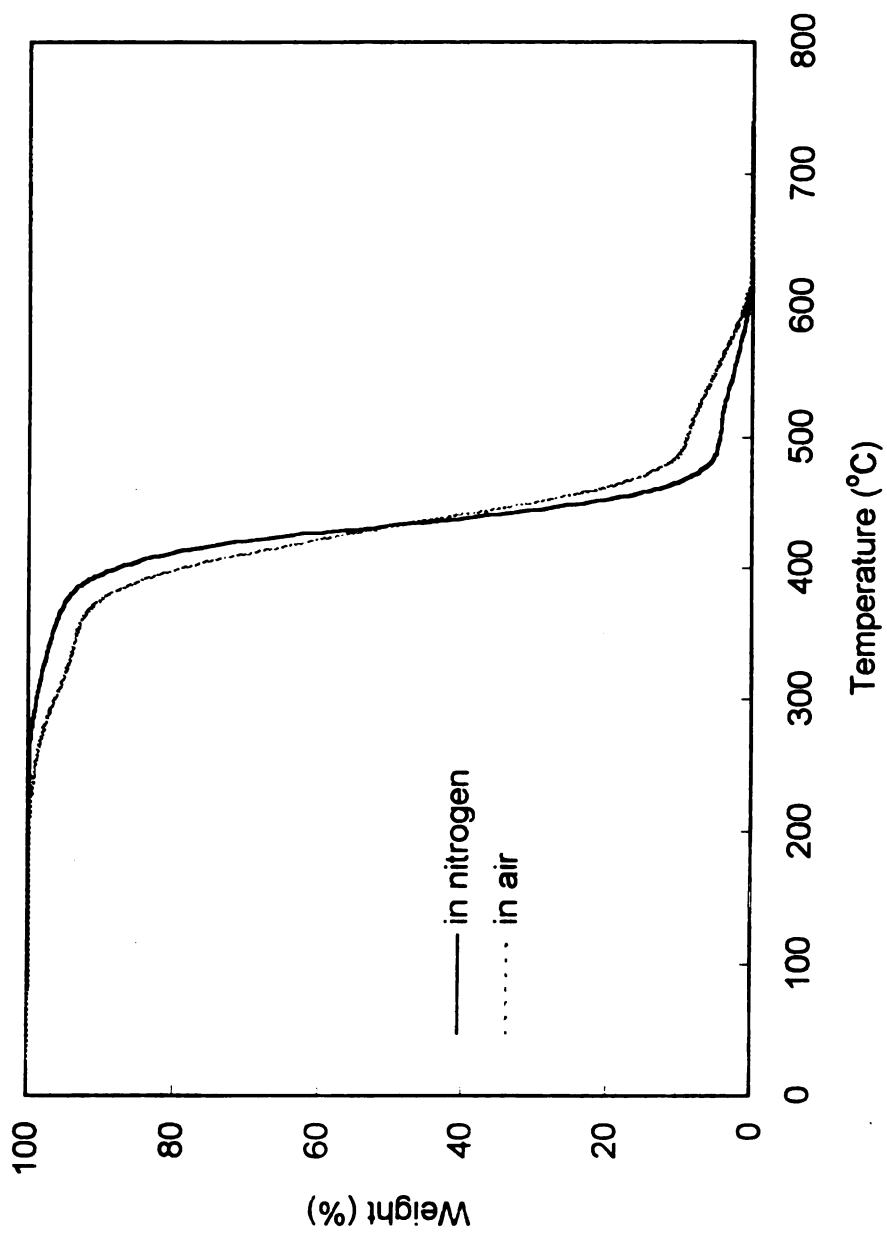


**Figure 16.** TGA profiles of PH2 (heating rate 10 °C/min).

**Table 5. Thermal Stability of the Unsaturated Polymers<sup>a</sup>**

| Polymer     | weight loss <sup>b</sup> in nitrogen |     |     | weight loss <sup>b</sup> in air |     |     |
|-------------|--------------------------------------|-----|-----|---------------------------------|-----|-----|
|             | 5%                                   | 50% | 90% | 5%                              | 50% | 90% |
| <b>PB2</b>  | 386                                  | 433 | 450 | 372                             | 430 | 464 |
| <b>PP2a</b> | 401                                  | 442 | 464 | 367                             | 424 | 457 |
| <b>PP2</b>  | 410                                  | 435 | 453 | 393                             | 427 | 451 |
| <b>PP3a</b> | 395                                  | 440 | 462 | 382                             | 430 | 451 |
| <b>PP3</b>  | 389                                  | 428 | 453 | 356                             | 422 | 454 |
| <b>PP4</b>  | 398                                  | 439 | 461 | 388                             | 433 | 454 |
| <b>PP4a</b> | 405                                  | 428 | 447 | 377                             | 418 | 453 |
| <b>PH2</b>  | 374                                  | 433 | 466 | 317                             | 432 | 487 |
| <b>PH3</b>  | 338                                  | 430 | 478 | 342                             | 424 | 469 |
| <b>PH4</b>  | 343                                  | 425 | 472 | 320                             | 424 | 478 |
| <b>PH5</b>  | 341                                  | 418 | 460 | 335                             | 421 | 460 |
| <b>PO2</b>  | 415                                  | 447 | 471 | 406                             | 443 | 474 |
| <b>PO4</b>  | 338                                  | 428 | 463 | 312                             | 421 | 466 |

<sup>a</sup> Temperatures are reported in °C.

<sup>b</sup> Defined as the temperature where the weight loss reached the indicated levels.

losses for all the unsaturated polymers. The temperatures where 5% weight loss occurred varied from 312 to 406 °C in air, with a shift to higher temperatures for measurements taken in nitrogen. Interestingly, the midpoint of the thermal breakdowns of all polymers appeared in a much smaller temperature range suggesting a common degradation mechanism. Usually a polymer lost 90% of its weight by the time temperature reached 450 °C.

### **5. Thermal behavior of the unsaturated polymers**

The unsaturated polymers were analyzed by DSC to study their thermal properties. Samples were heated at 10 °/min from -100 to 100 °C, quenched to -100 °C at 200 °C/min, heated at 10 °/min to 100 °C, and finally cooled to -100 °C at 10 °/min. As described below, nearly all samples exhibited unique thermal properties with combinations of crystallization and melting transitions.

The thermograms in **Figure 17** are the second DSC heating and cooling scans for **PB2**. After a glass transition seen at -72 °C in the heating scan, an exothermic crystallization at -33 °C was followed by two overlapping melting peaks at -9 and 0 °C respectively. No crystallizing or melting transitions were observed in the second cooling scan.

The thermal behavior of polymers **PP2 (Figure 18)** and **PP3 (Figure 19)** is simple. Except for the glass transition, no other peaks appeared during the measurements, indicating these two polymers are amorphous over the whole temperature range.

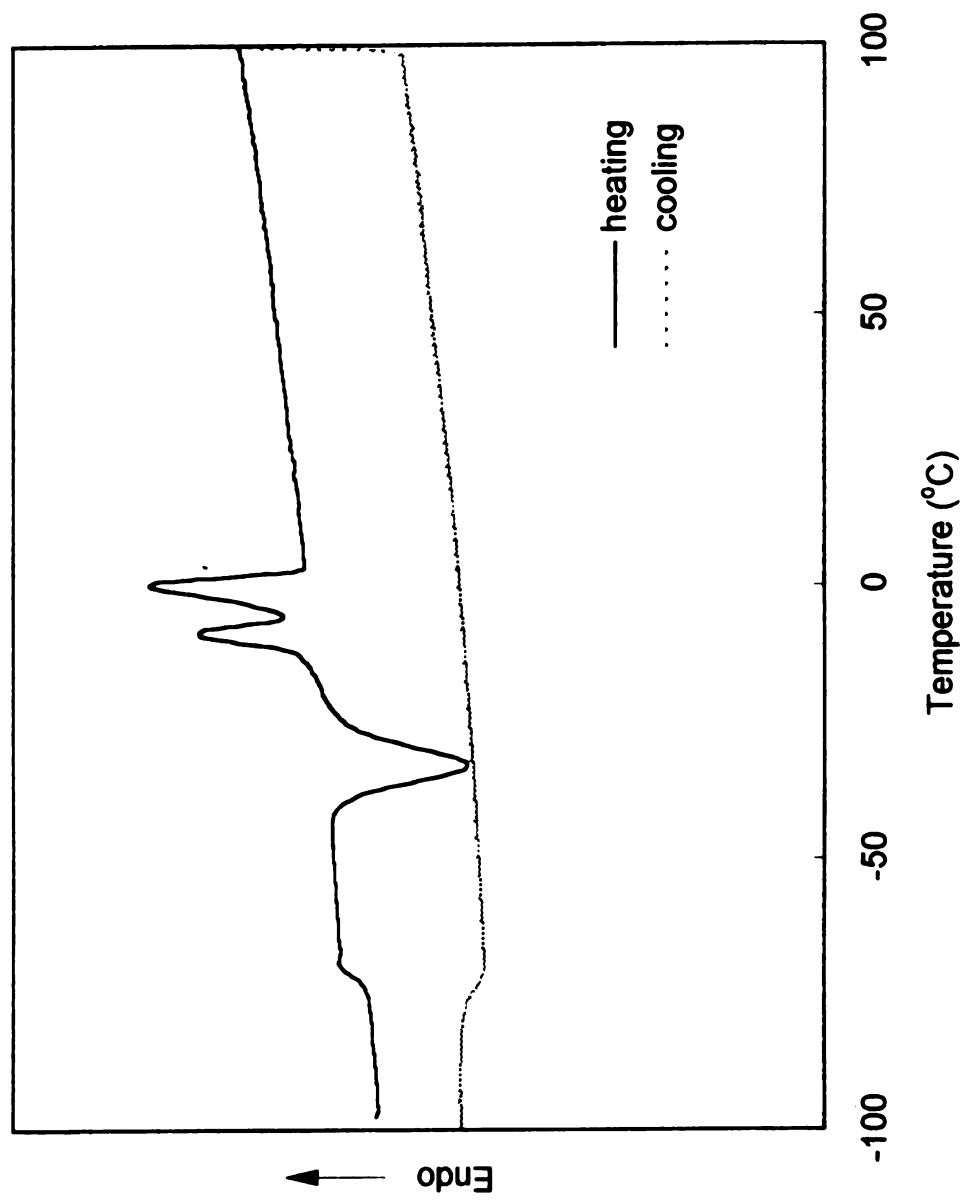


**Figure 17.** Second DSC heating and cooling scans for PB2 (heating and cooling rate 10 °C/min).

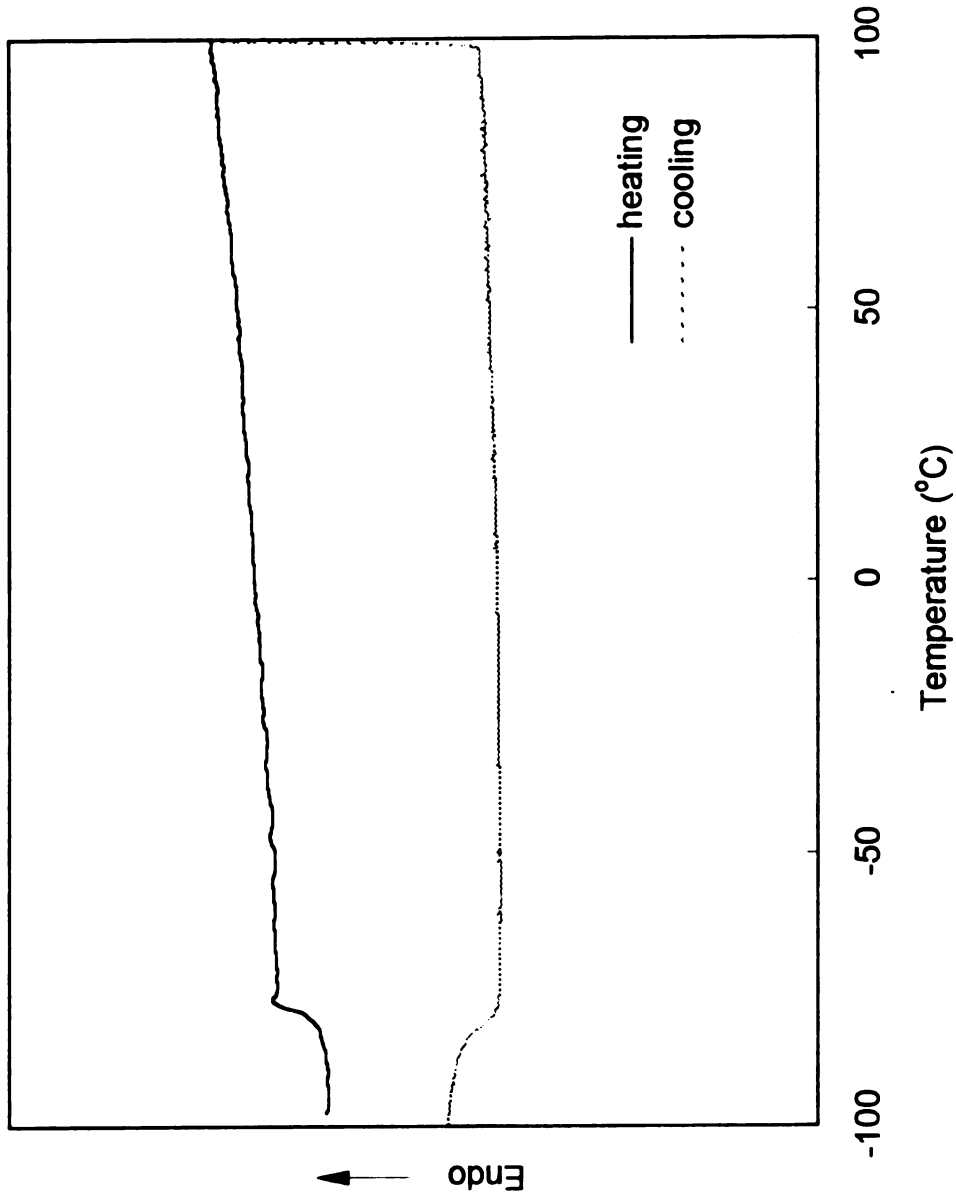


**Figure 18.** Second DSC heating and cooling scans for **PP2** (heating and cooling rate 10 °C/min).

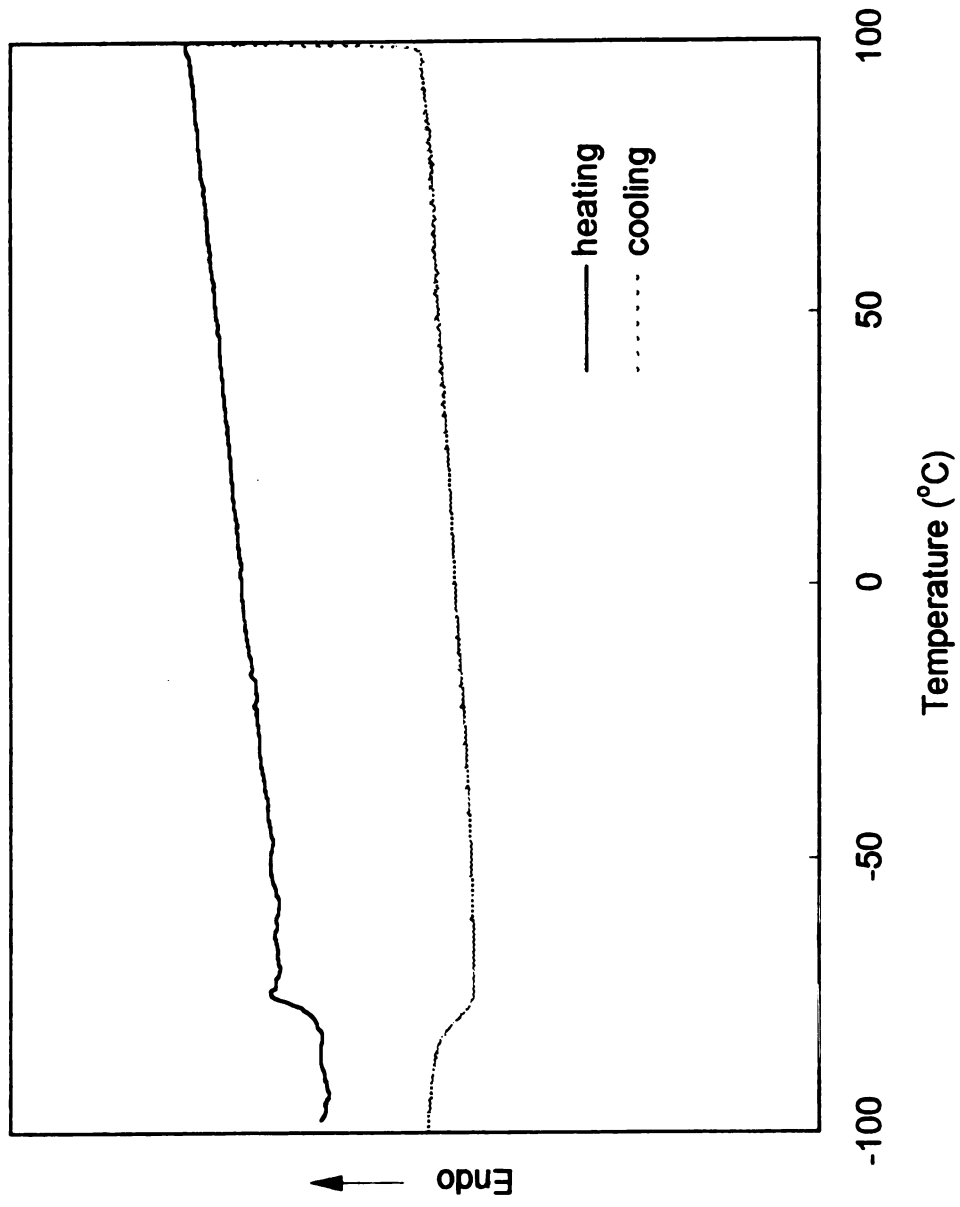


**Figure 19.** Second DSC heating and cooling scans for PP3 (heating and cooling rate 10 °C/min).

The second heating scan for **PP4 (Figure 20)** includes a glass transition and multiple crystallizations and melting transitions in the low temperature range. However, peaks corresponding to the crystalline phase changes were again not seen in the cooling scan, similar to the data for **PB2**.

The second DSC heating and cooling scans for polymers **PH2, PH3, PH4** and **PH5** are plotted in **Figures 21, 22, 23** and **24** respectively. In all cases, glass transitions were observed at low temperatures. The DSC heating scans for polymers **PH2** and **PH3** have similar features. Above the glass transition, a broad crystallization peak is followed by two melting transitions at higher temperatures. For polymers **PH4** and **PH5**, there were multiple crystallization and melting peaks. Usually a crystalline phase formed and melted, followed by formation and melting of another crystalline phase as the temperature increased.

Finally, DSC thermograms for **PO2 (Figure 25)** show adjacent twin melting peaks in the heating scan and a sharp crystallizing peak in the cooling scan. In **Figure 26**, **PO4** with a longer ethylene oxide segment possesses one broad melting transition in heating scan and a sharp crystallizing peak in the cooling scan.

The characteristics of the thermal transitions for the unsaturated polymers are summarized in **Table 6**. Values of the melting transition temperature,  $T_m$ , were taken as the temperature at the peak of the melting transitions in second heating scans, and the crystallization temperature,  $T_c$ , was taken as the temperature at the peak of the crystallization transitions in the second cooling

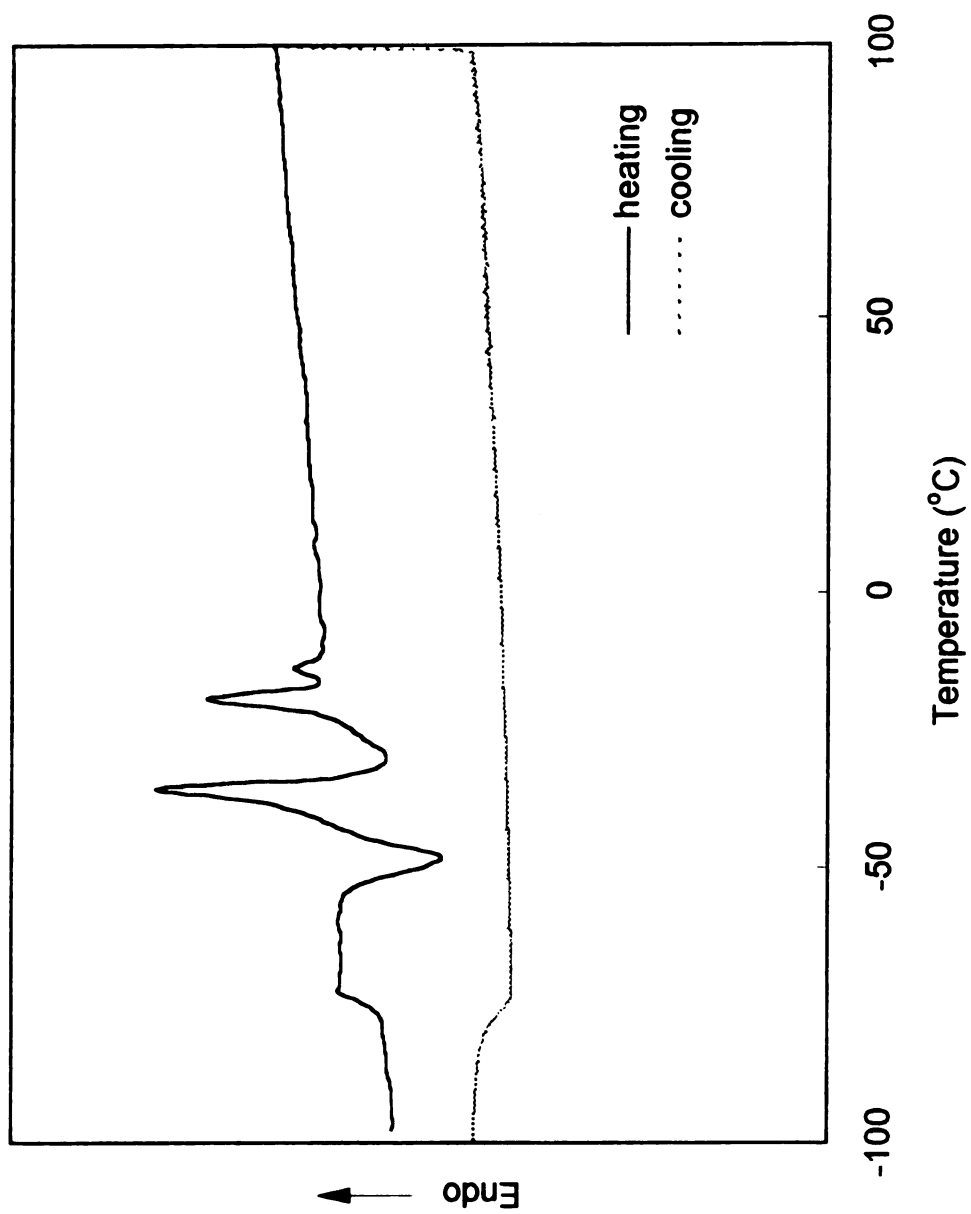


**Figure 20.** Second DSC heating and cooling scans for **PP4** (heating and cooling rate 10 °C/min).

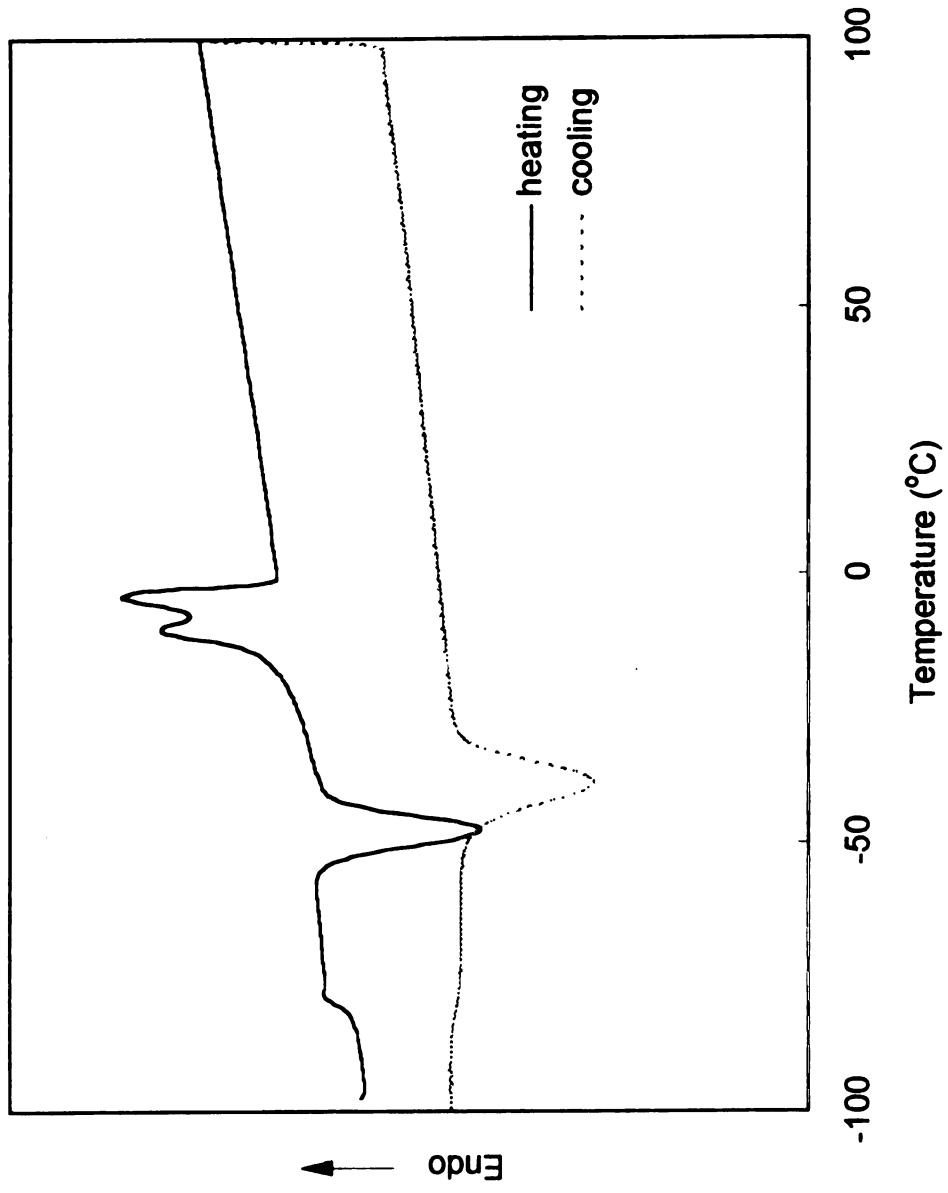


**Figure 21.** Second DSC heating and cooling scans for PH2 (heating and cooling rate 10 °C/min).

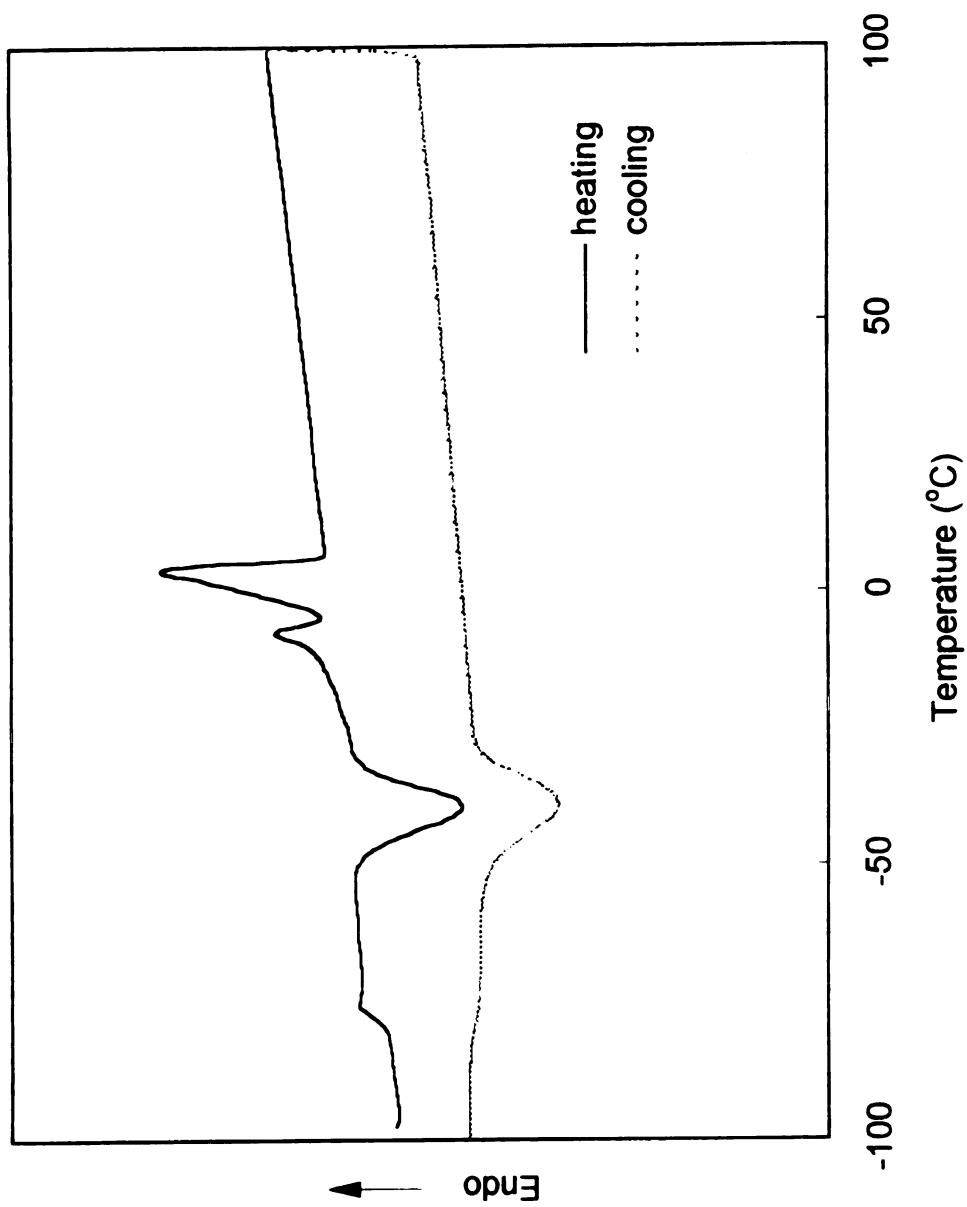


**Figure 22.** Second DSC heating and cooling scans for PH3 (heating and cooling rate 10 °C/min).

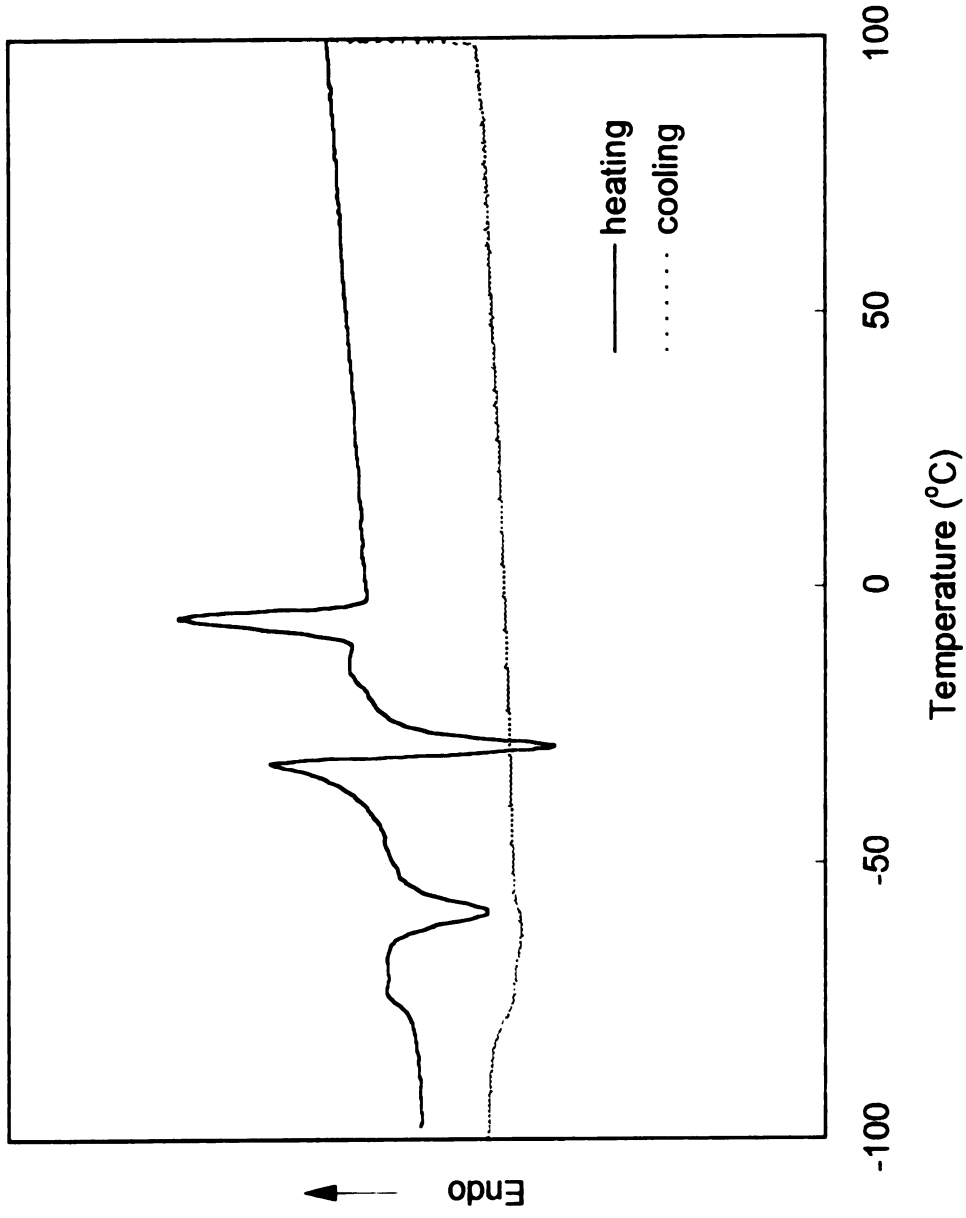


**Figure 23.** Second DSC heating and cooling scans for PH4 (heating and cooling rate 10 °C/min).

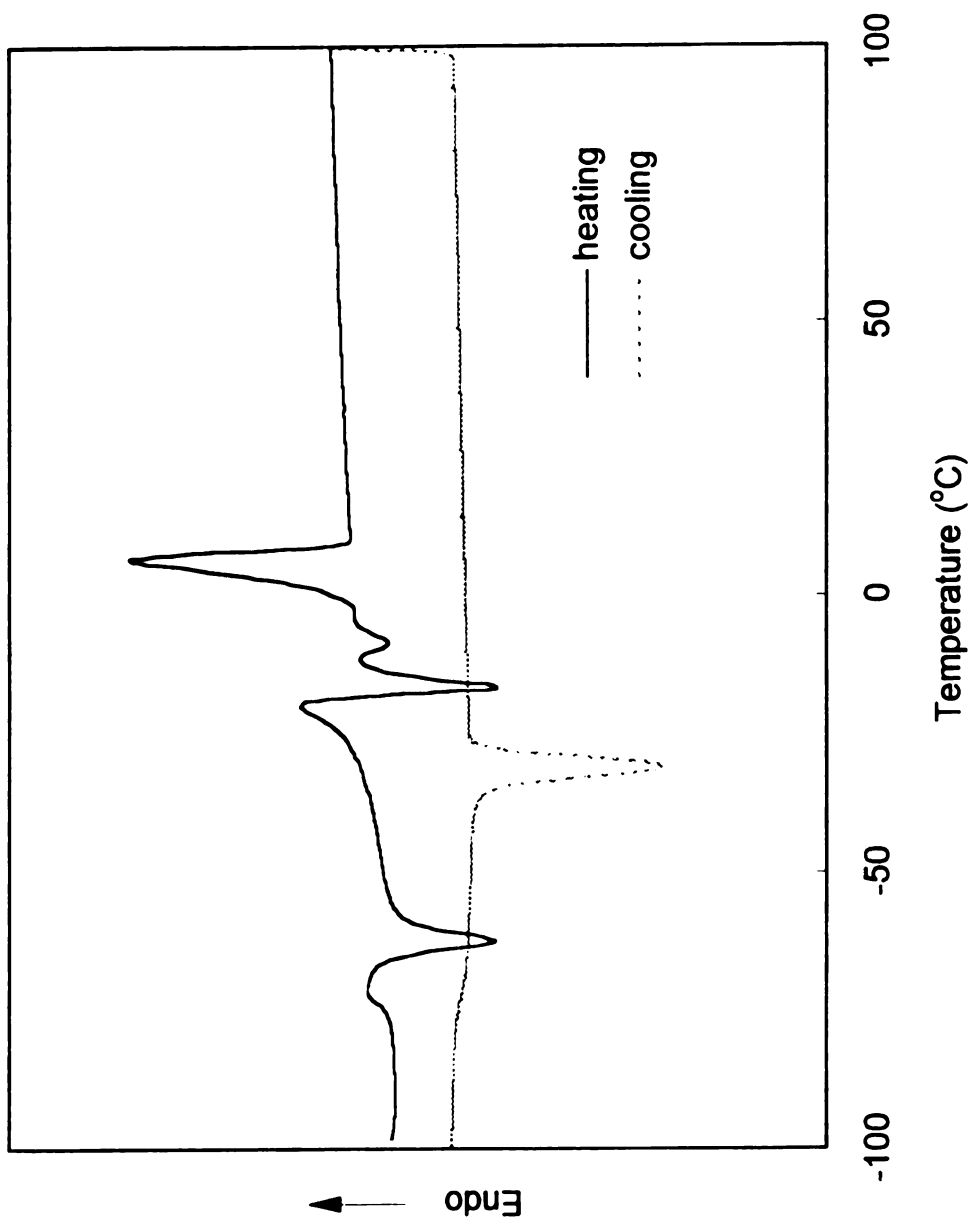


**Figure 24.** Second DSC heating and cooling scans for PH5 (heating and cooling rate 10 °C/min).

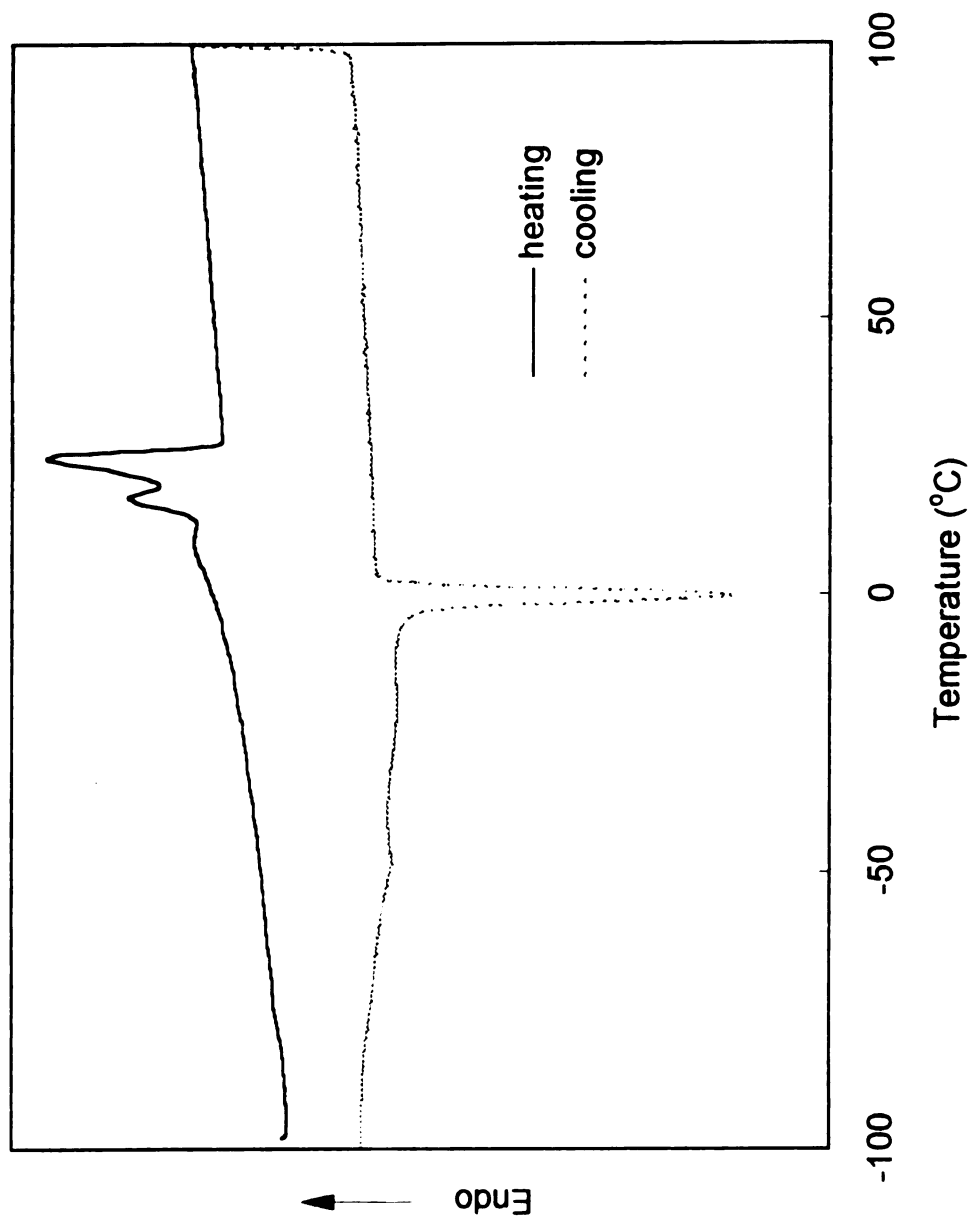


**Figure 25.** Second DSC heating and cooling scans for **PO<sub>2</sub>** (heating and cooling rate 10 °C/min).

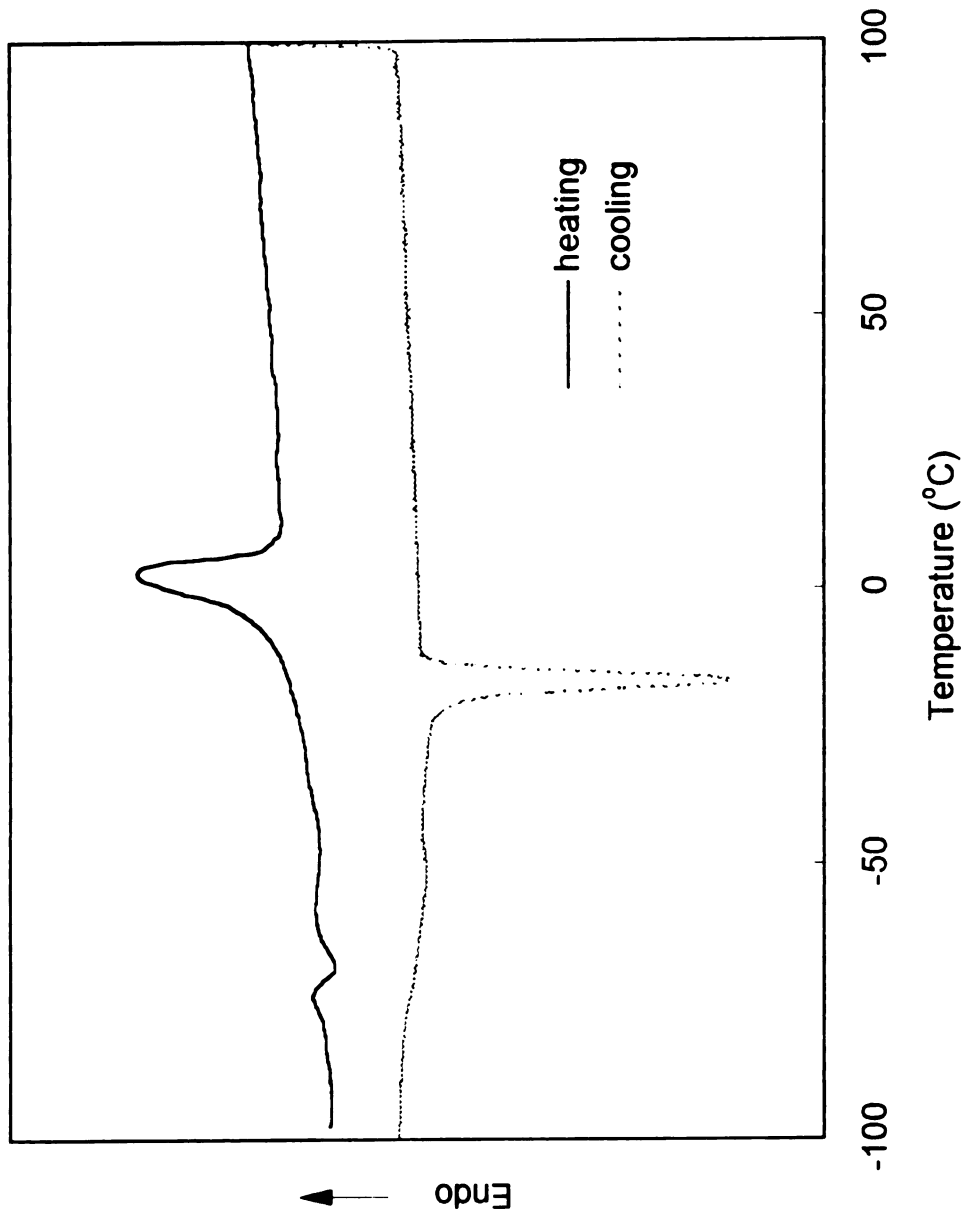


**Figure 26.** Second DSC heating and cooling scans for PO4 (heating and cooling rate 10 °C/min).

**Table 6. Thermal Transition of the Unsaturated Polymers**

| Polymer    | T <sub>g</sub> (°C) | T <sub>m</sub> <sup>a</sup> (°C) | T <sub>c</sub> <sup>b</sup> (°C) | T <sub>g</sub> /T <sub>m</sub> <sup>c</sup> |
|------------|---------------------|----------------------------------|----------------------------------|---|
| <b>PB2</b> | -72                 | -9, 0                            |                                  | 0.74  |
| <b>PP2</b> | -79                 |                                  |                                  |   |
| <b>PP3</b> | -77                 |                                  |                                  |   |
| <b>PP4</b> | -75                 | -36, -19, -14                    |                                  | 0.76  |
| <b>PH2</b> | -81                 | -10, -4                          | -38                              | 0.71  |
| <b>PH3</b> | -79                 | -8, 4                            | -39                              | 0.70  |
| <b>PH4</b> | -77                 | -32, -5                          | -29                              | 0.73  |
| <b>PH5</b> | -74                 | -20, 7                           | -31                              | 0.71  |
| <b>PO2</b> |                     | 18, 25                           | 0                                |   |
| <b>PO4</b> | -78                 | 3                                | -17                              | 0.71  |

<sup>a</sup> Taken as the temperature of the peak of the melting endotherm.

<sup>b</sup> Taken as the temperature of the peak of the crystallization exotherm in the DSC cooling scans.

<sup>c</sup> Calculated using absolute temperature values.

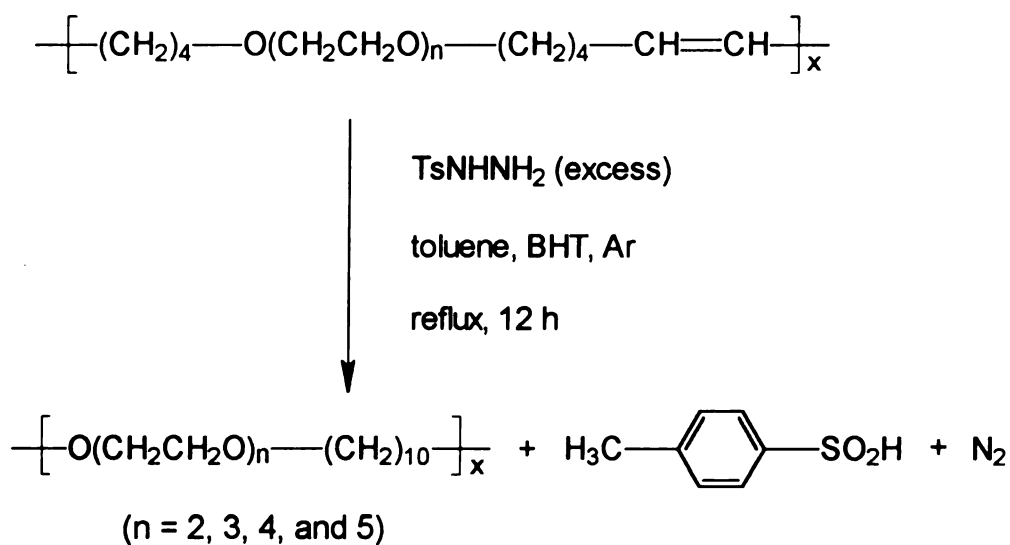
scans. Each  $T_g/T_m$  value was calculated as the ratio of  $T_g$  to the highest  $T_m$  for that polymer sample, where T is expressed in Kelvin (K).

### III. Alternating (AB)<sub>n</sub> Copolymers from Unsaturated Polymers

#### 1. Reduction of the unsaturated polymers

Four unsaturated polymers, **PH2**, **PH3**, **PH4** and **PH5**, were reduced to form hydrogenated polymers, **PH2H**, **PH3H**, **PH4H**, and **PH5H** respectively, as outlined in **Scheme 20**. The reduction reaction involved the hydrogenation of the carbon-carbon double bonds in the unsaturated polymers with *p*-toluenesulfonylhydrazide, which was believed to decompose and form diimide as an intermediate during the reaction.<sup>76-79</sup> Diimide is very reactive and reduces symmetrical double bonds readily by neutral hydrogen atom transfer to the substrate.

**Scheme 20. Hydrogenation of the unsaturated polymers**



for

con

spe

co

**27**

the

eth

**PH**

inte

in t

ref

130

not

poi

by

hya

**Tat**

mol

was

The hydrogenation reaction was carried out smoothly in refluxing toluene for 12 h and the reducing reagent was employed in large excess to ensure a complete reduction of all carbon-carbon double bonds. The  $^1\text{H}$  and  $^{13}\text{C}$  NMR spectra of the hydrogenated polymers provided spectroscopic evidence that complete reduction was achieved in all four polymers. As an example, **Figure 27** displays the  $^1\text{H}$  NMR spectrum of hydrogenated polymer **PH5H**. In this figure, the multiple peaks between 3.63 and 3.54 ppm belong to the protons on the ethylene oxide units. Their position and pattern are unchanged from **PH5** to **PH5H**. The multiplet peak at 5.35 ppm that corresponded to proton on the internal double bond, however, is absent, indicating double bonds no longer exist in this hydrogenated polymer. The structural change from **PH5** to **PH5H** is reflected in the  $^{13}\text{C}$  NMR spectrum (**Figure 28**) as well. The adjacent peaks at 130.24 and 129.74 ppm characteristic of internal *trans* and *cis* double bonds can not be detected in the spectrum. NMR data proved that perfectly alternating polyethylene/polyethylene oxide  $(\text{AB})_n$  copolymers were successfully prepared by the reduction reaction shown in **Scheme 20**.

## 2. Physical properties of the hydrogenated polymers

The molecular weights and molecular weight distributions of the hydrogenated polymers are listed with those of the unsaturated polymers in **Table 7**. Interestingly, there was a remarkable decrease in number-average molecular weight during hydrogenation for each pair. For example,  $M_n$  of **PH2** was 44,700, but after reduction,  $M_n$  of **PH2H** dropped to

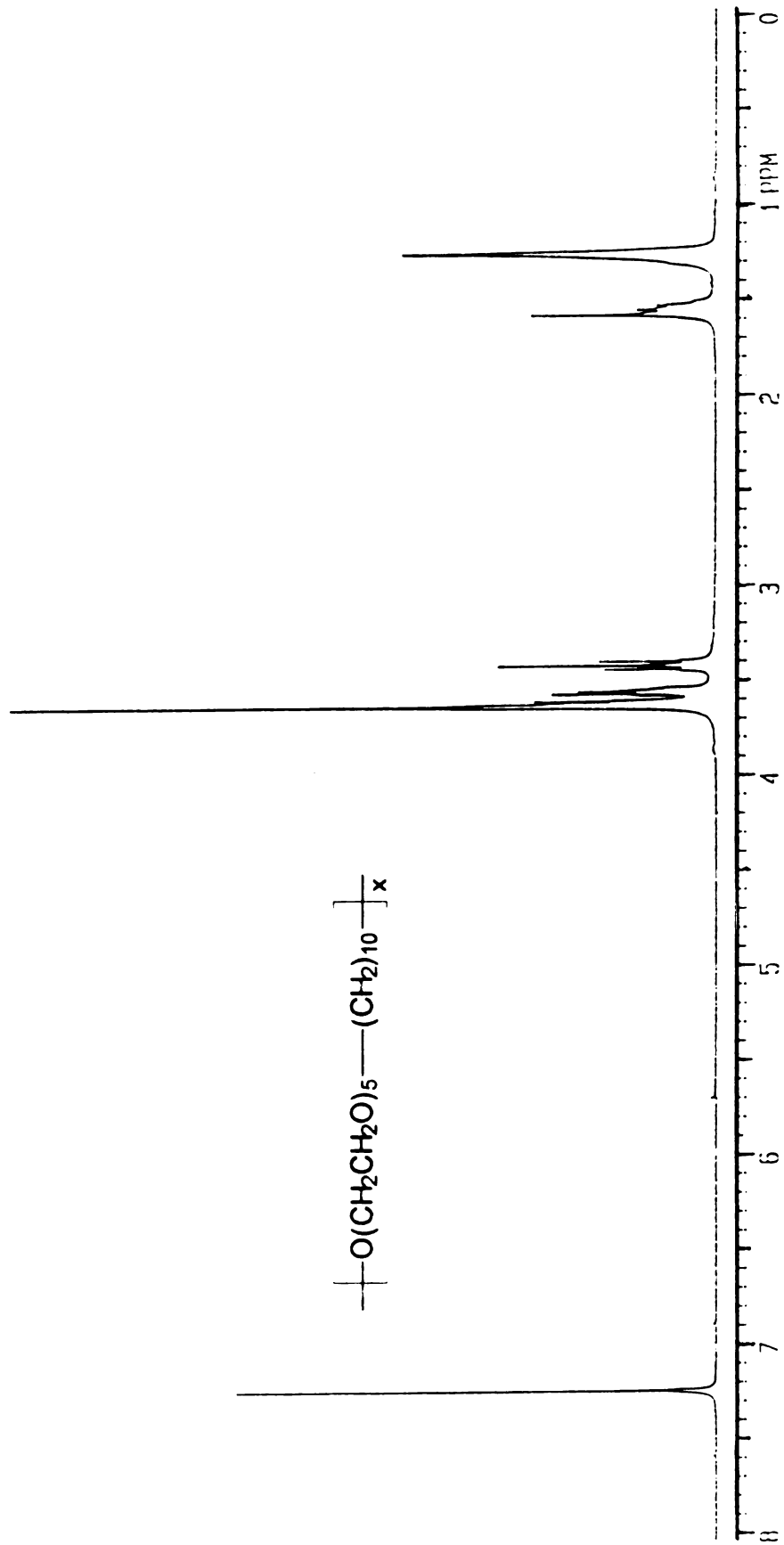
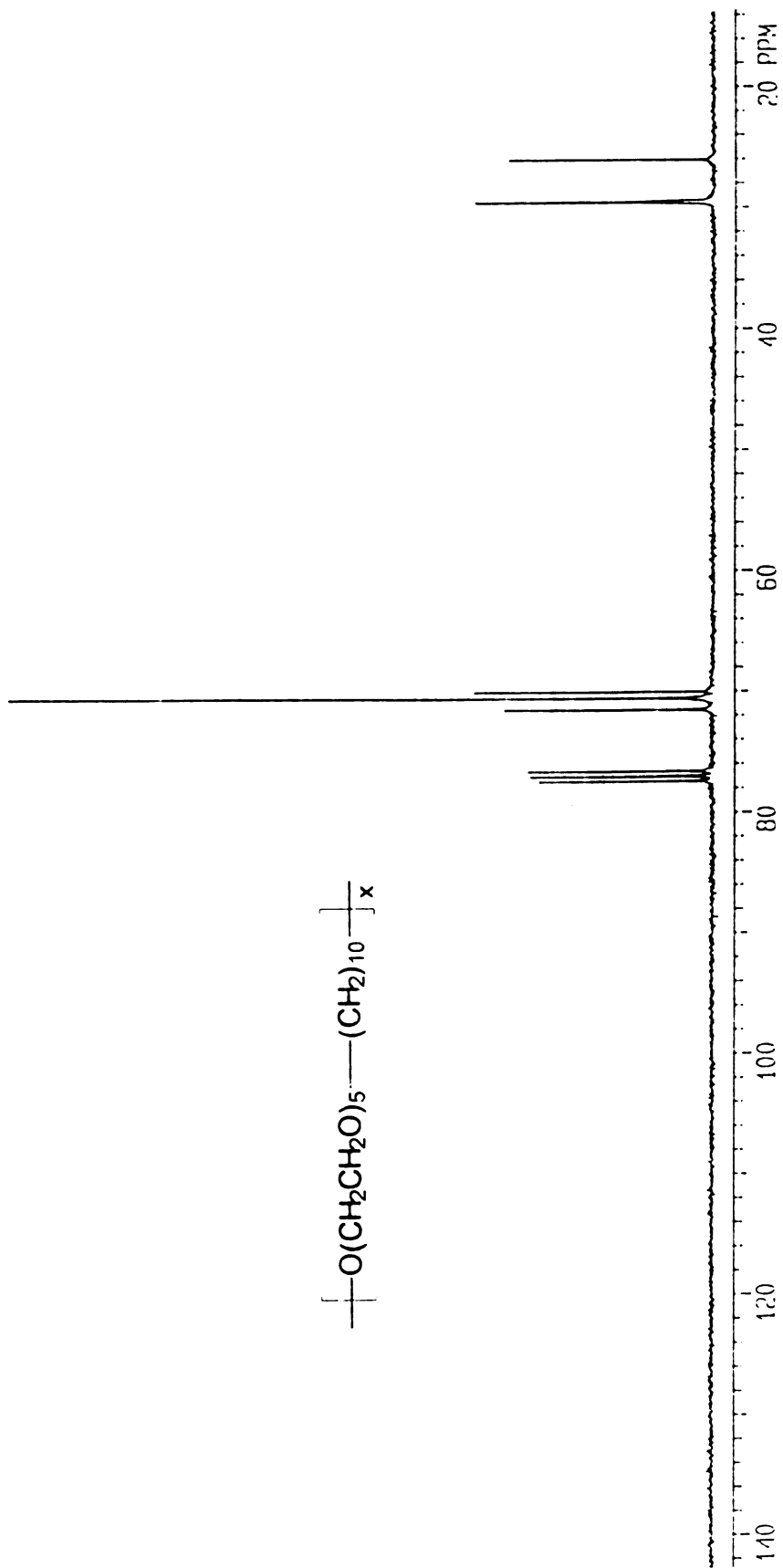


Figure 27.  $^1\text{H}$  NMR spectrum of hydrogenated polymer PH5H.



**Figure 28.**  $^{13}\text{C}$  NMR spectrum of hydrogenated polymer PH5H.

po

of

ma

mo

do

sg

Ta

—

—

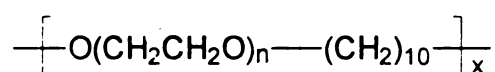
—

of n

uns

24,800. Since the molecular weights were measured relative to monodisperse polystyrene standards by GPC, each molecular weight is not an absolute value of the true molecular weight but a relative one reflecting the coil sphere size of macromolecules in dilute solution. From the chemical structure, the absolute molecular weight change of each polymer before and after reduction of the double bonds is negligible. The decrease of relative molecular weight may be a sign of decrease of coil sphere size for the saturated polymers.

**Table 7. GPC Data Comparison Between the Hydrogenated Polymers and Their Unsaturated Precursors**



| n | Unsaturated Polymer |      | Hydrogenated Polymer |      |
|---|---------------------|------|----------------------|------|
|   | M <sub>n</sub>      | PDI  | M <sub>n</sub>       | PDI  |
| 2 | 44,700              | 2.74 | 24,800               | 2.09 |
| 3 | 32,200              | 2.12 | 24,900               | 2.00 |
| 4 | 28,100              | 2.16 | 13,100               | 2.06 |
| 5 | 31,500              | 2.01 | 18,400               | 1.81 |

The saturated polymers **PH2H**, **PH3H**, **PH4H** and **PH5H** show a number of notable properties, some of which differentiate them from the original unsaturated polymers. Unlike the unsaturated polymers that have a greenish

brown

remn

polym

polar

same

precu

carb

hygr

DSC

DSC

to ti

th.s

ma

the

roc

wa

IF

D,

C-

brown color, these polymers appear to be opaque with a white color. The remnants of the molybdenum catalyst may have been removed from the polymers after the reduction reaction and work-up procedure. Because the polarity of the saturated polymers is not significantly altered, they exhibit the same good solubility in a variety of organic solvents that dissolve the unsaturated precursors, such as toluene, tetrahydrofuran, methylene chloride, chloroform, carbon tetrachloride, and acetonitrile. The hydrogenated polymers are hygroscopic and tend to gradually absorb moisture from environment.

### 3. Thermal behavior of the hydrogenated polymers

The thermal properties of the four hydrogenated polymers were studied by DSC analysis in the same way as for the unsaturated polymers. The second DSC heating and cooling scans of **PH2H** is displayed in **Figure 29**. In contrast to the unsaturated polymers, the glass transition of **PH2H** is not clearly defined in this plot. Following a minor melting peak and a minor crystallization peak, a major melting transition was seen with a peak melting temperature of 46 °C in the heating scan. This transition confirms that **PH2H** is a crystalline polymer at room temperature. When the sample was cooled, a sharp crystallization peak was observed at 29 °C.

Similarly, the  $T_g$  of **PH3H** was not detected in its DSC thermograms (**Figure 30**). A melting transition appeared at 37 °C in the heating scan, followed by a minor second melting peak. In the cooling scan a well-defined crystallization transition was observed at 22 °C. Both  $T_m$  and  $T_c$  of **PH3H** are

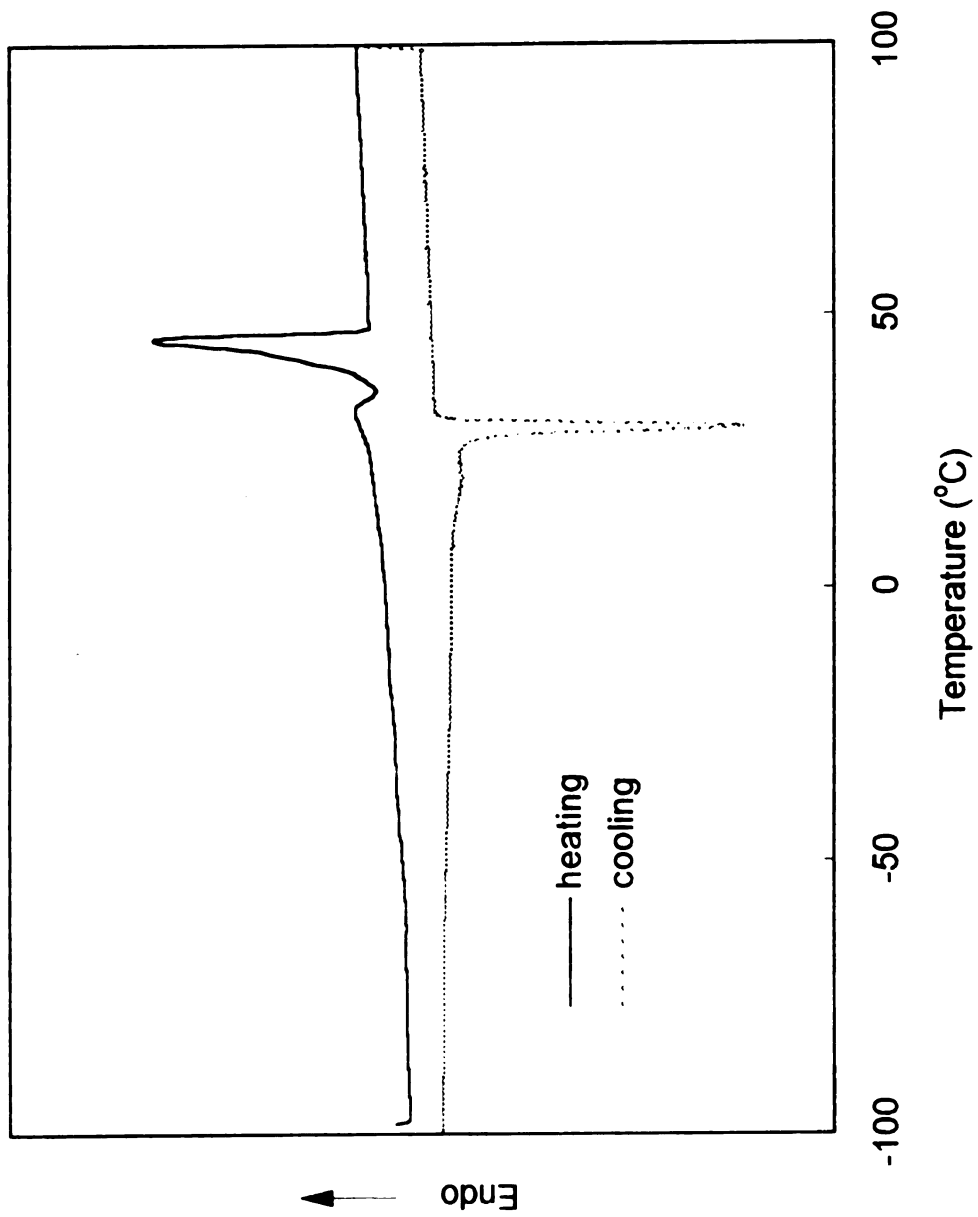


**Figure 29.** Second DSC heating and cooling scans for PH2H (heating and cooling rate 10 °C/min).

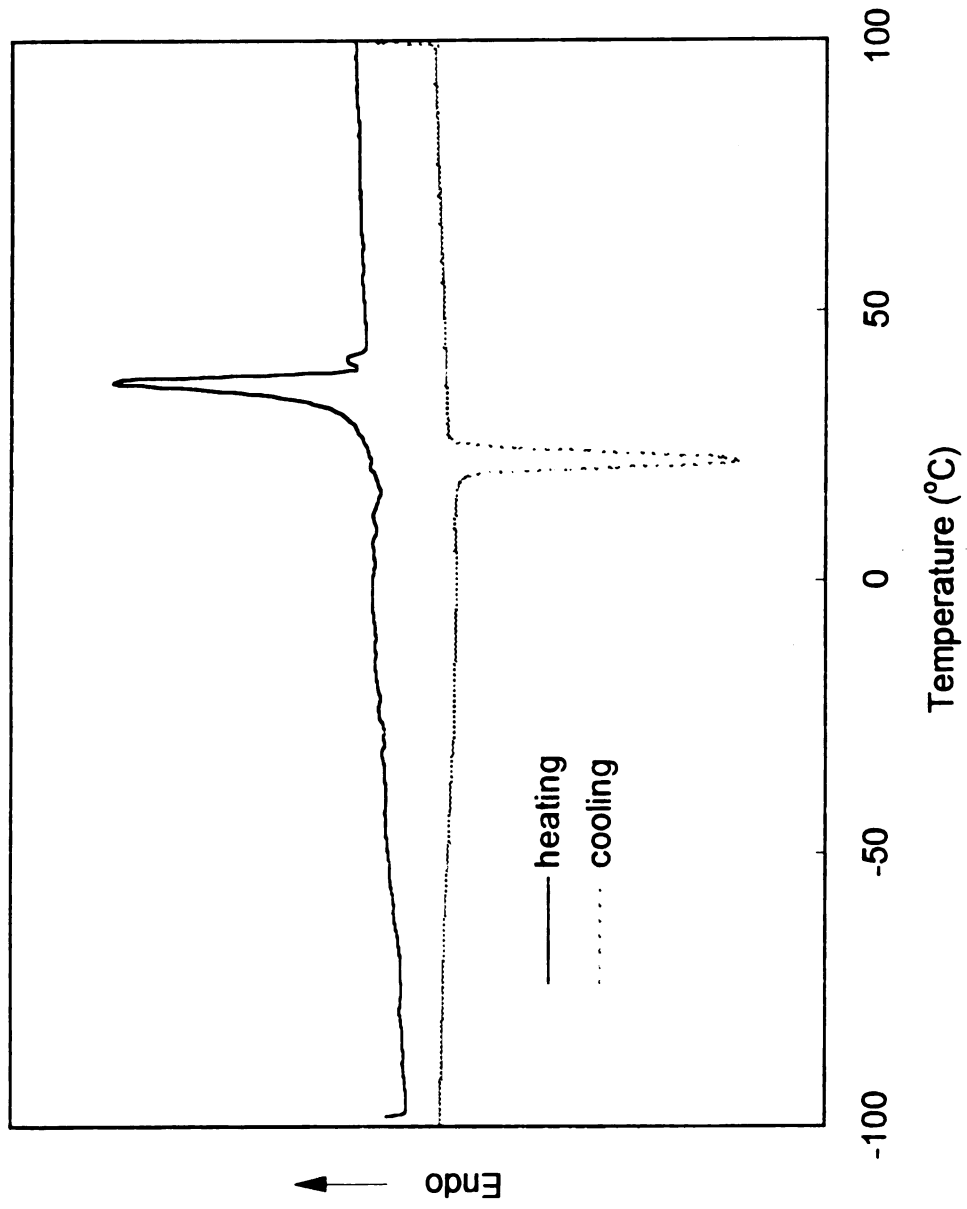


**Figure 30.** Second DSC heating and cooling scans for PH3H (heating and cooling rate 10 °C/min).

lower than corresponding  $T_m$  and  $T_c$  of **PH2H**, which has one less ethylene oxide unit in the repeating unit.

The  $T_g$  of **PH4H** was not seen in its DSC thermograms (**Figure 31**). Compared with corresponding unsaturated polymer **PH4** (**Figure 23**), the thermal transitions of **PH4H** show a strikingly similar pattern in its heating scan, though the transition temperatures are higher. After a melting peak followed by a crystallizing peak, the main melting transition appeared at 29 °C. The cooling curve for **PH4H** is much simpler, showing only one crystallizing peak at 4 °C.

In the second heating scan of **PH5H** (**Figure 32**), the hydrogenated polymer exhibits multiple melting and crystallizing transitions in the heating scan, with the major melting peak at the same temperature as the  $T_m$  of **PH4H**. Its crystallizing temperature measured during cooling is also close to that of **PH4H**.

The DSC study proves that all hydrogenated polymers are crystalline at room temperature. The absence of observable  $T_g$ 's for the polymers probably reflects the high crystallinity in these materials. The thermal transition temperatures of the hydrogenated polymers are summarized in **Table 8**.

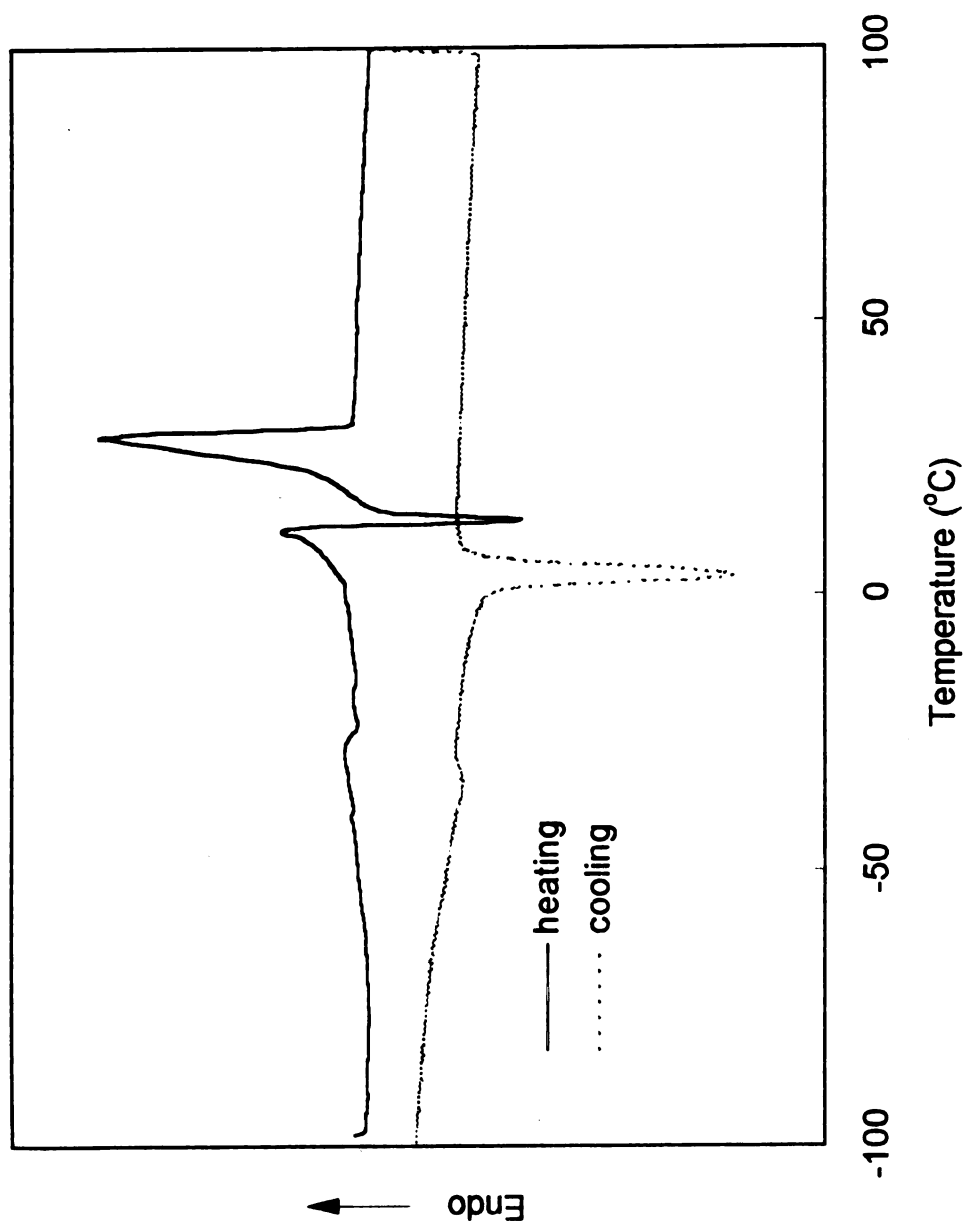


**Figure 31.** Second DSC heating and cooling scans for PH4H (heating and cooling rate 10 °C/min).

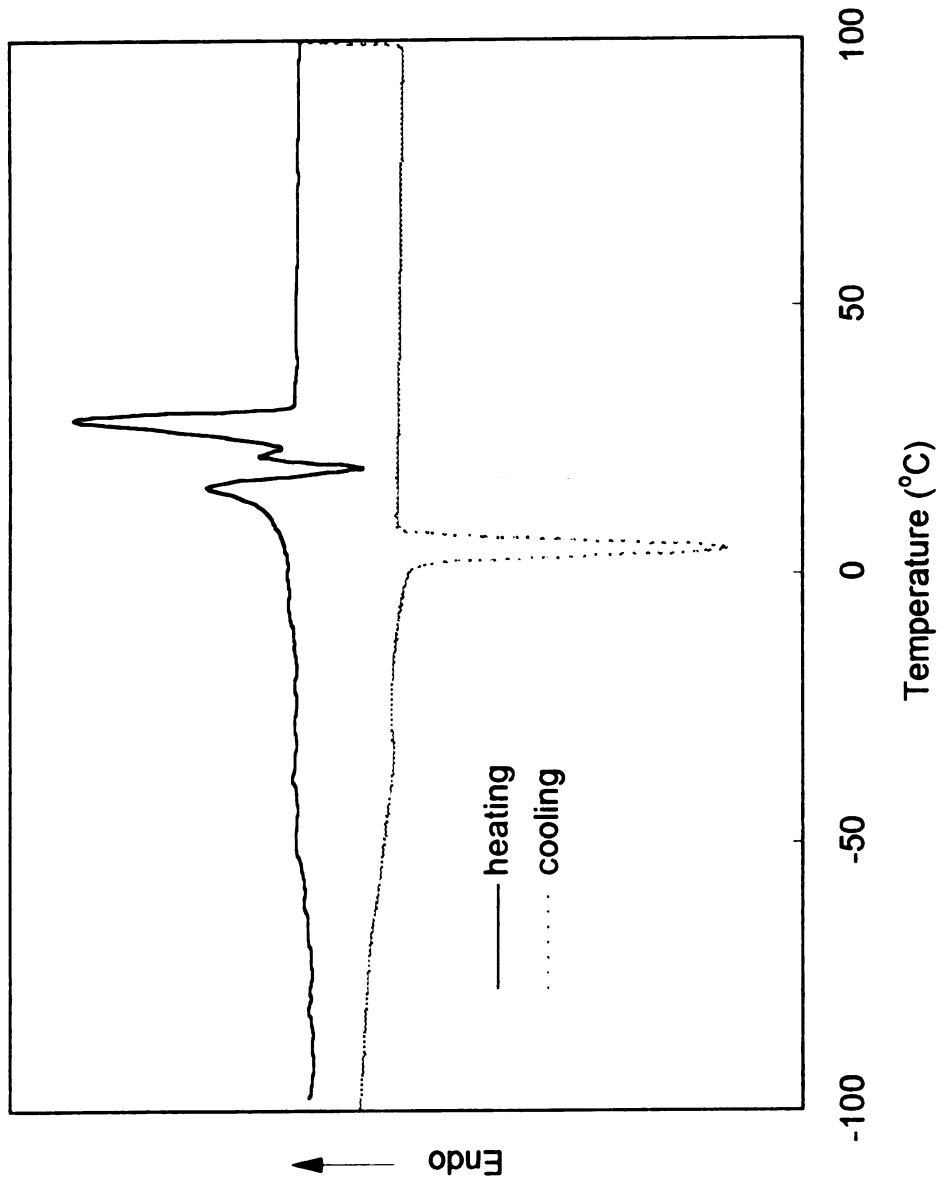


**Figure 32.** Second DSC heating and cooling scans for PH5H (heating and cooling rate 10 °C/min).

**Table 8. Thermal Transition Temperatures for the Hydrogenated Polymers.**

| Polymer     | T <sub>g</sub> (°C) | T <sub>m</sub> (°C) <sup>b</sup> | T <sub>c</sub> (°C) <sup>c</sup> |
|-------------|---------------------|----------------------------------|----------------------------------|
| <b>PH2H</b> | ND <sup>a</sup>     | 46                               | 29                               |
| <b>PH3H</b> | ND <sup>a</sup>     | 37                               | 22                               |
| <b>PH4H</b> | ND <sup>a</sup>     | 29                               | 4                                |
| <b>PH5H</b> | ND <sup>a</sup>     | 29                               | 5                                |

<sup>a</sup> Not detected.

<sup>b</sup> Taken as the temperature at the peak of the major melting transition in the second heating scan.

<sup>c</sup> Taken as the temperature at the peak of the major crystallization transition in the second cooling scan.

#### **4. Morphology of the hydrogenated polymers**

The crystalline phase in the hydrogenated polymers was directly observed by polarized optical microscopy. After being melted and hot pressed between two glass slides, the hydrogenated polymer films were allowed to cool. At room temperature, crystalline regions were seen to form slowly in the thin polymer films. As the polarized light optical micrograph of **PH2H** shows in **Figure 33**, this hydrogenated polymer consisted of scattered crystalline domains after extended cooling at room temperature. The typical Maltese cross pattern

4  $\mu\text{m}$



**Figure 33.** Polarized light optical micrograph of PH2H.

4  $\mu\text{m}$

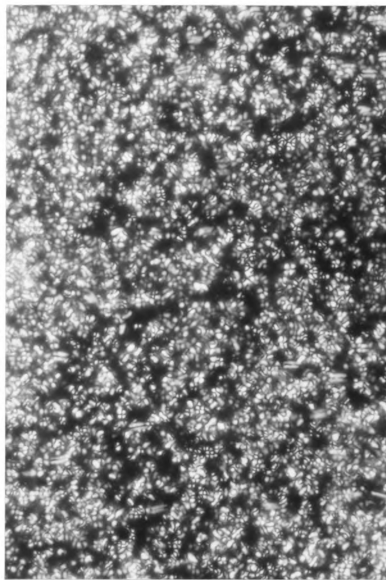


**Figure 34.** Polarized light optical micrograph of **PH3H**.

W  
T  
W  
S

was observed, indicating the formation of spherulites in the crystalline polymer.

The cross pattern is more easily seen in the micrograph of **PH3H (Figure 34)**, which showed better developed spherulites. The same characteristics were also seen in the micrographs of **PH4H** and **PH5H**.

#### IV. Polymer Electrolytes Based on the Unsaturated Polymers

Polymer electrolytes formed from the unsaturated polymers **PP2**, **PP3**, **PP4**, **PH3**, **PH4** and **PH5** with various  $\text{LiClO}_4$  contents were studied. Thermal properties of these polymer electrolytes were examined by DSC analysis, and their ionic conductivities were measured by impedance spectroscopy over the temperature range of 20 to 100 °C.

##### 1. Thermal behavior of the polymer electrolytes

DSC analysis of the polymer electrolytes was performed in the same way as for the unsaturated polymers. The second heating scans of **PP2** and its  $\text{LiClO}_4$  salt complexes at different salt concentrations are compiled in **Figure 35**. The DSC curves show a glass transition for each sample that increases with increasing salt concentration in the sample (**Figure 36**). No other thermal transition was observed for these samples, indicating **PP2**-salt complexes are amorphous in the salt concentration range studied.

The DSC curves recorded for amorphous polymer **PP3** and its salt complexes are shown in **Figure 37**. Similar to polymer electrolytes from **PP2**, the glass transition was the only thermal transition observed for electrolytes from **PP3**. These polymer-salt complexes exhibited higher  $T_g$ 's for higher salt contents (**Figure 38**).

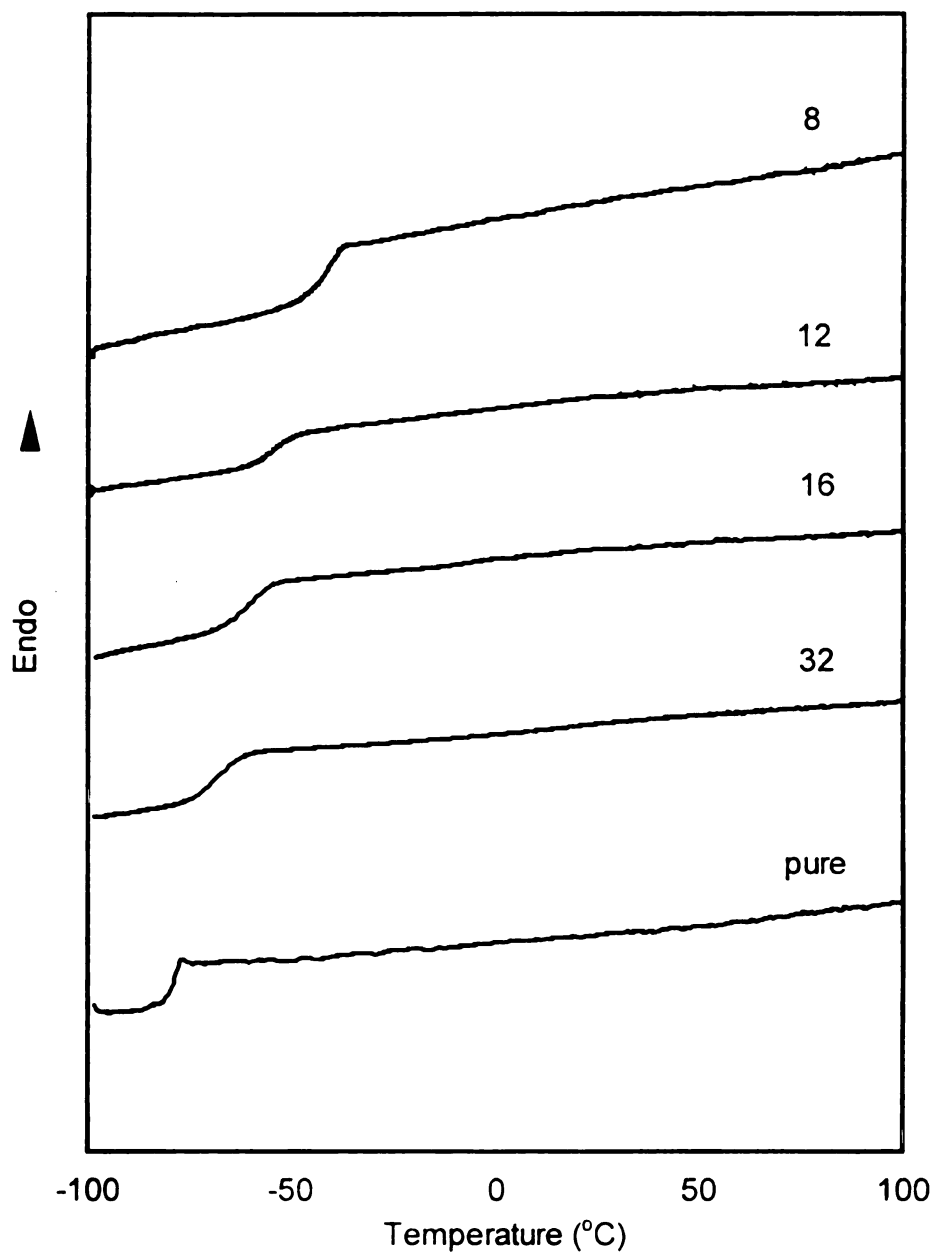


**Figure 35.** 2nd heating DSC scans of PP2 and its LiClO<sub>4</sub> salt complexes at different salt concentrations. Numbers refer to molar O:Li ratios for each sample. Heating rate is 10 °C/min.

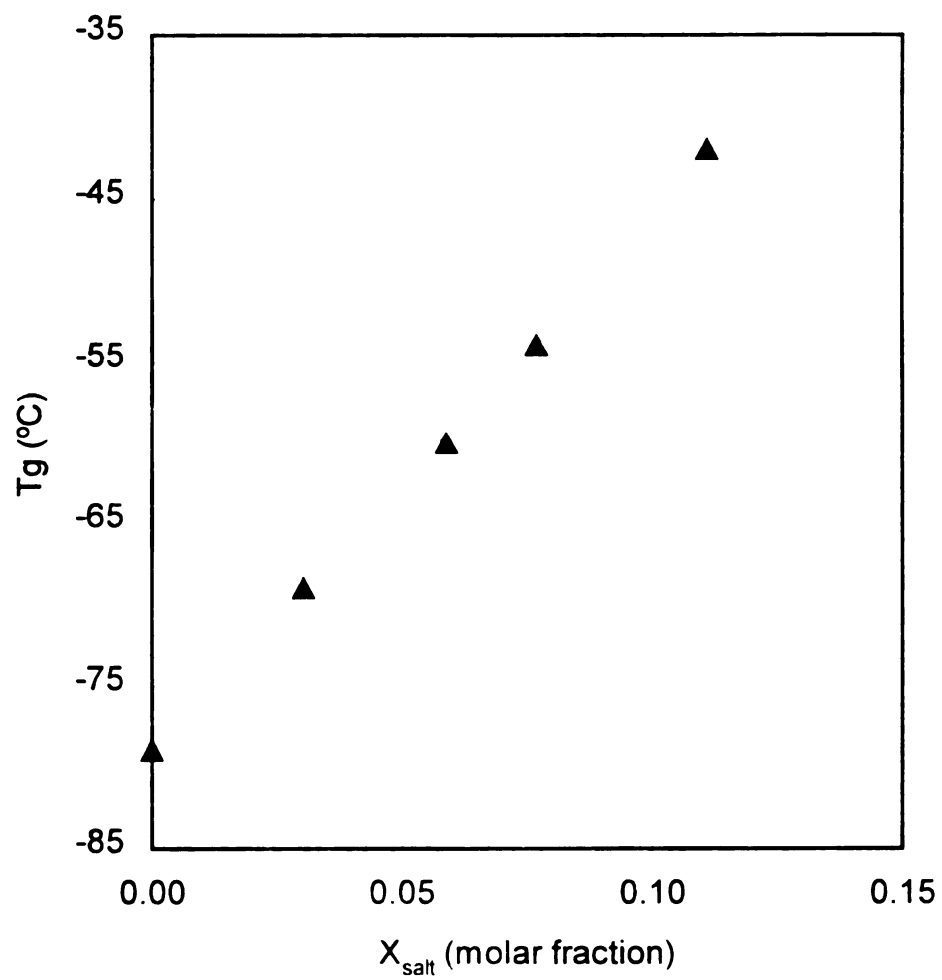


**Figure 36**  $T_g$  as a function of the salt molar fraction for PP2-salt complexes.

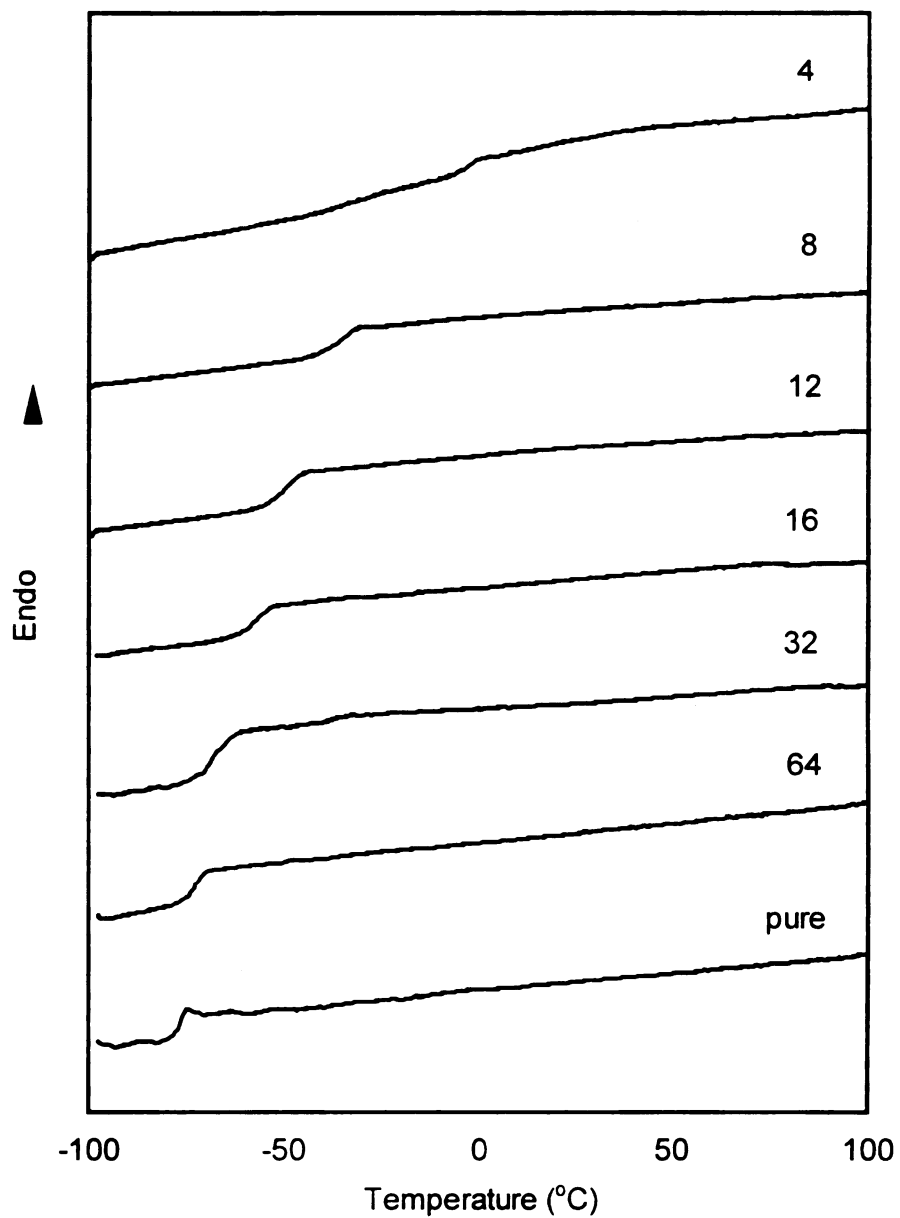


**Figure 37.** 2nd heating DSC scans of **PP3** and its  $\text{LiClO}_4$  salt complexes at different salt concentrations. Numbers refer to molar O:Li ratios for each sample. Heating rate is  $10\text{ }^\circ\text{C}/\text{min}$ .

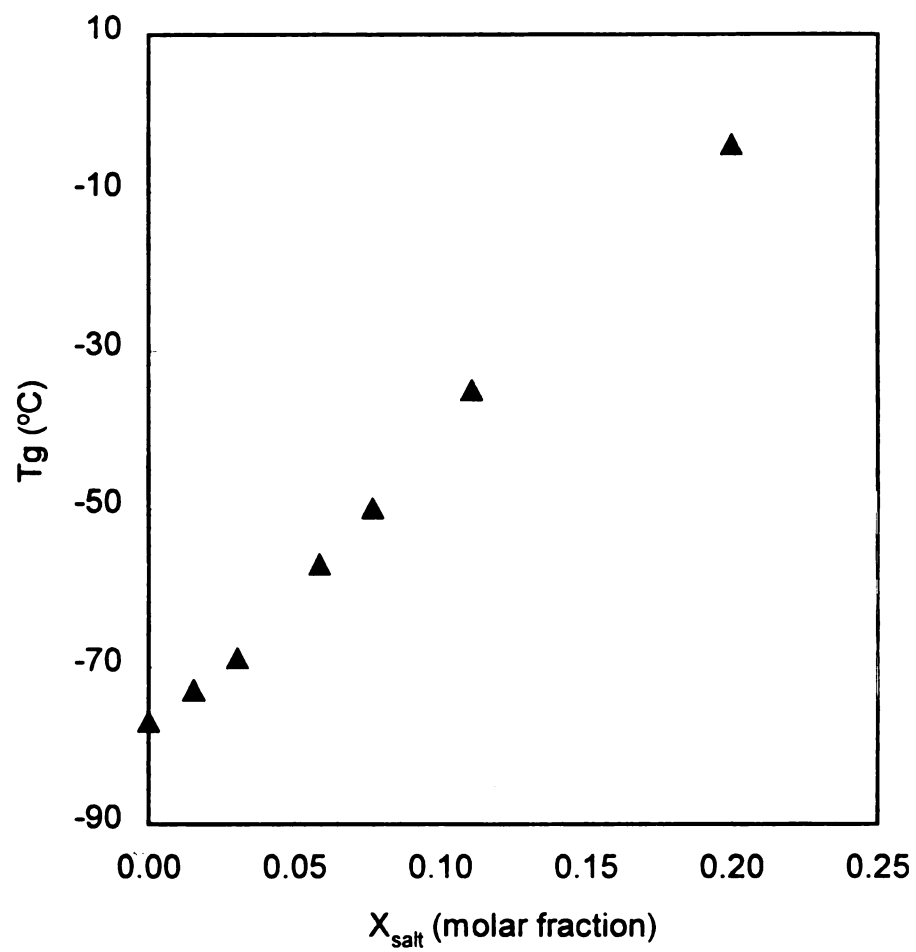


**Figure 38**  $T_g$  as a function of the salt molar fraction for **PP3**-salt complexes.

PP4

disp

displ

howe

of sa

is am

low te

the p

displa

comp

seen

follow

64). h

crysta

lowere

crystal

temper

PH3. V

corresp

The cor

transiti

**Figure 39** depicts the second heating DSC scans of polymer **PP4** and **PP4- LiClO<sub>4</sub>** salt complexes. As for **PP2** and **PP3**, polymer electrolytes from **PP4** displayed increasing  $T_g$ s as the salt concentration increased (**Figure 40**). **PP4** displayed interesting multiple melting and crystallization transitions above its  $T_g$ , however, none of these thermal transitions appeared in the DSC measurements of salt complexes from **PP4**. Even the **PP4**-salt complex with an O:Li ratio of 64 is amorphous, suggesting the crystalline phase present in the pure polymer at low temperature can easily be eliminated by dissolving a small amount of salt in the polymer.

The second DSC heating scans of **PH3** and its salt complexes are displayed in **Figure 41**. As increasing amounts of salt are dissolved in the complexes, their  $T_g$  values increase accordingly (**Figure 42**), the same trend seen in previous cases. Pure **PH3** shows a crystallization transition peak followed by two melting peaks. The thermal behavior of its salt complex (O:Li = 64), however, was affected by the presence of salt. Compared with **PH3**, the crystallization peak shifted to a higher temperature, while the peak intensity lowered, indicating increased difficulty for crystallization and a decreased overall crystallinity. The melting peaks decreased as well, but the corresponding temperatures stayed the same, suggesting that the crystalline phase was pure **PH3**. When the molar O:Li ratio is 32 in the salt complex, only small bumps corresponding to crystallization and melting were seen in the DSC heating scan. The complexes become totally amorphous and free of crystallization and melting transitions when the O:Li ratio is 16 and lower.

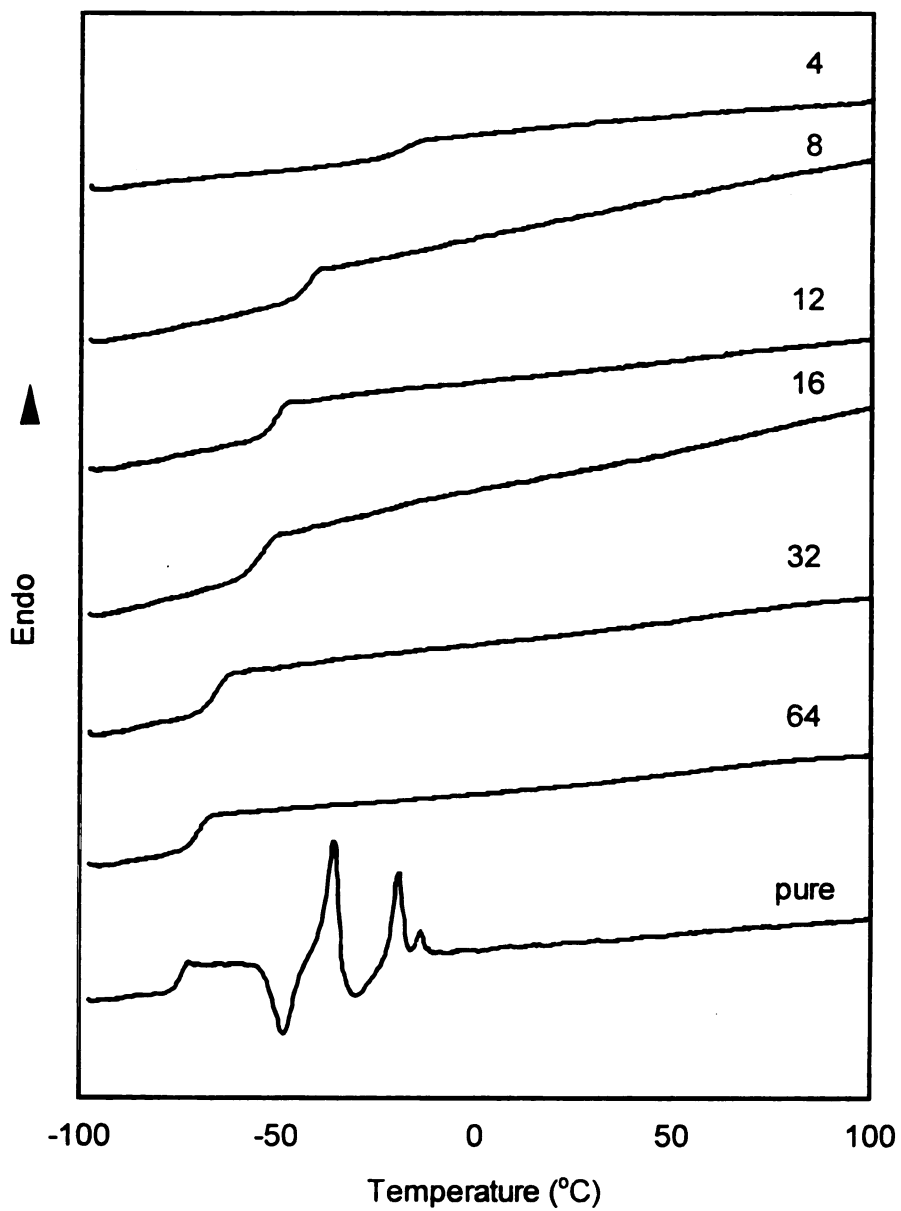


**Figure 39.** 2nd heating DSC scans of PP4 and its LiClO<sub>4</sub> salt complexes at different salt concentrations. Numbers refer to molar O:Li ratios for each sample. Heating rate is 10 °C/min.

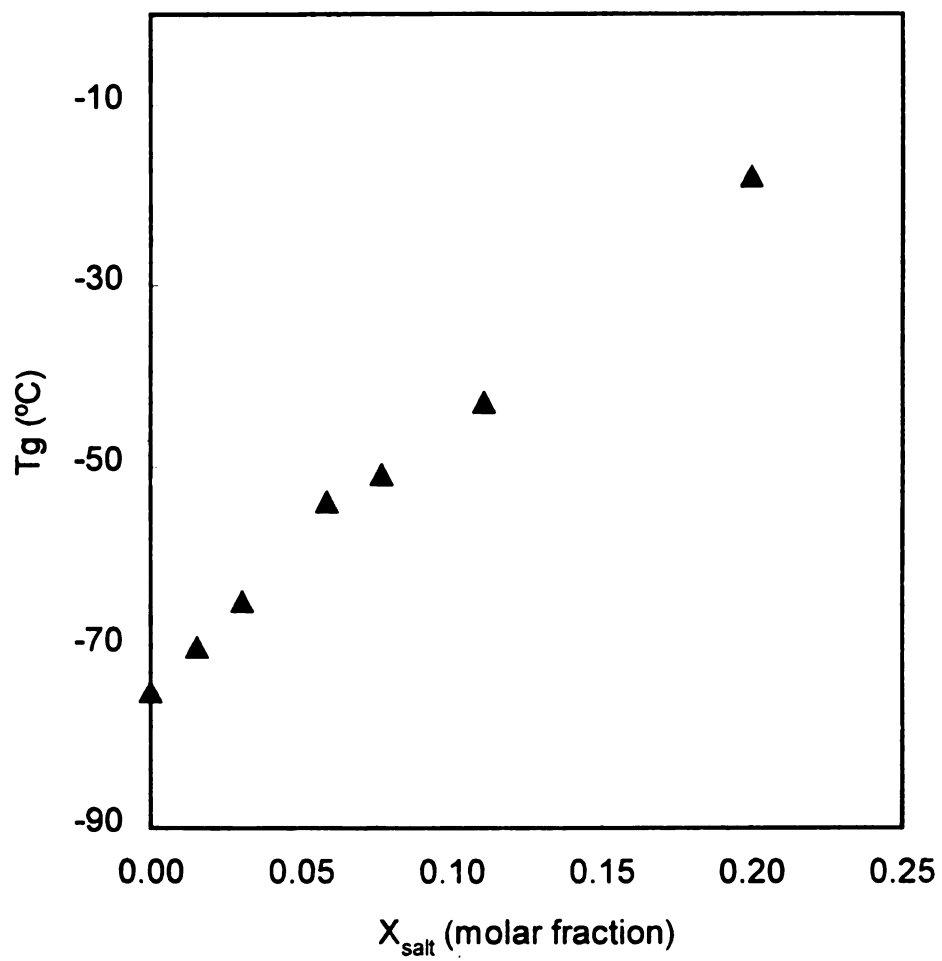


**Figure 40.**  $T_g$  as a function of the salt molar fraction for **PP4**-salt complexes.

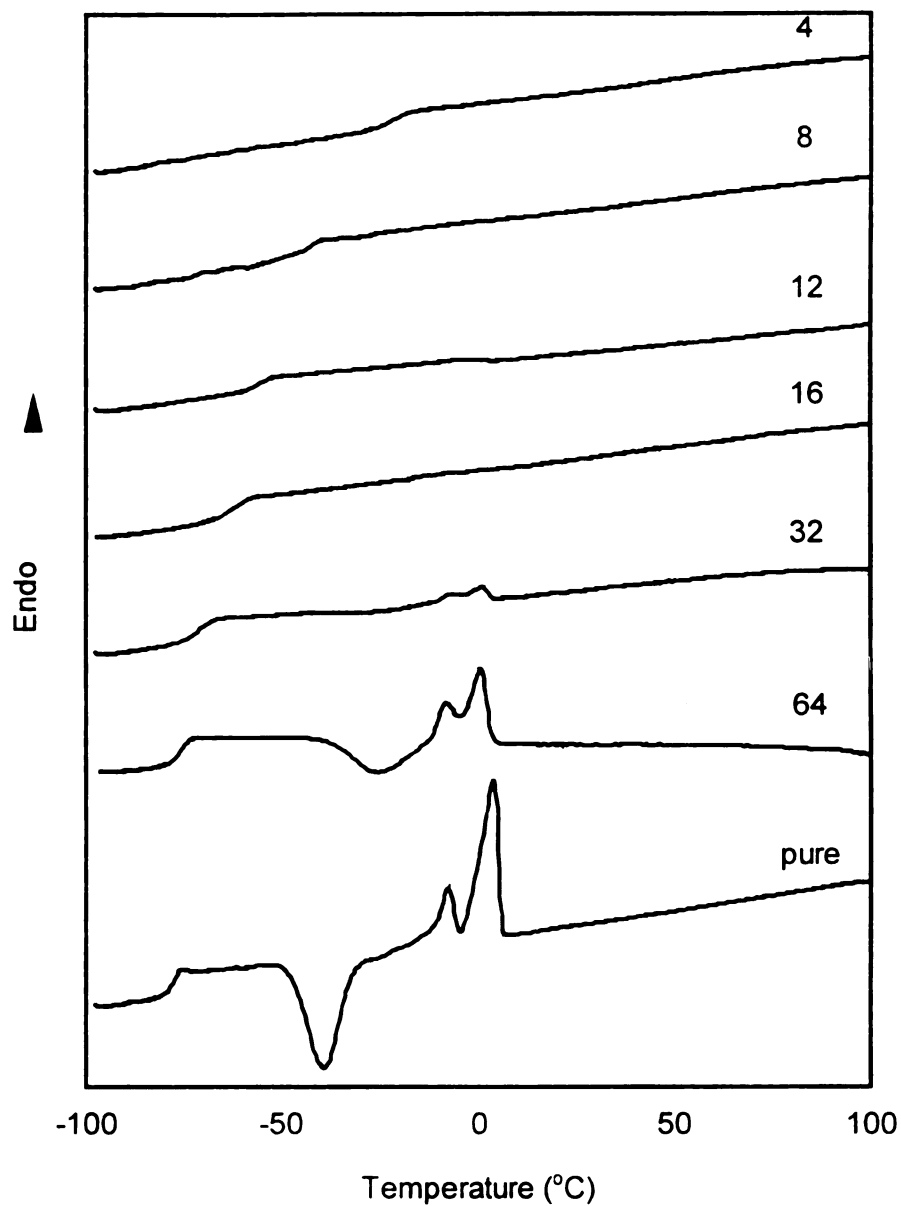


**Figure 41.** 2nd heating DSC scans of PH<sub>3</sub> and its LiClO<sub>4</sub> salt complexes at different salt concentrations. Numbers refer to molar O:Li ratios for each sample. Heating rate is 10 °C/min.

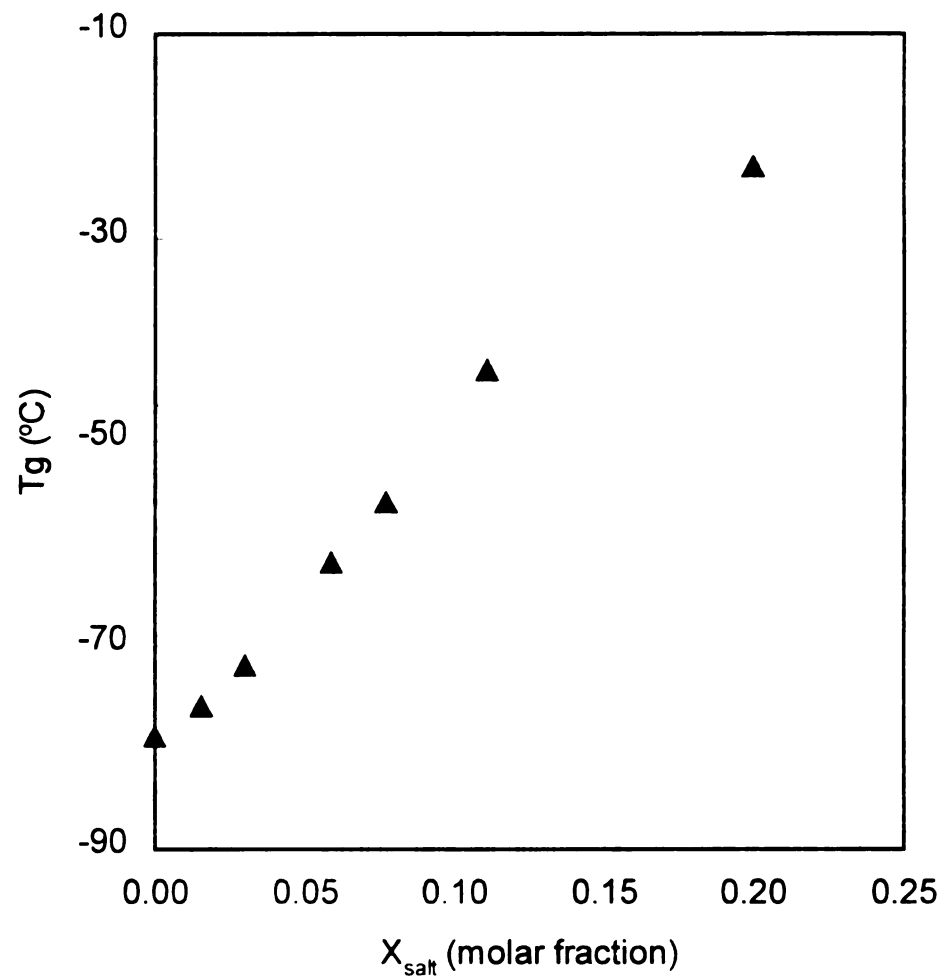


**Figure 42.**  $T_g$  as a function of the salt molar fraction for PH3-salt complexes.

**Figure 43** includes the second heating DSC curves of **PH4** and polymer electrolytes from **PH4** at various salt concentrations. The common feature observed in the other polymer electrolytes is also seen in this figure: an increasing  $T_g$  for polymer electrolytes with higher salt content (**Figure 44**). In addition, the multiple crystallization and melting transitions seen in **PH4** were also found for **PH4**-salt complexes with O:Li ratios of 64, 48, and 32. The crystallization following the glass transition also moved to noticeably higher temperatures as the salt content increased. While the temperature at which the melting peaks appeared did not change appreciably, the intensity of the peaks decreased with decreasing O:Li ratios. Similar to electrolytes from **PH3**, the crystallization and melting transitions of **PH4** remained visible in DSC scans to O:Li ratios of 32, but for O:Li<24, the polymer electrolytes were amorphous and only glass transitions were observed.

The last polymer electrolytes studied by DSC were those from unsaturated polymer **PH5** and the results were plotted in **Figures 45** and **46**. Except for the detailed shapes of the melting and crystallization peaks, the results mirror those of **PH3** and **PH4**.

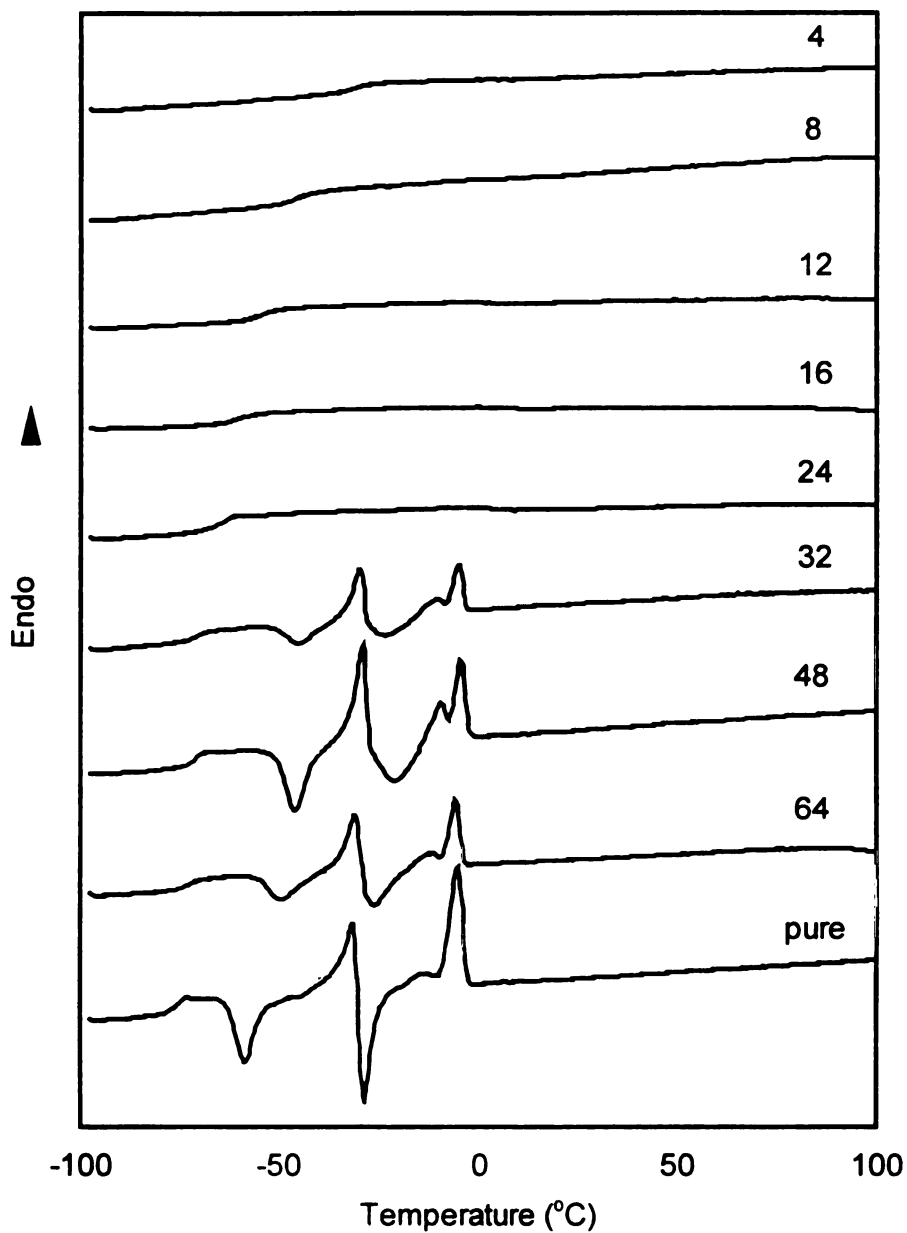


**Figure 43.** 2nd heating DSC scans of PH4 and its LiClO<sub>4</sub> salt complexes at different salt concentrations. Numbers refer to molar O:Li ratios for each sample. Heating rate is 10 °C/min.

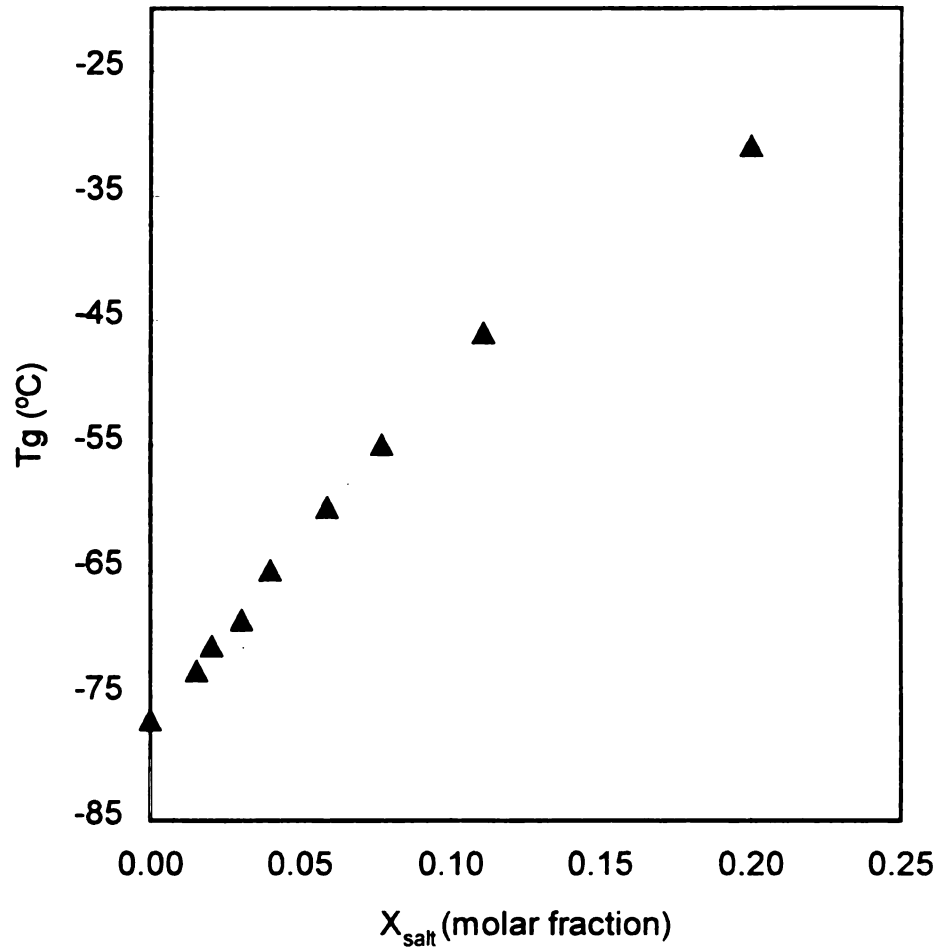


**Figure 44.**  $T_g$  as a function of the salt molar fraction for PH4-salt complexes.

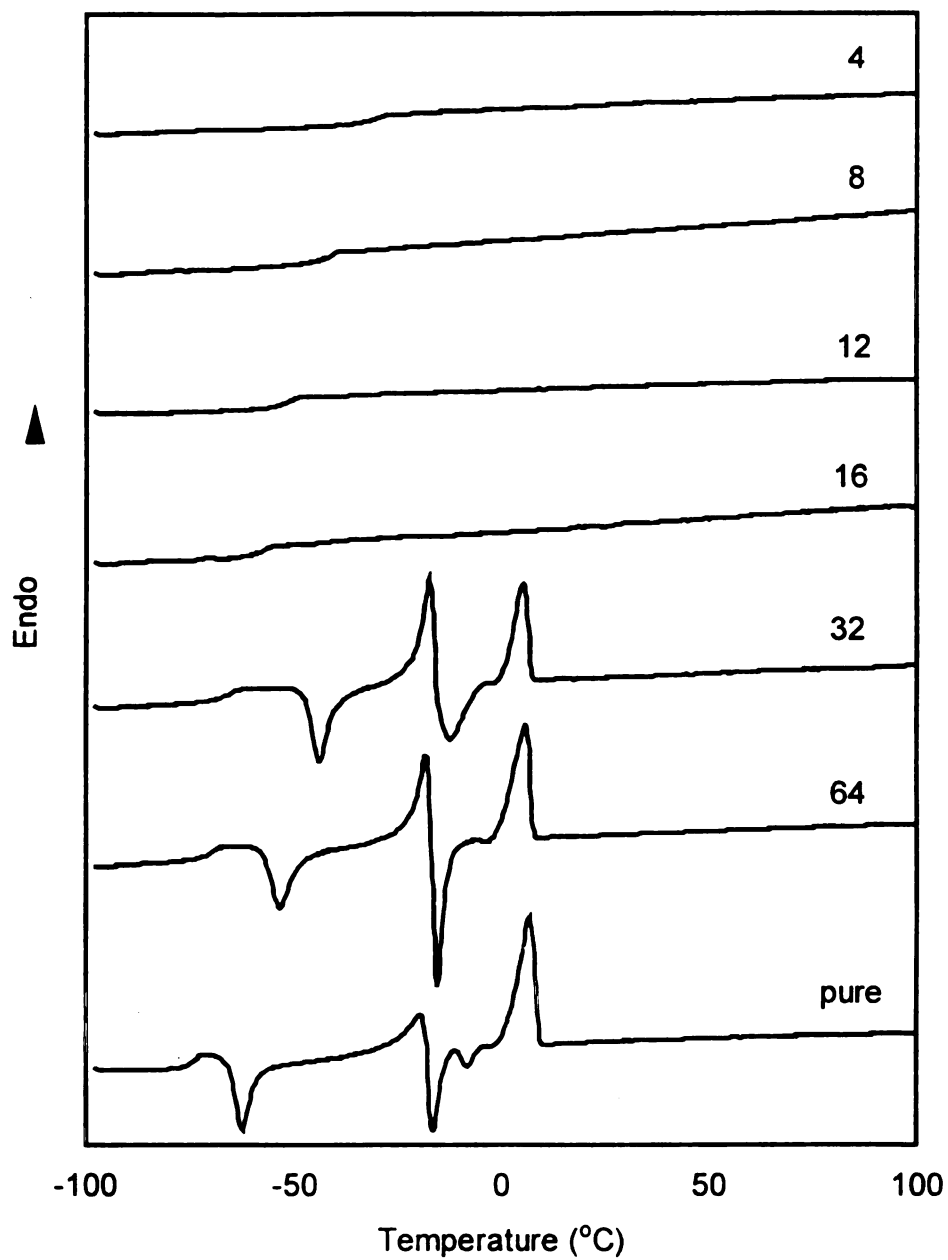


**Figure 45.** 2nd heating DSC scans of PH5 and its LiClO<sub>4</sub> salt complexes at different salt concentrations. Numbers refer to molar O:Li ratios for each sample. Heating rate is 10 °C/min.

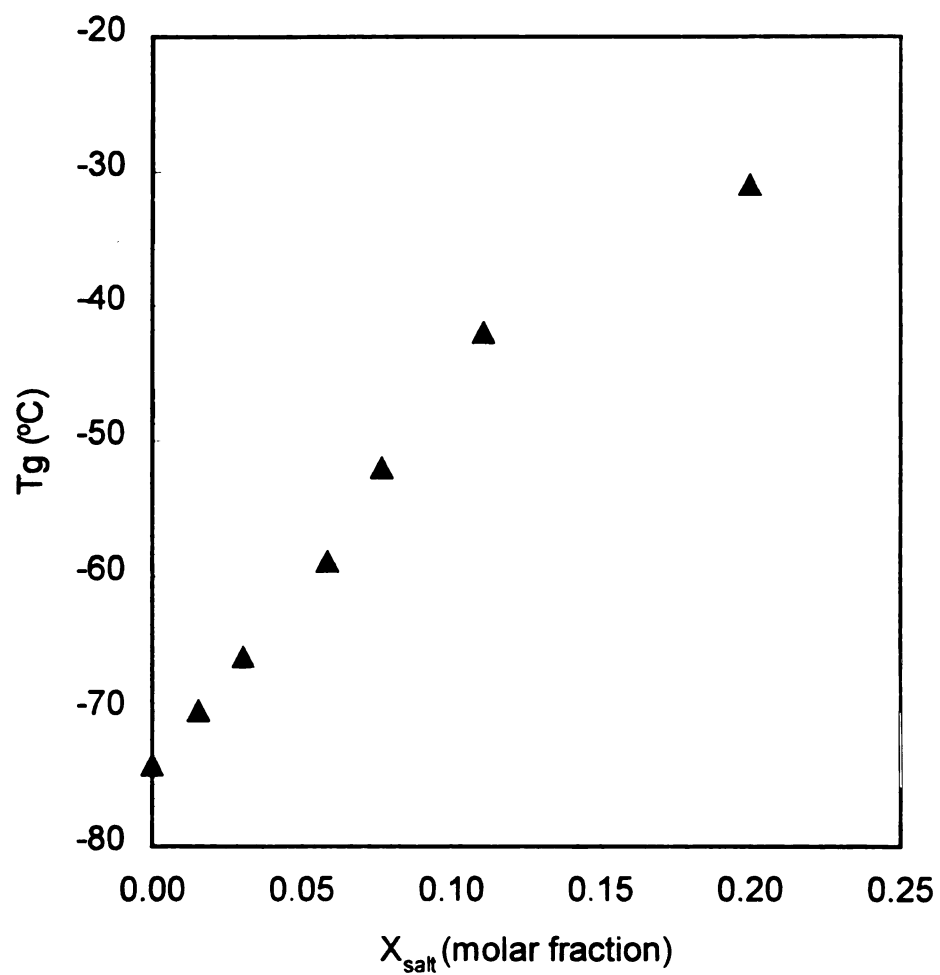


**Figure 46.**  $T_g$  as a function of the salt molar fraction for PH5-salt complexes.

## 2. Impedance spectroscopy of the polymer electrolytes

Impedance spectroscopy measurements were used to measure the ionic conductivities of the unsaturated polymer electrolytes at different temperatures. At each temperature, both the real and imaginary components of a sample's impedance were obtained over the frequency range of 5 Hz to 10 MHz. The plot of the imaginary impedance vs. the real impedance resulted in a complex impedance diagram, as exemplified in **Figure 47**. This complex impedance diagram, obtained for a **PP4**-salt complex (O:Li = 4) at 50 °C, is composed of an arc that describes the complex impedance of the sample cell at high frequencies, and a linear spike following the arc that corresponds to the impedance at low frequency. The intercept of that line on the real axis, 7.2 K $\Omega$ , was taken as the bulk resistance of the electrolyte cell. As the dimensions of the cell were known, the conductivity of **PP4**-salt complex (O:Li = 4) at 50 °C could be derived by simple calculation.

**Figure 48** shows the complex impedance diagram for a **PH4**-salt complex (O:Li = 32) at 30 °C. The arc in this figure is incomplete near the origin, because the upper frequency limit of the measurement was too low to obtain the complex impedance in that region. This phenomenon is usually seen when the bulk impedance of the sample is small, but it does not affect the extrapolation of the linear portion of the data. From the intercept on the real axis, a bulk resistance of 2.2 K $\Omega$  was obtained for this sample.

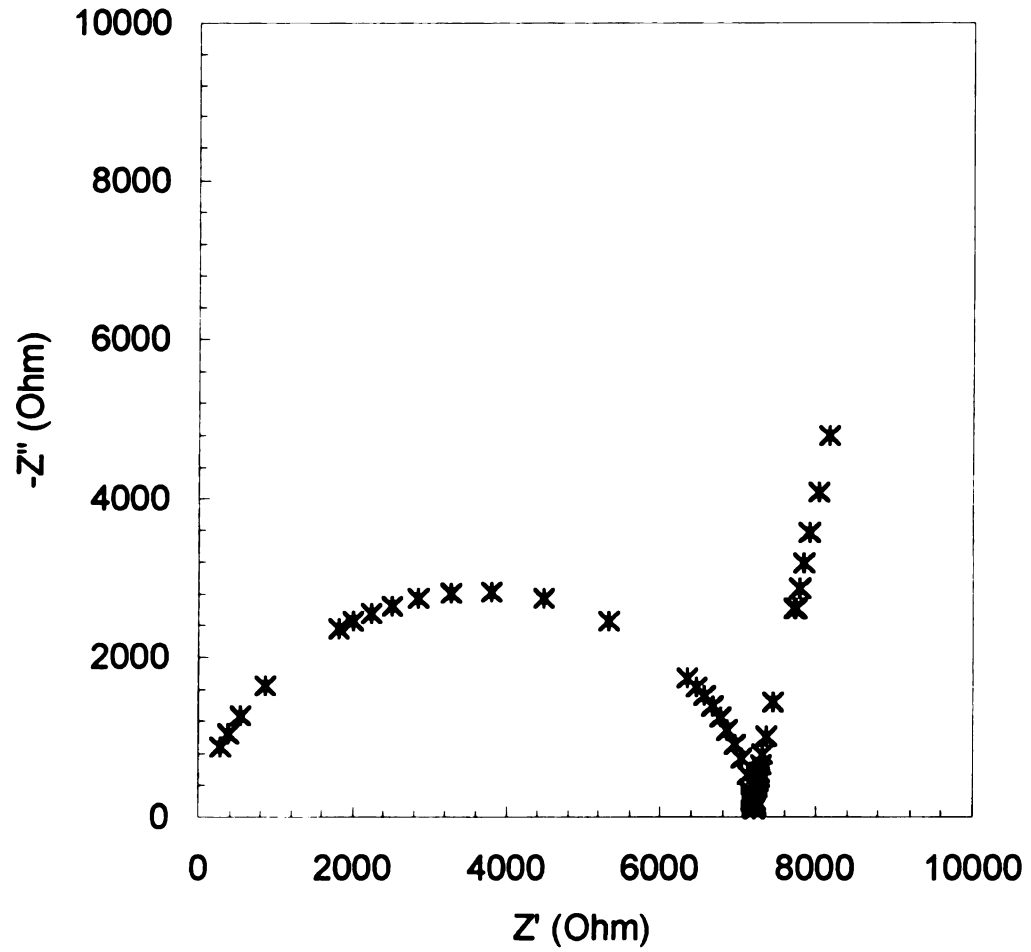


**Figure 47.** Complex impedance diagram for **PP4**-salt complex (O:Li = 4) at 50 °C.

Fig

C.

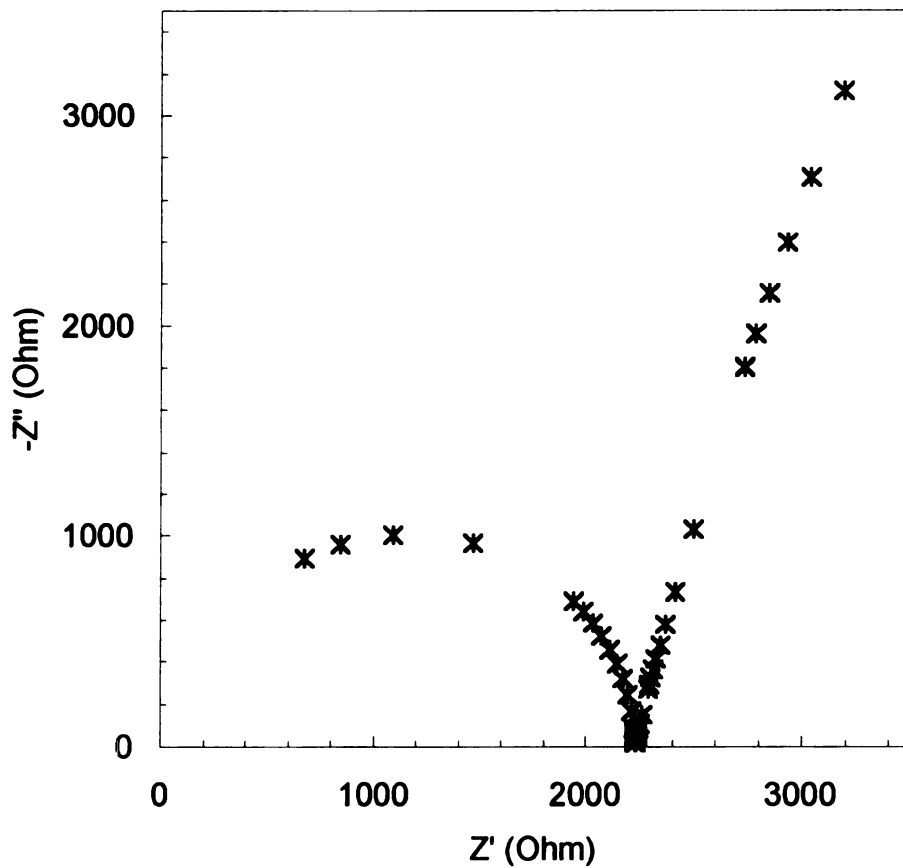


**Figure 48.** Complex impedance diagram for PH4-salt complex (O:Li = 32) at 30 °C.

c

s

c

Ti

°C

2.0

incr

conc

of 12

movi

tempe

and 50

The ionic conductivities of the unsaturated polymer-salt complexes at various temperatures appear in the Appendix.

### 3. Conductivity behavior of the polymer electrolytes

The effects of salt concentration and temperature on ionic conductivity of the unsaturated polymer-LiClO<sub>4</sub> complexes were examined. **Figures 49-54** display the results for the **PP2, PP3, PP4, PH3, PH4, and PH5** salt complexes. At each temperature, for example, 20 °C, the conductivity increases as the salt content in the electrolyte increases. After reaching a maximum, the conductivity decreases with further increases in salt content. The conductivity also shows strong dependence on the temperature. The conductivity of all salt concentrations increases systematically as a result of increased temperature. The peak conductivity for electrolyte from **PP2 (Figure 49)** is  $7.9 \times 10^{-6}$  S/cm at 20 °C, increases to  $3.5 \times 10^{-5}$  S/cm at 50 °C, and reaches  $1.7 \times 10^{-4}$  S/cm at 100 °C.

For **PP3 (Figure 50)** the room temperature conductivity maximum of  $2.0 \times 10^{-5}$  S/cm was achieved with a molar O:Li ratio of 12. This conductivity increased to  $7.9 \times 10^{-5}$  S/cm at 50 °C, and  $4.1 \times 10^{-4}$  S/cm at 100 °C. Although the conductivity maximum was obtained at almost the same salt content (O:Li ratio of 12) for all three temperatures, the peak conductivity shows a tendency of moving toward higher salt concentration. It is also interesting to see that as the temperature increases, the conductivity peak becomes broader.

The conductivity of **PP4**-salt complex as a function of salt content at 20 °C and 50 °C are shown in **Figure 51**. The conductivity of an amorphous PEO-

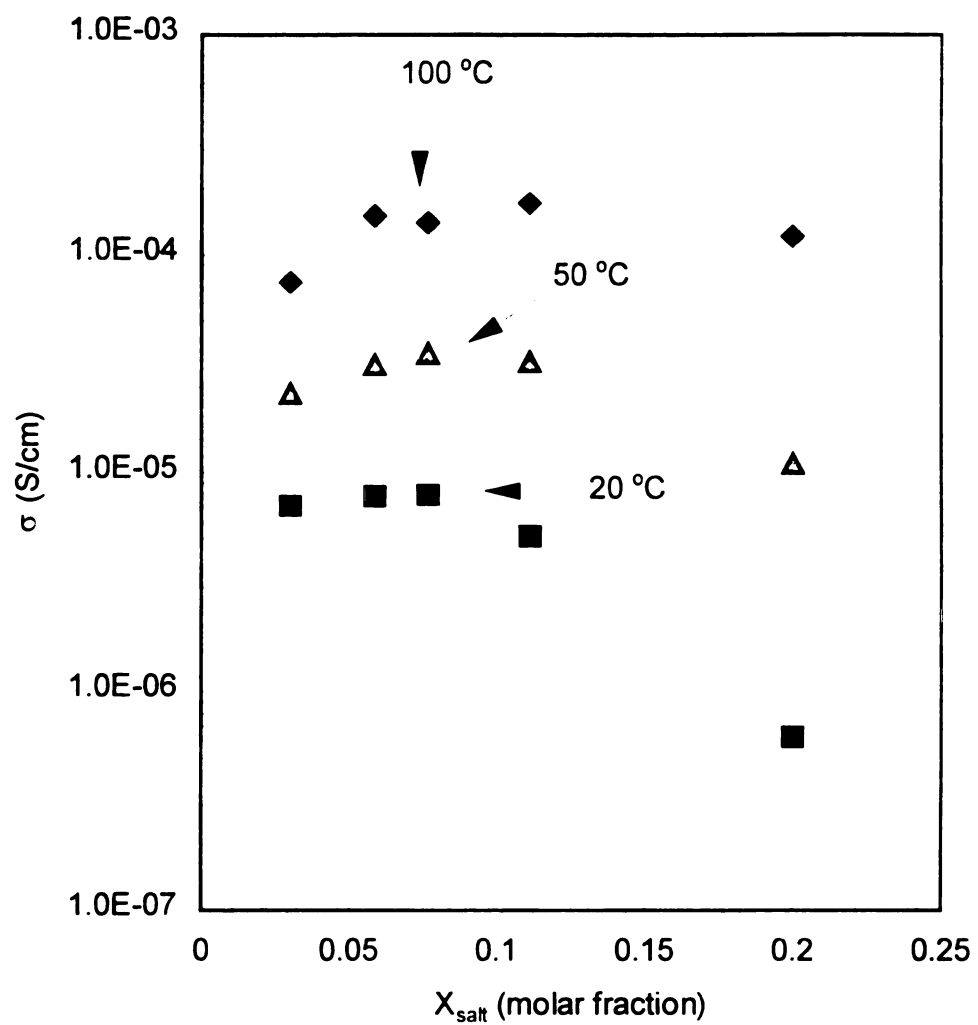


**Figure 49.** Conductivity of PP2-LiClO<sub>4</sub> complexes as a function of salt content at 20 °C, 50 °C and 100 °C.

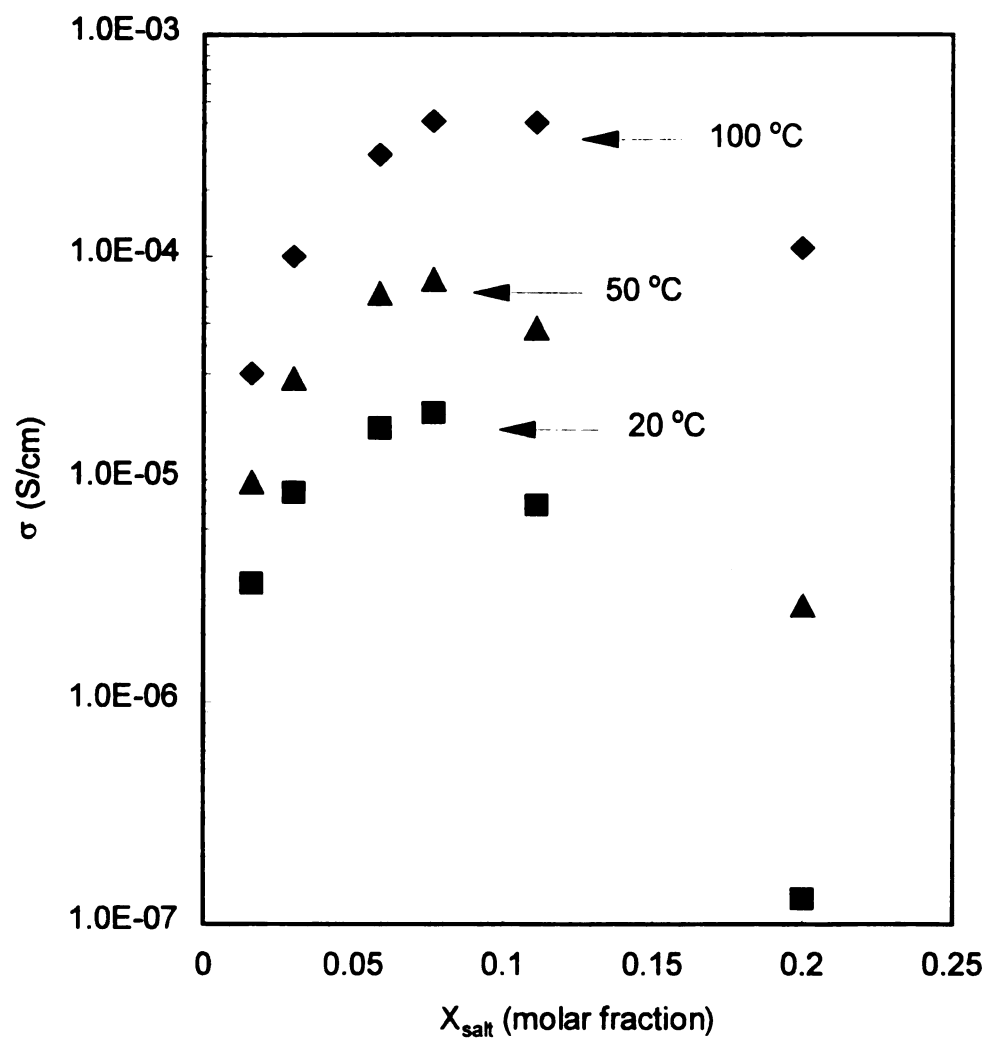


**Figure 50.** Conductivity of PP3-LiClO<sub>4</sub> complexes as a function of salt content at 20 °C, 50 °C and 100 °C.

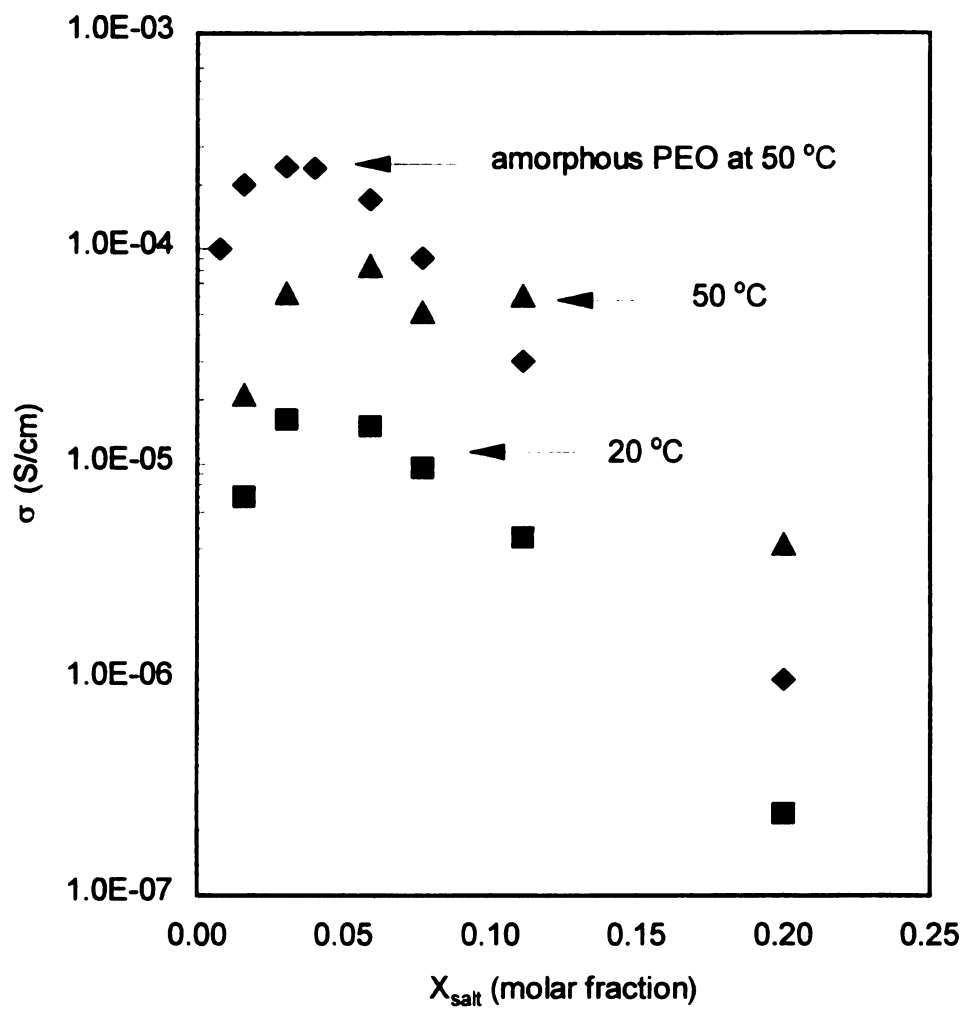


**Figure 51.** Conductivity of electrolytes from PP4 and amorphous PEO as a function of salt content at 20 °C and 50 °C.

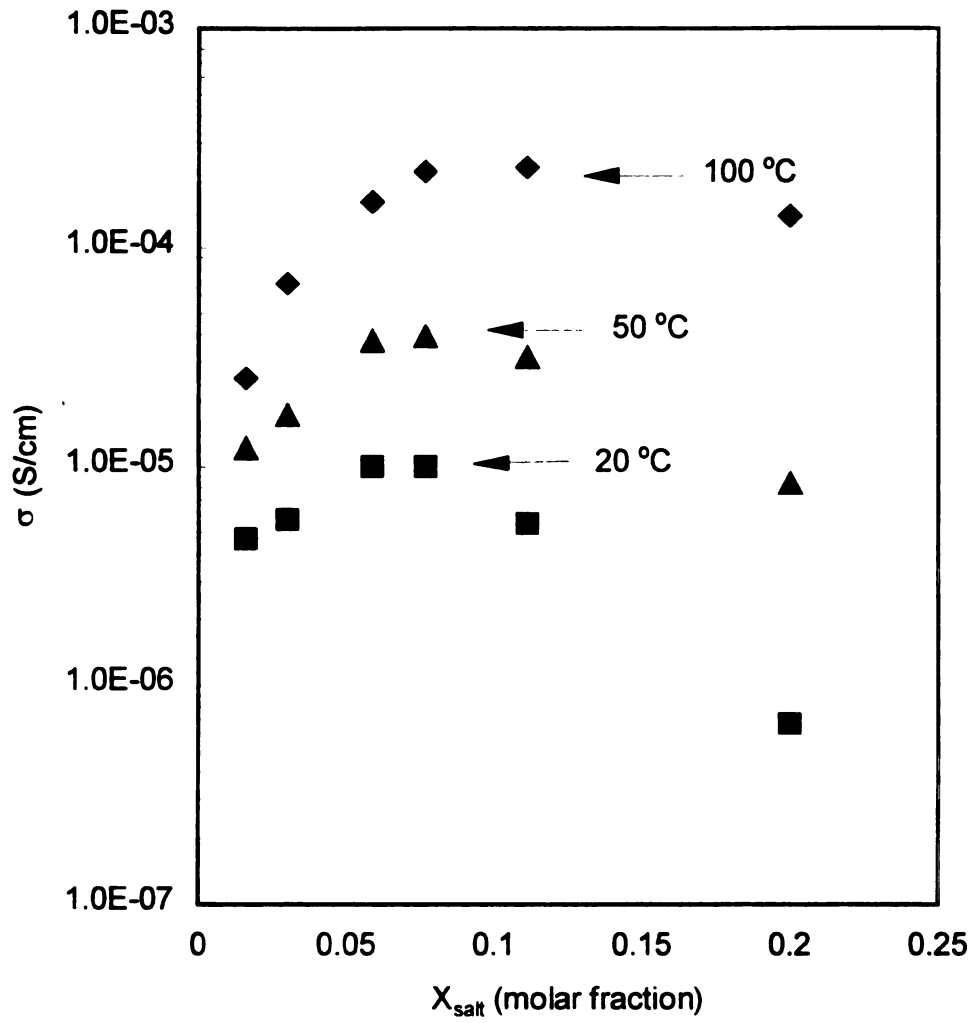


**Figure 52.** Conductivity of  $\text{PH}_3\text{-LiClO}_4$  complexes as a function of salt content at 20 °C, 50 °C and 100 °C.

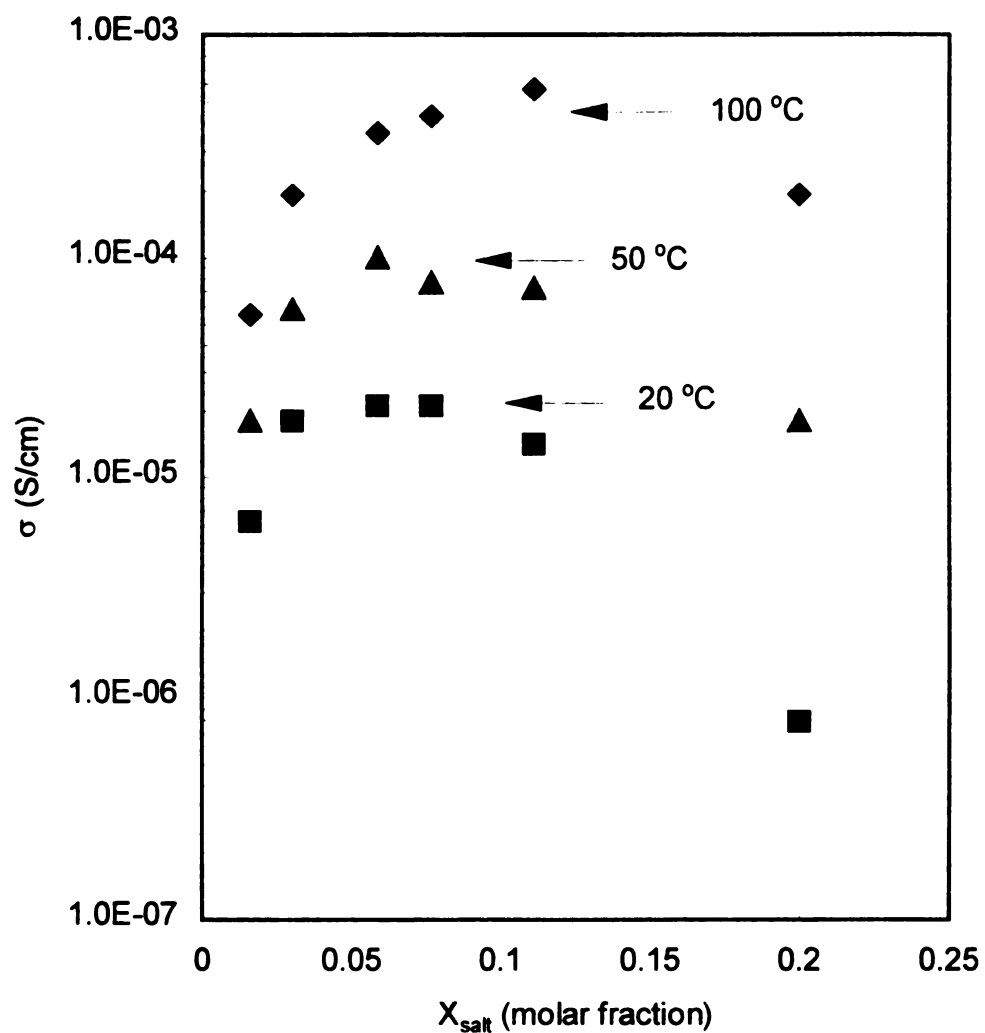


**Figure 53.** Conductivity of  $\text{PH}_4\text{-LiClO}_4$  complexes as a function of salt content at 20 °C, 50 °C and 100 °C.

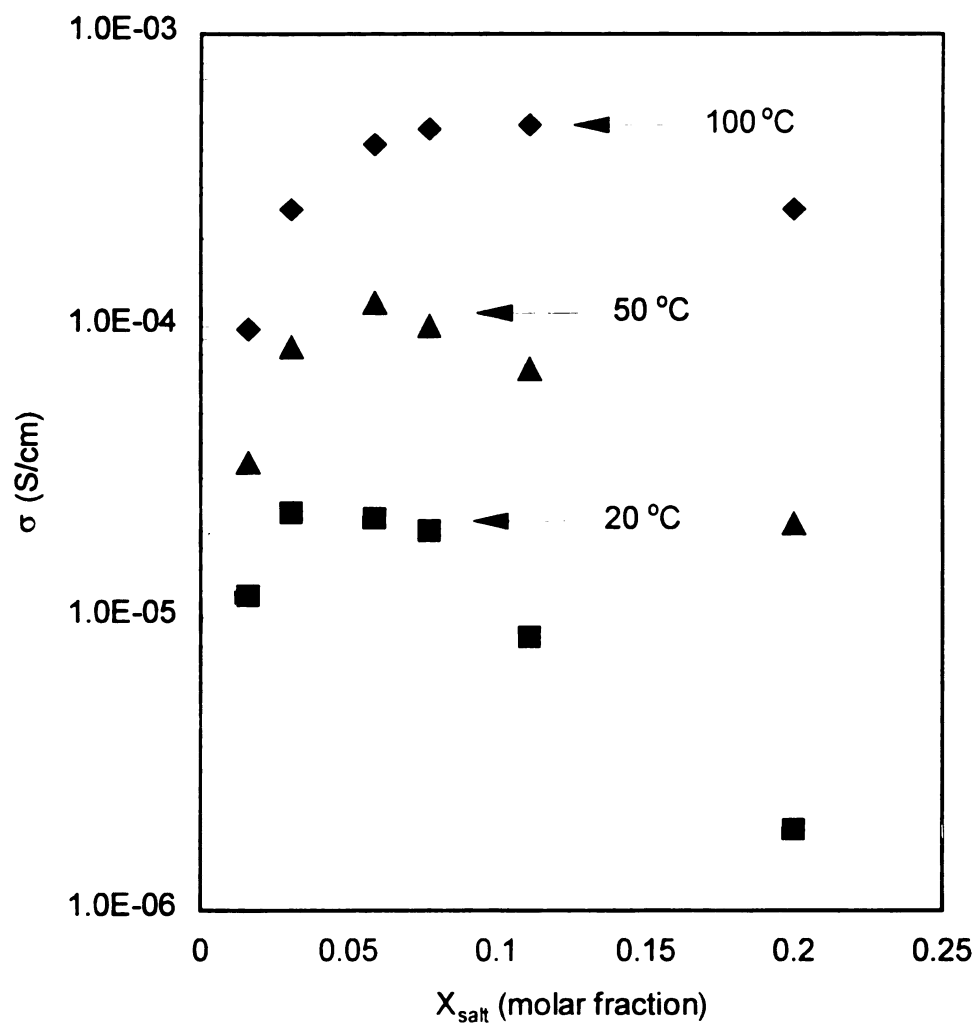


**Figure 54.** Conductivity of PH5-LiClO<sub>4</sub> complexes as a function of salt content at 20 °C, 50 °C and 100 °C.

$\text{LiClO}_4$  complex as a function of salt content at 50 °C is also included in the same figure. For **PP4**, the room temperature conductivity maximum was  $1.6 \times 10^{-5}$  S/cm at a molar O:Li ratio of 32, and  $8.3 \times 10^{-5}$  S/cm at 50°C with an O:Li ratio of 16. The highest conductivity of amorphous PEO electrolytes was reported to be  $2.4 \times 10^{-4}$  S/cm at 50 °C.<sup>9</sup> The conductivity of **PP4**-salt complexes at 50 °C is comparable to that of amorphous PEO- $\text{LiClO}_4$  complexes at the same temperature, but the peak conductivity was achieved at a higher O:Li ratio for **PP4**-salt complexes.

The salt concentration-dependent conductivity of **PH3**- $\text{LiClO}_4$  complexes is given in **Figure 52**. The dependence of conductivity on salt concentration observed for electrolytes from **PP2**, **PP3** and **PP4** holds for electrolytes from **PH3**. The peak conductivity at room temperature was found to be  $1.0 \times 10^{-5}$  S/cm for the sample with an O:Li ratio of 16. The peak value improved to  $3.9 \times 10^{-5}$  S/cm with an O:Li ratio of 12 at 50 °C. The highest conductivity for **PH3** electrolytes was obtained as  $2.3 \times 10^{-4}$  S/cm at 100 °C with an O:Li ratio of 8.

The relationship between conductivity of electrolytes from **PH4** and the salt concentration was also examined (**Figure 53**). For example, the peak conductivity of **PH4** electrolytes was determined to be  $2.1 \times 10^{-5}$  S/cm,  $1.0 \times 10^{-4}$  S/cm and  $5.7 \times 10^{-4}$  S/cm at 20 °C, 50 °C and 100 °C respectively.

As expected, the conductivity of electrolytes from **PH5** showed the same dependence on the salt concentration as observed for other electrolytes in this research (**Figure 54**). The conductivity maximum of electrolytes from **PH5** was determined to be  $2.3 \times 10^{-5}$  S/cm for an O:Li ratio of 32 at 20 °C,  $1.2 \times 10^{-4}$  S/cm for

an O:Li ratio of 16 at 50 °C, and  $4.9 \times 10^{-4}$  S/cm for an O:Li ratio of 8 at 100 °C respectively.

#### 4. Temperature dependent conductivity

The VTF equation has been commonly used to model the temperature dependent conductivity of polymer electrolytes.<sup>80</sup> Here we used the VTF equation to examine the relationship between the structure and conductivity of the unsaturated polymer-based electrolytes.

**Figure 55** shows the VTF plots for PP2-LiClO<sub>4</sub> complexes at four salt concentrations. The O:Li ratios are 32, 16, 12, and 4 respectively. Values of  $T_0$  were taken as the  $T_g$ 's of the corresponding electrolytes measured in the DSC studies. At each salt concentration, a linear relationship was well established between logarithm of the conductivity ( $\text{Log } \sigma$ ) and  $1/(T - T_0)$ , as predicted by the VTF equation. Although the four lines are not perfectly parallel to each other, they appear to have similar slopes (same activation energy), suggesting the conduction mechanism is the same in all samples.

**Figures 56-60** give the VTF plots for PP3, PP4, PH3, PH4 and PH5-LiClO<sub>4</sub> complexes. All plots of  $\text{Log } \sigma$  vs.  $1/(T - T_0)$  are linear, agreeing well with the VTF equation. In many cases, slopes of the samples from each polymer are found to have similar values.

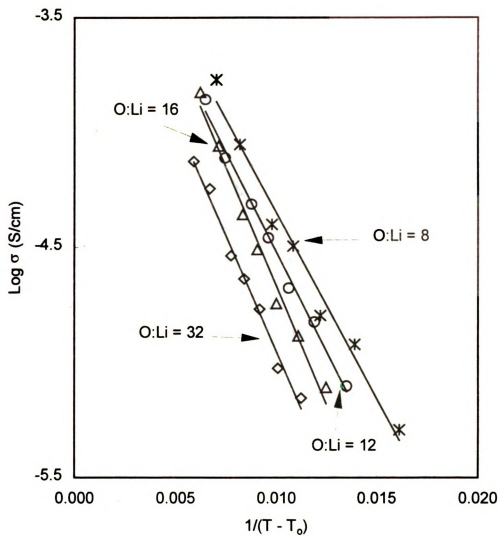


**Figure 55.** VTF plots for PP2-LiClO<sub>4</sub> complexes with O:Li ratio of 32, 16, 12, and

4.

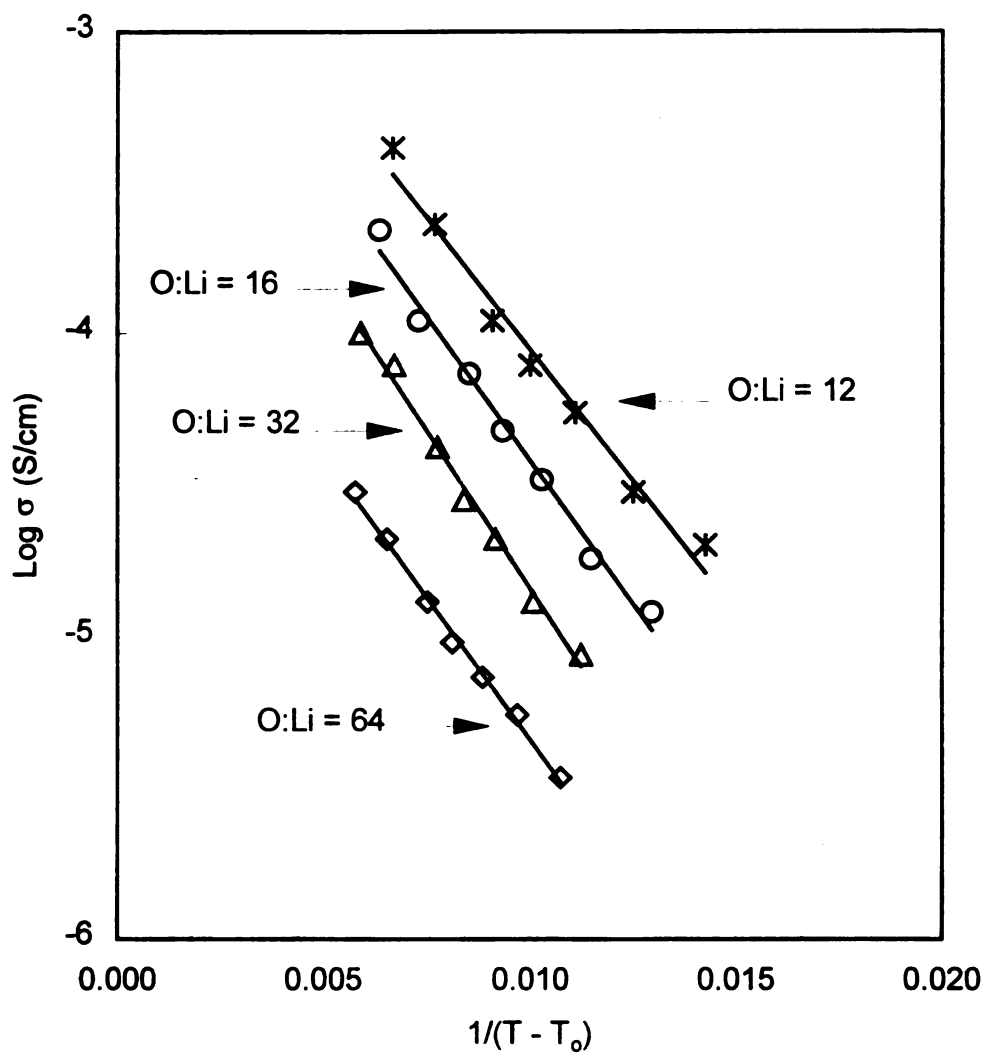


**Figure 56.** VTF plots for PP3-LiClO<sub>4</sub> complexes with O:Li ratio of 64, 32, 16, and 12.

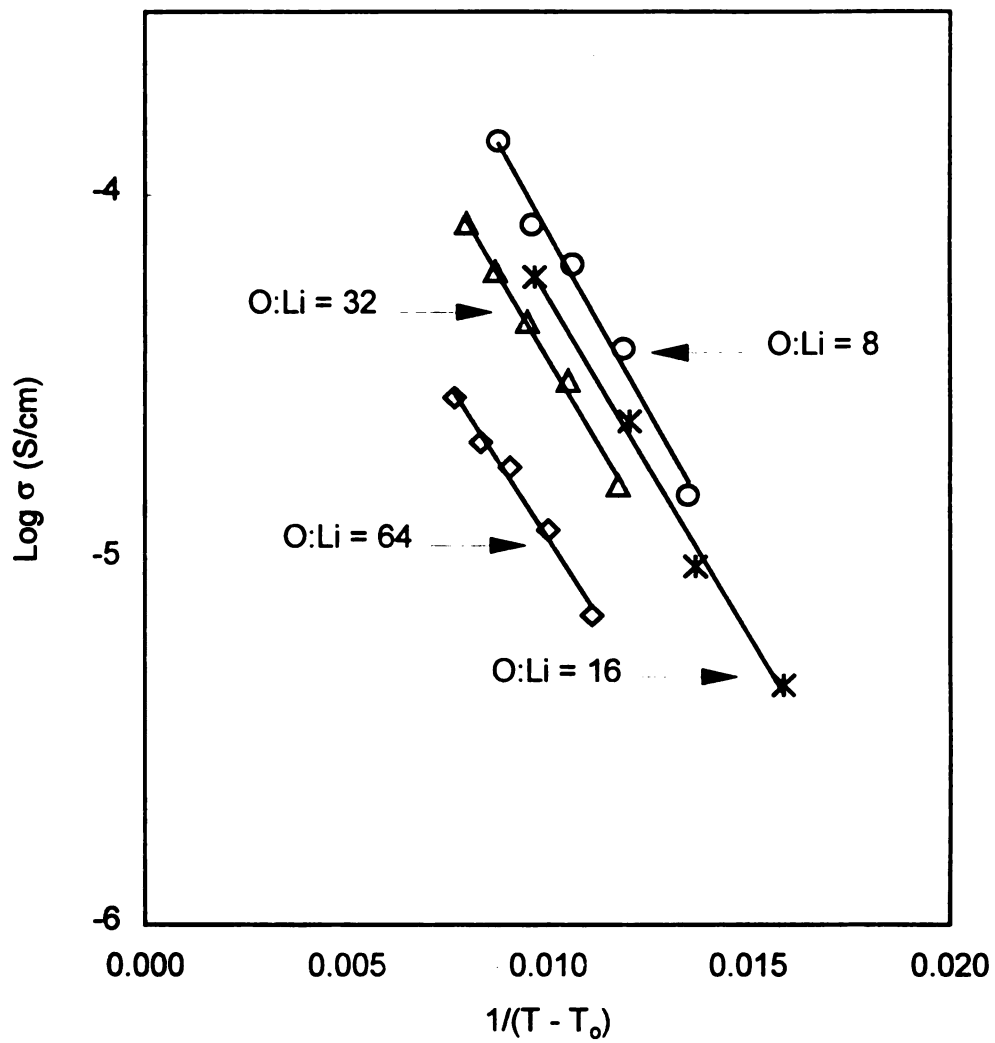


**Figure 57.** VTF plots for  $\text{PP}_4\text{-LiClO}_4$  complexes with O:Li ratio of 64, 32, 16, and 8.

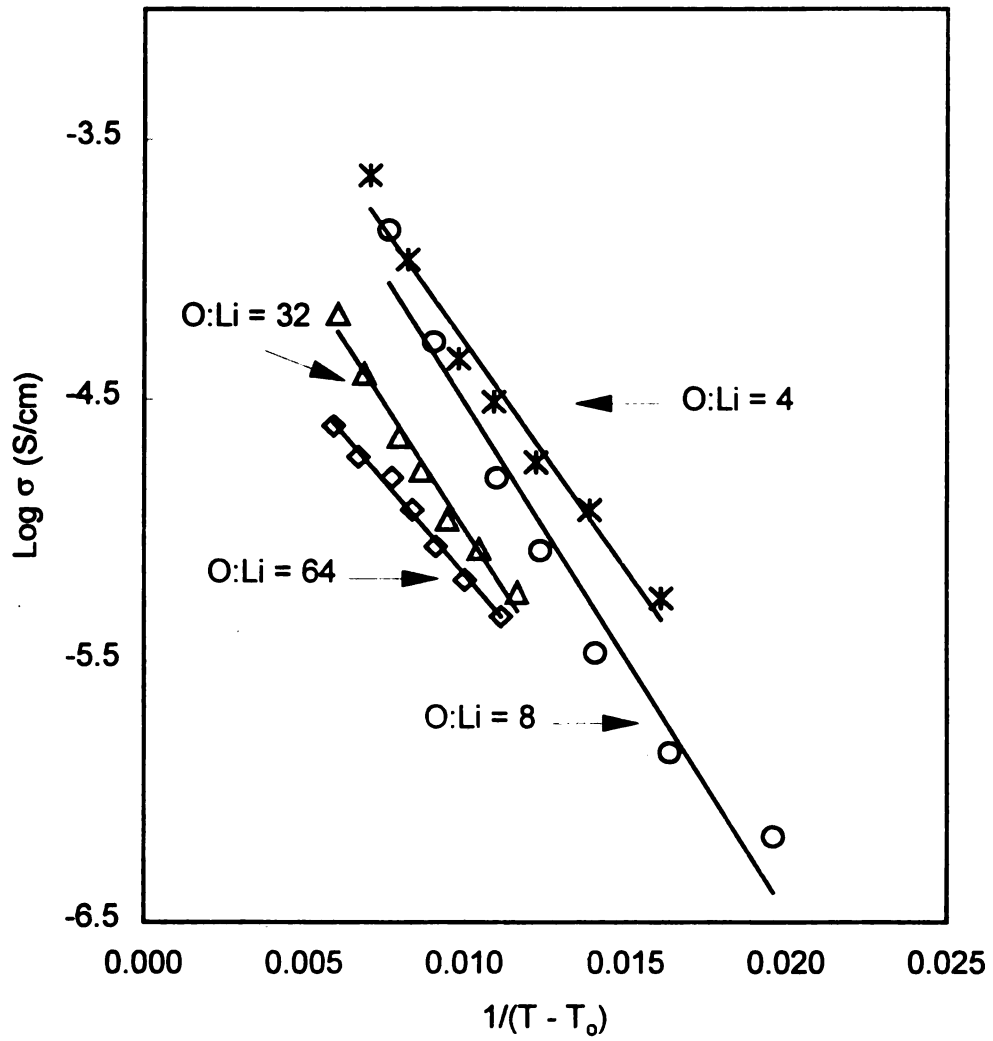


**Figure 58.** VTF plots for  $\text{PH}_3\text{-LiClO}_4$  complexes with O:Li ratio of 64, 32, 8, and 4.

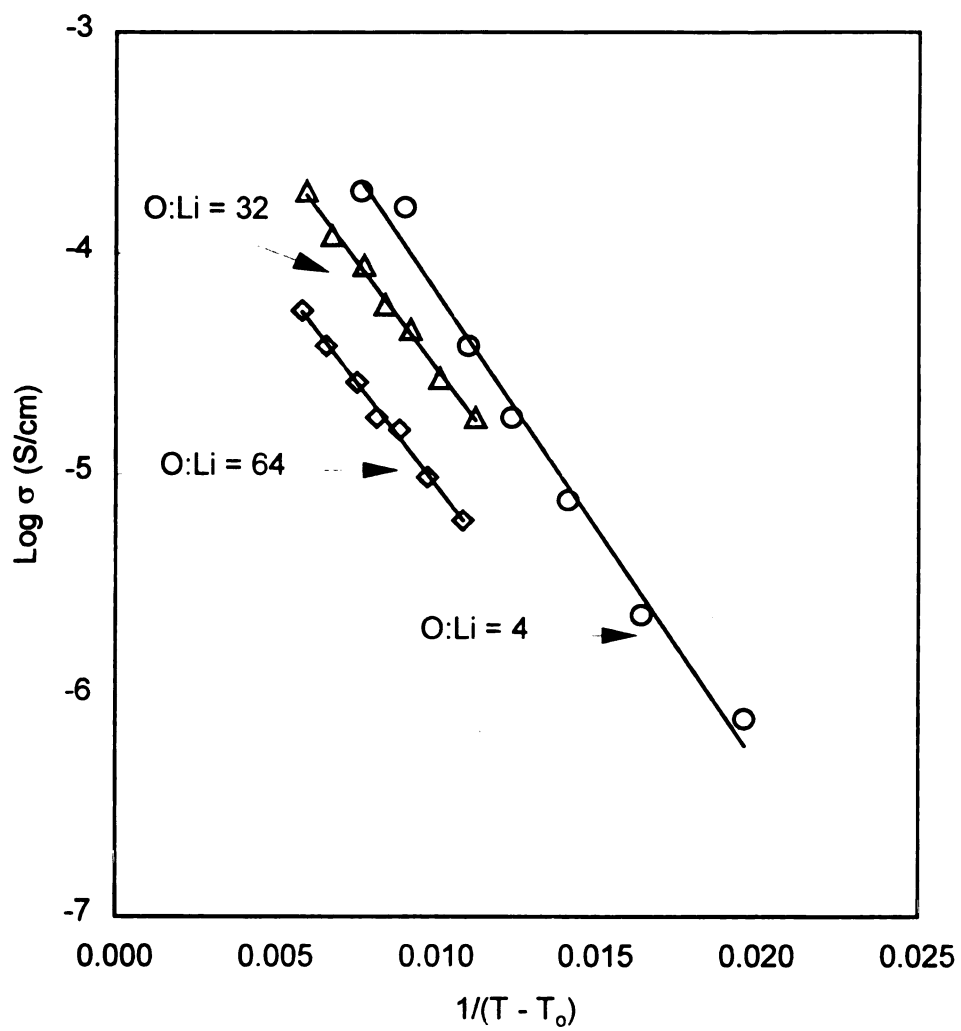


**Figure 59.** VTF plots for  $\text{PH}_4\text{-LiClO}_4$  complexes with O:Li ratio of 64, 32, and 4.

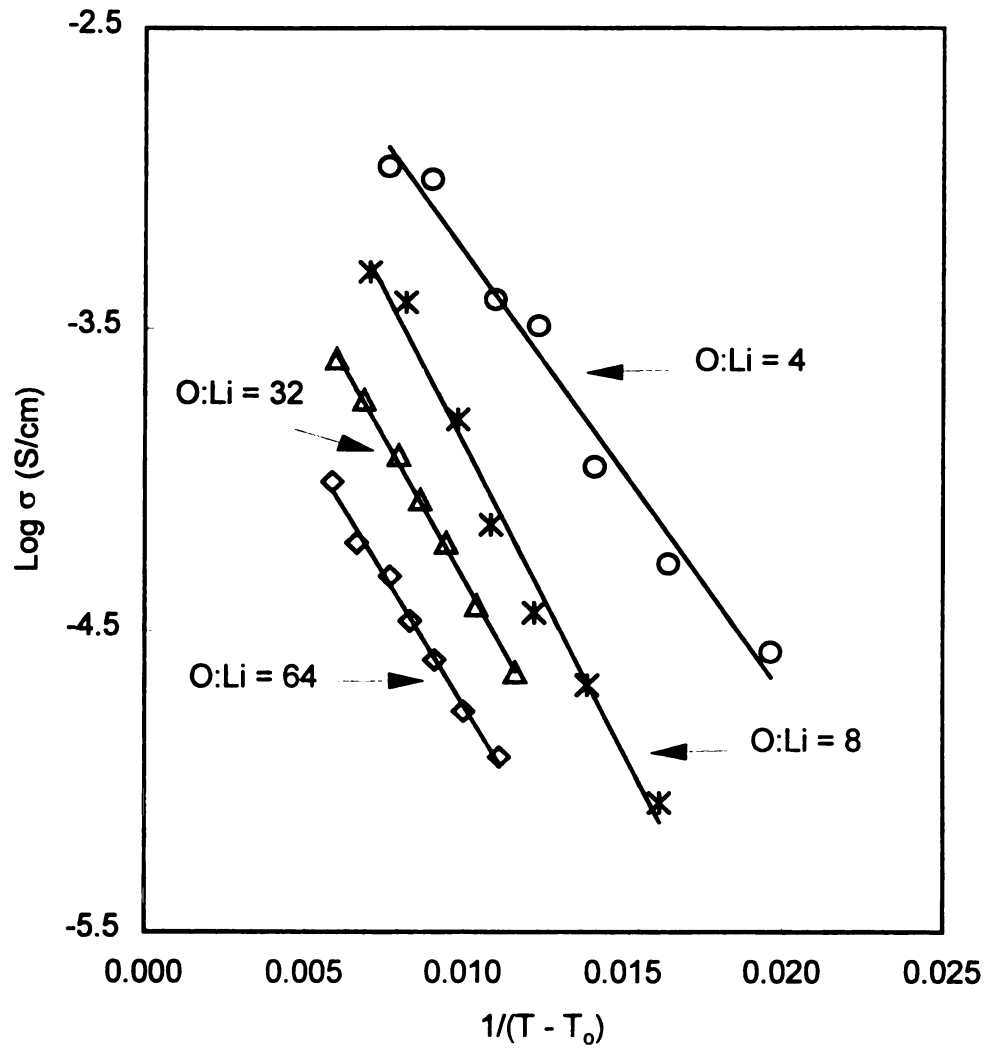


**Figure 60.** VTF plots for PH<sub>5</sub>-LiClO<sub>4</sub> complexes with O:Li ratio of 64, 32, 8, and

4.

## DISCUSSION

### I. Scope of ADMET Polymerization in Synthesizing Target Polymers

Three aspects of ADMET polymerization were examined in the present research: (1) the effectiveness of metathesis catalysts in the synthesis of target polymers; (2) how monomer structure affects the polymerizability of monomers in ADMET polymerization; and (3) the ease of ADMET polymerization in giving polymers in the desired molecular weight range.

#### 1. ADMET polymerization catalysts

While ADMET polymerization has proven to be a convenient method to prepare various unsaturated polymers, only a limited number of metathesis catalysts are capable of polymerizing acyclic dienes with different functionalities. In an effort to find a suitable catalyst for the preparation of the target polymers, the reactivity of both a conventional metathesis catalyst,  $\text{WCl}_6/\text{Sn}(\text{CH}_3)_4/\text{PrOAc}$  system, and Schrock's Mo alkylidene catalyst were tested with oligo(ethylene oxide) segmented  $\alpha,\omega$ -diene monomers.

It was reported that 1,4-polybutadiene oligomer ( $M_n = 2,970$ ,  $\text{PDI} = 2.43$ ) was successfully prepared<sup>54</sup> when  $\text{WCl}_6/\text{Sn}(\text{CH}_3)_4$  mixture was applied to the hydrocarbon monomer, by introducing a Lewis base, *n*-propyl acetate, into the catalyst mixture to quench unwanted side reactions. However, the

$WCl_6/Sn(CH_3)_4/PrOAc$  system failed to polymerize **P3** and **H4**. The ether structures in these two monomers were expected to provide additional difficulty for this Lewis acid catalyst, since the oxygen atoms in monomers **P3** and **H4** can easily coordinate to the center W atom. Such interactions may hinder or totally destroy the metathesis reactivity of the catalyst, and give rise to side reactions.

However, Schrock's molybdenum alkylidene catalyst was successful in the synthesis of the target polymers. The use of this Lewis acid free metathesis catalyst effected a clean and efficient polymerization that generated a variety of unsaturated ethylene oxide segmented polymers.<sup>81</sup> Although Schrock's Mo catalyst is a very well designed metathesis catalyst, it has several limitations in practical applications. First, the preparation of this catalyst requires a multistep organometallic synthesis in an oxygen and moisture-free environment. As a result, the cost of this catalyst is high. Second, since it is an extremely oxygen and moisture-sensitive compound, great care is needed in storing, handling, and transferring this catalyst. The monomers for ADMET polymerization also must be dry and of high purity. Third, it is difficult to remove catalyst traces from the products, and ADMET polymers usually have an undesirable greenish brown color. Nevertheless, as demonstrated by the work of Wagener *et al.* and results in this research, Schrock's well-defined single-component molybdenum alkylidene catalyst is an excellent choice for ADMET polymerizations.

## 2. Polymerizability of the monomers

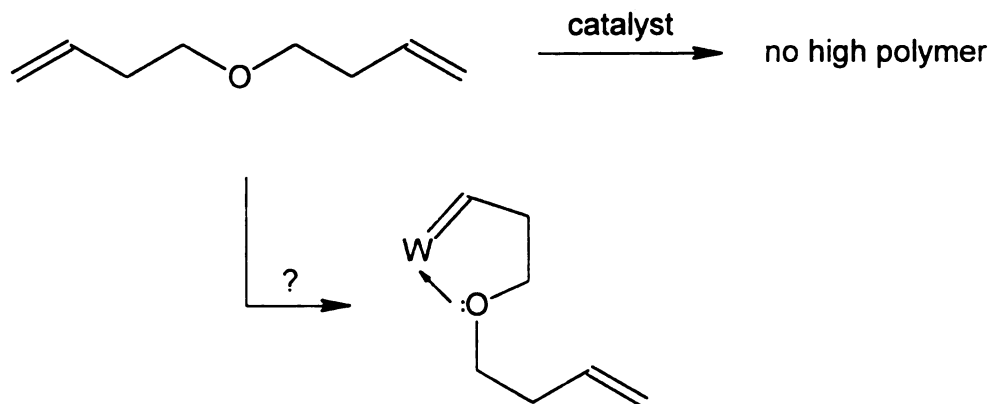
The potential application of the target polymers as solid polymer electrolytes also requires a good understanding of the structure-property relationship in the target polymers. The general structure of the target polymers (shown in **Scheme 8**) suggested that both the number of methylene units and the length of ethylene oxide chain could be altered to refine the properties of the unsaturated polymers. From the polymer synthesis point of view, this offered some challenging questions. First, is there a limit to the number of methylene units that can be incorporated into a monomer and still lead to a successful polymerization? If there is, what are structural features that prevent that monomer from being polymerized by ADMET?

In the synthesis of the unsaturated polymers, it was found that monomers with 3, 4, and 6 methylene units between the vinyl group and the oligo(ethylene oxide) segment all polymerized *via* ADMET. The number of ethylene oxide units in these monomers ranged from 2 to 5, and had no effect on the polymerizability of these monomers. This result agreed well with Wagener's work,<sup>46</sup> which showed that when two or more methylene groups separate oxygen atoms from the terminal double bond, ADMET polymerization proceeds and generates high polymers.

Wagener *et al*<sup>46</sup> further found that Schrock's W catalyst failed to polymerize di-3-butenyl ether (**Scheme 21**). Since there were only two methylene units to separate oxygen atom and the vinyl end group, it was proposed that an interaction between the carbon-carbon double bond and the

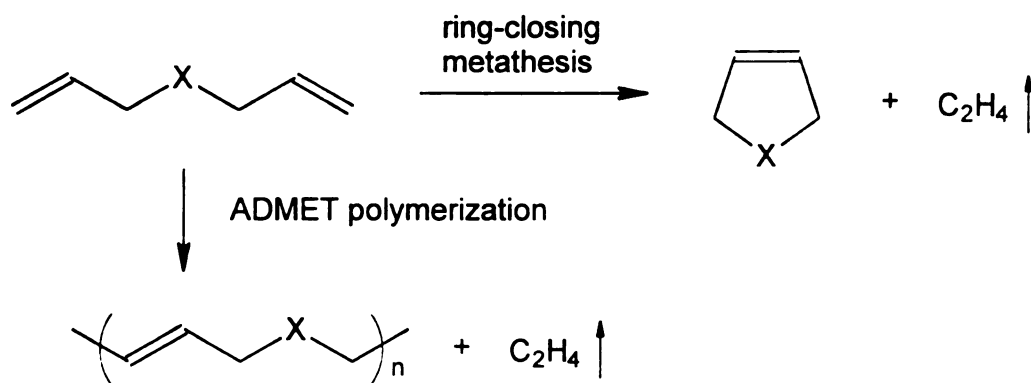
oxygen atom with the catalyst metal atom may block the metathesis reaction and poison the catalyst.

**Scheme 21. Failed ADMET polymerization to make an unsaturated polyether**

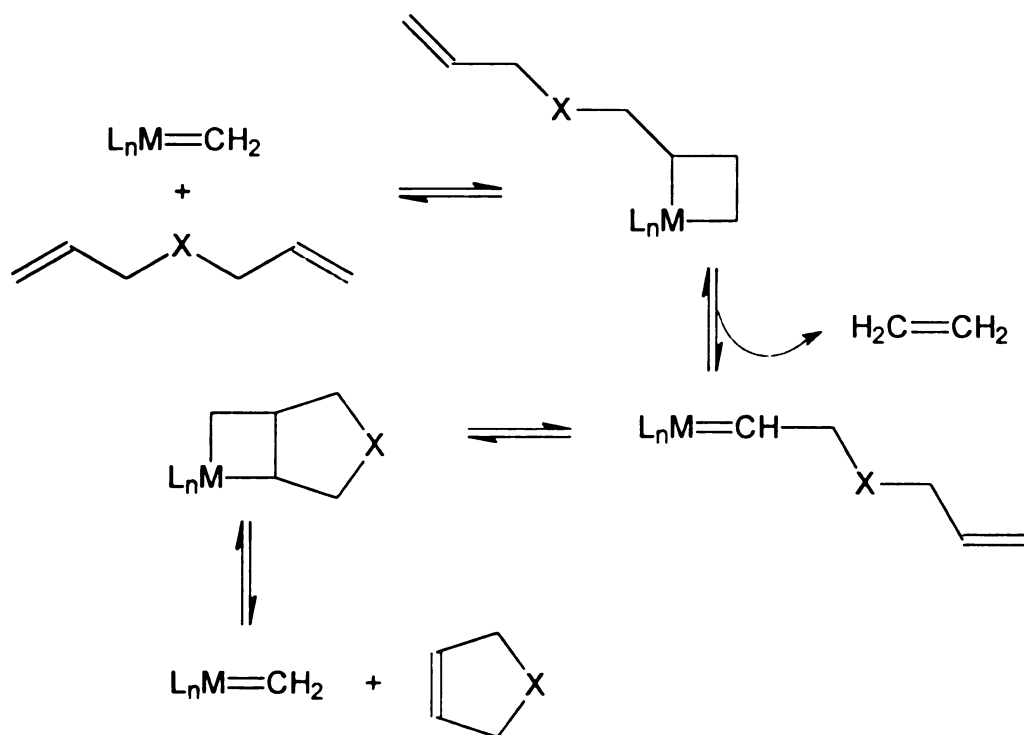


Another possible explanation is suggested by recent work by Grubbs and coworkers<sup>82-89</sup> on ring-closing metathesis reactions. Ring-closing metathesis, outlined in **Scheme 22**, competes with ADMET polymerization. Instead of forming an unsaturated linear polymer, an acyclic diene can be cyclized by a metathesis catalyst. Similar to ADMET polymerization, the mechanism of a ring-closing reaction (**Scheme 23**) involves formation of two metallocyclobutane rings as reactive intermediates. After the first metathesis forms a new carbene species, the second metallocyclobutane ring forms by reacting with another double bond from the same diene. Ring-closing reactions are usually carried out in solution with a low concentration of the acyclic diene, so that the probability

**Scheme 22. Competition between ring-closing metathesis reaction and ADMET polymerization**



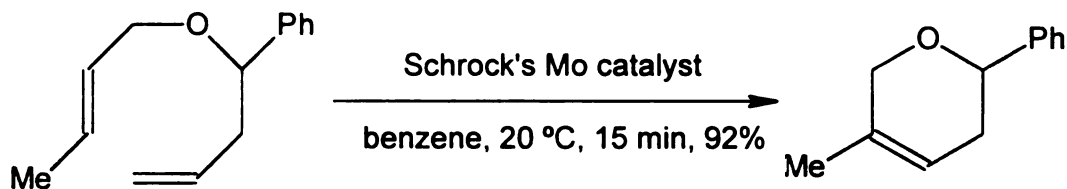
**Scheme 23. Mechanism for ring-closing metathesis reaction**



of metathesis reaction between double bonds on the same diene (intramolecular) is higher than the reaction between different diene molecules. A favorable ring size is equally important in a ring-closing reaction; five-, six-, seven- and even eight-membered carbocyclic and heterocyclic products are most commonly seen.

Various heterocycles, such as cyclic ethers<sup>82</sup> and nitrogen-containing heterocycles,<sup>83</sup> were prepared by ring-closing metathesis reaction. A ring-closing metathesis reaction example relevant to ADMET polymerization in this research is given in **Scheme 24**.<sup>82</sup> In the starting diene, one carbon-carbon double bond was separated from the oxygen atom by one carbon atom, the other double bond was separated from the oxygen by two. A six-membered cyclic ether was produced in this metathesis reaction. This example implies that it is possible for monomers with one or two carbon atoms separating terminal double bond and oxygen atom to undergo ADMET polymerization, if ring formation can be suppressed.

**Scheme 24.** An example of ring-closing metathesis reaction to prepare a cyclic ether



Even though di-4-butenyl ether could not be polymerized into high molecular weight polymer, monomer **B2**, a structurally homologous molecule, polymerized using Schrock's Mo catalyst. Compared to di-4-butenyl ether, **B2** is longer by two ethylene oxide units, long enough to inhibit the ring-closing reaction, which occurs easily with di-4-butenyl ether.

It is now necessary to consider the ADMET polymerization of monomer **A2**, which contains only one methylene group between the double bond and oxygen atom. When catalyst was added to **A2**, ethylene gas was released, but the polymerization never yielded oligomer or polymer of reasonable molecular weight. However, the reasons behind this failed polymerization are complicated. When the **A2** and **B2** monomers were purified, they could not be dried with a sodium mirror, as it was found that monomers with one or two methylene units between double bond and oxygen atom reacted with sodium metal to give unknown products. They were only purified by repeated distillation over  $\text{CaH}_2$ , so they may not be absolutely anhydrous. Other possibilities, such as catalyst poisoning caused by monomer structure, and a competing ring-closing reaction, can not be excluded at this time. The polymerizability of monomer **A2** needs further investigation.

### 3. Controlling molecular weights

ADMET polymerization of **P2**, **P3** and **P4** was carried out for 48 h and for 168 h, to gain an understanding about the achievable molecular weight and

polymerization rates at high conversion. The GPC data of the six polymers **PP2a**, **PP2**, **PP3a**, **PP3**, **PP4a** and **PP4** are listed in **Table 4**.

When the reaction time for the polymerization of **P2** was extended from 48 h to 168 h, higher molecular weight was achieved for **PP2** (168 h) than for **PP2a** (48 h). The same trend can be seen for polymers **PP3** and **PP3a**, and **PP4** and **PP4a**. In all cases, longer polymerization time resulted in higher molecular weights. In a stepwise ADMET polymerization with perfect stoichiometry and no side reactions that lead to chain ends without double bonds, the degree of polymerization,  $X_n$  is given by the Carothers equation

$$X_n = 1/(1 - p)$$

where  $p$  is the fractional conversion of terminal vinyl groups to internal double bonds. Thus, the extension of polymerization time enhanced the ADMET conversion, and thus increased the molecular weight.

## II. Unsaturated Ethylene Oxide-Segmented Polymers

### 1. Segment length dependent glass transition temperature

The glass transition temperature is a parameter of great importance for new synthetic polymers, since its value usually defines potential applications for the polymer. In this project, it is generally desirable to have polymers with low glass transitions so that polymer chains are mobile, and enhance the conductivity of polymer electrolytes. Therefore, an understanding of the effect of chemical structure on  $T_g$  in ethylene oxide segmented polymers would help in the design of improved polymer electrolytes.

The  $T_g$ 's of two series of unsaturated polymers are plotted in **Figure 61** as a function of number of ethylene oxide units in the repeating unit. When there are three methylene units in the polymer structure ( $m = 3$ , polymers **PP2**, **PP3** and **PP4**), the  $T_g$  increases about 2 °C per ethylene oxide unit (solid triangles) in the repeating unit of the polymer.

The same trend can be seen when there are four methylene units in the structure ( $m = 4$ , polymers **PH2**, **PH3**, **PH4** and **PH5**). Polymer **PH2** has the lowest  $T_g$  (-81 °C), and  $T_g$  increases by 2 to 3 °C with each additional ethylene oxide unit (solid circles) for **PH3**, **PH4** and **PH5**.

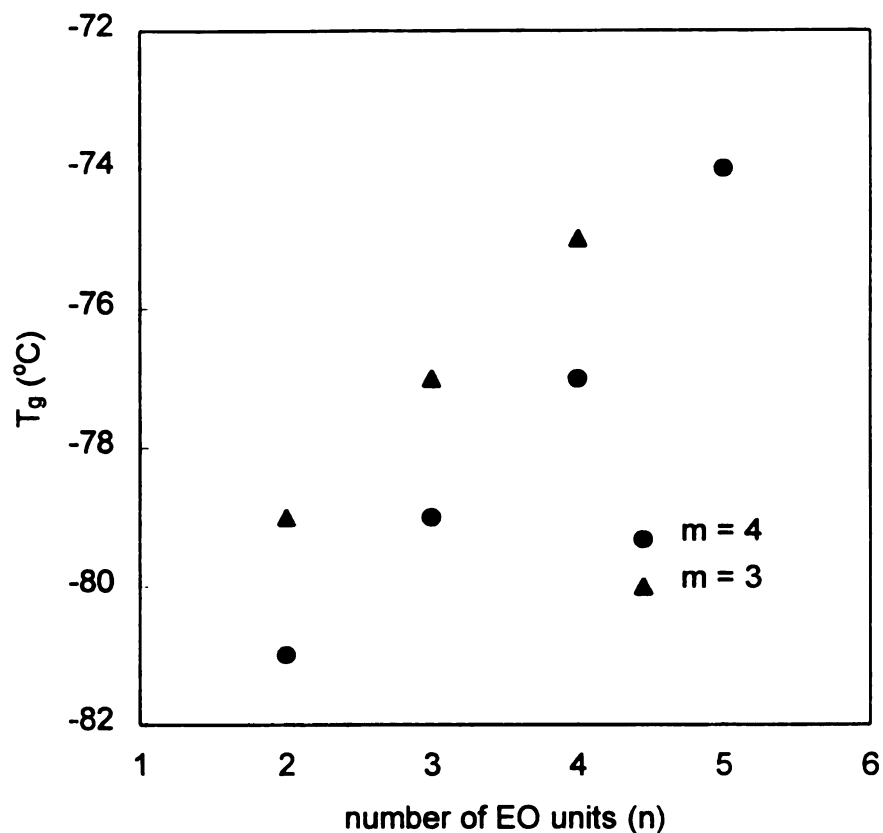
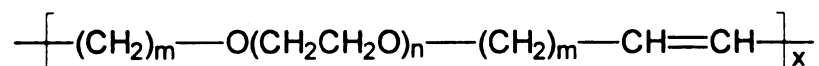


**Figure 61.** Ethylene oxide segment length dependent  $T_g$  in unsaturated polymers



The unsaturated polymers **PB2**, **PP2** and **PH2** all have two ethylene oxide units in their repeating units but a different number of methylene units. Their  $T_g$ 's are plotted as a function of number of methylene units, as shown in **Figure 62** (solid squares). In this polymer series,  $T_g$  decreases with increasing numbers of methylene units, from  $-72$  °C for  $m = 2$ , to  $-79$  °C for  $m = 3$ , to  $-81$  °C for  $m = 4$ .

The  $T_g$ 's of polymers **PP4**, **PH4** and **PO4** (four ethylene oxide units in the repeating unit) decrease as the methylene content increases (solid diamonds in **Figure 62**), similar to the trend observed for **PB2**, **PP2** and **PH2**.

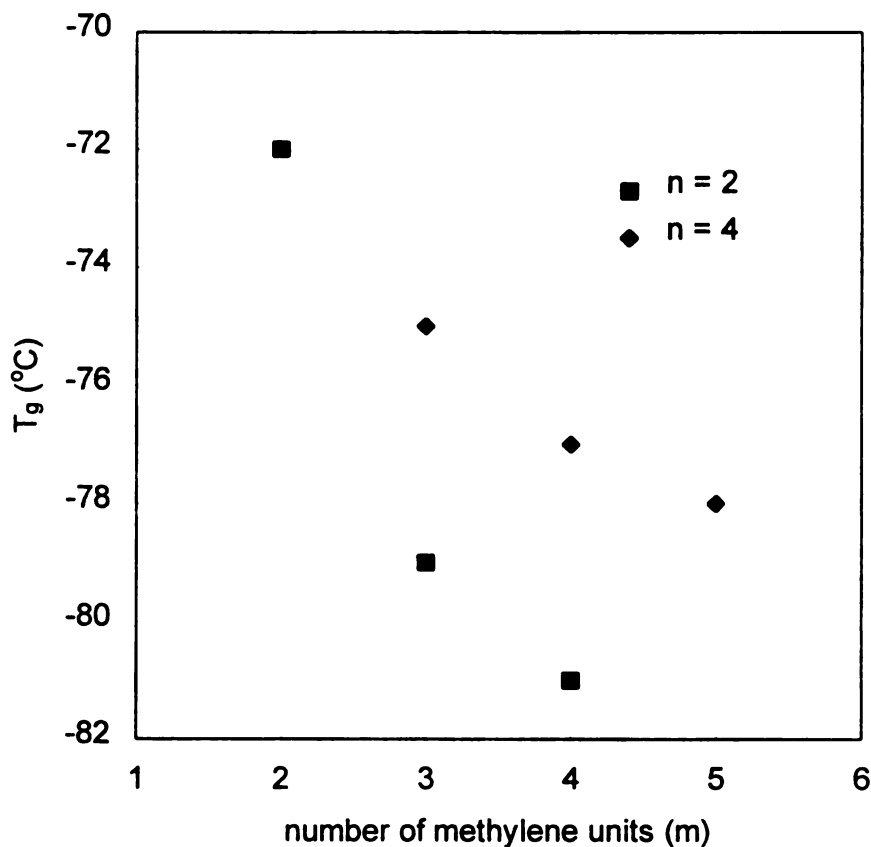
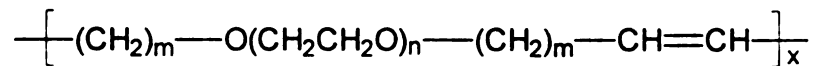


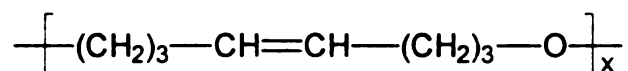
**Figure 62.** Methylene unit dependent  $T_g$  in several unsaturated polymers



The dependence of the  $T_g$  of a one-phase copolymer on the  $T_g$ 's of its two components is given by a simple equation<sup>90</sup>

$$T_g = w_1 T_{g1} + w_2 T_{g2}$$

where  $w_1$  and  $w_2$  are the weight fractions of components 1 and 2 in the copolymer respectively, while  $T_{g1}$  and  $T_{g2}$  are the glass transition temperatures of homopolymers of component 1 and component 2. This equation was applied to several unsaturated polymers prepared in this project. For example, polymers **PP2**, **PP3** and **PP4** can be generally regarded as  $(AB)_n$  segmented copolymers, with the hydrocarbon chain one segment and oligo(ethylene oxide) the other. The glass transition temperature of PEO is known to be  $-65\text{ }^\circ\text{C}$ , but the  $T_g$  of the unsaturated polyether



was not reported in the article that described its synthesis.<sup>46</sup> We derived a value of  $-88\text{ }^\circ\text{C}$  by using the above equation and the  $T_g$  of **PP2** obtained from DSC measurements. Based on these data, the  $T_g$ 's of **PP3** and **PP4** were calculated. In the same way, the  $T_g$  of **PH3**, **PH4** and **PH5** were obtained.

The experimental and calculated  $T_g$ 's of several polymers are listed in **Table 9**. Except for **PH5**, the calculated  $T_g$  for each polymer is in good agreement with the DSC measurements, indicating the equation provides a reliable  $T_g$  prediction for other unsaturated polymers in this project. These results further confirmed that there is no phase separation in the unsaturated polymers.

**Table 9. The Measured and Calculated  $T_g$  of Some Unsaturated Polymers**

| Polymer    | Measured $T_g$ ( $^{\circ}\text{C}$ ) | Calculated $T_g$ ( $^{\circ}\text{C}$ ) |
|------------|---------------------------------------|---|
| <b>PP3</b> | -77                                   | -77                                     |
| <b>PP4</b> | -75                                   | -75                                     |
| <b>PH3</b> | -79                                   | -79                                     |
| <b>PH4</b> | -77                                   | -77                                     |
| <b>PH5</b> | -74                                   | -76                                     |

The equation can also be used to explain qualitatively the segmental dependence of  $T_g$  in the unsaturated polymers. There is a linear relationship between the  $T_g$  of a copolymer and the  $T_g$ 's of the homopolymers of the two components A and B in the copolymer. If the  $T_g$  of homopolymer A is higher than the  $T_g$  of homopolymer B, the higher the weight fraction of A, the higher the  $T_g$  of the copolymer. In contrast, the higher the weight fraction of B, the lower the  $T_g$  of the copolymer. Unsaturated polyethers that have no ethylene oxide units have lower  $T_g$ 's than PEO. Therefore, for polymers with the same number of methylenes in the repeat unit, increasing the number of ethylene oxide units in a repeating unit gives higher  $T_g$ 's, and for a fixed number of ethylene oxide units, the more methylene units in a repeating unit, the lower the  $T_g$  of the polymer.

## 2. Melting transitions

Many of the unsaturated polymers displayed well-defined crystallizing and melting transitions in their DSC thermograms. As shown in Table 6, the  $T_g/T_m$  ratios for these polymers fall between 0.70 to 0.76. These values are close to  $2/3$ , the suggested ratio of  $T_g/T_m$  for nonsymmetrical crystalline polymers by the Boyer-Beaman rule.<sup>91</sup>

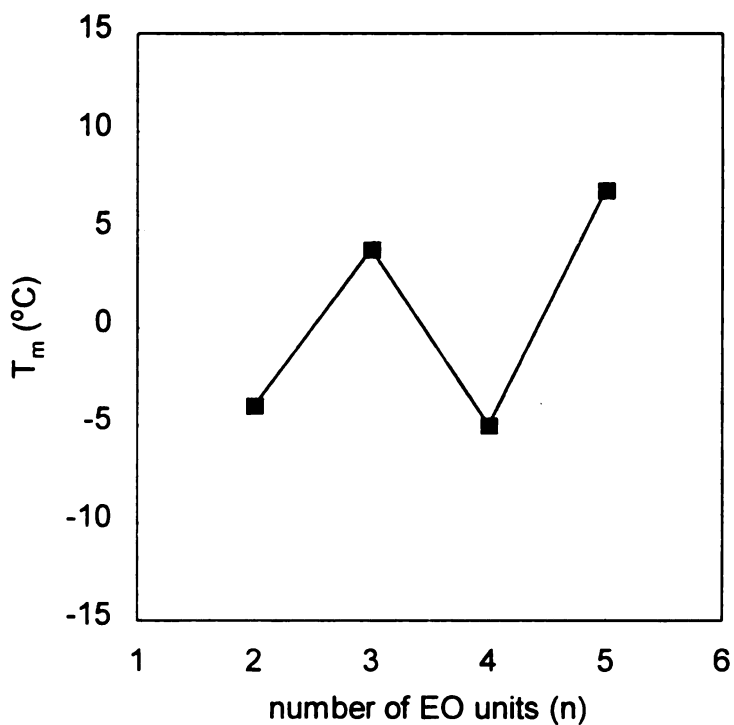
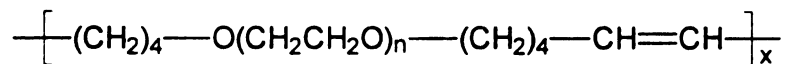


**Figure 63.** Melting temperature as a function number of ethylene oxide units in unsaturated polymers



The melting points for the highest melting phases of polymers **PH2**, **PH3**, **PH4** and **PH5** are plotted in **Figure 63**. Polymers with an even number of ethylene oxide units (**PH2** and **PH4**) have lower melting points than those with odd number of ethylene oxide units (**PH3** and **PH5**).

The study on the relationship between structure and crystalline transitions of unsaturated polymers and the hydrogenated polymers is currently underway in our group.

### III. Electrolytes from the Unsaturated Polymers

#### 1. Conductivity and EO content

The highest conductivities obtained for each electrolyte at three temperatures are compiled in **Table 10**. The weight fraction of the ethylene oxide segment in each polymer is also included. Except for the **PP4**-salt complex at 20 °C, the conductivity of  $\text{LiClO}_4$  salt complexes from **PP2**, **PP3** and **PP4** increases with increasing EO content. Since the hydrocarbon segment in each polymer acts as a filler and does not contribute to the conductivity, the conductivity in these three polymers is generally low. Therefore an increase in EO segment fraction in the polymers is expected to result in higher conductivity.

A similar trend can be seen for electrolytes from polymers **PH3**, **PH4** and **PH5**. Except for conductivity of **PH4**-salt complex at 100 °C, conductivity of other samples increases as EO content increases at the same temperature.

As the conductivity of electrolytes from the unsaturated polymers is not satisfactory at this stage, the dependence of conductivity on the EO content in these polymers offers an effective approach to increase the overall conductivity of the unsaturated polymers.

**Table 10. Peak Conductivity<sup>a</sup> of the Unsaturated Polymers  
at 20 °C, 50 °C and 100 °C**

| Polymer    | EO (%) <sup>b</sup> | $\sigma_{\text{peak}}$ (S/cm) |                      |                      |
|------------|---------------------|-------------------------------|----------------------|----------------------|
|            |                     | 20 °C                         | 50 °C                | 100 °C               |
| <b>PP2</b> | 49                  | $7.9 \times 10^{-6}$          | $3.5 \times 10^{-5}$ | $1.7 \times 10^{-4}$ |
| <b>PP3</b> | 57                  | $2.0 \times 10^{-5}$          | $7.9 \times 10^{-5}$ | $4.1 \times 10^{-4}$ |
| <b>PP4</b> | 64                  | $1.6 \times 10^{-5}$          | $8.3 \times 10^{-5}$ |                      |
| <b>PH3</b> | 52                  | $1.0 \times 10^{-5}$          | $3.9 \times 10^{-5}$ | $2.2 \times 10^{-4}$ |
| <b>PH4</b> | 58                  | $2.1 \times 10^{-5}$          | $1.0 \times 10^{-4}$ | $5.7 \times 10^{-4}$ |
| <b>PH5</b> | 63                  | $2.3 \times 10^{-5}$          | $1.2 \times 10^{-4}$ | $4.9 \times 10^{-4}$ |

<sup>a</sup> Highest conductivity measured for that polymer at a temperature.

<sup>b</sup> Weight fraction percentage of ethylene oxide segment in a polymer.

## 2. Parameters in the VTF equation

The parameters A and B for the VTF equation,  $\sigma(T) = A \exp[-B/(T - T_0)]$ , were obtained in the polymer-salt complexes with an O:Li ratio of 32 in **Table 11**. The values of A for samples from **PP2**, **PP3** and **PP4** increase as the EO fraction in the polymer increased. This again shows the dependence of conductivity on the EO content in the unsaturated polymers. Similarly, A increases for electrolytes from **PH3**, **PH4** and **PH5** with increasing EO fraction.

It is interesting to note that the values of B for all six samples are similar. Since parameter B in the VTF equation is related to the activation energy for the ionic conduction, comparable B values for the six electrolytes indicate that they likely have the same conduction mechanism.

**Table 11. The VTF Parameters for Polymer-Salt Complexes  
with an O:Li Ratio of 32**

| Polymer | EO (%) <sup>a</sup> | T <sub>c</sub> (°C) <sup>b</sup> | A (S/cm)             | B (K) |
|---------|---------------------|----------------------------------|----------------------|-------|
| PP2     | 49                  | -69                              | 1.2x10 <sup>-3</sup> | 549   |
| PP3     | 57                  | -69                              | 1.7x10 <sup>-3</sup> | 568   |
| PP4     | 64                  | -65                              | 2.7x10 <sup>-3</sup> | 508   |
| PH3     | 52                  | -72                              | 0.8x10 <sup>-3</sup> | 530   |
| PH4     | 58                  | -69                              | 2.6x10 <sup>-3</sup> | 525   |
| PH5     | 63                  | -66                              | 3.5x10 <sup>-3</sup> | 555   |

<sup>a</sup> Weight fraction percentage of ethylene oxide segment in a polymer.

<sup>b</sup> Taken as the T<sub>g</sub> of the sample in the DSC measurement.

#### IV. Summary

In this research, the unsaturated ethylene oxide-segmented polymers were designed and successfully prepared from oligo(ethylene glycol)  $\alpha,\omega$ -dialkenyl ethers via ADMET polymerization with Schrock's well-defined molybdenum alkylidene metathesis catalyst. The polymerizations proceeded to give high molecular weight polymers in good yields (above 92%). Spectroscopic methods, including  $^1\text{H}$  and  $^{13}\text{C}$  NMR and IR, were used to confirm the structure of the polymers. Internal double bonds on unsaturated polymer backbone typically had a *trans* geometry (among 82 to 86%). Due to the presence of both hydrophilic and hydrophobic segments in the polymer chain, the unsaturated polymers dissolved well in a variety of polar and nonpolar organic solvents.

TGA analysis demonstrated that the unsaturated polymers have good thermal stability both in air and in nitrogen. No significant thermal degradation took place for these polymers at 300 °C, but a rapid thermal breakdown followed at higher temperatures and only traces were left when the temperature reached 500 °C. The unsaturated polymers showed segment length-dependent  $T_g$ 's from DSC measurements. Some of the unsaturated polymers are crystalline at low temperature and interesting multiple crystallization and melting transitions were observed in their DSC scans.

Four unsaturated polymers were hydrogenated to yield perfectly alternating polyethylene/polyethylene oxide (AB)<sub>n</sub> copolymers. The

hydrogenation reaction was carried out in refluxing toluene using *p*-toluenesulfonhydrazide for several hours, and NMR monitoring showed that a full reduction was achieved. The resulting hydrogenated polymers are crystalline at room temperature, and their thermal behavior was studied by DSC measurements.

The polymer-LiClO<sub>4</sub> complexes were prepared by combining the unsaturated polymers and salt in acetonitrile and drying the samples. The T<sub>g</sub> of each of these polymer electrolytes was found to increase with increasing salt content. The ionic conductivities of the polymer electrolytes were measured in IS experiments. The conductivity isotherms of the polymer-salt complexes indicated that the conductivity increased at low salt contents, reached a maximum and then decreased. The conductivity also increased as the temperature increased. The temperature-dependent conductivities fit the Vogel-Tammann-Fulcher (VTF) equation. Finally, electrolytes with higher ethylene oxide content displayed higher conductivities.

## V. Suggestions for Further Research

Based on the results in this work, several directions can be taken in future research. First, a better understanding of relationship between polymerizability and monomer structure is necessary. Investigation can be carried out on ADMET polymerization of monomers with one methylene spacer separating the terminal vinyl group and ethylene oxide segment. Monomers having different numbers of ethylene oxide units, which can be prepared using the same preparation for this work, should be considered.

Recent work by Grubbs *et al.*<sup>63 65</sup> provided another type of efficient metathesis catalysts, the ruthenium carbene catalysts. Compared with Schrock's molybdenum alkylidene catalyst, the ruthenium catalysts have several advantages, such as easier preparation and handling, and tolerance toward moisture and oxygen. As purification and drying of monomers with longer ethylene oxide segment is expected to become harder, the ruthenium catalysts may substitute for Schrock's catalyst in polymer preparation.

Both unsaturated and hydrogenated ethylene oxide-segmented polymers displayed interesting segment length-dependent thermal behavior in DSC study. Efforts can be directed toward the understanding in the molecular level factors that govern the thermal changes.

The ionic conductivity of the polymer electrolytes prepared from the unsaturated polymers is still low at room temperature. One approach to improve the conductivity is suggested by structure-property relationship discovered in the

present work. As the conductivity showed a systematic increase as the ethylene oxide content increased, future unsaturated polymers should be prepared with longer ethylene oxide chains to enhance overall conducting segment fraction. Increasing the EO content in the polymer can also be achieved by attaching EO side chains to the double bond functionality to make comb-branched polymers with EO segments on both backbone and side chains of the material.

## EXPERIMENTAL

### I. General

Unless otherwise specified, ACS reagent grade starting materials were used as received from commercial suppliers without further purification. Melting points and boiling points were uncorrected. Glassware used for ADMET polymerization was soaked in a potassium hydroxide/ethanol base bath overnight, thoroughly rinsed with distilled water, and oven dried at 160 °C for one day.

Proton and carbon nuclear magnetic resonance ( $^1\text{H}$  and  $^{13}\text{C}$  NMR) analyses of monomers and polymers were carried out at room temperature in deuterated chloroform ( $\text{CDCl}_3$ ) on a Varian Gemini-300 spectrometer, the solvent proton and carbon signals being used as chemical shift standards respectively. Quantitative  $^{13}\text{C}$  NMR spectra used to determine the *trans* / *cis* ratio of the internal double bonds on polymer backbone were obtained on a VXR-300 NMR spectrometer. Infrared (IR) spectra of both monomers and polymers were recorded as  $\text{CCl}_4$  solutions under nitrogen at room temperature on a Nicolet IR/42 Fourier Transform IR spectrometer. The spectrum of each pure compound was obtained by subtracting the  $\text{CCl}_4$  spectrum from that of the solution. High resolution mass spectra of the monomers were measured by the Michigan State University Mass Spectroscopy Facility, with a heated direct inlet on a JEOL AX-505H double-

focusing mass spectrometer. Elemental analyses were carried out by the Microanalysis Laboratory at University of Illinois, Urbana-Champaign, using a CE440 Carbon, Hydrogen, Nitrogen Analyzer (Exeter Analytical, Inc.). Molecular weights were determined by gel permeable chromatography (GPC) using a PLgel 20m Mixed A column at room temperature with THF as eluting solvent at a flow rate of 1 mL/min. The concentration of the polymer samples were 2 mg/mL. Detection was by a Waters R401 Differential Refractometer. The results were calibrated with monodisperse polystyrene standards. Thermogravimetric analyses (TGA) of the polymers were obtained from a Perkin Elmer TGA 7 instrument at a heating rate of 10 °C/min, usually in the temperature range of 30 to 800 °C. For each polymer, one run was performed in air and one in nitrogen. Differential scanning calorimetry (DSC) analysis of the polymers and polymer electrolytes was performed in aluminum pans under a nitrogen/helium atmosphere on a Perkin Elmer DSC 7 instrument, calibrated with indium. Coolant for the system was liquid nitrogen. Each run was carried out by heating from -100 °C to 100 °C at a rate of 10 °C/min, quenching immediately to -100 °C at a rate of 200 °C/min, heating to 100 °C at a rate of 10 °C/min, and cooling back to -100 °C at a rate of 10 °C/min. The glass transition temperature,  $T_g$ , was defined as midpoint temperature of the transition, and the melting point was taken as the temperature at the peak of the melting endotherm. The polymer samples (2 - 4 mg) for microscopy were prepared by heating samples to 80 °C on a Mettler FP 82 HT hot stage and pressing the sample between two clean glass slides. Polarized optical microscopy of the hydrogenated polymers PH2H,

**PH3H, PH4H and PH5H** was carried out with a Nikon Optiphot2-Pol Microscope in polarized light at ambient temperature after the polymers crystallized and became opaque. Micrographs were taken with a Nikon FX-35DX camera that was directly connected to the microscope. Polymer electrolyte cells for impedance spectroscopy (IS) measurements were prepared by sandwiching bulk electrolytes between two stainless steel electrodes separated by a Teflon O-ring, and pressing with a Carver Laboratory Press (Model 2112) at 80 °C. The polymer electrolytes thus prepared typically had a diameter of 1.12 cm and ranged from 400 to 600 microns in thickness as determined with a Mitutoyo 101-103 micrometer. The impedance spectra of the polymer/LiClO<sub>4</sub> complexes were measured using a Hewlett-Packard 4192A LF Impedance Analyzer in a frequency range of 5 Hz to 10 MHz. Measurements were made from 20 to 100 °C by heating the cells in a VWR Scientific 1410D oven. The thickness and area of each cell was measured at 20 °C and was not corrected for different operating temperatures. Data collection and processing were performed through an HPIB interface using software from this laboratory on a Gateway 2000 4DX2-66V personal computer.

### **1. Solvents**

Acetonitrile was distilled over phosphorus pentoxide (P<sub>2</sub>O<sub>5</sub>) under nitrogen and was stored over activated 4 Å molecular sieves. Reagent grade diethyl ether was distilled from sodium benzophenone ketyl under nitrogen. Anhydrous dimethoxyethane (99.5%) was distilled from sodium benzophenone ketyl under

nitrogen. Reagent grade pentane (4 L) was vigorously stirred over concentrated sulfuric acid ( $\text{H}_2\text{SO}_4$ , 300 mL), which was changed every 12 h until the acid remained colorless. The pentane was then stirred over a 500 mL solution of potassium permanganate ( $\text{KMnO}_4$ , 0.5 M) and  $\text{H}_2\text{SO}_4$  (3 M) for one day. After separation from the aqueous phase, the pentane was washed with distilled water (4x500 mL), saturated solution of sodium bicarbonate ( $\text{NaHCO}_3$ , 500 mL) and distilled water (2x500 mL), and dried over anhydrous magnesium sulfate ( $\text{MgSO}_4$ ). The pentane was filtered and distilled from calcium hydride and then from sodium benzophenone ketyl under nitrogen. Tetrahydrofuran (THF) was dried first by distilling from calcium hydride and then from sodium benzophenone ketyl under nitrogen. Toluene was dried by distilling first from calcium hydride and then from sodium benzophenone ketyl under nitrogen.

## 2. Argon

Argon used in air-sensitive reactions was deoxygenated by passing it through a 60 cm (8 cm in diameter)  $\text{Mn}^0/\text{SiO}_2$  column.

**Raw column filling material.** An acidic manganese nitrate [ $\text{Mn}(\text{NO}_3)_2$ ] solution was prepared by mixing  $\text{Mn}(\text{NO}_3)_2(\text{H}_2\text{O})_x$  (500 g), concentrated nitric acid ( $\text{HNO}_3$ , 50 mL) and distilled water (500 mL). The clear light pink solution was blended with silica gel (60 - 200 mesh, 500 g). The blended silica gel was transferred into a 2000 mL beaker and the beaker was heated with a silicone oil bath at 180 °C in a well-ventilated hood for 72 h, with occasional stirring until no  $\text{NO}$  and  $\text{NO}_2$  were no longer evolved. The raw filling material was black.

**Column generation/regeneration.** The quartz column wrapped with heating wire and filled with the raw filling material was heated to at least 450 °C under a flow of hydrogen gas ( $H_2$ ). The color of the filling material turned from black to brown to green, and moisture was evolved from the column. The generation process lasted about 10 h and was followed by switching the  $H_2$  flow to argon for 2 h with continued heating. Traces of  $H_2O$  were removed by connecting the column to vacuum for 30 min.

After it was used for a period of time, the filling material in the column turned from green to brown, and the column regeneration process was repeated.

### **3. Sodium mirror**

Sodium mirror coated Schlenk flasks were prepared by heating a piece of fresh sodium metal (0.2 g) inside a clean flask with a burner under high vacuum until the molten sodium vaporized and coated the walls of the flask.

## II. Preparation of Monomers

### 1. Diethylene glycol $\alpha,\omega$ -diallyl ether (A2)

A mixture of sodium hydride powder (6.70 g, 95% purity, 0.265 mol) in dry THF (450 mL) was placed in a nitrogen filled 1000 mL flask equipped with a Claisen adapter, a cold water condenser and a dropping funnel. To this stirred mixture was slowly added a solution of allyl alcohol (12.8 g, 0.221 mol) in THF (30 mL) over a period of 30 min, while a stream of hydrogen evolved. The reaction mixture was stirred at room temperature for 12 h. Then a solution of diethylene glycol di-*p*-tosylate (43.5 g, 0.105 mol) in THF (150 mL) was added and the reaction was stirred under reflux for 72 h. The mixture was cooled to room temperature and was filtered through a coarse fritted funnel with a 2 cm layer of Celite<sup>®</sup> to removed insoluble solids. The resulting solution was concentrated and the product was purified by repeated distillation over CaH<sub>2</sub> under vacuum, to yield a clear colorless liquid. Yield: 16.6 g (85.0 %). B.P.: 38.2 - 39.9 °C / <0.05 mm Hg. <sup>1</sup>H NMR (300 MHz, CDCl<sub>3</sub>)  $\delta$  (ppm): 5.90 (ddt, J= 17.3, 10.4, 5.7 Hz, 2H), 5.25 (dq, J= 17.2, 1.6 Hz, 2H), 5.16 (dq, J= 10.4, 1.4 Hz, 2H), 4.01 (dt, J= 5.7, 1.4 Hz, 4H), 3.67-3.57 (m, 8H). <sup>13</sup>C NMR (300 MHz, CDCl<sub>3</sub>)  $\delta$  (ppm): 134.68, 116.90, 72.11, 70.57, 69.34. IR (CCl<sub>4</sub>): cm<sup>-1</sup> 3083, 3017, 2865, 1647, 1551, 1451, 1420, 1345, 1107, 995, 926, 884, 745. HRMS *m/z* calc for C<sub>10</sub>H<sub>18</sub>O<sub>3</sub> (M<sup>+</sup>) 186.1256, found 186.1225; calc for C<sub>10</sub>H<sub>19</sub>O<sub>3</sub> (M<sup>+</sup>+1) 187.1334, found 187.1320.

## 2. Diethylene glycol $\alpha,\omega$ -di-3-butenyl ether (B2)

Monomer B2 was prepared in a similar way as for A2. The reaction of 3-buten-1-ol (12.5 g, 0.173 mol), NaH (5.68 x 95% g, 0.225 mol), and diethylene glycol di-*p*-tosylate (34.2 g, 0.0824 mol) in THF (650 mL) yielded 11.4 g (64.4 %) of clear colorless product after repeated vacuum distillation over CaH<sub>2</sub>. B.P.: 46.1 - 48.3 °C / <0.05 mm Hg. <sup>1</sup>H NMR (300 MHz, CDCl<sub>3</sub>)  $\delta$  (ppm): 5.80 (ddt, J= 17.1, 10.3, 6.8 Hz, 2H), 5.10-4.99 (m, 4H), 3.65-3.56 (m, 8H), 3.51 (t, J= 6.9 Hz, 4H), 2.33 (qt, J= 6.8, 1.3 Hz, 4H). <sup>13</sup>C NMR (300 MHz, CDCl<sub>3</sub>)  $\delta$  (ppm): 135.08, 116.19, 70.57, 70.53, 70.08, 34.05. IR (CCl<sub>4</sub>): cm<sup>-1</sup> 3081, 3002, 2980, 2941, 2872, 2838, 1981, 1837, 1642, 1555, 1480, 1456, 1431, 1418, 1325, 1296, 1244, 1138, 1048, 990, 916, 878, 747, 639. HRMS *m/z* calc for C<sub>12</sub>H<sub>22</sub>O<sub>3</sub> (M<sup>+</sup>) 214.1569, found 214.1543.

## 3. Diethylene glycol $\alpha,\omega$ -di-4-pentenyl ether (P2)

5-Iodo-1-pentene was prepared from 5-bromo-1-pentene, according to a literature procedure.<sup>92</sup> In a 1000 mL flask with a condenser and a drying tube, a mixture of 5-bromo-1-pentene (42.8 g, 0.287 mol) and sodium iodide (300 g, 2.00 mol) in acetone (600 mL) was refluxed in darkness. After 20 h, the acetone solution from the reaction was combined with distilled water (500 mL) to give a homogeneous solution, which was extracted with ether (3x300 mL). The combined ether extracts were washed with saturated NaCl solution (3x500 mL)

and distilled water (500 mL), and dried over anhydrous  $\text{MgSO}_4$ . Ether and  $\text{MgSO}_4$  were removed and the resulting liquid was distilled. The product was collected at 144 - 147 °C as a light pink liquid (41.6 g, 74.0%).  $^1\text{H}$  NMR (300 MHz,  $\text{CDCl}_3$ )  $\delta$  (ppm): 5.74 (ddt,  $J$ = 17.1, 10.3, 6.7 Hz, 1H), 5.10-4.98 (m, 2H), 3.18 (t,  $J$ = 6.9 Hz, 2H), 2.15 (q,  $J$ = 7.0 Hz, 2H), 1.89 (q,  $J$ = 7.0 Hz, 2H).

To a 500 mL round-bottom flask at room temperature under argon and charged with a stirred mixture of sodium hydride (3.79 g, 95% purity, 0.150 mol) in dry THF (250 mL), was added dropwise a solution of diethylene glycol (5.30 g, 0.0500 mol) in THF (40 mL). After 12 h a solution of 5-iodo-1-pentene (29.4 g, 0.150 mol) in THF (30 mL) was added dropwise. The reaction was heated to reflux after 6 h and the course of the reaction was followed by  $^1\text{H}$  NMR. After an extended time (more than 72 h) the reaction mixture was filtered through a coarse fritted funnel with a 3 cm layer of Celite<sup>®</sup>. After removal of solvent, the resulting liquid was distilled over  $\text{CaH}_2$  in *vacuo* to yield a clear colorless liquid. It was further purified by stirring over a fresh sodium mirror in a 50 mL Schlenk flask, followed by a second vacuum distillation, and was stored in helium filled drybox for future use. Yield: 7.53 g (62.2%). B.P.: 67.4 - 68.5 °C/ $<0.05$  mm Hg.  $^1\text{H}$  NMR (300 MHz,  $\text{CDCl}_3$ )  $\delta$  (ppm): 5.80 (ddt,  $J$ = 17.0, 10.2, 6.7 Hz, 2H), 5.04-4.91 (m, 4H), 3.65-3.55 (m, 8H), 3.45 (t,  $J$ = 6.6 Hz, 4H), 2.09 (q,  $J$ = 7.2 Hz, 4H), 1.66 (q,  $J$ = 7.1 Hz, 4H).  $^{13}\text{C}$  NMR (300 MHz,  $\text{CDCl}_3$ )  $\delta$  (ppm): 138.28, 114.65, 70.69, 70.62, 70.11, 30.21, 28.75. IR ( $\text{CCl}_4$ ):  $\text{cm}^{-1}$  3081, 2977, 2942, 2927,

2869, 1642, 1551, 1451, 1350, 1298, 1250, 1121, 994, 914, 631. HRMS  $m/z$  calc for  $C_{14}H_{26}O_3$  ( $M^+$ ) 242.1882, found 242.1884.

#### 4. Triethylene glycol $\alpha,\omega$ -di-4-pentenyl ether (P3)

An argon-filled 500 mL flask at room temperature was charged with sodium hydride (3.79 g, 95% purity, 0.150 mol) in dry THF (200 mL). Added dropwise to the stirred mixture was a solution of triethylene glycol (7.51 g, 0.0500 mol) in dry THF (40 mL). After stirring for 24 h, 5-bromo-1-pentene (25.5 g, 0.171 mol) was added, and the reaction was heated to reflux for 96 h. Following the same work-up and drying procedure as for diethylene glycol  $\alpha,\omega$ -di-4-pentenyl ether, triethylene glycol  $\alpha,\omega$ -di-4-pentenyl ether was obtained as a clear liquid by vacuum distillation at 92.8 - 93.4 °C/<0.05 mm Hg. Yield: 10.6 g (73.8%). It was degassed with four freeze-pump-thaw cycles and then stored in a helium-filled drybox for future use.  $^1H$  NMR (300 MHz,  $CDCl_3$ )  $\delta$  (ppm): 5.79 (ddt,  $J= 17.1, 10.3, 6.7$  Hz, 2H), 5.03-4.91 (m, 4H), 3.64-3.54 (m, 12H), 3.45 (t,  $J= 6.7$  Hz, 4H), 2.09 (q,  $J= 7.2$  Hz, 4H), 1.66 (q,  $J= 7.1$  Hz, 4H).  $^{13}C$  NMR (300 MHz,  $CDCl_3$ )  $\delta$  (ppm): 138.28, 114.65, 70.68, 70.61, 70.09, 30.21, 28.76. IR ( $CCl_4$ ):  $cm^{-1}$  3081, 2998, 2942, 2917, 2869, 1642, 1451, 1350, 1296, 1246, 1121, 994, 876, 637. HRMS  $m/z$  calc for  $C_{16}H_{30}O_4$  ( $M^+$ ) 286.2144, found 286.2138.

### 5. Tetraethylene glycol $\alpha,\omega$ -di-4-pentenyl ether (P4)

Monomer **P4** was prepared as described for diethylene glycol  $\alpha,\omega$ -di-4-pentenyl ether using tetraethylene glycol (8.74 g, 0.045 mol) in THF (120 mL), NaH (3.41 g, 95% purity, 0.135 mol), and 5-bromo-1-pentene (14.9 g, 0.100 mol) in dry THF (50 mL). The colorless liquid tetraethylene glycol di-4-pentenyl ether was purified by distillation at 124.1 - 125.0 °C/<0.05 mm Hg. Yield: 12.1 g (81.2%).  $^1\text{H}$  NMR (300 MHz,  $\text{CDCl}_3$ )  $\delta$  (ppm): 5.79 (ddt,  $J$ = 17.1, 10.3, 6.7 Hz, 2H), 5.03-4.91 (m, 4H), 3.64-3.54 (m, 16H), 3.45 (t,  $J$ = 6.7 Hz, 4H), 2.09 (q,  $J$ = 7.2 Hz, 4H), 1.66 (q,  $J$ = 7.1 Hz, 4H).  $^{13}\text{C}$  NMR (300 MHz,  $\text{CDCl}_3$ )  $\delta$  (ppm): 138.28, 114.67, 70.69, 70.59, 70.10, 30.21, 28.76. IR ( $\text{CCl}_4$ ):  $\text{cm}^{-1}$  3081, 2998, 2979, 2942, 2919, 2869, 1642, 1451, 1350, 1296, 1246, 1121, 994, 914, 641. HRMS  $m/z$  calc for  $\text{C}_{18}\text{H}_{34}\text{O}_5$  ( $\text{M}^+$ ) 330.2406, found 330.2416.

### 6. Diethylene glycol $\alpha,\omega$ -di-5-hexenyl ether (H2)

Diethylene glycol  $\alpha,\omega$ -di-5-hexenyl ether was prepared as described for **A2**. After repeated vacuum distillation over  $\text{CaH}_2$  and a sodium mirror, a clear colorless liquid was obtained (23.8 g, 84.0%). B.P.: 87.2 - 88.4 °C /<0.05 mm Hg.  $^1\text{H}$  NMR (300 MHz,  $\text{CDCl}_3$ )  $\delta$  (ppm): 5.78 (ddt,  $J$ = 17.0, 10.3, 6.7 Hz, 2H), 5.02-4.90 (m, 4H), 3.65-3.54 (m, 8H), 3.44 (t,  $J$ = 6.7 Hz, 4H), 2.04 (q,  $J$ = 7.1 Hz, 4H), 1.58 (m, 4H), 1.42 (m, 4H).  $^{13}\text{C}$  NMR (300 MHz,  $\text{CDCl}_3$ )  $\delta$  (ppm): 138.60, 114.36, 71.12, 70.54, 69.99, 33.43, 28.97, 25.27. IR ( $\text{CCl}_4$ ):  $\text{cm}^{-1}$  3079, 2938,

### 7. Triethylene glycol $\alpha,\omega$ -di-5-hexenyl ether (H3)

Triethylene glycol  $\alpha,\omega$ -di-5-hexenyl ether was prepared as described for A2. A clear colorless liquid was obtained after repeated vacuum distillation over  $\text{CaH}_2$  and sodium mirrors. Yield: 23.5 g (71.3%). B.P.: 105.5 - 88.4 °C  $\pm$ 0.05 mm Hg.  $^1\text{H}$  NMR (300 MHz,  $\text{CDCl}_3$ )  $\delta$  (ppm): 5.78 (ddt, J = 17.0, 10.3, 6.7 Hz, 2H), 5.01-4.89 (m, 4H), 3.63-3.54 (m, 12H), 3.44 (t, J = 6.6 Hz, 4H), 2.04 (q, J = 7.1 Hz, 4H), 1.63-1.53 (m, 4H), 1.46-1.36 (m, 4H).  $^{13}\text{C}$  NMR (300 MHz,  $\text{CDCl}_3$ )  $\delta$  (ppm): 138.58, 114.36, 71.10, 70.48, 69.94, 33.40, 28.94, 25.24. IR ( $\text{CCl}_4$ ):  $\text{cm}^{-1}$  3079, 2938, 2867, 1827, 1642, 1551, 1456, 1441, 1416, 1350, 1323, 1298, 1246, 1121, 1044, 994, 913, 745, 633. HRMS  $m/z$  calc for  $\text{C}_{18}\text{H}_{35}\text{O}_4$  ( $\text{M}^+ + 1$ ) 315.2491, found 315.2506.

### 8. Tetraethylene glycol $\alpha,\omega$ -di-5-hexenyl ether (H4)

Tetraethylene glycol  $\alpha,\omega$ -di-5-hexenyl ether was prepared as described for A2 to give a clear colorless liquid. Yield: 29.3 g (77.9%). B.P.: 132.1 - 133.5 °C, < 0.05 mm Hg.  $^1\text{H}$  NMR (300 MHz,  $\text{CDCl}_3$ )  $\delta$  (ppm): 5.78 (ddt, J = 17.0, 10.2, 6.7 Hz, 2H), 5.02-4.90 (m, 4H), 3.64-3.54 (m, 16H), 3.44 (t, J = 6.6 Hz, 4H), 2.04 (q, J = 7.1 Hz, 4H), 1.58 (m, 4H), 1.41 (m, 4H).  $^{13}\text{C}$  NMR (300 MHz,  $\text{CDCl}_3$ )  $\delta$  (ppm): 138.55, 114.34, 71.07, 70.45, 69.92, 33.38, 28.92, 25.22. IR ( $\text{CCl}_4$ ):  $\text{cm}^{-1}$  3079, 2938, 2867, 1827, 1642, 1551, 1456, 1441, 1350, 1323, 1298, 1246, 1121,

1042, 994, 949, 913, 745, 633. HRMS  $m/z$  calc for  $C_{20}H_{38}O_5$  ( $M^+$ ) 358.2719, found 358.2737.

### 9. Pentaethylene glycol $\alpha,\omega$ -di-5-hexenyl ether (H5)

Using the same procedure used to prepare **A2**, **H5** was obtained as a clear colorless liquid, after purification by distillation over  $CaH_2$  and a Na mirror. Yield: 28.9 g (68.5%). B.P.: 155.9 - 157.2 °C/ $<0.05$  mm Hg.  $^1H$  NMR (300 MHz,  $CDCl_3$ )  $\delta$  (ppm): 5.79 (ddt,  $J = 17.1, 10.3, 6.7$  Hz, 2H), 5.03-4.91 (m, 4H), 3.64-3.54 (m, 20H), 3.45 (t,  $J = 6.7$  Hz, 4H), 2.04 (q,  $J = 7.1$  Hz, 4H), 1.64-1.53 (m, 4H), 1.45-1.36 (m, 4H).  $^{13}C$  NMR (300 MHz,  $CDCl_3$ )  $\delta$  (ppm): 138.58, 114.36, 71.10, 70.45, 69.93, 33.40, 28.92, 25.24. IR ( $CCl_4$ ):  $cm^{-1}$  3079, 2938, 2867, 1831, 1642, 1551, 1456, 1416, 1350, 1323, 1298, 1248, 1121, 1042, 994, 948, 913, 747. HRMS  $m/z$  calc for  $C_{22}H_{42}O_6$  ( $M^+$ ) 402.2981, found 402.2918.

### 10. Diethylene glycol $\alpha,\omega$ -di-7-octenyl ether (O2)

7-Octen-1-ol, a colorless oil, was prepared by dehydrochlorination of 8-chloro-1-octanol according to the literature method.<sup>93-94</sup> To a stirred mixture of potassium *t*-butoxide (31.3 g, 95% purity, 0.265 mol) in dry dimethyl sulfoxide (DMSO, 700 mL) in a 2000 mL flask, was added dropwise a solution of 8-chloro-1-octanol (29.2 g, 0.177 mol) in DMSO (50 mL) under argon at room temperature. After 2 h, the reaction mixture was combined with ether (500 mL) and washed with 1 M acetic acid (300 mL), 2M NaOH solution (300 mL), and

distilled water (3 x 500 mL). After filtration and removal of solvent, the crude product was distilled under vacuum. Yield: 15.3 g (67.5 %).  $^1\text{H}$  NMR (300 MHz,  $\text{CDCl}_3$ )  $\delta$  (ppm): 5.79 (ddt,  $J= 17.0, 10.3, 6.7$  Hz, 1H), 5.01-4.89 (m, 2H), 3.62 (t,  $J= 6.6$  Hz, 2H), 2.03 (q,  $J= 7.0$  Hz, 2H), 1.55 (m, 2H), 1.33 (m, 6H), 1.33 (s, 1H).

Diethylene glycol  $\alpha,\omega$ -di-7-octenyl ether was prepared using the method described for **A2** from 7-octen-1-ol and diethylene glycol *p*-ditosylate as a clear colorless liquid. Yield: 7.70 g (82.9%). B.P.: 138.2 - 140.5  $^\circ\text{C}$ <0.05 mm Hg.  $^1\text{H}$  NMR (300 MHz,  $\text{CDCl}_3$ )  $\delta$  (ppm): 5.78 (ddt,  $J= 17.0, 10.2, 6.7$  Hz, 2H), 5.02-4.88 (m, 4H), 3.64-3.54 (m, 8H), 3.43 (t,  $J= 6.8$  Hz, 4H), 2.02 (q,  $J= 6.6$  Hz, 4H), 1.56 (m, 4H), 1.41-1.31 (m, 12H).  $^{13}\text{C}$  NMR (300 MHz,  $\text{CDCl}_3$ )  $\delta$  (ppm): 138.95, 114.10, 71.36, 70.57, 70.01, 33.63, 29.50, 28.85, 28.76, 25.86. IR ( $\text{CCl}_4$ ):  $\text{cm}^{-1}$  3079, 2932, 2881, 1642, 1551, 1456, 1415, 1350, 1323, 1298, 1246, 1121, 1042, 995, 912, 804. HRMS  $m/z$  calc for  $\text{C}_{20}\text{H}_{38}\text{O}_3$  ( $\text{M}^+$ ) 326.2821, found 326.2866.

### 11. Tetraethylene glycol $\alpha,\omega$ -di-7-octenyl ether (**O4**)

Monomer **O4**, a clear colorless liquid, was prepared using the method described for **A2**. Yield: 12.0 g (78.4%). B.P.: 174.5 - 177.2  $^\circ\text{C}$ <0.05 mm Hg.  $^1\text{H}$  NMR (300 MHz,  $\text{CDCl}_3$ )  $\delta$  (ppm): 5.78 (ddt,  $J= 17.0, 10.2, 6.8$  Hz, 2H), 5.02-4.88 (m, 4H), 3.63-3.54 (m, 16H), 3.43 (t,  $J= 6.8$  Hz, 4H), 2.03 (q,  $J= 6.7$  Hz, 4H), 1.55 (m, 4H), 1.42-1.31 (m, 12H).  $^{13}\text{C}$  NMR (300 MHz,  $\text{CDCl}_3$ )  $\delta$  (ppm): 138.65, 113.92, 71.10, 70.33, 69.80, 33.41, 29.29, 28.63, 28.54, 25.65. IR ( $\text{CCl}_4$ ):  $\text{cm}^{-1}$

3079, 2932, 2861, 1642, 1549, 1456, 1350, 1324, 1296, 1242, 1119, 1042, 995,

912, 804. HRMS  $m/z$  calc for  $C_{24}H_{46}O_5$  ( $M^+$ ) 414.3345, found 414.3343.

### III. ADMET Polymerization Catalysts

$\text{WCl}_6/\text{Sn}(\text{CH}_3)_4/\text{PrOAc}$  was prepared as described by Nubel, Lutman and Yokelson.<sup>54</sup>  $\text{Mo}(\text{CHCMe}_2\text{Ph})(\text{NAr})[\text{OMe}(\text{CF}_3)_2]_2$ , Schrock's molybdenum alkylidene catalyst was prepared starting from  $\text{MoO}_2$ , using the five-step synthesis reported in literature procedure.<sup>62</sup>

#### IV. Synthesis of Unsaturated Ethylene Oxide-Segmented Polymers

##### 1. Polymer from diethylene glycol $\alpha,\omega$ -di-3-butenyl ether (PB2)

In a helium filled drybox, monomer **B2** (0.500 g,  $2.34 \times 10^{-3}$  mol) was placed in a 30 mL Schlenk tube with a stir bar. To this was added Schrock's Mo catalyst (15 mg) and the mixture was vigorously stirred at room temperature. The reaction vessel was removed from the drybox and high vacuum ( $<0.02$  mm Hg) was applied to the system to remove ethylene generated during the polymerization. After 6 h, the reaction temperature was raised to  $50\text{ }^{\circ}\text{C}$  by heating with a silicone oil bath. When the reaction mixture became too viscous to stir, toluene (3 mL) and Schrock's Mo catalyst (3 mg) were added. The polymerization was terminated after 7 days by exposing it to air. The toluene solution of the product was filtered through Celite<sup>®</sup> and polymer **PB2** was precipitated into *n*-heptane and dried in *vacuo* at room temperature until constant weight was reached. Yield: 0.394 g (92.8%).  $M_n = 15,100$ , PDI = 1.86.  $^1\text{H NMR}$  (300 MHz,  $\text{CDCl}_3$ ):  $\delta$  (ppm) 5.45 (m, 2H), 3.63-3.54 (m, 8H), 3.44 (t,  $J = 7.1$  Hz, 4H), 2.29-2.23 (m, 4H).  $^{13}\text{C NMR}$  (300 MHz,  $\text{CDCl}_3$ ):  $\delta$  (ppm) 128.24, 127.38, 70.97, 70.46, 69.96, 32.89, 27.85. IR ( $\text{CCl}_4$ ):  $\text{cm}^{-1}$  2867, 1549, 1456, 1350, 1324, 1296, 1242, 1119, 1041, 970, 885, 804.

##### 2. Polymer from diethylene glycol $\alpha,\omega$ -di-4-pentenyl ether (PP2)

**PP2a.** Under helium environment in a drybox, monomer **P2** (2.00 g,  $8.26 \times 10^{-3}$  mol) was placed in a 50 mL Schlenk tube with a magnetic stir bar.

After the catalyst (15 mg) was added, the mixture was vigorously stirred at room temperature for 20 min, and the reaction vessel was connected to high vacuum (<0.02 mm Hg). As for polymerization of **B2**, the reaction was heated to 50 °C after 6 h. When the reaction mixture became too viscous to stir, toluene (10 mL) and catalyst (5 mg) were added. The polymerization was terminated after 48 h by exposing it to air. **PP2a** was purified in the same manner as for **PB2**. Yield: 1.68 g (95.0 %).  $M_n = 17,700$ , PDI = 2.15.  $^1\text{H NMR}$  (300 MHz,  $\text{CDCl}_3$ ):  $\delta$  (ppm) 5.38 (m, 2H), 3.64-3.53 (m, 8H), 3.42 (t,  $J = 6.7$  Hz, 4H), 2.09-1.98 (m, 4H), 1.61 (q,  $J = 7.1$  Hz, 4H).  $^{13}\text{C NMR}$  (300 MHz,  $\text{CDCl}_3$ ):  $\delta$  (ppm) 129.94, 129.51, 70.74, 70.54, 70.03, 29.35, 28.94, 23.60. IR ( $\text{CCl}_4$ ):  $\text{cm}^{-1}$  2940, 2914, 2867, 1555, 1449, 1350, 1294, 1246, 1121, 968, 879, 754. Anal. Calcd. for  $(\text{C}_{12}\text{H}_{22}\text{O}_3)_x$  (**PP2-1**): C, 67.25; H, 10.35; O, 22.40. Found: C, 66.50; H, 10.51; O, 22.99.

**PP2**. A 7-day polymerization of **P2** (2.00 g,  $8.26 \times 10^{-3}$  mol), carried out in the same way as for **PP2a**, gave 1.73 g (97.8 %) of **PP2**.  $M_n = 93,900$ , PDI = 2.29. Anal. Calcd. for  $(\text{C}_{12}\text{H}_{22}\text{O}_3)_x$  (**PP2**): C, 67.25; H, 10.35; O, 22.40. Found: C, 67.66; H, 10.91; O, 21.43.

### 3. Polymer from triethylene glycol $\alpha,\omega$ -di-4-pentenyl ether (**PP3**)

**PP3-1a**. The polymer was prepared by ADMET polymerization of **P3** (2.00 g,  $6.99 \times 10^{-3}$  mol) with Mo catalyst (15 mg) in the same way as for **PP2a**. Yield: 1.72 g (95.3 %).  $M_n = 18,300$ , PDI = 3.10.  $^1\text{H NMR}$  (300 MHz,  $\text{CDCl}_3$ ):  $\delta$  (ppm) 5.38 (m, 2H), 3.64-3.53 (m, 12H), 3.42 (t,  $J = 6.7$  Hz, 4H), 2.09-1.97 (m,

4H), 1.61 (q,  $J = 6.9$  Hz, 4H).  $^{13}\text{C}$  NMR (300 MHz,  $\text{CDCl}_3$ ):  $\delta$  (ppm) 129.96, 129.54, 70.78, 70.55, 70.03, 29.38, 28.96, 23.63. IR ( $\text{CCl}_4$ ):  $\text{cm}^{-1}$  2949, 2909, 2869, 1551, 1451, 1350, 1262, 1119, 968, 868, 754. Anal. Calcd. for  $(\text{C}_{14}\text{H}_{26}\text{O}_4)_x$ : C, 65.08; H, 10.14; O, 24.78. Found: C, 65.57; H, 10.60; O, 23.83.

**PP3.** A 7-day polymerization of **P3**, done in the same way as for **PP3a**, gave 1.73 g (95.9 %) of **PP3**.  $M_n = 55,000$ , PDI = 2.57. Anal. Calcd. for  $(\text{C}_{14}\text{H}_{26}\text{O}_4)_x$ : C, 65.08; H, 10.14; O, 24.78. Found: C, 65.22; H, 10.60; O, 24.18.

#### 4. Polymer from tetraethylene glycol $\alpha,\omega$ -di-4-pentenyl ether (**PP4**)

**PP4a.** The polymer was prepared by ADMET polymerization of **P4** (2.00 g,  $6.06 \times 10^{-3}$  mol) with Mo catalyst (15 mg) in the same way as for **PP2a**. Yield: 1.77 g (96.7 %).  $M_n = 37,300$ , PDI = 2.21.  $^1\text{H}$  NMR (300 MHz,  $\text{CDCl}_3$ ):  $\delta$  (ppm) 5.38 (m, 2H), 3.63-3.53 (m, 16H), 3.42 (t,  $J = 6.7$  Hz, 4H), 2.09-1.97 (m, 4H), 1.60 (q,  $J = 7.1$  Hz, 4H).  $^{13}\text{C}$  NMR (300 MHz,  $\text{CDCl}_3$ ):  $\delta$  (ppm) 129.942, 129.50, 70.73, 70.50, 69.99, 29.34, 28.92, 23.59. IR ( $\text{CCl}_4$ ):  $\text{cm}^{-1}$  2940, 2916, 2869, 1549, 1451, 1350, 1296, 1248, 1121, 968, 874, 744. Anal. Calcd. for  $(\text{C}_{16}\text{H}_{30}\text{O}_5)_x$ : C, 63.54; H, 10.00; O, 26.46. Found: C, 62.56; H, 10.41; O, 26.03.

**PP4.** A 7-day polymerization of **P4** (2.00 g,  $6.06 \times 10^{-3}$  mol), carried out in the same way as for **PP4a**, gave 1.79 g (97.8 %) of **PP4**.  $M_n = 66,400$ , PDI = 2.24. Anal. Calcd. for  $(\text{C}_{16}\text{H}_{30}\text{O}_5)_x$ : C, 63.54; H, 10.00; O, 26.46. Found: C, 63.74; H, 10.64; O, 25.62.

### 5. Polymer from diethylene glycol $\alpha,\omega$ -di-5-hexenyl ether (PH2)

The polymer was prepared by ADMET polymerization of H2 (6.20 g, 0.0230 mol) with Mo catalyst (30 mg) as described for PB2. Polymerization time: 7 days. Yield: 5.28 g (95.0 %).  $M_n = 44,700$ , PDI = 2.74.  $^1\text{H NMR}$  (300 MHz,  $\text{CDCl}_3$ ):  $\delta$  (ppm) 5.35 (m, 2H), 3.63-3.53 (m, 8H), 3.42 (t,  $J = 6.7$  Hz, 4H), 2.03-1.92 (m, 4H), 1.60-1.50 (m, 4H), 1.40-1.30 (m, 4H).  $^{13}\text{C NMR}$  (300 MHz,  $\text{CDCl}_3$ ):  $\delta$  (ppm) 130.18, 129.67, 71.26, 70.53, 69.98, 32.26, 29.16 (cis), 29.02, 26.91 (cis), 26.10 (cis), 25.94. IR ( $\text{CCl}_4$ ):  $\text{cm}^{-1}$  2938, 2865, 1549, 1456, 1350, 1299, 1249, 1121, 970, 801. Anal. Calcd. for  $(\text{C}_{14}\text{H}_{26}\text{O}_3)_x$ : C, 69.39; H, 10.82; O, 19.79. Found: C, 68.50; H, 10.49; O, 21.01.

### 6. Polymer from triethylene glycol $\alpha,\omega$ -di-5-hexenyl ether (PH3)

The polymer was prepared by ADMET polymerization of H3 (12.5 g, 0.0398 mol) with Mo catalyst (30 mg) as described for PB2. Polymerization time: 7 days. Yield: 11.1 g (97.4 %).  $M_n = 32,200$ , PDI = 2.12.  $^1\text{H NMR}$  (300 MHz,  $\text{CDCl}_3$ ):  $\delta$  (ppm) 5.34 (m, 2H), 3.62-3.52 (m, 12H), 3.41 (t,  $J = 6.7$  Hz, 4H), 2.03-1.92 (m, 4H), 1.59-1.49 (m, 4H), 1.39-1.29 (m, 4H).  $^{13}\text{C NMR}$  (300 MHz,  $\text{CDCl}_3$ ):  $\delta$  (ppm) 130.01, 129.51, 71.07, 70.35, 69.80, 32.09 (trans), 29.00 (cis), 28.85 (trans), 26.75 (cis), 25.94 (cis), 25.78 (trans). IR ( $\text{CCl}_4$ ):  $\text{cm}^{-1}$  2942, 2869, 1549, 1456, 1349, 1249, 1121, 970, 800, 743. Anal. Calcd. for  $(\text{C}_{18}\text{H}_{30}\text{O}_4)_x$ : C, 67.09; H, 10.56; O, 22.35. Found: C, 66.51; H, 10.66; O, 22.83.

**7. Polymer from tetraethylene glycol  $\alpha,\omega$ -di-5-hexenyl ether (PH4)**

The polymer was prepared by ADMET polymerization of H4 (15.0 g, 0.0419 mol) with Mo catalyst (30 mg) as described for PB2. Polymerization time: 7 days. Yield: 13.4 g (97.1 %).  $M_n = 28,100$ , PDI = 2.16.  $^1\text{H NMR}$  (300 MHz,  $\text{CDCl}_3$ ):  $\delta$  (ppm) 5.38 (m, 2H), 3.63-3.53 (m, 16H), 3.42 (t,  $J = 6.7$  Hz, 4H), 2.04-1.92 (m, 4H), 1.60-1.50 (m, 4H), 1.40-1.30 (m, 4H).  $^{13}\text{C NMR}$  (300 MHz,  $\text{CDCl}_3$ ):  $\delta$  (ppm) 130.01, 129.51, 71.07, 70.33, 69.80, 32.09 (*trans*), 28.99 (*cis*), 28.85 (*trans*), 26.74 (*cis*), 25.94 (*cis*), 25.78 (*trans*). IR ( $\text{CCl}_4$ ):  $\text{cm}^{-1}$  2937, 2890, 1549, 1456, 1350, 1322, 1299, 1249, 1121, 970, 802. Anal. Calcd. for  $(\text{C}_{18}\text{H}_{34}\text{O}_5)_x$ : C, 65.47; H, 10.37; O, 24.22. Found: C, 66.16; H, 10.20; O, 23.64.

**8. Polymer from pentaethylene glycol  $\alpha,\omega$ -di-5-hexenyl ether (PH5)**

The polymer was prepared by ADMET polymerization of H5 (12.8 g, 0.0318 mol) with Mo catalyst (30 mg) as described for PB2. Polymerization time: 7 days. Yield: 11.6 g (97.5 %).  $M_n = 31,500$ , PDI = 2.01.  $^1\text{H NMR}$  (300 MHz,  $\text{CDCl}_3$ ):  $\delta$  (ppm) 5.35 (m, 2H), 3.63-3.53 (m, 20H), 3.42 (t,  $J = 6.7$  Hz, 4H), 2.04-1.93 (m, 4H), 1.63-1.50 (m, 4H), 1.40-1.30 (m, 4H).  $^{13}\text{C NMR}$  (300 MHz,  $\text{CDCl}_3$ ):  $\delta$  (ppm) 130.24, 129.74, 71.33, 70.53, 70.01, 32.32, 29.22 (*cis*), 29.08, 26.98 (*cis*), 26.16 (*cis*), 26.00. IR ( $\text{CCl}_4$ ):  $\text{cm}^{-1}$  2946, 2844, 1549, 1456, 1350, 1299, 1241 1121, 970, 802, 742. Anal. Calcd. for  $(\text{C}_{20}\text{H}_{38}\text{O}_6)_x$ : C, 64.14; H, 10.23; O, 25.63. Found: C, 64.39; H, 10.50; O, 25.11.

**9. Polymer from diethylene glycol  $\alpha,\omega$ -di-7-octenyl ether (PO2)**

The polymer was prepared by ADMET polymerization of **O2** (5.00 g, 0.0168 mol) with Mo catalyst (15 mg) as described for **PB2**. Polymerization time: 4 days. Yield: 4.39 g (96.1 %).  $M_n = 57,100$ , PDI = 2.45.  $^1\text{H NMR}$  (300 MHz,  $\text{CDCl}_3$ ):  $\delta$  (ppm) 5.35 (m, 2H), 3.64-3.53 (m, 8H), 3.42 (t,  $J = 6.8$  Hz, 4H), 1.94 (m, 4H), 1.59-1.51 (m, 4H), 1.28 (m, 12H).  $^{13}\text{C NMR}$  (300 MHz,  $\text{CDCl}_3$ ):  $\delta$  (ppm) 130.10, 129.54, 71.37, 70.63, 70.01, 34.89, 29.44, 29.02, 26.95, 25.50, 25.94. IR ( $\text{CCl}_4$ ):  $\text{cm}^{-1}$  2932, 2859, 1459, 1350, 1324, 1299, 1245, 1121, 1042, 968, 901, 804.

**10. Polymer from tetraethylene glycol  $\alpha,\omega$ -di-7-octenyl ether (PO4)**

The polymer was prepared by ADMET polymerization of **O4** (8.50 g, 0.0205 mol) with Mo catalyst (20 mg) as described for **PB2**. Polymerization time: 4 days. Yield: 7.53 g (95.0 %).  $M_n = 35,400$ , PDI = 2.35.  $^1\text{H NMR}$  (300 MHz,  $\text{CDCl}_3$ ):  $\delta$  (ppm) 5.35 (m, 2H), 3.63-3.53 (m, 16H), 3.43 (t,  $J = 6.8$  Hz, 4H), 1.93 (m, 4H), 1.60-1.50 (m, 4H), 1.28 (m, 12H).  $^{13}\text{C NMR}$  (300 MHz,  $\text{CDCl}_3$ ):  $\delta$  (ppm) 130.17, 129.62, 71.31, 70.55, 69.97, 34.80, 29.41, 29.00, 26.97, 25.53, 25.88. IR ( $\text{CCl}_4$ ):  $\text{cm}^{-1}$  2933, 2861, 1458, 1350, 1324, 1296, 1245, 1119, 1042, 968, 901, 804.

## V. Preparation of Saturated Ethylene Oxide-Segmented Polymers

### 1. Hydrogenated polymer from PH2 (PH2H)

The hydrogenation of unsaturated polymer PH2 was done according to the documented procedure.<sup>76-79</sup> To a 250 mL Schlenk flask was added a solution of the unsaturated polymer PH2 (1.00 g) in dry toluene (150 mL), *p*-toluenesulfonhydrazide (10 equivalent of the number of the double bonds) and 2,6-di-*t*-butyl-4-methylphenol (butylated hydroxytoluene, BHT, 0.005 g) as the radical inhibitor. The mixture was degassed with three freeze-pump-thaw cycles. Then a cold water condenser with argon inlet and outlet was attached to the flask under argon environment, and the mixture was heated to reflux in argon with an oil bath. After 12 h, the mixture was cooled to room temperature and was filtered through a 60 mL coarse fritted funnel under vacuum. The solution was washed with 2 M HCl solution (3x150 mL), saturated NaCl solution (3x150 mL) and distilled water (150 mL), and was concentrated with a rotary evaporator. The resulting polymer was further purified by repeated precipitation into *n*-heptane from toluene solution and dried in *vacuo* until constant weight was observed. The hydrogenated polymer was then stored in a desiccator for future characterization. Yield: 0.427 g (42.7 %).  $M_n = 24,800$ , PDI = 2.09.  $^1\text{H}$  NMR (300 MHz,  $\text{CDCl}_3$ ):  $\delta$  (ppm) 3.64-3.54 (m, 8H), 3.42 (t,  $J = 6.8$  Hz, 4H), 1.55 (m, 4H), 1.25 (m, 12H).  $^{13}\text{C}$  NMR (300 MHz,  $\text{CDCl}_3$ ):  $\delta$  (ppm) 71.52, 70.61, 70.04,

29.62, 29.53, 29.47, 26.07. IR ( $\text{CCl}_4$ ):  $\text{cm}^{-1}$  2934, 2863, 1643, 1456, 1349, 1324, 1299, 1249, 1119, 1048, 992, 954, 913, 810, 742.

## 2. Hydrogenated polymer from PH3 (PH3H)

**PH3H** was prepared and purified by the same procedure as used for **PH2H**. Yield: 0.293 g (29.3 %).  $M_n = 24,900$ , PDI = 2.00.  $^1\text{H}$  NMR (300 MHz,  $\text{CDCl}_3$ ):  $\delta$  (ppm) 3.64-3.54 (m, 12H), 3.42 (t,  $J = 6.7$  Hz, 4H), 1.55 (m, 4H), 1.25 (m, 12H).  $^{13}\text{C}$  NMR (300 MHz,  $\text{CDCl}_3$ ):  $\delta$  (ppm) 71.43, 70.50, 69.94, 29.52, 29.44, 29.38, 25.98. IR ( $\text{CCl}_4$ ):  $\text{cm}^{-1}$  2932, 2861, 1455, 1355, 1324, 1292, 1117, 1048, 992, 954, 913, 810, 742.

## 3. Hydrogenated polymer from PH4 (PH4H)

**PH4H** was prepared and purified by the same procedure used for **PH2H**. Yield: 0.330 g (33.0 %).  $M_n = 13,100$ , PDI = 2.06.  $^1\text{H}$  NMR (300 MHz,  $\text{CDCl}_3$ ):  $\delta$  (ppm) 3.63-3.53 (m, 16H), 3.42 (t,  $J = 6.8$  Hz, 4H), 1.55 (m, 4H), 1.25 (m, 12H).  $^{13}\text{C}$  NMR (300 MHz,  $\text{CDCl}_3$ ):  $\delta$  (ppm) 71.52, 70.54, 69.99, 29.59, 29.53, 29.46, 26.05. IR ( $\text{CCl}_4$ ):  $\text{cm}^{-1}$  2932, 2861, 1732, 1549, 1456, 1350, 1324, 1296, 1249, 1117, 1042, 992, 948, 913, 806, 742.

## 4. Hydrogenated polymer from PH5 (PH5H)

**PH5H** was prepared and purified by the same procedure as used for **PH2H**. Yield: 0.389 g (38.9 %).  $M_n = 18,400$ , PDI = 1.81.  $^1\text{H}$  NMR (300 MHz,

$\text{CDCl}_3$ ):  $\delta$  (ppm) 3.63-3.54 (m, 20H), 3.42 (t,  $J = 6.8$  Hz, 4H), 1.55 (m, 4H), 1.25 (m, 12H).  $^{13}\text{C}$  NMR (300 MHz,  $\text{CDCl}_3$ ):  $\delta$  (ppm) 71.49, 70.53, 69.99, 29.58, 29.50, 29.43, 26.03. IR ( $\text{CCl}_4$ ):  $\text{cm}^{-1}$  2932, 2863, 1456, 1350, 1324, 1292, 1249, 1117, 1042, 986, 947, 913, 886, 823, 742.

## VI. Preparation of Polymer Electrolytes

Polymer electrolytes were prepared from unsaturated polymers and lithium perchlorate ( $\text{LiClO}_4$ ).  $\text{CH}_3\text{CN}$  (6 - 8 mL) was added to a vial containing the polymer sample (usually 0.400 - 0.600 g) and the appropriate amount of  $\text{LiClO}_4$ . The mixture was stirred until a homogeneous solution was obtained. The solution was concentrated by solvent evaporation at 70 °C, followed by drying under high vacuum for 24 h. Samples were further dried under high vacuum at 120 °C for 2 h. Polymer electrolytes from **PP2, PP3, PP4, PH3, PH4** and **PH5** were prepared, generally with O:Li ratios of 64:1, 32:1, 16:1, 12:1, 8:1 and 4:1 for each polymer. The polymer electrolytes were stored in a dry and inert atmosphere.

## **APPENDIX**

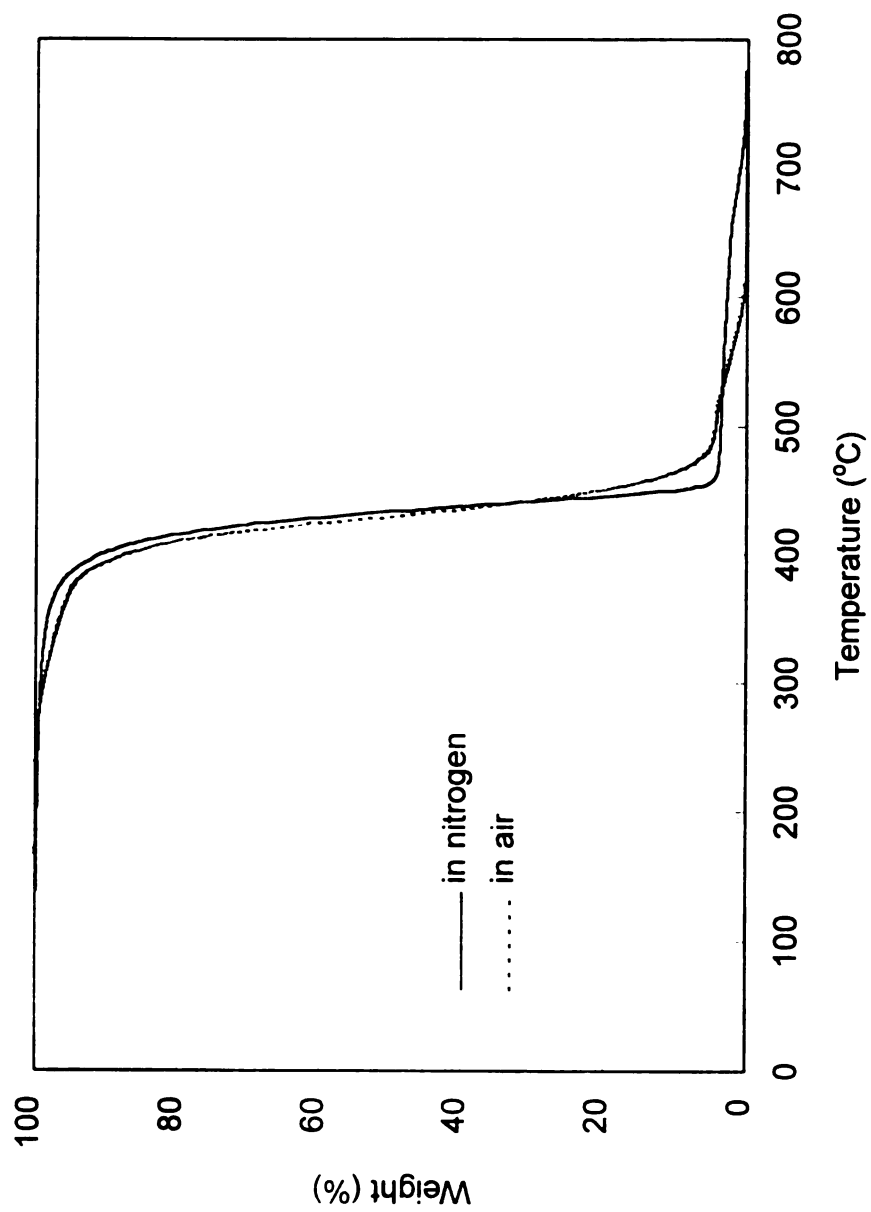


Figure 64. TGA profiles of PB2 (heating rate 10 °C/min).

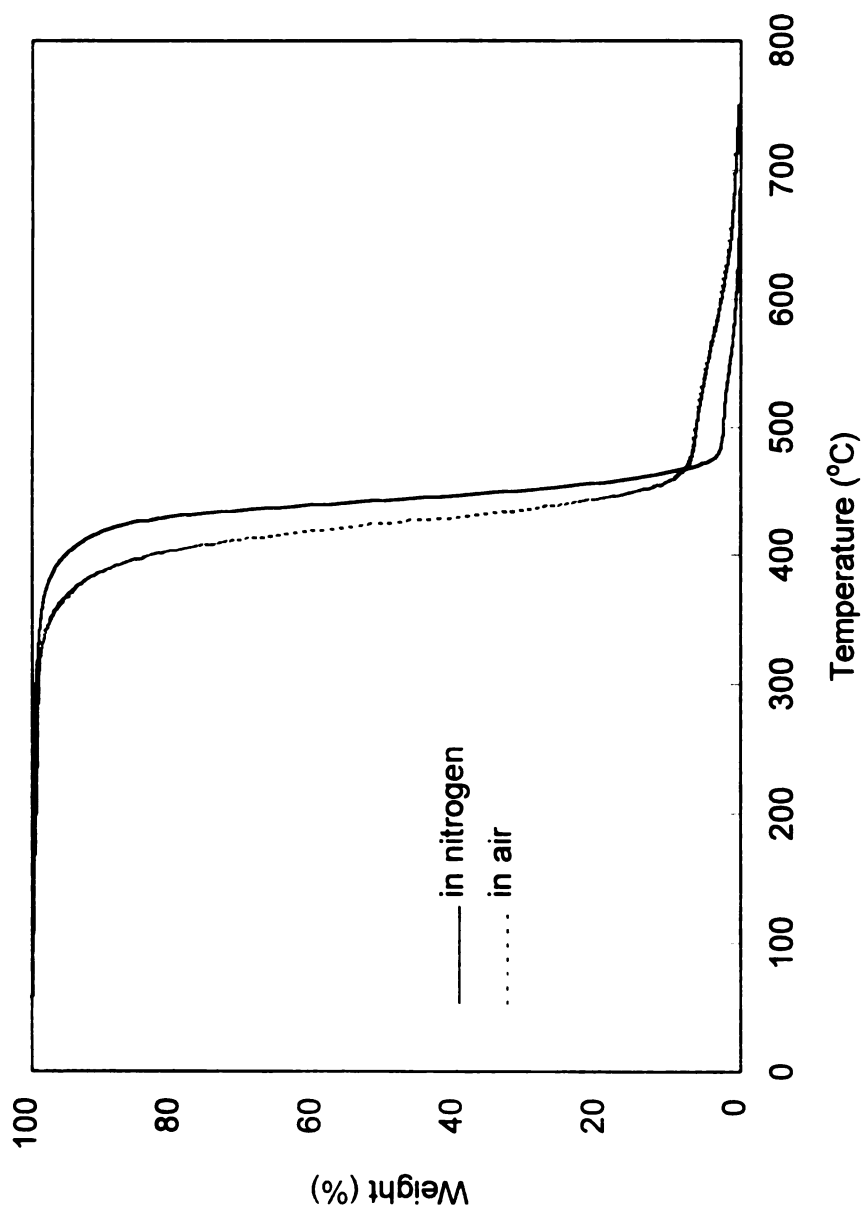
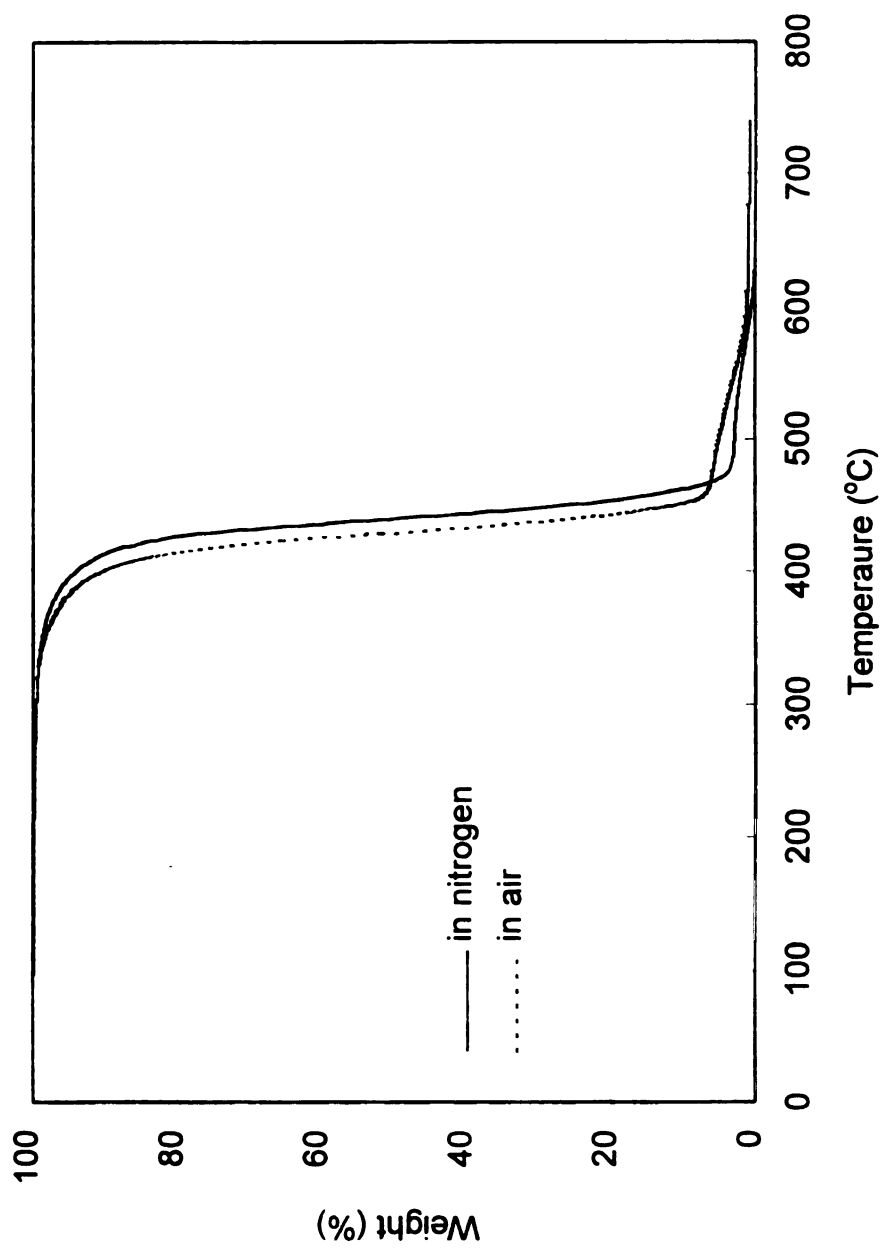
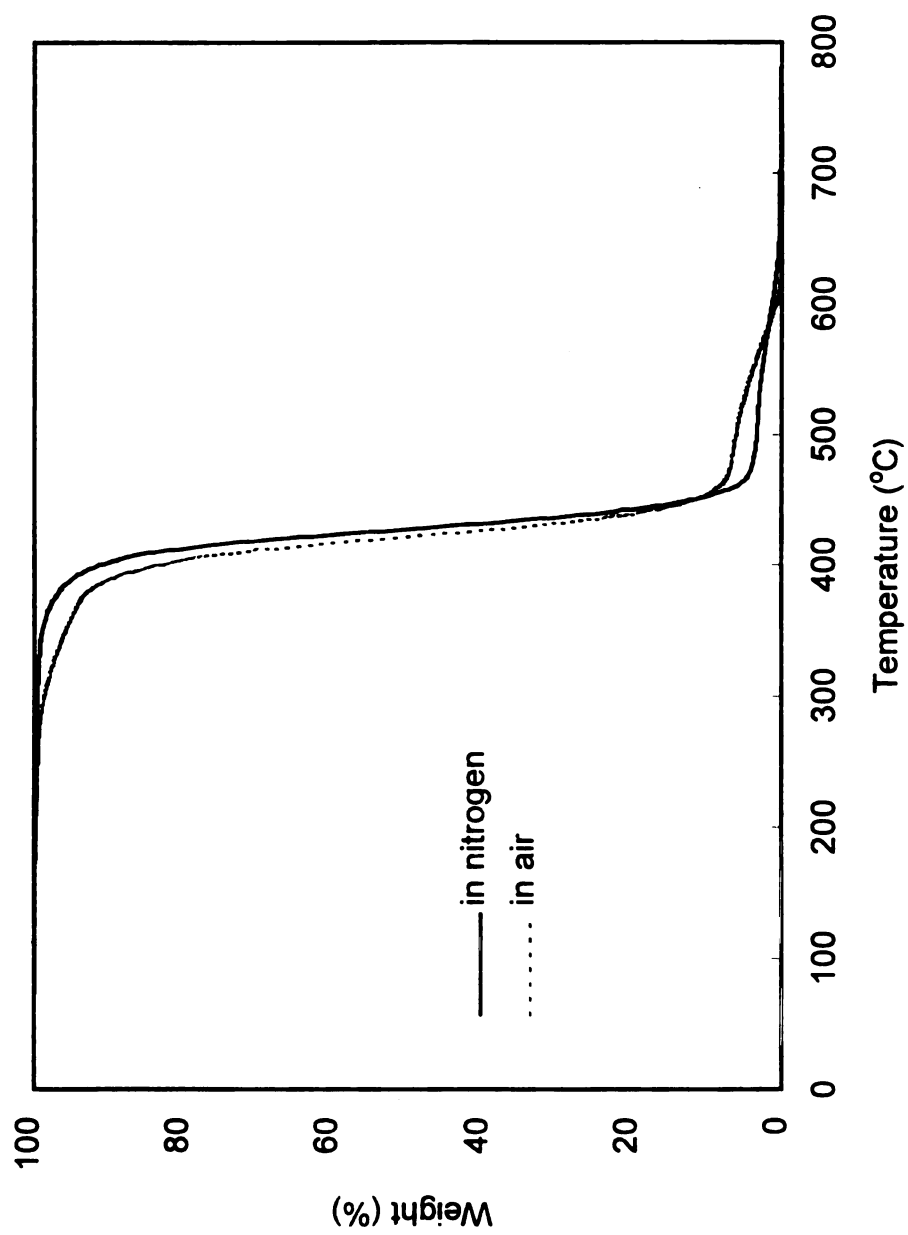


Figure 65. TGA profiles of PP2a (heating rate 10 °C/min).



**Figure 66.** TGA profiles of PP3a (heating rate 10 °C/min).



**Figure 67.** TGA profiles of PP3 (heating rate 10 °C/min).

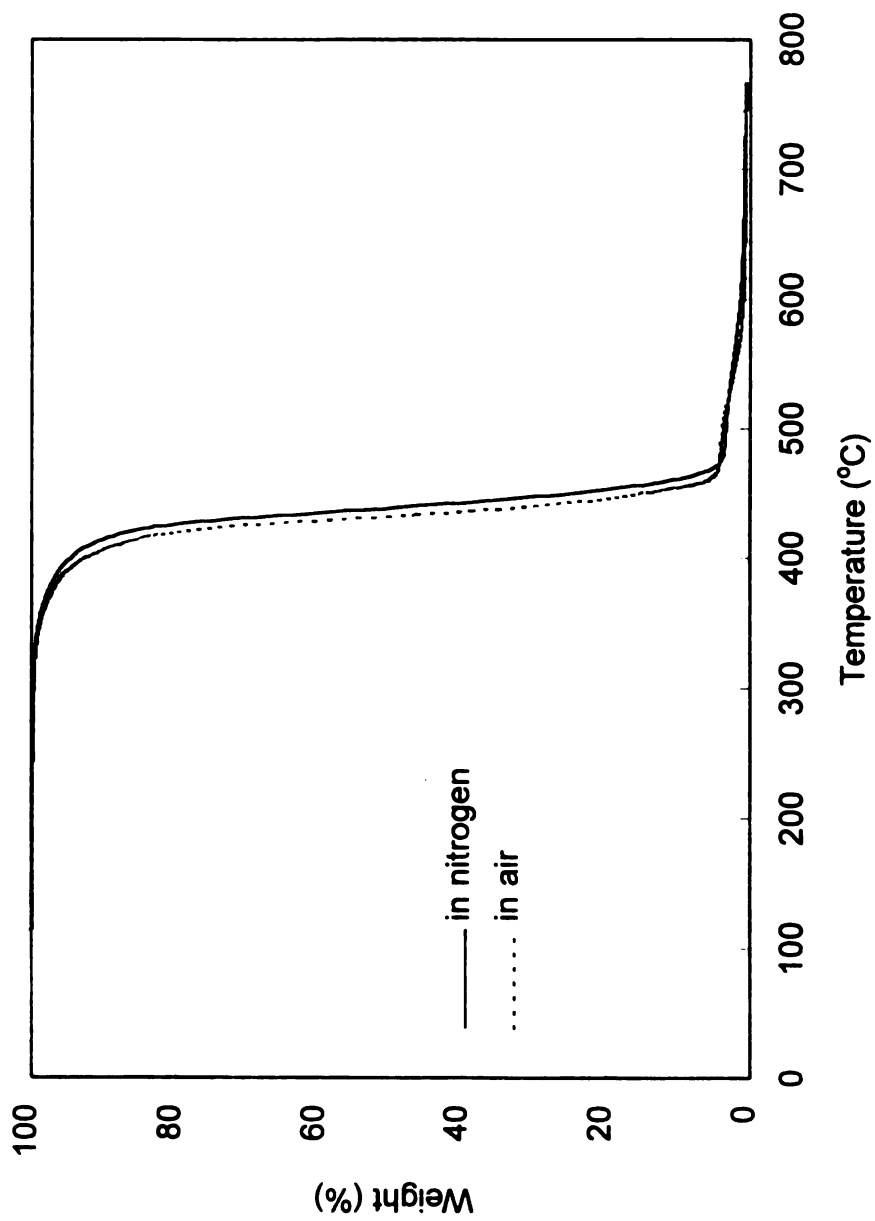


**Figure 68.** TGA profiles of PP4a (heating rate 10 °C/min).

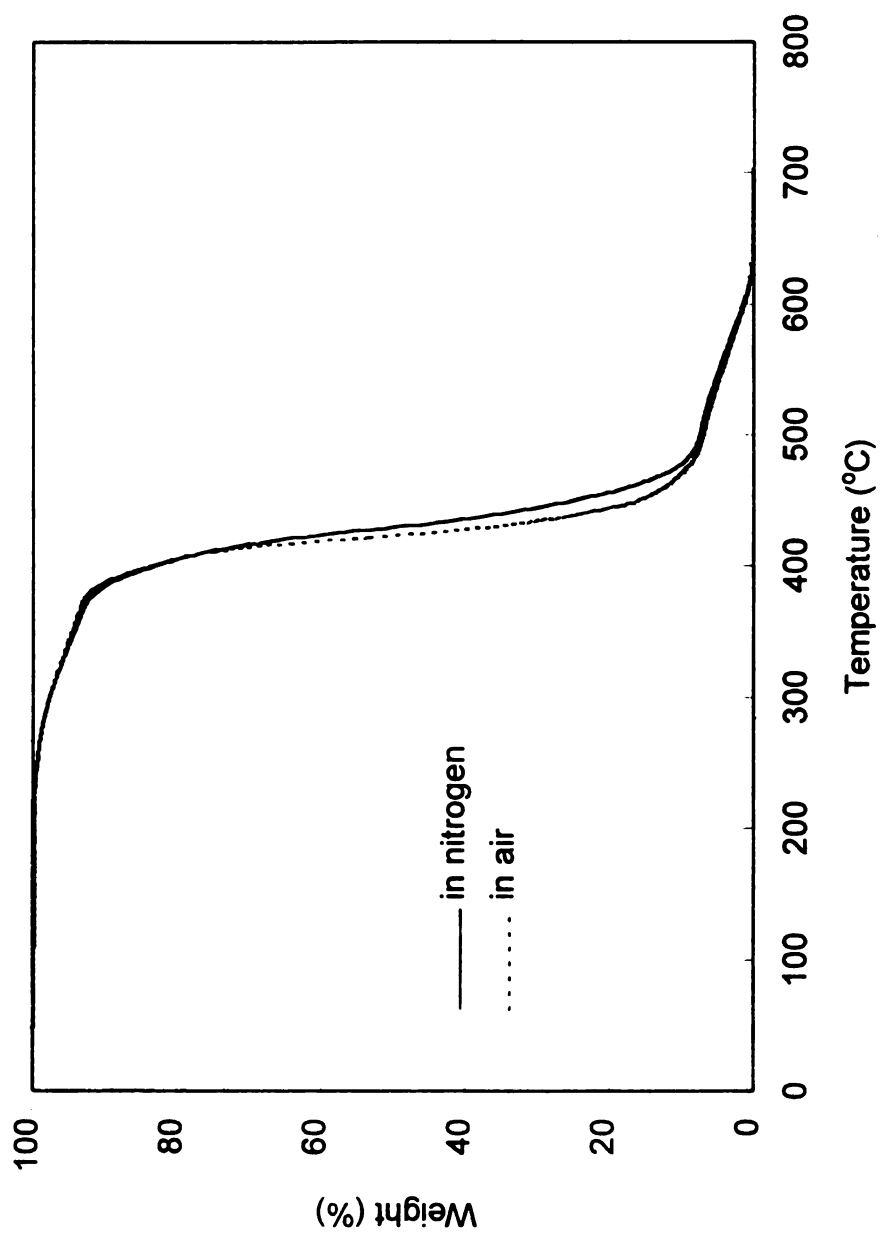


**Figure 69.** TGA profiles of PH3 (heating rate 10 °C/min).

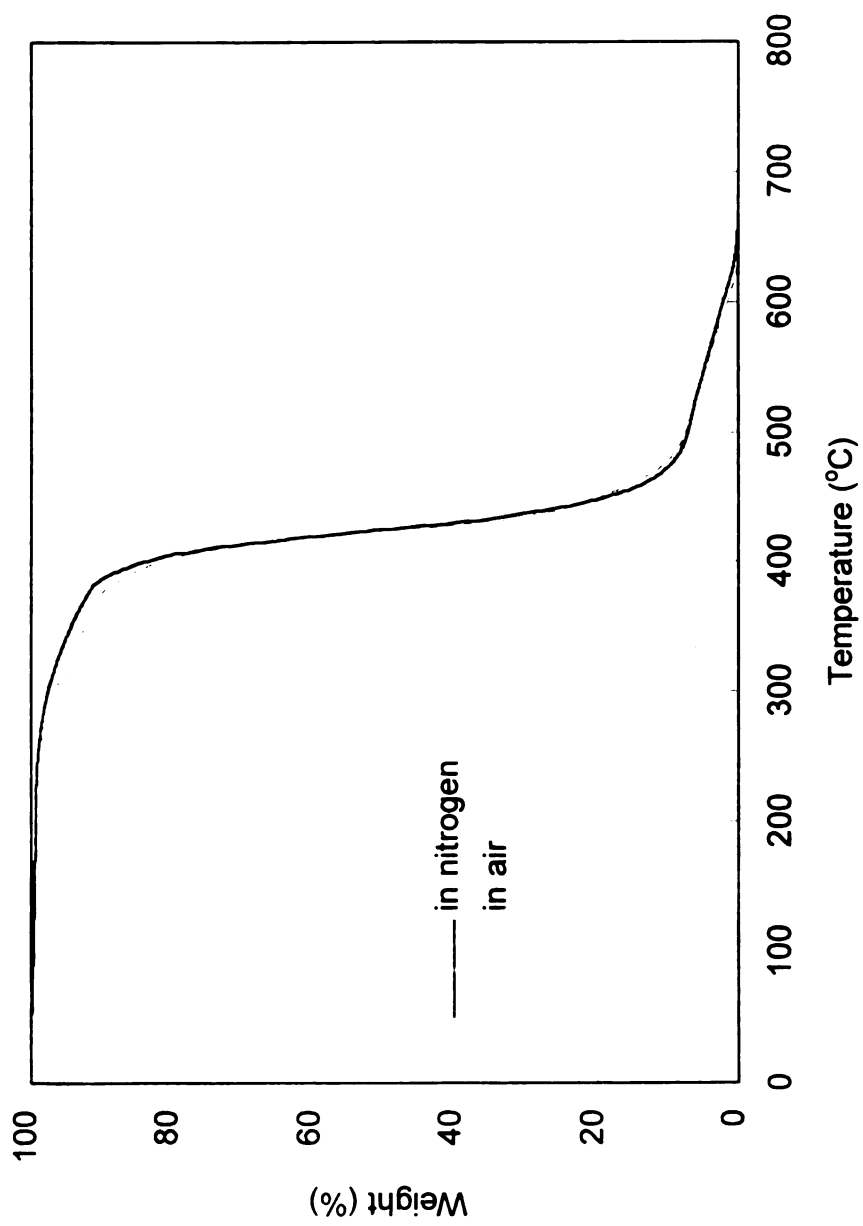


**Figure 70.** TGA profiles of PH4 (heating rate 10 °C/min).

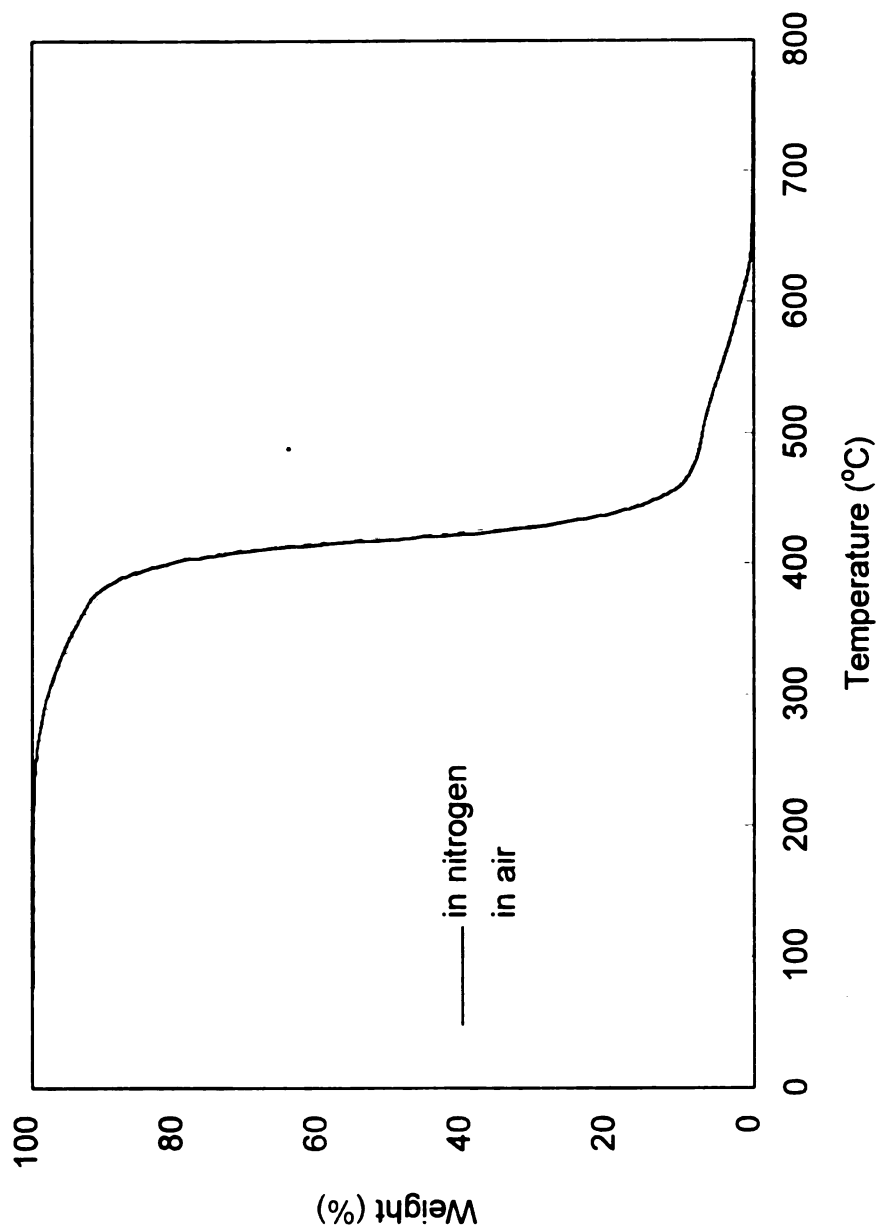


**Figure 71.** TGA profiles of PH5 (heating rate 10 °C/min).

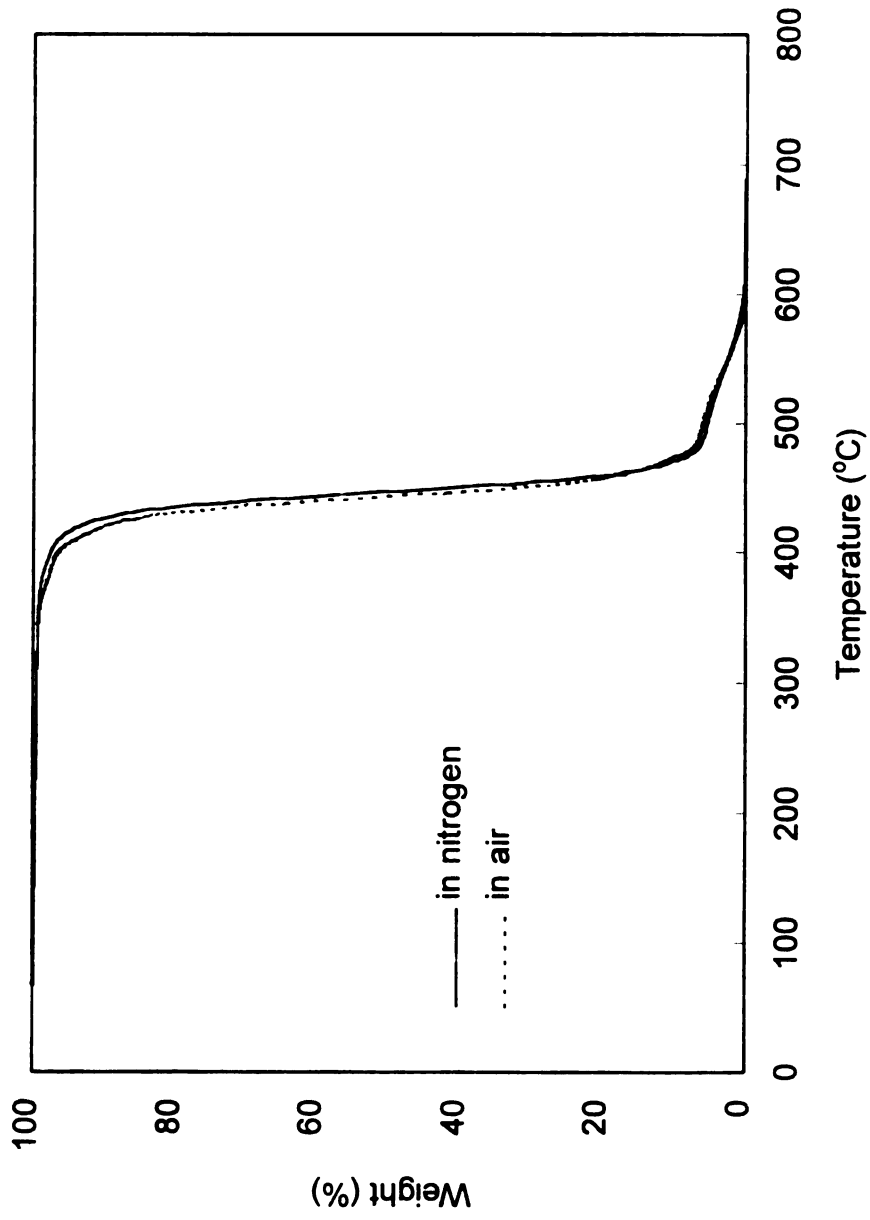


Figure 72. TGA profiles of PO<sub>2</sub> (heating rate 10 °C/min).

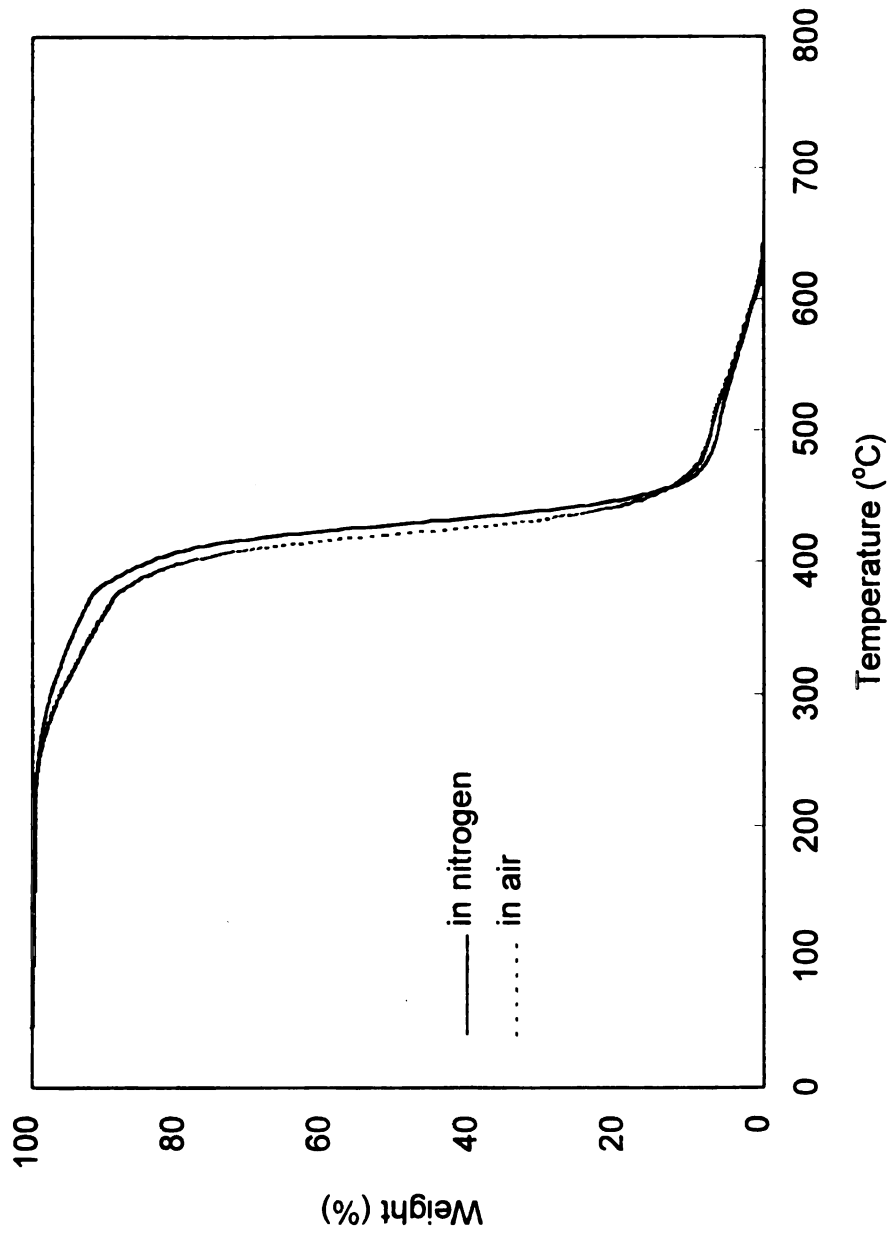


Figure 73. TGA profiles of PO4 (heating rate 10 °C/min).

Table 12. Conductivity Data<sup>a</sup> for PP2-LiClO<sub>4</sub> Complexes

| O:Li ratio | 20 °C                | 30 °C                | 40 °C                | 50 °C                | 60 °C                | 80 °C                | 100 °C               |
|------------|----------------------|----------------------|----------------------|----------------------|----------------------|----------------------|----------------------|
| 64         | 7.0x10 <sup>-6</sup> | 9.4x10 <sup>-6</sup> | 1.7x10 <sup>-5</sup> | 2.3x10 <sup>-5</sup> | 2.9x10 <sup>-5</sup> | 5.7x10 <sup>-5</sup> | 7.5x10 <sup>-5</sup> |
| 32         | 7.8x10 <sup>-6</sup> | 1.3x10 <sup>-5</sup> | 1.8x10 <sup>-5</sup> | 3.1x10 <sup>-5</sup> | 4.4x10 <sup>-5</sup> | 8.8x10 <sup>-5</sup> | 1.5x10 <sup>-4</sup> |
| 16         | 7.9x10 <sup>-6</sup> | 1.5x10 <sup>-5</sup> | 2.1x10 <sup>-5</sup> | 3.5x10 <sup>-5</sup> | 4.9x10 <sup>-5</sup> | 7.8x10 <sup>-5</sup> | 1.4x10 <sup>-4</sup> |
| 12         | 5.1x10 <sup>-6</sup> | 1.2x10 <sup>-5</sup> | 1.6x10 <sup>-5</sup> | 3.2x10 <sup>-5</sup> | 4.0x10 <sup>-5</sup> | 8.9x10 <sup>-5</sup> | 1.7x10 <sup>-4</sup> |
| 8          | 5.1x10 <sup>-6</sup> | 1.2x10 <sup>-5</sup> | 1.6x10 <sup>-5</sup> | 3.2x10 <sup>-5</sup> | 4.0x10 <sup>-5</sup> | 8.9x10 <sup>-5</sup> | 1.7x10 <sup>-4</sup> |
| 4          | 6.2x10 <sup>-7</sup> | 1.8x10 <sup>-6</sup> | 4.9x10 <sup>-6</sup> | 1.1x10 <sup>-5</sup> | 1.7x10 <sup>-5</sup> | 6.2x10 <sup>-5</sup> | 1.2x10 <sup>-4</sup> |

<sup>a</sup> Value reported in S/cm.

Table 13. Conductivity Data<sup>a</sup> for PP3-LiClO<sub>4</sub> Complexes

| O:Li ratio | 20 °C                | 30 °C                | 40 °C                | 50 °C                | 60 °C                | 80 °C                | 100 °C               |
|------------|----------------------|----------------------|----------------------|----------------------|----------------------|----------------------|----------------------|
| 64         | 3.4x10 <sup>-6</sup> | 5.5x10 <sup>-6</sup> | 7.3x10 <sup>-6</sup> | 9.6x10 <sup>-6</sup> | 1.3x10 <sup>-5</sup> | 2.1x10 <sup>-5</sup> | 3.0x10 <sup>-5</sup> |
| 32         | 8.7x10 <sup>-6</sup> | 1.3x10 <sup>-5</sup> | 2.1x10 <sup>-5</sup> | 2.8x10 <sup>-5</sup> | 4.2x10 <sup>-5</sup> | 7.9x10 <sup>-5</sup> | 1.0x10 <sup>-4</sup> |
| 16         | 1.2x10 <sup>-5</sup> | 1.8x10 <sup>-5</sup> | 3.3x10 <sup>-5</sup> | 4.8x10 <sup>-5</sup> | 7.4x10 <sup>-5</sup> | 1.1x10 <sup>-4</sup> | 2.2x10 <sup>-4</sup> |
| 12         | 2.0x10 <sup>-5</sup> | 3.0x10 <sup>-5</sup> | 5.5x10 <sup>-5</sup> | 7.9x10 <sup>-5</sup> | 1.1x10 <sup>-4</sup> | 2.3x10 <sup>-4</sup> | 4.1x10 <sup>-4</sup> |
| 8          | 7.7x10 <sup>-6</sup> | 1.3x10 <sup>-5</sup> | 2.8x10 <sup>-5</sup> | 4.7x10 <sup>-5</sup> | 8.1x10 <sup>-5</sup> | 2.4x10 <sup>-4</sup> | 4.0x10 <sup>-4</sup> |
| 4          | 1.3x10 <sup>-7</sup> | 2.7x10 <sup>-7</sup> | 1.1x10 <sup>-6</sup> | 2.7x10 <sup>-6</sup> | 9.3x10 <sup>-6</sup> | 3.4x10 <sup>-5</sup> | 1.1x10 <sup>-4</sup> |

<sup>a</sup> Value reported in S/cm.

Table 14. Conductivity Data<sup>a</sup> for PP4-LiClO<sub>4</sub> Complexes

| O:Li ratio | 20 °C                | 30 °C                | 40 °C                | 50 °C                | 60 °C                | 80 °C <sup>b</sup> | 100 °C <sup>b</sup> |
|------------|----------------------|----------------------|----------------------|----------------------|----------------------|--------------------|---------------------|
| 64         | 7.0x10 <sup>-6</sup> | 1.2x10 <sup>-5</sup> | 1.8x10 <sup>-5</sup> | 2.1x10 <sup>-5</sup> | 2.8x10 <sup>-5</sup> | -                  | -                   |
| 32         | 1.6x10 <sup>-5</sup> | 3.1x10 <sup>-5</sup> | 4.5x10 <sup>-5</sup> | 6.2x10 <sup>-5</sup> | 8.4x10 <sup>-5</sup> | -                  | -                   |
| 16         | 1.5x10 <sup>-5</sup> | 3.8x10 <sup>-5</sup> | 6.5x10 <sup>-5</sup> | 8.3x10 <sup>-5</sup> | 1.4x10 <sup>-4</sup> | -                  | -                   |
| 12         | 9.5x10 <sup>-6</sup> | 2.3x10 <sup>-5</sup> | 3.5x10 <sup>-5</sup> | 5.1x10 <sup>-5</sup> | 8.9x10 <sup>-5</sup> | -                  | -                   |
| 8          | 4.5x10 <sup>-6</sup> | 9.6x10 <sup>-6</sup> | 2.4x10 <sup>-5</sup> | 6.0x10 <sup>-5</sup> | 6.0x10 <sup>-5</sup> | -                  | -                   |
| 4          | 2.4x10 <sup>-7</sup> | 6.0x10 <sup>-7</sup> | 2.8x10 <sup>-6</sup> | 4.2x10 <sup>-6</sup> | 1.1x10 <sup>-5</sup> | -                  | -                   |

<sup>a</sup> Value reported in S/cm.<sup>b</sup> Not measured

**Table 15. Conductivity Data<sup>a</sup> for PH<sub>3</sub>-LiClO<sub>4</sub> Complexes**

| O:Li ratio | 20 °C                | 30 °C                | 40 °C                | 50 °C                | 60 °C                | 80 °C                | 100 °C               |
|------------|----------------------|----------------------|----------------------|----------------------|----------------------|----------------------|----------------------|
| 64         | 4.7x10 <sup>-6</sup> | 6.4x10 <sup>-6</sup> | 8.8x10 <sup>-6</sup> | 1.2x10 <sup>-5</sup> | 1.6x10 <sup>-5</sup> | 1.9x10 <sup>-5</sup> | 2.5x10 <sup>-5</sup> |
| 32         | 5.7x10 <sup>-6</sup> | 8.6x10 <sup>-6</sup> | 1.1x10 <sup>-5</sup> | 1.7x10 <sup>-5</sup> | 2.3x10 <sup>-5</sup> | 4.0x10 <sup>-5</sup> | 6.8x10 <sup>-5</sup> |
| 16         | 1.0x10 <sup>-5</sup> | 1.8x10 <sup>-5</sup> | 2.5x10 <sup>-5</sup> | 3.7x10 <sup>-5</sup> | 5.0x10 <sup>-5</sup> | 1.2x10 <sup>-4</sup> | 1.6x10 <sup>-4</sup> |
| 12         | 9.9x10 <sup>-6</sup> | 1.8x10 <sup>-5</sup> | 2.8x10 <sup>-5</sup> | 3.9x10 <sup>-5</sup> | 5.1x10 <sup>-5</sup> | 1.2x10 <sup>-4</sup> | 2.2x10 <sup>-4</sup> |
| 8          | 5.5x10 <sup>-6</sup> | 1.2x10 <sup>-5</sup> | 1.8x10 <sup>-5</sup> | 3.1x10 <sup>-5</sup> | 4.6x10 <sup>-5</sup> | 1.1x10 <sup>-4</sup> | 2.3x10 <sup>-4</sup> |
| 4          | 6.7x10 <sup>-7</sup> | 1.4x10 <sup>-6</sup> | 3.4x10 <sup>-6</sup> | 8.3x10 <sup>-6</sup> | 1.6x10 <sup>-5</sup> | 5.4x10 <sup>-5</sup> | 1.4x10 <sup>-4</sup> |

<sup>a</sup> Value reported in S/cm.

Table 16. Conductivity Data<sup>a</sup> for PH<sub>4</sub>-LiClO<sub>4</sub> Complexes

| O:Li ratio | 20 °C                | 30 °C                | 40 °C                | 50 °C                | 60 °C                | 80 °C                | 100 °C               |
|------------|----------------------|----------------------|----------------------|----------------------|----------------------|----------------------|----------------------|
| 64         | 6.2x10 <sup>-6</sup> | 9.7x10 <sup>-6</sup> | 1.6x10 <sup>-5</sup> | 1.8x10 <sup>-5</sup> | 2.6x10 <sup>-5</sup> | 3.8x10 <sup>-5</sup> | 5.5x10 <sup>-5</sup> |
| 32         | 1.8x10 <sup>-5</sup> | 2.7x10 <sup>-5</sup> | 4.5x10 <sup>-5</sup> | 5.8x10 <sup>-5</sup> | 8.7x10 <sup>-5</sup> | 1.2x10 <sup>-4</sup> | 1.9x10 <sup>-4</sup> |
| 16         | 2.1x10 <sup>-5</sup> | 3.7x10 <sup>-5</sup> | 5.3x10 <sup>-5</sup> | 1.0x10 <sup>-4</sup> | 1.4x10 <sup>-4</sup> | 3.0x10 <sup>-4</sup> | 3.6x10 <sup>-4</sup> |
| 12         | 2.1x10 <sup>-6</sup> | 4.0x10 <sup>-5</sup> | 5.3x10 <sup>-5</sup> | 7.7x10 <sup>-5</sup> | 1.4x10 <sup>-4</sup> | 3.7x10 <sup>-4</sup> | 4.3x10 <sup>-4</sup> |
| 8          | 1.4x10 <sup>-5</sup> | 2.5x10 <sup>-5</sup> | 4.2x10 <sup>-5</sup> | 7.2x10 <sup>-5</sup> | 1.2x10 <sup>-4</sup> | 3.2x10 <sup>-4</sup> | 5.7x10 <sup>-4</sup> |
| 4          | 7.8x10 <sup>-7</sup> | 2.3x10 <sup>-6</sup> | 7.6x10 <sup>-6</sup> | 1.8x10 <sup>-5</sup> | 3.8x10 <sup>-5</sup> | 1.6x10 <sup>-4</sup> | 1.9x10 <sup>-4</sup> |

<sup>a</sup> Value reported in S/cm.

Table 17. Conductivity Data<sup>a</sup> for PH5-LiClO<sub>4</sub> Complexes

| O:Li ratio | 20 °C                | 30 °C                | 40 °C                | 50 °C                | 60 °C                | 80 °C                | 100 °C               |
|------------|----------------------|----------------------|----------------------|----------------------|----------------------|----------------------|----------------------|
| 64         | 1.2x10 <sup>-5</sup> | 1.7x10 <sup>-5</sup> | 2.5x10 <sup>-5</sup> | 3.4x10 <sup>-5</sup> | 4.8x10 <sup>-5</sup> | 6.2x10 <sup>-5</sup> | 9.8x10 <sup>-5</sup> |
| 32         | 2.3x10 <sup>-5</sup> | 3.8x10 <sup>-5</sup> | 6.1x10 <sup>-5</sup> | 8.5x10 <sup>-5</sup> | 1.2x10 <sup>-4</sup> | 1.8x10 <sup>-4</sup> | 2.5x10 <sup>-4</sup> |
| 16         | 2.2x10 <sup>-5</sup> | 4.3x10 <sup>-5</sup> | 8.2x10 <sup>-5</sup> | 1.2x10 <sup>-4</sup> | 1.7x10 <sup>-4</sup> | 3.4x10 <sup>-4</sup> | 4.2x10 <sup>-4</sup> |
| 12         | 2.0x10 <sup>-5</sup> | 4.0x10 <sup>-5</sup> | 7.3x10 <sup>-5</sup> | 1.0x10 <sup>-4</sup> | 1.8x10 <sup>-4</sup> | 3.9x10 <sup>-4</sup> | 4.7x10 <sup>-4</sup> |
| 8          | 8.6x10 <sup>-6</sup> | 2.1x10 <sup>-5</sup> | 3.6x10 <sup>-5</sup> | 7.1x10 <sup>-5</sup> | 1.6x10 <sup>-4</sup> | 3.9x10 <sup>-4</sup> | 4.9x10 <sup>-4</sup> |
| 4          | 1.9x10 <sup>-6</sup> | 4.3x10 <sup>-6</sup> | 9.2x10 <sup>-6</sup> | 2.1x10 <sup>-5</sup> | 4.0x10 <sup>-5</sup> | 1.0x10 <sup>-4</sup> | 2.5x10 <sup>-4</sup> |

<sup>a</sup> Value reported in S/cm.

## BIBLIOGRAPHY

1. Vincent, C. A. *Prog. Solid St. Chem.* **1987**, *17*, 145.
2. MacCallum, J. R.; Vincent, C. A. "Polymer Electrolyte Review-1" Elsevier Applied Science, London (1987).
3. MacCallum, J. R.; Vincent, C. A. "Polymer Electrolyte Review-2" Elsevier Applied Science, London (1989).
4. Gray, F. M. "Solid Polymer Electrolytes: Fundamentals and Technological Applications" VCH Publishers, Inc., New York (1991).
5. Fenton, D. E.; Parker, J. M.; Wright, P. V. *Polymer* **1973**, *14*, 589.
6. Armand, M. B.; Chabagno, J. M.; Duclot, M. J. in *Fast Ion Transport in Solids*, Vashista, P.; Mundy, J. N.; Shenoy, G. K. eds. Elsevier, New York (1979); p131.
7. Ratner, M. A.; Shriver, D. F. *Chem. Rev.* **1988**, *88*, 109.
8. Furukawa, J.; Tsuruta, T.; Sakata, T.; Saegusa, T.; Kawaski, A. *Macromol. Chem.* **1960**, *40*, 64.
9. Vachon, C.; Labreche, C.; Vallee, A.; Besner, S.; Dumont, M.; Prud'homme, J. *Macromolecules* **1995**, *28*, 5585.
10. Chiang, C. K.; Davis, G. T.; Harding, C. A.; Takahashi, T. *Macromolecules* **1985**, *18*, 825.
11. Harris, C. S.; Shriver, D. F.; Ratner, M. A. *Macromolecules* **1986**, *19*, 987.

12. Clancy, S.; Shriver, D. F.; Ochrymowycz, L. A. *Macromolecules* **1986**, *19*, 606.
13. Armstrong, R. D.; Clarke, M. D. *Electrochimica Acta*. **1984**, *29*, 1443.
14. Watanabe, M.; Rikukawa, M.; Sanui, K.; Ogata, N.; Kato, H.; Kobayashi, T.; Ohtaki, Z. *Macromolecules* **1984**, *17*, 2902.
15. Watanabe, M.; Togo, M.; Sanui, K.; Ogata, N.; Kobayashi, T.; Ohtaki, Z. *Macromolecules* **1984**, *17*, 2908.
16. Tadokoro, H.; Chatani, Y.; Yoshihara, T.; Tahara, S.; Murahashi, S.. *Makromol. Chem.* **1964**, *73*, 109.
17. Robitaille, C. D.; Fauteux, D. *J. Electrochem. Soc.* **1986**, *133*, 315.
18. Berthier, C.; Gorecki, W.; Minier, M.; Armand, M. B.; Chabagno, J. M.; Rigaud, P. *Solid State Ionics* **1983**, *11*, 91.
19. Chabagno, J. M. Thesis, Institut National Polytechnique, Grenoble, 1980.
20. Craven, J. R.; Mobbs, R. H.; Booth, C.; Giles, J. R. M. *J. Macromol. Chem. Rapid Commun.* **1986**, *7*, 81.
21. Nicholas, C. V.; Wilson, D. J.; Booth, C.; Giles, J. R. M. *Br. Polymer J.* **1988**, *20*, 289.
22. Liao, B.; Chen, Y.; Booth, C.; Luo, Y. *Polym. Commun.* **1991**, *32*, 348.
23. Nagaoka, K.; Naruse, H.; Shinohara, I.; Watanabe, M. *J. Polym. Sci. Polym. Lett. Ed.* **1984**, *22*, 659.
24. Manaresi, P.; Bignozzi, M. C.; Pilati, F.; Munari, A.; Mastragostino, M.; Meneghello, L.; Chiolle, A. *Polymer* **1993**, *34*, 2422.

25. Passiniemi, P.; Takkumaki, S.; Kankare, J.; Syrjama, M. *Solid State Ionics* **1988**, 28-30, 1001.
26. Hall, P. G.; Davies, G. R.; McIntyre, J. E.; Ward, I. M.; Bannister, D. J.; Le Brocq, K. M. F. *Polym. Commun.* **1986**, 27, 98.
27. Fish, D.; Khan, I. M.; Smid, J. *J. Makromol. Chem. Rapid Commun.* **1986**, 7, 115.
28. Fish, D.; Khan, I. M.; Wu, E.; Smid, J. *Br. Polym. J.* **1988**, 20, 281.
29. Khan, I. M.; Yuan, Y.; Fish, D.; Wu, E.; Smid, J. *Macromolecules* **1988**, 21, 2684.
30. Blonsky, P. M.; Shriver, D. F.; Austin, P.; Allcock, H. R. *J. Am. Chem. Soc.* **1984**, 106, 6854.
31. Lerner, M. M.; Lyons, L. J.; Tonge, J. S.; Shriver, D. F. *Chem. Mater.* **1989**, 1, 601.
32. Lerner, M. M.; Tipton, A. L.; Shriver, D. F.; Dembek, A. A.; Allcock, H. R. *Chem. Mater.* **1991**, 3, 1117.
33. Allcock, H. R.; Kuharcik, S. E.; Reed, C. S.; Napierala, M. E. *Macromolecules*, **1996**, 29, 3384.
34. Tonge, J. S.; Shriver, D. F. *J. Electrochem. Soc.* **1987**, 134, 269.
35. Bennett, J. L.; Dembek, A. A.; Allcock, H. R.; Heyen, B. J.; Shriver, D. F. *Chem. Mater.* **1989**, 1, 14.
36. Pomerantz, M.; Krishnan, G.; Victor, M. W.; Wei, C.; Rajeshwar, K. *Chem. Mater.* **1993**, 5, 705.

37. Xia, D. W.; Smid, J. *J. Polym. Sci. Polym. Lett. Ed.* **1984**, *22*, 617.
38. Selvaraj, I. I.; Chaklanois, S.; Chandrasekhar, V. *J. Polym. Sci. Polym. Chem.* **1993**, *31*, 2643.
39. Selvaraj, I. I.; Chaklanois, S.; Manoravi, P.; Chandrasekhar, V. *Polymer* **1995**, *36*, 2603.
40. Cowie, J. M. G.; Ferguson, R. *J. Polym. Sci. Polym. Phys.* **1985**, *23*, 2181.
41. Inoue, K.; Nishikawa, Y.; Tanigaki, T. *J. Am. Chem. Soc.* **1991**, *113*, 7069.
42. Inoue, K.; Takiue, K.; Tanigaki, T. *J. Polym. Sci. Polym. Chem.* **1996**, *34*, 1331.
43. Lestel, L.; Cheradame, H.; Boileau, S. *Polymer* **1990**, *31*, 1154.
44. Lindmark-Hamberg, M.; Wagener, K. B. *Macromolecules* **1987**, *20*, 2949.
45. Wagener, K. B.; Boncella, J. M.; Nel, J. G. *Macromolecules* **1991**, *24*, 2649.
46. Wagener, K. B.; Brzezinska, K. *Macromolecules* **1991**, *24*, 5273.
47. Wagener, K. B.; Smith, Jr., D. W. *Macromolecules* **1991**, *24*, 6073.
48. Patton, J. T.; Boncella, J. M.; Wagener, K. B. *Macromolecules* **1992**, *25*, 3862.
49. Wagener, K. B.; Patton, J. T. *Macromolecules* **1993**, *26*, 249.
50. Smith, Jr., D. W.; Wagener, K. B. *Macromolecules* **1993**, *26*, 1633.

51. Marmo, J. C.; Wagener, K. B. *Macromolecules* **1993**, *26*, 2137.
52. O'Gara, J. E.; Portmess, J. D.; Wagener, K. B. *Macromolecules* **1993**, *26*, 2837.
53. Tao, D.; Wagener, K. B. *Macromolecules* **1994**, *27*, 1281.
54. Nubel, P. O.; Lutman, C. A.; Yokelson, H. B. *Macromolecules* **1994**, *27*, 7000.
55. Konzelman, J.; Wagener, K. B. *Macromolecules* **1995**, *28*, 4686.
56. Walba, D. M.; Keller, P.; Shao, R.; Clark, N. A.; Hillmyer, M.; Grubbs, R. H. *J. Am. Chem. Soc.* **1996**, *118*, 2740.
57. Chauvin, Y.; Saussine, L. *Macromolecules* **1996**, *29*, 1163.
58. Odian, G. "Principles of Polymerization", 3rd Ed.; John Wiley & Sons, Inc.: New York (1991); p40.
59. Schaverien, C. J.; Dewan, J. C.; Schrock, R. R. *J. Am. Chem. Soc.* **1986**, *108*, 2771.
60. Schrock, R. R.; DePue, R. T.; Feldman, J.; Schaverien, C. J.; Dewan, J. C.; Liu, A. H. *J. Am. Chem. Soc.* **1988**, *110*, 1423.
61. Murdzek, J. S.; Schrock, R. R. *Organometallics* **1987**, *6*, 1373.
62. Schrock, R. R.; Murdzek, J. S.; Bazan, G. C.; Robbins, J.; DiMare, M.; O'Regan, M. *J. Am. Chem. Soc.* **1990**, *112*, 3875.
63. Nguyen, S. T.; Johnson, L. K.; Grubbs, R. H. *J. Am. Chem. Soc.* **1992**, *114*, 3974.
64. Nguyen, S. T.; Grubbs, R. H.; Ziller, J. W. *J. Am. Chem. Soc.* **1993**, *115*, 9858.

65. Schwab, P.; France, M. B.; Ziller, J. W.; Grubbs, R. H. *Angew. Chem. Int. Ed. Engl.* **1995**, *34*, 2039.
66. Grubbs, R. H.; Tumas, W. *Science* **1989**, *243*, 907.
67. Schrock, R. R. *Acc. Chem. Res.* **1990**, *23*, 158.
68. Wu, Z.; Benedicto, A. D.; Grubbs, R. H. *Macromolecules* **1993**, *26*, 4975.
69. Kanaoka, S.; Grubbs, R. H. *Macromolecules* **1995**, *28*, 4707.
70. Konzelman, J.; Wagener, K. B. *Macromolecules* **1995**, *28*, 4686.
71. MacDonald, J. R. *J. Chem. Phys.* **1973**, *58*, 4982.
72. MacDonald, J. R. *J. Chem. Phys.* **1974**, *61*, 3977.
73. Bruce, P. G. in "Polymer Electrolyte Review-1", MacCallum, J. R.; Vincent, C. A. eds. Elsevier Applied Science, London (1987); p.237.
74. MacDonald, J. R. "Impedance Spectroscopy" John Wiley & Sons, Inc., New York (1987).
75. Growcock, F. B. *Chemtech* **1989**, 564.
76. Van Tamelen, E. E.; Dewey, R. S.; Timmons, R. J. *J. Am. Chem. Soc.* **1961**, *83*, 3725.
77. Dewey, R. S.; van Tamelen, E. E. *J. Am. Chem. Soc.* **1961**, *83*, 3729.
78. Van Tamelen, E. E.; Dewey, R. S.; Lease, M. F.; Pirkle, W. H. *J. Am. Chem. Soc.* **1961**, *83*, 4302.
79. Wu, Z.; Grubbs, R. H. *Macromolecules* **1994**, *27*, 6700.
80. Moynihan, C. T. in "Ionic Interactions from Dilute Solutions to Fused Salts"; Petrucci, S., Ed.; Academic Press: New York (1971); Vol. I; p261.

81. Qiao, J.; Baker, G. L. *Polym. Mater. Sci. Eng.* **1995**, *73*, 515.
82. Fu, G. C.; Grubbs, R. H. *J. Am. Chem. Soc.* **1992**, *114*, 5426.
83. Fu, G. C.; Grubbs, R. H. *J. Am. Chem. Soc.* **1992**, *114*, 7324.
84. Fu, G. C.; Grubbs, R. H. *J. Am. Chem. Soc.* **1993**, *115*, 3800.
85. Fu, G. C.; Nguyen, S. T.; Grubbs, R. H. *J. Am. Chem. Soc.* **1993**, *115*, 9856.
86. Fujimura, O.; Fu, G. C.; Grubbs, R. H. *J. Org. Chem.* **1994**, *59*, 4029.
87. Kim, S.-H.; Bowden, N.; Grubbs, R. H. *J. Am. Chem. Soc.* **1994**, *116*, 10801.
88. Miller, S. J.; Grubbs, R. H. *J. Am. Chem. Soc.* **1995**, *117*, 5855.
89. Grubbs, R. H.; Miller, S. J.; Fu, G. C. *Acc. Chem. Res.* **1995**, *28*, 446.
90. Sperling, L. H. "Introduction to Physical Polymer Science", 2nd Ed., John Wiley & Sons, Inc. (New York): 1992; p355.
91. Van Krevelen, D. W. "Properties of Polymers", Elsevier (Amsterdam, Netherland): 1990; p166.
92. Abraham, E. P.; Smith, J. C. *J. Chem. Soc.* **1936**, 1605.
93. Wood, N. F.; Chang, F. C. *J. Org. Chem.* **1965**, *30*, 2054.
94. Traynham, J. G.; Stone, D. B.; Couvillion, B. R. *J. Org. Chem.* **1967**, *32*, 510.

MICHIGAN STATE UNIV. LIBRARIES



31293015550548